

The Sedimentary and Tectonic Evolution of the Nam Co Basin, Tibetan Plateau, since the Middle Pleistocene

—

A Seismoacoustic Study on Lake Sediments

Dissertation
zur Erlangung des Doktorgrades der Naturwissenschaften
am Fachbereich Geowissenschaften
der Universität Bremen

vorgelegt von:
Nora Schulze

Bremen, Dezember 2020



Supervisor: Prof. Dr. Volkhard Spieß, University of Bremen, Germany
2nd Supervisor: Prof. Dr. Sebastian Krastel, Kiel University, Germany

Date of the colloquium: 22.03.2021

“Science makes people reach selflessly for truth and objectivity;
it teaches people to accept reality, with wonder and admiration,
not to mention the deep awe and joy that the natural order of things
brings to the true scientist.”

— Lise Meitner

Preface

This thesis was submitted for the degree of Doctor of Natural Sciences (Dr. rer. nat.) at the Department of Geosciences, University of Bremen. The research was conducted in the research group Marine Technology – Environmental Research under the supervision of Prof. Dr. Volkhard Spieß. The second thesis reviewer is Prof. Dr. Sebastian Krastel from Kiel University.

The doctoral project was carried out in cooperation with our partners at the Friedrich-Schiller-University Jena, in particular with Dr. Gerhart Daut and our Chinese partners, led by Dr. Liping Zhu and Dr. Junbo Wang from the Institute of Tibetan Plateau Research (Chinese Academia of Science) in Beijing.

Data acquisition, processing, and analysis were funded by the German Research Foundation (DFG) within the ICDP priority program (Grant SP296/36-1, Grant SP296/36-2). Additional funding for data acquisition was provided to our Chinese partners by the Strategic Priority Research Program of the Chinese Academy of Sciences (XDA20070101) and the Chinese Ministry of Science and Technology project (2012FY111400).

The Bremen International Graduate School for Marine Sciences (GLOMAR) provided further financial support for international conferences and workshop participations.

Nora Schulze

Bremen, December 2020

Contents

Preface.....	V
Contents.....	VII
List of acronyms and abbreviations.....	X
Abstract.....	11
Zusammenfassung.....	13
Thesis outline and declaration of co-author contributions	17
Chapter 1: Introduction	21
1.1 Motivation and Objectives.....	21
1.1.1 Climate change threatens vital resources.....	21
1.1.2 Research effort on past climate change.....	22
1.1.3 ICDP effort.....	23
1.1.4 Scientific objectives.....	24
1.2 Tectonic, climate, and regional setting	26
1.2.1 Tectonic evolution of the Tibetan Plateau.....	26
1.2.2 Atmospheric circulations and climate.....	29
1.2.3 Modern settings and characteristics of Nam Co.....	31
1.2.4 Paleoenvironmental studies at Nam Co.....	32
Chapter 2: Data and Methods.....	35
2.1 Parametric sub-bottom profiler	36
2.2 Multichannel Seismic	37
2.3 Multichannel seismic data processing.....	37
2.3.1 Pre-Processing.....	38
2.3.2 Pre-Stack Processing.....	39
2.3.3 Post-stack Processing	41
2.3.4 Basement processing.....	41
2.4.1 Seismic Stratigraphy	42
2.4.2 Horizon maps, calculations, and grids.....	42
2.4.3 Fault database	42
2.4.4 SES and Core intergration	43
Chapter 3: Sediment distribution processes and lake-level variations since the LGM.....	45
3.1 Abstract	45
3.2 Introduction	46
3.2.1 Motivation.....	46
3.2.2 Study site / Geologic and climate setting	47
3.2.3 General lake sedimentary processes	49
3.3 Methods.....	50
3.3.1 Sediment Echo Sounder data.....	50
3.3.2 SES data interpretation.....	50
3.3.3 Age Model and Integration of SES and Core data.....	51

3.4	Results.....	51
3.4.1	Description of Acoustic Facies	51
3.4.2	Description of Acoustic Units	51
3.4.3	Additional reflectors and amplitude anomalies.....	54
3.4.4	Integration of Core data and hydro-acoustic data.....	54
3.4.5	Sediment distribution characteristics.....	56
3.4.6	Sediment extents and thicknesses during the Holocene.....	56
3.5	Discussion	58
3.5.1	Correlation of AF and AU with sediment characteristics.....	58
3.5.2	Sedimentation in Nam Co	59
3.5.3	Lake level reconstruction based on primary sedimentation process.....	61
3.6	Conclusion	67
3.7	Acknowledgements.....	68
Chapter 4: Climate-induced lake-level variations of the Tibetan lake Nam Co since the Middle Pleistocene.....		71
4.1	Abstract	71
4.2	Introduction.....	72
4.2.1	Paleoclimate reconstructions on the Tibetan Plateau	72
4.2.2	Geologic and climatic setting of the Nam Co region	75
4.2.3	Research results on Nam Co's lake-level variation	75
4.3	Methods.....	76
4.3.1	Acquisition and processing of MCS data.....	76
4.3.2	Interpretation procedures of MCS data	77
4.4	Results.....	77
4.4.1	Perceptions from Multichannel seismic data	77
4.4.2	Seismic stratigraphy.....	80
4.5	Interpretation and Discussion.....	84
4.5.1	Depositional environments of seismic facies	84
4.5.2	Chronology of relative lake-level variations	85
4.5.3	Sedimentary responses to climate forcing	88
4.6	Conclusion	93
4.7	Acknowledgements.....	94
Chapter 5: The transtensional tectonic system at Nam Co		95
5.1	Abstract	95
5.2	Introduction.....	96
5.2.1	E-W extension on the Tibetan Plateau.....	96
5.2.2	Regional tectonic setting around Nam Co.....	98
5.3	Material and methods.....	99
5.3.1	2D Reflection seismic surveys data	99

5.3.2	Acquisition.....	99
5.3.3	Processing and interpretation	99
5.3.4	Characterization and classification of faults.....	100
5.3.5	Application of H-T-Plots	100
5.4	Results.....	100
5.4.1	Fault initiation and behavior	101
5.4.2	Fault classification and identification of fault surfaces	102
5.4.3	Areas	1023
5.5	Discussion.....	109
5.5.1	Character of observed faults	109
5.5.2	Unresolved basin evolution of Nam Co.....	109
5.5.3	Extensional and strike-slip characteristics of defined areas	110
5.5.4	Interpretation of extensional and strike-slip-dominated scenarios	114
5.6	Conclusion.....	116
5.7	Acknowledgements.....	117
Chapter 6: Conclusion and Outlook		119
Acknowledgments		125
List of Figures.....		126
List of Tables.....		128
References		129
Appendix		143

List of acronyms and abbreviations

AMS	Accelerator mass spectrometry
ASM	Asian Summer Monsoon
AWM	Asian Winter Monsoon
CMP	Common midpoint
CVS	Common velocity stack
EASM	East Asian Summer Monsoon
ICDP	International Continental Scientific Drilling Program
IOSM	Indian Ocean Summer Monsoon
ITP-CAS	Institute of Tibetan Plateau Research - Chinese Academy of Sciences
L(L)GM	Last (local) glacial maximum
LSR	Linear sedimentation rate
masl	Meters above sea level
mbll/mall	Meters below lake level/ meters above lake level
MCS	Multichannel seismic
NMO	Normal moveout
NQTL	Nyainqêntanglha Mountain Range
SAR	Sediment accumulation rate
SES	Sediment echo sounder
SRME	Surface related multiple elimination
TP	Tibetan Plateau
TR	Throw rate
TWT	Two way travel time
WD	Water depth

Abstract

Advancing climate change threatens the supply of water and sediment resources provided by the Tibetan Plateau for most Asian countries. This could expose one-fifth of the global population to significant societal, ecological, and economic adversity. Accurate climate models based on data of past climatic changes are, therefore, essential to prepare best for the effects of climate change. However, prolonged and continuous datasets on the Tibetan Plateau are rare. A promising and yet undeveloped climate archive is Nam Co (Co= Tibetan for Lake).

This doctoral thesis contributes substantially to the sedimentary, climatic, and tectonic understanding of Nam Co and its vicinity as part of the evaluation of Nam Co's potential as a high-resolution and extensive climate archive. In detail, this thesis investigates 1) sedimentary structures, distribution, and deposition processes of the last 20.5 kyrs, 2) long-term climate-driven lake-level variations throughout the last 700 kyrs, and 3) the transtensional tectonic setting of Nam Co.

High-resolution hydro-acoustic data, comprising sediment echo sounder (SES) and multichannel reflection seismic (MCS) data, build the basis of the presented studies.

1400 km of SES profiles recorded the upper 25 m of Nam Co's subsurface with decimeter resolution. Combined with the chronology and logs of the sediment core NC01/08 from the center of Nam Co, the SES dataset enabled a detailed spatial study of the recent sediments and the uppermost seven meters of deposits, reaching 20.5 ka in age. The youngest clayey and silty sediments (<1 ka) start to deposit at a water depth of 66 m. This indicates a dominant distribution of fine-grained sediments via interflows, steered by a boundary layer in the water column (e.g., a pycnocline). The reconstruction of paleo-lake-levels from older sediment onlaps implies that the pycnocline depth was stable throughout the Holocene and had a similar depth during a high lake-level stand around 12.2 ka. During climatic periods with a lower lake level than today, lake stratification was potentially unstable, and hyperpycnal flows controlled the transport and distribution of suspended material in the lake basin. The identified sediment onlaps from 20.5 ka until 16.7 ka are linked to paleo-beach ridges, implying a lake-level rise from ~80 m to ~58 m below lake level (mbll). During cold but moist climatic conditions between 16.5 and 13.4 ka, the sediment onlaps represent relative lake-level variations in the range of 60 to 20 mbll. Around 12.2 ka, the water level rose to a maximum of +16.1 m above lake level. During the Holocene, the lake level oscillated quickly, as short lake-level minima occurred during a general high water level.

To extend our comprehension of lake-level variations at Nam Co to long time-scales, MCS data were analyzed. The MCS dataset spans more than 860 km of profiles and indicates that the sediment infill at Nam Co exceeds 670 m in thickness. The presented detailed facies analysis revealed a cyclic alternation in seismic reflection amplitude, directly correlated to lake level (e.g., low seismic

amplitudes indicate the sedimentation of fine-grained material in a low energy environment during a high lake level). This relation was used to establish a relative lake-level curve representative for Nam Co. The seismic stratigraphic framework, derived through the correlation of the lake-level cycles with the global glacial cycles (Marine Isotope Stages; MIS), indicates the unique record of eight glacial-interglacial cycles back to 712 ka. The findings reveal further that the environmental influences at Nam Co were similar for individual glacial cycles, as the calculated linear sedimentation rates (LSR) show almost constant values of 0.52 mm/yr for full glacial-interglacial cycles. Interpolating this LSR for the entire sediment infill indicates that the deepest sediments in Nam Co may exceed more than one million years in age. Comparing the relative lake-level curve with climate-proxy records of global and supra-regional scale exposed that the lake-level behavior of Nam Co correlates to the shift of the Asian summer monsoon on short (20.5 kyrs) and long (700 kyr) time scales. Deviations possibly indicate local climate feedback caused by enhanced meltwater supply and thawing permafrost and triggered quick, high amplitude lake-level variations as observed for the interglacial substages of MIS 5. Overall, precipitation steered lake-level variations at Nam Co.

The MCS data moreover exposed a previously unknown amount of faults in the lacustrine infill of Nam Co and documented, for the first time, tectonic extension since the Middle Pleistocene in southern Tibet. The analysis of the fault structures revealed 1) primary strike-slip faults along a NW-SE directed wrench zone, parallel to the dextral Beng Co Fault, NE of Nam Co, and 2) secondary faults with normal or strike-slip faults characteristics. A transtensional regime with a dominating extensional W-E direction is proposed to represent the overall tectonic setting at Nam Co. Calculated cumulative throw rates stay in the range of 0.3 mm/yr in WSW-ENE direction to 0.9 mm/yr in WNW-ESE direction and are similar to rates reported from the southern Yadong-Gulu rift system. The cumulative throw along the WNW-ESE direction sums up to a total of 315 m. Lateral extension rates range between 0.5 and 0.7 mm/yr and comprise nearly half of the total extension compared to the southern Yadong-Gulu rift system, or ~7% compared to the whole south Tibet extension. Faulting was initiated in Nam Co at ~350 ka. This result is a novel perception of the tectonic extension in southern Tibet. Faulting was continuously active with short exceptions for periods of very high lake levels during wet, interglacial conditions in MIS 5e and since the Holocene.

Overall, this thesis comprises new findings regarding the seismo-stratigraphic framework, precipitation-driven lake-level variations, and extensional regime of Nam Co and set the essential basis for selecting suitable drill sites for the ICDPdrilling campaign 'NamCore'.

Zusammenfassung

Der voranschreitende Klimawandel bedroht die Versorgung der meisten asiatischen Länder mit Wasser und Sedimentressourcen, die vom Tibetischen Plateau bereitgestellt werden. Dies könnte ein Fünftel der Weltbevölkerung enormen sozialen, ökologischen und ökonomischen Notlagen aussetzen. Aussagekräftige Klimamodelle basierend auf Daten vorheriger Klimaveränderungen sind daher wesentlich um auf die Folgen des Klimawandels bestmöglich vorbereitet zu sein. Lang zurückreichende, kontinuierliche Klimaarchive vom tibetischen Hochland sind jedoch rar. Ein vielversprechendes und bisher unerschlossenes Archiv stellt der tibetische See Nam Co (Co= Tibetisch für See) dar.

Im Rahmen der Untersuchungen zur Eignung der Seesedimente als hochauflösendes und weit zurückreichendes Klimaarchiv trägt diese Doktorarbeit wesentlich zu einem Ausbau des sedimentären, klimatischen und tektonischen Grundverständnisses des Nam Co und seiner Umgebung bei. Im Detail untersucht diese Arbeit 1) sedimentäre Strukturen, Verteilungs- und Ablagerungsprozesse der letzten 20,5 tausend Jahre (ka), 2) lang-zeitige, klimabedingte Seespiegelveränderungen bis 700 ka und 3) das transtensionale, tektonische System des Nam Co.

Die vorliegenden Forschungen basieren auf hochauflösenden hydroakustischen Daten, welche Sedimentecholotdaten und Mehrkanalseismik (MCS) umfassen.

1400 km lange SES-Profile bilden die oberen 25 m des Untergrundes dezimetergenau ab. Zusammen mit der zeitlichen Abfolge und den Messungen des Sedimentkerns NC08/01 aus dem Zentrum des Nam Co, erlaubt dieser Datensatz eine detaillierte, räumliche Erforschung der jüngsten Sedimente und der obersten sieben Meter der Ablagerungen, welche bis zu 20,5 ka alt sind. Die jüngsten tonigen und siltigen Sedimente (<1 ka) fangen ab einer Wassertiefe von 66 m an abzulagern. Dies deutet darauf hin, dass die vorherrschende feinkörnige Sedimentverteilung von ‚Interflows‘ (Zwischeneinströmungen) dominiert wird, welche durch eine Sprungschicht in der Wassersäule (z.B. eine Pycnokline) gesteuert wird. Die Rekonstruktion der Paleo-Seespiegel, basierend auf älteren Sedimentanlagerungen (sediment onlap) weist darauf hin, dass die Pycnokline im Holozän stabil und während eines Seespiegelhochstands um 12,2 ka ähnlich tief war. In Klimaperioden mit einem niedrigeren Seespiegel als heute war die Stratifikation hingegen vermutlich instabil und Trübestrome kontrollierten den Transport und die Verteilung der Suspensionsfracht im Seebecken.

Die erkannten Sedimentanlagerungen im Zeitraum von 0,5 bis 16,4 ka stehen in Verbindung mit Paleo-Strandkämmen und weisen auf einen Seespiegelanstieg von ~80 m auf 58 m unter Seespiegel (m u.S.) hin. In den kalten aber feuchten Klimabedingungen im Zeitraum von 16,5 bis 13,4 ka zeigen die Sedimentanlagerungen relative Seespiegelveränderungen im Bereich von 60 bis

20 m u.S. an. Um 12,2 ka stieg der Wasserstand auf ein Maximum von 16,1 m über Seespiegel. Während des Holozäns schwankte der Seespiegel schnell, da kurze Tiefstände während eines generell hohen Seespiegels auftraten.

Um unser Verständnis der Seespiegelveränderungen auf langzeitliche Skalen auszudehnen, wurden MCS Daten ausgewertet. Die MCS Daten umfassen mehr als 860 km und deuten an, dass die Sedimentfüllung Nam Cos die Mächtigkeit von 670 m übersteigt. Die hier präsentierte, detaillierte Faziesanalyse zeigt eine zyklische Abwechslung der seismischen Reflektionsamplituden, welche direkt mit dem Seespiegel korrelieren (z.B. weist eine niedrige seismische Amplitude auf feinkörniges Material hin, das in einer niedrig-energetischen Umgebung während eines Seespiegelhochstandes abgelagert wurde). Diese Beziehung wurde genutzt um eine relative Seespiegelkurve zu entwickeln, welche repräsentativ für Nam Co ist. Der seismo-stratigraphische Rahmen, abgeleitet aus der Korrelation der Seespiegelzyklen mit den Zyklen der globalen Vergletscherung (Marine Sauerstoff-Isotopen-Stufen) stellt eine einzigartige Aufzeichnung von acht Glazial-Interglazial-Zyklen dar, die bis auf 712 ka zurückreicht.

Diese Ergebnisse zeigen des Weiteren, dass sich die Umwelteinflüsse der einzelnen Zyklen am Nam Co ähnelten, da die berechneten linearen Sedimentationsraten (LSR) beinahe konstante Werte von 0,52 mm/yr aufweisen. Interpoliert man diese Rate für die komplette Sedimentfüllung, so ergibt sich, dass die tiefsten Sedimente im Nam Co mehr als eine Million Jahre alt sein könnten.

Der Vergleich der relativen Seespiegelkurve mit regionalen und überregionalen Klimaproxyaufzeichnungen zeigt, dass das kurz- (~20,5 ka) und langzeitliche (~700 ka) Seespiegelverhalten des Nam Co mit der Verschiebung des asiatischen Sommermonsuns korreliert. Abweichungen deuten möglicherweise lokale Klimarückkopplungen an, die durch verstärkte Schmelzwasserbeiträge und tauenden Permafrostboden freigesetzt wurden und schnelle Seespiegelschwankungen hoher Amplitude auslösten, wie sie auch während der interglazialen Substadien von Sauerstoff-Isotopen-Stufe 5 beobachtet wurden. Folglich steuert der Niederschlag die Seespiegelveränderungen des Nam Co.

Die MCS Daten zeigen außerdem eine zuvor unbekannte Anzahl an Störungen in der lakustrinen Verfüllung des Nam Co und dokumentieren zum ersten Mal die tektonische Dehnung des südlichen Tibets seit dem Mittelpleistozän. Die Untersuchung der Störungsstrukturen ergab 1) primäre Verschiebungsstörungen entlang einer NW-SO ausgerichteten Verwerfungszone, parallel zur dextralen Beng Co-Störung nordöstlich von Nam Co und 2) sekundäre Störungen mit Ab- oder Verschiebungs-Charakteristika. Für das gesamte tektonische System des Nam Co wird ein transtensionales Regime mit vorherrschender W-O-Ausdehnung vorgeschlagen. Die berechneten kumulativen Versatzraten bewegen sich im Rahmen von 0,3 mm/yr in WSW-ONO-Richtung bis

zu 0,9 mm/yr in WNO-OSO-Richtung und sind dokumentierten Raten aus dem südlichen Yadong-Gulu Rift ähnlich. Der gesamte vertikale Versatz entlang der WNW OSO Richtung beläuft sich auf 315 m. Laterale Ausdehnungsraten bewegen sich im Rahmen von 0,5 bis 0,7 mm/yr und umfassen somit im Vergleich zum Yadong-Gulu Rift ca. die Hälfte oder im Vergleich zum gesamten südlichen Tibet ca. 7% der gesamten Ausdehnung. Die Störungen wurden um 350 ka ausgelöst. Dieses Ergebnis stellt eine neuartige Auffassung der tektonischen Ausdehnung im südlichen Tibet dar. Die Störungen sind, bis auf kurze Ausnahmen, während sehr hoher Seespiegelstände und feuchten, interglazialen Bedingungen in Sauerstoff-Isotopen-Stufe 5e und des Holozänes kontinuierlich aktiv.

Diese Arbeit liefert neue, aufschlussreiche Erkenntnisse in Bezug auf den seismo-stratigraphischen Rahmen, die niederschlagsgesteuerten Seespiegelstände und die Ausdehnungstektonik des Nam Co und bildet eine wesentliche Grundlage für die Auswahl geeigneter Bohrstandort für das ICDP Bohrprojekt ‚NamCore‘.

Thesis outline and declaration of co-author contributions

This thesis is written in the cumulative format. It comprises an introductory chapter (Chapter 1), which highlights the general scientific context, the objectives and aims of this thesis, as well as the geological background of the working area. Chapter 2 describes the utilized datasets, their acquisition, the processing of multichannel seismic data, and the data integration in detail. Chapters 3 to 5 represent the body of the thesis in the form of three joint-authorship manuscripts. The three stand-alone research manuscripts will additionally be submitted as joint-author articles to international peer-reviewed journals. The last chapter of this thesis (Chapter 6) summarizes the main conclusions, points out future research opportunities, and provides an outlook on the ICDP drilling Project 'NamCore'. An additional joint-authorship manuscript comprising the scientific opportunities and logistical framework of an ICDP drilling (Haberzettl et al., 2019) is provided in the Appendix.

The following section provides information on the individual contributions of each co-author to the individual manuscripts and the current manuscript status:

Chapter 3: Sediment distribution processes and lake-level variations since the LLGM in the Tibetan lake Nam Co - reconstructed from high-resolution hydro-acoustic data

Authors: Nora Schulze, Thomas Kasper, Gerhard Daut, Volkhard Spieß, Junbo Wang, and Liping Zhu

Status: to be submitted to *The Journal of Quaternary Science*

This chapter focuses on the modern sediment distribution and deposition processes in Nam Co and complies with reconstructing the lake level back to the last local glacial maximum.

The utilized hydro-acoustic sediment echosounder data (SES) originate from several research cruises. In 2005 and 2006, the SES data were acquired by the Friedrich-Schiller University of Jena in cooperation with the Institute of Tibetan Plateau Research of the Chinese Academy of Sciences (ITP-CAS). Gerhard Daut provided the dataset. In 2016, SES data were recorded in a joint expedition by the Universities of Jena and Bremen and the ITP-CAS. All authors except for Thomas Kasper and Liping Zhu participated in the 2016 cruise. Junbo Wang and Liping Zhu were leading and coordinating the fieldwork. Gerhard Daut was responsible for the SES acquisition.

I confirm that I processed the SES data from 2016, interpreted the entire dataset, developed the scientific concept, created all figures/tables, and wrote all sections of the manuscript. The overall idea development was a flowing process, which benefited from discussions with the co-authors.

Furthermore, Volkhard Spieß, Thomas Kasper, and Gerhard Daut made significant intellectual contributions and reviewed the manuscript. (Personal contribution: 90%).

Chapter 4: Climate-induced lake level variations of the Tibetan lake Nam Co since the Middle Pleistocene - inferred from seismic stratigraphic analysis

Authors: Nora Schulze, Volkhard Spiess, Gerhard Daut, Junbo Wang, and Liping Zhu

Status: to be submitted to *Geochemistry, Geophysics, Geosystems*

This chapter discusses the seismic stratigraphy of multichannel seismic data and the cyclic lake-level changes in Nam Co compared to global and supra-regional climatic indicators and atmospheric circulation.

The utilized multichannel seismic data (GeoB14 & GeoB16) were acquired during pre-site surveys on Nam Co in 2014 and 2016. The research cruises were a joint effort of the Universities of Jena and Bremen and the ITP-CAS. Junbo Wang and Liping Zhu were leading and coordinating the fieldwork. In 2014, Fabian Meisenbacher (formerly known as Fabian Gernhardt), Volkhard Spieß, and Stefan Wenau were responsible for the multichannel seismic data acquisition. Fabian Meisenbacher conducted the processing of the data set in the scope of his master thesis. In 2016, Fenna Bergmann, Fabian Meisenbacher, Julia Haberkern, Volkhard Spieß, and I were responsible for the multichannel seismic data acquisition.

I confirm that I processed and interpreted all multichannel seismic data from 2016, developed the scientific concept, created all figures/tables, and wrote all sections of the manuscript. Bor Gonzalez Usach provided a python script to facilitate the age interpolation for the correlation steps. The development of the overall idea was a flowing process, which greatly benefited from practical advice and discussions with the co-authors. Furthermore, they made significant intellectual contributions and reviewed the manuscript. (Personal contribution: 90%)

Chapter 5: The transtensional tectonic system at Nam Co, SE Tibet - Results from high-resolution 2D seismic data

Authors: Nora Schulze, Jérôme van der Woerd, Volkhard Spieß, Junbo Wang, and Liping Zhu

Status: to be submitted to *Journal of Geophysical Research: Solid Earth*

This chapter discusses the activity and regime of the local tectonic system in Nam Co as well as its setting in the regional context.

The seismic datasets (GeoB14 & GeoB16) utilized in this study originate from two research cruises. The research cruises were a joint effort of the Universities of Jena and Bremen and the ITP-CAS. Junbo Wang and Liping Zhu were leading and coordinating the fieldwork. The GeoB14 dataset was acquired in 2014, during which Fabian Meisenbacher (formerly known as Fabian

Gernhardt), Volkhard Spieß, and Stefan Wenau were responsible for the acoustic data acquisition. Fabian Meisenbacher processed the 2014 MCS profiles in the scope of his master thesis.

The GeoB16 data are from the pre-site survey on Nam Co in 2016. Fenna Bergmann, Julia Haberkern, Fabian Meisenbacher, Volkhard Spieß, and I were responsible for the multichannel seismic data acquisition.

I confirm that I processed the GeoB16 seismic data, carried out the interpretation of all utilized data, developed the scientific concept in close communication with my co-authors, created all figures/tables, and wrote all sections of the manuscript. In cooperation with Carlos Ramos Cordova, a Python script was written to extract fault properties from the interpreted seismic data.

The overall scientific concept benefitted greatly from regular discussions with Volkhard Spieß and Jerome von der Woerd, who also made significant intellectual contributions and reviewed the manuscript. (Personal contribution: 85%)

Chapter 1: Introduction

1.1 Motivation and Objectives

1.1.1 Climate change threatens vital resources

One of the most pressing concerns of our future will be the demand for water. Water is an essential element for the daily life of every human, animal, and plant and, at the same time, an equally important material for the industry. However, the rapid increase in population on earth, industrialization, and climate change threaten water security (Rodda, 2007).

The Tibetan Plateau (TP), for example, provides freshwater from the so-called 'Water Tower of Asia' to more than one-fifth of the world's population (Cuo & Zhang, 2017; Immerzeel et al., 2010, 2020). The largest rivers of Asia (Yangtze, Huang He /Yellow River, Mekong, Salween, Irrawaddy, Brahmaputra, Ganges, and Indus) have their headwaters in Tibet (Figure 1.1). Each river transports several thousand cubic meters of freshwater per second (Gupta, 2008) into China, India, Nepal, Bhutan, Bangladesh, Pakistan, Vietnam, Myanmar/Burma, Cambodia, Laos, and Thailand. Besides water, the rivers also transport sediments to the associated mega deltas covering areas of more than 10,000 km² (Cruz et al. 2007). These mega deltas accommodate megacities like Tianjin, Shanghai or Dhaka, and are home to millions of people (Figure 1.1).



Figure 1.1: Geographical location of the Tibetan Plateau. The eight largest rivers originate in Tibet and distribute freshwater and sediment toward their deltas (highlighted by red triangles). The prevailing atmospheric circulations are indicated with orange arrows (AWM= Asian Winter monsoon; IOSM= Indian Ocean Summer Monsoon; EASM = East Asian Summer Monsoon). Geographical extent of the TP (Zhang et al., 2002), glacier extent (ice-blue, GLIMS & NSIDC (2005), updated 2020); GEBCO topography (GEBCO-Compilation-Group, 2020), Projection in WGS84.

The 5th assessment report of 2014 and the special report on 'The Ocean and Cryosphere in a Changing Climate' of 2019 by the International Panel of Climate Change (IPCC) highlighted how prone the hydrological cycle on the TP is to future climate change (Hijioka et al., 2014; Hock et al., 2019). Presently, the TP contains the world's third-largest amount of ice (Qiu, 2008) with about 54,429 glaciers and a total ice volume of $3,270 \pm 850 \text{ km}^3$ (in 2017; Farinotti et al. (2019)). Even though glacial melt varies significantly on the TP (e.g., Sun et al. (2018)), the observed retreat could result in the loss of two-thirds of the glaciers by 2050 (Qiu, 2008). Subsequently, rivers like the Ganges, Brahmaputra, and Indus might become seasonal (Cruz et al., 2007).

So far, no confident projections on how climate change will impact, e.g., future precipitation on a sub-regional scale or the availability of water and sediment resources have been established (Hijioka et al., 2014).

However, the vulnerability assessment of the 'Water Tower of Asia' (Immerzeel et al., 2020) showed that rapid melting of glaciers and enhanced climate variability threatens water and home security for millions of people in many Asian regions (Hijioka et al., 2014) and will, therefore, have a significant societal, ecological, and economic impact.

1.1.2 Research effort on past climate change

Major questions on the system's responses to climate change arise, regarding the glacier melting, river discharge, the sediment transport downstream as well as the effect on the monsoon system and changing precipitation patterns. This lack of knowledge highlights the need for detailed investigations of the climate evolution on the TP. Based on our understanding of the past, it will then be possible to assess the extent of climate pattern dynamics and their impact in the future (Hou et al., 2017; Sun et al., 2015).

One crucial puzzle piece in this system is studying the Tibetan Plateau's reaction to climate changes in the past and the former influence on the hydrologic system. Essential in this effort is our understanding of thresholds, timing, pace, and intensity of past climatic changes (Haberzettl et al., 2019). Initiated by this significant scientific and societal interest, many studies have taken place on the TP in the last decades to understand the recent and the past climate.

Lake sediments have proven to be sensitive archives for studying the effects of climate variability in general as they offer an abundant spectrum of physical, chemical, and biological proxies (e.g., De Batist & Chapron, 2008) that can be used to reconstruct paleoclimate. The sediments of endorheic lake basins on the TP provide valuable insights into past lake levels and hence the interplay of precipitation, evaporation, and glacier melting in the past (Günther et al., 2016). Many short, lacustrine paleoenvironmental records exist on the TP, covering the Holocene to the last glacial period. To date, the longest record spanned 32 cal kyrs BP and was retrieved in Lake Qinghai in NE

Tibet (An et al., 2012; Figure 1.1). Hence, a continuous record covering several glacial-interglacial cycles is still lacking; however, it is highly desired to understand climate variability fully.

1.1.3 ICDP effort

The search for a long and continuous record has brought attention to the third-largest and ~100 m deep lake Nam Co in the center of the Tibetan Plateau (Figure 1.1). Recent research on this lacustrine system (see Chapter 1.2.4) has highlighted the unique potential of its sediments as a high-resolution archive for palaeoclimate, -ecology, and -environment (Haberzettl et al., 2019).

In that context, Nam Co has become a scientific drilling target with multi-purpose requirements, e.g., understanding the Asian monsoon and the biological response of fauna at high altitudes. Joint Sino-German seismic pre-site surveys were carried out in 2014 and 2016 to constrain the sedimentary and tectonic architecture of the lacustrine Nam Co basin. Expeditions and data acquisition were realized and partially funded by the Universities Jena and Bremen and the Institute of Tibetan Plateau Research of the Chinese Academy of Sciences (ITP-CAS), supported by the DFG's ICDP Priority Programme and the Strategic Priority Research Program of the Chinese Academy of Sciences and the Chinese Ministry of Science and Technology.

During the research cruises, high-resolution multichannel reflection seismic profiles were acquired, building the foundation of this thesis. Data processing and interpretation were carried out as part of the DFG project 'Seismic Pre-Site Survey for ICDP Drilling Locations at Lake Nam Co, Tibet' funded within the ICDP Priority Programme.

The conducted work contributed to the ICDP workshop in Beijing in 2018 (see Haberzettl et al., 2019, Appendix) and reinforced the revised full drilling proposal submitted to ICDP by twelve principal investigators from seven different countries under the leadership of T. Haberzettl. The proposal was accepted in 2020. Dependent on appropriate co-funding, drilling is planned to be conducted within the next three years.

Besides the aim of this work to support the ICDP effort with a high-grade processed seismic dataset, several scientific goals were set to enhance the comprehensive understanding of Nam Co's sedimentary and tectonic environment.



Figure 1.2: NamCore Logo of the ICDP Nam Co Drilling Project.

1.1.4 Scientific objectives

The main scientific objectives of this thesis are enumerated in the following:

- (1) Improved comprehension of lacustrine sediment distribution and deposition processes (Chapter 3)

Modern sediment distribution processes and depositional patterns have to be apprehended in the context of contemporary climate. This is an essential prerequisite before performing interpretations for similar climate periods in the past or drawing conclusions about paleoenvironmental and paleoclimatic conditions during cold climate periods.

While most variables (e.g., grain size, n-alkanes, ^{210}Pb and ^{137}Cs activities), analyzed in 67 surface samples throughout the basin (Wang et al., 2015a, 2012) exhibited spatial variability associated with water depth (Wang et al., 2015a), a detailed model on the sediment distribution parameters is lacking.

The analysis of high-resolution sediment echo sounder (SES) data enables a detailed spatial study of the recent deposits. Combined with the lithological and chrono-stratigraphic information from the 10.4 m long sediment core NC08/01, the dataset permits an acoustic facies and stratigraphic analysis reaching from the recent sediments back to the last local glacial maximum (LLGM). Hence, we can test the application of the modern sediment distribution and deposition processes back to the LLGM.

- (2) Development of a seismo-stratigraphic concept of the lacustrine sediments (Chapter 4)

The stratigraphy of the lacustrine sediment in Nam Co is uncertain except for the coring depth of ~10.4 meters (NC08/01). However, low-reflectivity seismic units similar to the Holocene are reoccurring at depth in the acquired multichannel datasets. As derived from SES, multichannel seismic of 2014, and core data, the low-reflectivity units represent low energy depositional environments and distant shorelines during high lake levels (=interglacial climate conditions), e.g., during the entire Holocene. In contrast, low lake levels resulted in shortened transport paths and the deposition of coarser grain sizes in the center of the basin during dry glacial climate conditions.

The deep penetrating MCS dataset indicates an extensive sediment infill, potentially spanning several glacial-interglacial cycles. Seismic facies analysis and thickness maps reveal how the modern interglacial and glacial patterns repeat in the past. Thus, the conduction of seismic stratigraphy of higher and lower lake levels allow for a novel estimate of the evolution history in Nam Co.

(3) Understanding the variability of lake level on long time scales and its climatic control (Chapter 4)

Reconstructions of paleo-lake-levels were conducted for many lakes on the TP on deglacial to Holocene timescales. However, the conclusions on paleoclimatic conditions drawn from these studies vary significantly (e.g., Alivernini et al., 2018; Fan et al., 2012; Wang et al., 2016; Yu et al., 2019). It remains debated whether precipitation, temperature changes, the extent of monsoonal influence, or glacier melting have been dominant features of the observed environmental changes (Saini et al., 2017; Jia et al., 2001).

Sediment core analyses from the 10.4 m long record NC08/01 revealed that the availability of fine-grained material is controlled by higher precipitation during associated interglacial conditions (Doberschütz et al. 2014; Kasper et al., 2015). Also, the sediment accumulation rate during interglacial conditions is lower than during glacial conditions (Kasper et al., 2015).

A detailed seismic facies analysis of the MCS data provides insights on the sediments deposited during high or low lake-level stands and allows for a relative lake-level reconstruction, covering several interglacial-glacial cycles. By comparing the lake-level reconstruction to other paleoclimate-proxy records, we disentangle local and supra-regional effects of the paleoclimate on the lake level of Nam Co in the southern Tibetan Plateau.

(4) Providing insights on the link between regional and supra-regional tectonics (Chapter 5)

Nam Co is located north and west of the extensional Yadong-Gulu rift system and south-west of the dextral strike-slip Beng Co fault. The fault system is exemplary for the southern Tibetan Plateau between the suture zones of Bangong-Nujiang in the North and the Indus Tsangpo in the South. Yet, the interaction of the Nam Co basin, the Nyainqêntanglha Mountain Range, and the graben structures of the Yadong-Gulu rift has not been appraised in much detail. However, a comprehensive understanding of the fault system is essential for evaluating the induced accommodation space and the assessment of modern seismicity. Faults in the vicinity or through Nam Co are tenuous or even contradictory in the literature (e.g., Tapponier & Molnar, 1977; Armijo et al., 1986; Schneider et al., 2003) and mostly inferred from satellite images as fieldwork is challenging in this remote area. The superior quality of lake seismic data elucidate details of the tectonic setting, the Nam Co basin development, and an estimate of tectonic movement rates, which cannot be determined from land-based investigations.

1.2 Tectonic, climate, and regional setting

Nam Co (30° 30' –30° 35'N, 90°16' –91° 05'E) is an endorheic basin situated on the central TP north of the Nyainqentanglha Mountain Range at an altitude of 4724.5 masl (meters above sea level; in 2016 (Hydroweb, n.d.) (Figure 1.1).

The development of the Tibetan Plateau, the location of the Nam Co basin as well as the climatic circulation with a focus on the influence of the monsoon are briefly introduced in this chapter. Finally, the recent studies at and on Nam Co are summarized.

1.2.1 Tectonic evolution of the Tibetan Plateau

The Tibetan Plateau (TP) is the largest (2.5 million km²) and highest (average ~4500 masl) plateau on earth. The geological history of the TP is closely related to that of the Himalayas. Both formed due to the collision of the Indian and the Eurasian continental plates in the Cenozoic (Figure 1.3). Current age estimates of the collision are based on stratigraphic, sedimentological, paleomagnetic, or U/Pb zircon dating analysis and range between 50 and 60 Ma, as summarized by van Hinsbergen et al. (2019). After the plate collision, India continued its movement further north into Asia, causing forceful folding, thrusting, and crustal thickening along the Indian continental margin leading to the elevation of the Himalayas. According to recent GPS measurements, the continental collision still accounts for about 36-40 mm/yr of north-south convergence (Zhang et al., 2004). The Indian crust has been traced up to 31°N beneath central Tibet (Nábelek et al., 2009), resulting in a current crust thickness of 75 to 80 km under central Tibet (Searle, 2020), twice as thick as regular continental crust.

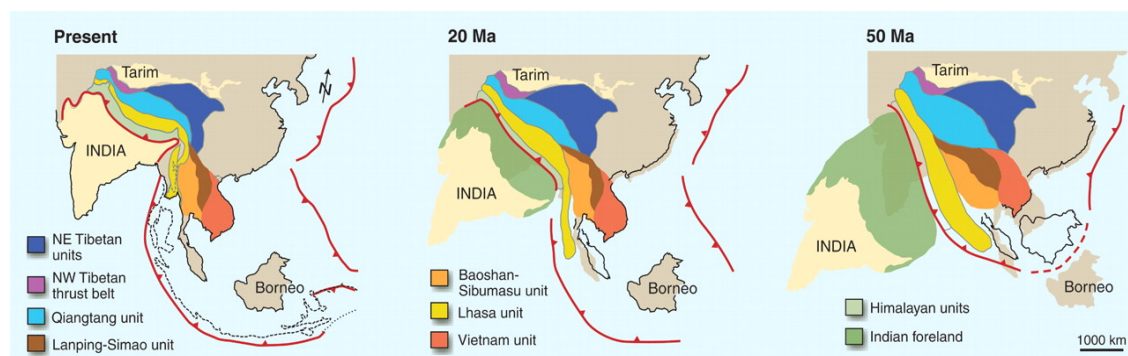


Figure 1.3: Tectonic reconstructions of the India-Eurasia-Collision at 50 Ma, 20 Ma, and today, major tectonic units are generalized by color, taken from Royden et al. (2008).

Like the collision itself, the exact timing and pace of the uplift of the TP are still debated (Guillot & Replumaz, 2013). Topics of discussion include, e.g., the stability, thickness, temperature of the lithospheric mantle beneath Tibet, and the mechanical coupling of the upper and lower crust and the mantle. Hence, different models on the subduction dynamic of the lithosphere exist.

The first and still widely accepted perspective is the model of underthrusting of Eurasia by India (Argand (1924) as cited in Webb et al., 2017; DeCelles et al., 2002)(Figure 1.4A). More recent studies derived tectonic models of lower crustal flow (e.g., Copley & McKenzie, 2007; Royden et al., 2008; Ryder et al., 2014)(Figure 1.4B), distributed shortening (e.g., England & McKenzie, 1982)(Figure 1.4C), extrusion (e.g., Molnar & Tapponnier, 1975) (Figure 1.4D), or intracontinental subduction (e.g., Guillot & Replumaz, 2013; Tapponnier et al., 2001) (Figure 1.4E).

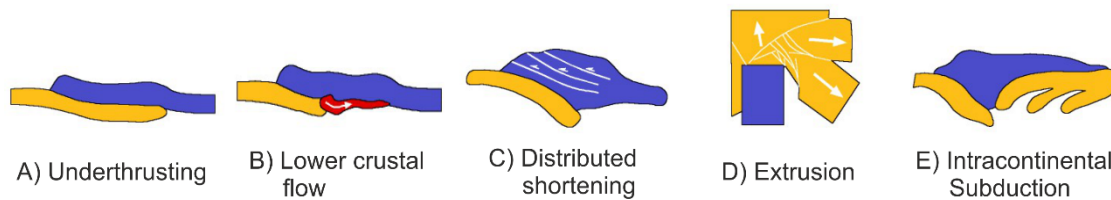


Figure 1.4: Sketches of proposed tectonic models, explaining uplift and thickening of the continental crust (modified after Özacar (n.d.)).

The advancing continental collision built the TP and the Himalayas from four tectonic zones, which extend over the length of the Himalaya and comprise from north to South: The Himalayan units, the Lhasa unit, the Qiangtang unit, and the NE Tibetan units (Royden et al., 2008)(Figure 1.3).

The Nam Co basin is located within the Lhasa Block (Lhasa unit in Figure 1.3, Figure 1.5), representing the Cretaceous Eurasian continental margin and hence an early, relatively stable and less deformed collisional unit (Kapp et al., 2007). The Lhasa Block is framed by the significant Indus-Tsangpo (ITS, Figure 1.5) and Bangong-Nuijiang Sutures (BNS) to the S and N, respectively (e.g., Pullen et al., 2008) (Figure 1.5), which were responsible for most of the shortening since the collision (e.g., Taylor et al., 2003). In the South of the Lhasa Block, the Gangdese batholiths belt intruded the folded marine sediments of early Mesozoic origin (Guillot & Replumaz, 2013). These Gangdese batholiths were formed during the Cretaceous to early Tertiary in an Andean-type subduction of the Tethys Ocean (e.g., Ding et al., 2014). The continental collision unearthed the Gangdese batholiths, which now form the Nyainqêntanglha Mountain Range (NQTL) to the South of Nam Co (Kapp et al., 2005)(Figure 1.7).

So far, no research has been done on how and when the Nam Co Basin was established. Nam Co has likely reached its present altitude in the upper Miocene (12-0 Ma) (Kapp et al., 2005a). Theories exist that the Nam Co basin evolved as an extensional or a pull-apart basin. This indicates a relatively recent development starting in the Upper Miocene or Pliocene. Also, the evolution as a foreland basin of the NQTL is possible as hinted at by Pullen et al. (2008) as the NQTL is interpreted as a part of a dextral restraining bend along NW thrusting fault zone during the Oligocene to Lower Miocene (Armijo et al., 1989; Tapponnier et al., 1986; Wu et al., 2007).

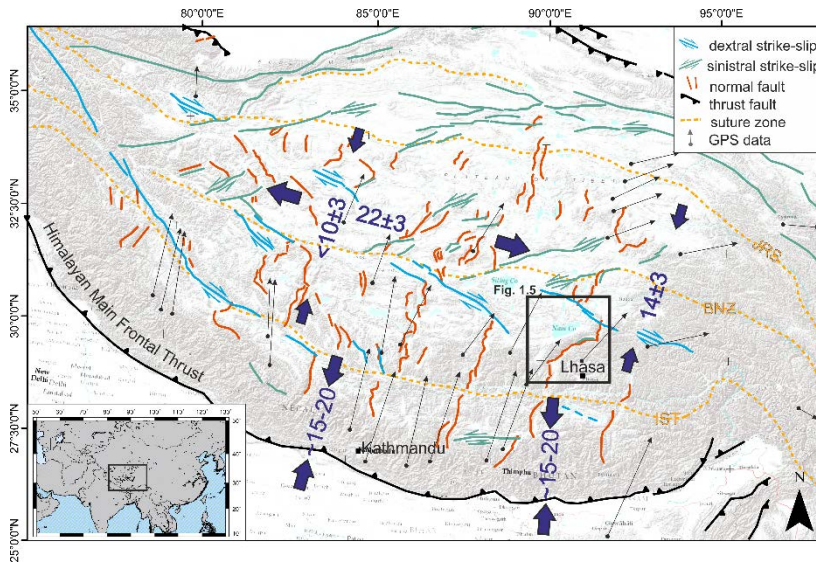


Figure 1.5: Tectonic map of the Tibetan Plateau, showing suture zones, GPS movements and rates (from (Zhang et al., 2004)), late Cenozoic faults. ITS = Indus Tsangpo Suture zone, BNS = Bangong- Nuijiang Suture, JRS = Jinsha River Suture. Compilation from Blisniuk et al. (2001), Taylor & Yin (2009), Langille et al. (2014) and Zhang et al. (2004) on a World Terrain Map from Esri, USGS, NOAA.

The TP's recent tectonic activity is characterized by normal and strike-slip faulting (Elliott et al., 2010) (Figure 1.6). These dominant E-W directed movements indicate extension and, hence, thinning of the upper crust. Related to the ongoing discussions on the uplift of the TP, the beginning of the E-W extension is not unambiguously resolved. In southern Tibet, onset times of middle to late Miocene ages are documented (e.g., Blisniuk et al., 2001; Kali et al., 2010; Leloup et al., 2010; Mahéo et al., 2007). The total ESE-WNW extension of 22 mm/yr in the TP is compensated by dextral and sinistral strike-slip faults and 15 to 20% by normal faults (Elliott et al., 2010) (Figure 1.5). Large N-S trending grabens south and numerous small graben structures north of the Bangong Suture characterize the modern appearance of the TP (Figure 1.5) (Armijo et al., 1986). Active tectonics of the Nam Co area are characterized by E-W extension with N-S directed faults in the Yadong-Gulu rift system and oblique NW-SE dextral faulting (Beng Co fault) in the north and SW-NE sinistral faulting close to Damxung (Figure 1.7) (Armijo et al., 1989).

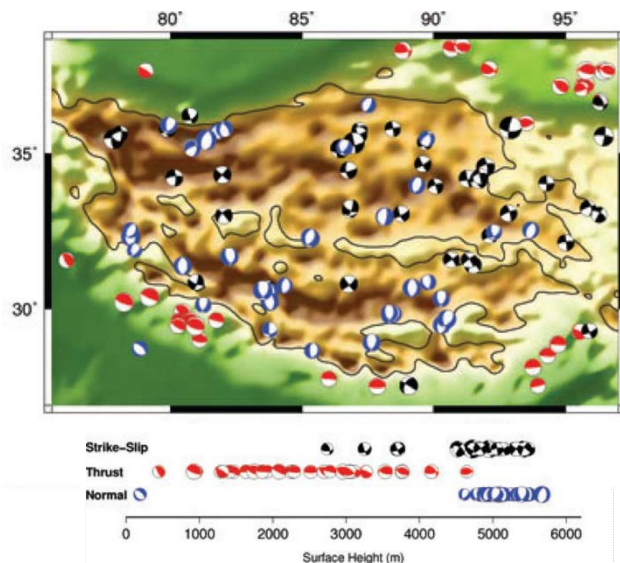


Figure 1.6: Distribution of earthquakes in and around the TP, indicating the correlation of normal and strike-slip fault movement with surface height of the TP (after Elliott et al., 2010).

Present-day tectonics and earthquake data indicate the current strain regime in the vicinity of Nam Co. Large earthquakes with magnitudes $M > 6$ occurred in 1924, 1951, 1952, and 2008 (U.S. Geological Survey, n.d.) (Figure 1.7). Amplified seismicity focused on the area of three meeting strike-slip faults in the East (Figure 1.7) (U.S. Geological Survey, n.d.). In the NW and N of the lake,

shallow, crustal earthquakes (< 15 km focal depths, red dots) occurred. Modern crustal motion measurements based on GPS (Figure 1.5, thin black arrows) further revealed that the movement of the upper crust begins to deflect to the East in the Nam Co region (90°E) (Zhang et al., 2004).

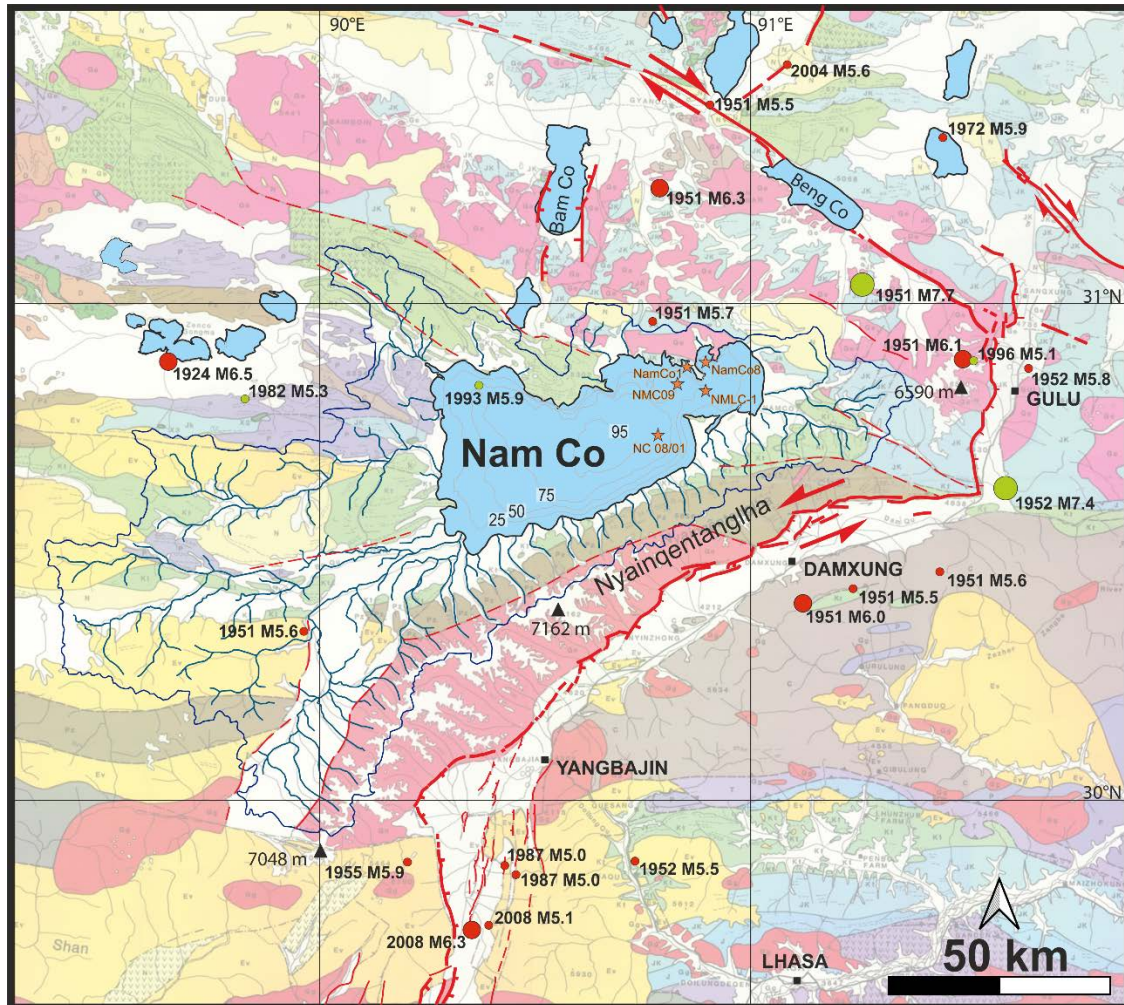


Figure 1.7: Catchment area of Nam Co (modified after Wang et al., 2009b) superimposed on the geologic map of the area (modified after Kidd et al., 1988). Fault compilation by Jerome van der Woerd (modified after Armijo et al., 1989; Kidd & Molnar, 1988). Documented earthquakes of magnitudes >5 are marked with red (focal depth <15 km) and green (focal depth ~ 30 km) circles (retrieved from U.S. Geological Survey, n.d.). Core site locations are marked with orange stars. Map extent as indicated in Figure 1.5.

1.2.2 Atmospheric circulations and climate

A complex interplay of multiple atmospheric circulations influences the climate on the TP and thus, the geographical and seasonal moisture supply and heat advection (An et al., 2001; Yao et al., 2013). These circulations include the Asian Summer Monsoon system (ASM), comprehending the East Asian Summer Monsoon (EASM) and the Indian Summer Monsoon (ISM), the subtropical jet stream (i.e., the Westerlies), as well as polar air masses (i.e., winter monsoon) (An et al., 1991, 2011; Chen et al., 2008; Zhu et al., 2015) (Figure 1.1).

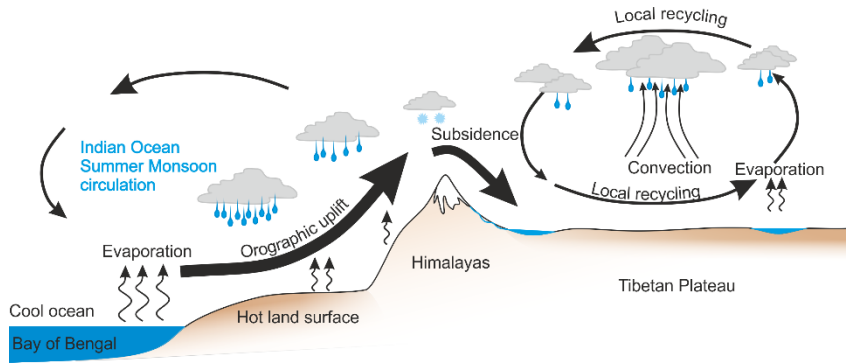


Figure 1.8: Sketch depicting the summer monsoon circulation, the orographic uplift effect due to the Himalayas, and the water cycle on the Tibetan Plateau, modified after Yao et al. (2013).

The monsoon winds are caused by the migration of the sun's zenith between the tropics and the temperature differences between land masses and the ocean. Due to the increased solar radiation in the summer season, the air over large landmasses warms up more than the air over oceans, and humid air masses move from the sea to the land during (e.g., Wang et al., 2017). Additionally, the Coriolis force causes a large wind deflection.

The tectonic uplift of the Tibetan Plateau is thought to have a significant effect on the monsoon system (e.g., An et al., 2001; Chen et al., 2014; Prell & Kutzbach, 1992; Wang et al., 2003). In contrast, Boos & Kuang (2010) propose that not the heating of the plateau but the heating of the Indian subcontinent and the orographic effect of the Himalayas are the critical factors for the formation of the Asian monsoons (Figure 1.8). The monsoon has been variable in the past on long and short time scales, and the underlying mechanisms and their interplay are under ongoing investigation (Wang et al., 2017; Webb et al., 2017). The reconstruction of the monsoonal variability and the extent of the monsoonal influence on the TP in the past are of substantial interest since the ASM precipitation provides the main humidity supply to the TP during the summer months.

Nam Co is located at the current intersection of the Westerlies and the ASM air masses. In the past, the extents of the Westerlies and the ASM shifted over Nam Co (Figure 1.9).

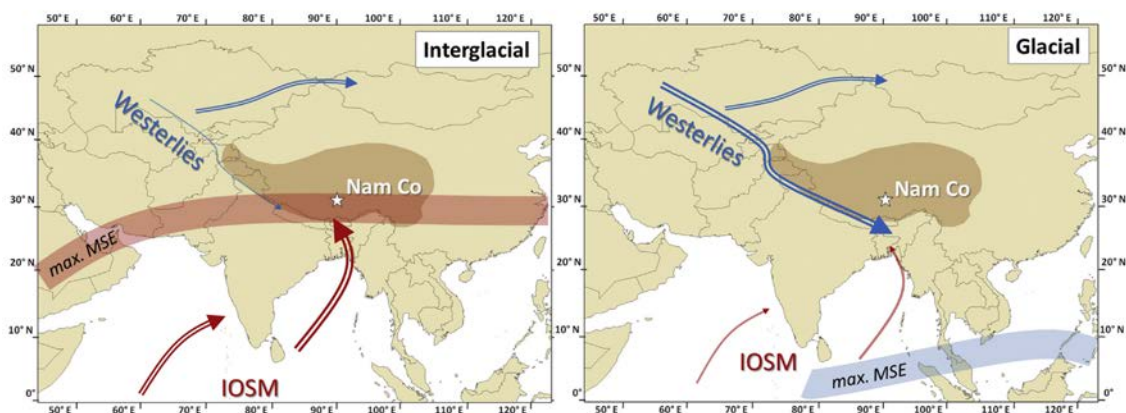


Figure 1.9: Basic pattern of summer circulation during the Last Glacial and the Holocene, displaying the interaction of the Westerlies and the Indian Ocean Summer Monsoon (IOSM). The Tibetan Plateau and the location of Nam Co are highlighted. From Günther et al. (2015).

1.2.3 Modern settings and characteristics of Nam Co

The Nam Co region is subject to arid to semi-arid continental climate (Wang et al., 2019). The mean annual temperature at the Nam Co Research Station is 0°C (min -21.5, max 13.3°C) (Anslan et al., 2020; Wang et al., 2020). The mean annual precipitation between 2006 and 2017 was about 406 mm/yr (291-568 mm/yr) (Anslan et al., 2020), of which >90% falls during the summer monsoon season from May to September (Huang et al., 2017). Nam Co is fed by >60 small streams sourced from the southern and eastern mountain chains. Lake water of Nam Co has a specific conductivity of 1850 $\mu\text{S}/\text{cm}$ and a pH of 9.2 (Wang et al., 2009b). Zhu et al. (2010b) calculated the entire lake volume to include about 86.4 km³ (in 2004). The Nam Co basin is morphologically divided into a western subbasin and an eastern subbasin with maximum water depths of 98 m and 60 m, respectively (Wang et al., 2009b). Since the last decades, the lake level has been rising by 0.3 m/yr on average (Kropáček et al., 2012). This accounts for about a third of the seasonal variability (Hydroweb, n.d.).

Nam Co is defined as a dimictic lake with a stable thermal stratification from June to November (Huang et al., 2017). Lake ice covers its surface for ~90 days during the winter season (Wang et al., 2019).

The modern sedimentation is mainly influenced by allochthonous input. Grain sizes of surface sediments in the shallow lakeshore areas are fine to very coarse, whereas, in the central basin areas, only clay and silt are found (Wang et al., 2015a). Recent autochthonous sedimentation includes carbonate precipitation due to the formation of Monohydrocalcite (Li et al., 2008, 2012) and the biological components of diatom and ostracod species (Zhu et al., 2010a).

Bedrock geology was mapped by Kidd et al. (1988) and Wu et al. (2011). According to their work (Figure 1.6, Figure 2.1), Cretaceous carbonates dominate the vicinity of Nam Co. Jurassic sediments occur to the East and Permian and Carboniferous bedrock occur to the South. Volcanic intrusions (granites, phonolites) disrupt these formations, particularly close to the lake's northeastern shore. Metamorphic rocks of the Gangdese batholith belt form the Nyainqêntanglha Mountain Range (NQTL) in the South. Deposits near the lakeshore are composed of unconsolidated Pleistocene to Holocene sediments of glacial, glaciofluvial, and fluvial origin (Schütt et al., 2008).

Glacial remains of valley glaciers were found in the southwestern part of the catchment (Keil et al., 2010; Lehmkuhl et al., 2002; Schütt et al., 2008). However, the corresponding terminal and ground moraines of the last maximum glacier advance are drowned under the current lake level (Schütt et al., 2008). Thus no accurate timing of the glacial advance, but an estimate of MIS 2 or 4 is available (Keil et al., 2010). In the southeast of Nam Co, no indications of valley glaciers reaching

into the present lake area were identified (Lehmkuhl et al., 2002; Schütt et al., 2008). Today, glaciers cover 2 % of the lake's catchment (Adnan et al., 2019; Biskop et al., 2016).

1.2.4 Paleoenvironmental studies at Nam Co

Several studies on the contemporary properties of the Nam Co basin were conducted in the last two decades. These studies range from the recording of current climate data at the Nam Co meteorological station or cataloging and the fauna and flora in and around Nam Co (e.g., Frenzel et al., 2010; Herrmann et al., 2010; Li, 2019; Lu et al., 2010; Yang et al., 2014b) to physicochemical analysis of lake and stream water (Keil et al., 2010; Wang et al., 2019, 2020) and glacial inventory studies (e.g., Bolch et al., 2010; Buckel et al., 2020; Zhou et al., 2010) or water balance modeling (e.g., Biskop et al., 2016; Zhou et al., 2013). These studies also support the comprehensive understanding of the steering mechanisms on proxies, essential for paleoclimate reconstructions (Haberzettl et al., 2019).

Table 1.1: List of sediment cores from Nam Co with conducted multiproxy studies.

Core Name	NC08/01	Nam Co 1	Nam Co 8	NMC09	NMLC-1
Position	30°44'14.70N 90°47'25.20"E	30°53'7.81"N 90°51'34.24"E	30°53'32.89"N 90°54'6.31"E	30°51'0.14"N 90°51'53.58"E	30°50'29.32"N 90°54'10.43"E
Water depth	93 m	26.5 m	31 m		59.5 m
Core length	10.4 m	4.47 m	2.7 m (?)	0.2 m	3.32 m
Coring type/system	gravity corer & uwitec piston corer (90 mm)	uwitec piston corer (63 mm)	uwitec piston corer (63 mm)	gravity coring	
Oldest measured age (method)	23180±330 cal a BP (AMS ¹⁴ C, ²¹⁰ Pb, ¹³⁷ Cs)	8996 ± 51 a BP		1857 AD (²¹⁰ Pb)	8510±40 a BP (AMS ¹⁴ C)
Publications	Doberschütz et al., 2014; Günther et al., 2015, 2016; Kasper et al., 2012, 2013, 2015; Su et al., 2013; Witt et al., 2016; Zhu et al., 2015	Daut et al., 2010	Mügler et al., 2010	Cong et al., 2013; Li et al., 2017	Li et al., 2008, 2011; Lin et al., 2008; Zhu et al., 2008, 2010a

In the last two decades, five sediment cores were collected in Nam Co, which allow insights into the climatic past of Nam Co via a broad range of paleoenvironmental proxies. Four short cores were retrieved from the eastern subbasin and one long core from the center of the western subbasin (Table 1.1). Multiproxy studies were conducted on the cores, NMLC-1, Nam Co 8, Nam Co 1, and NC08/01, as has been summarized by Haberzettl et al. (2019). These include research on inorganic geochemistry, sedimentology, and mineralogy (Doberschütz et al., 2014; Kasper et al., 2015; Li et

al., 2008, 2012; Mügler et al., 2010; Zhu et al., 2008), organic geochemistry and *n*-alkanes (Günther et al., 2015, 2016; Witt et al., 2016), paleomagnetic and environmental magnetic examinations (Haberzettl et al., 2015; Kasper et al., 2012; Su et al., 2013), and modern and fossil pollen composite (Zhu et al., 2015). Micropaleontological analyses were also conducted on additional short cores in the eastern subbasin (Frenzel et al., 2010; Wrozyńska et al., 2012; Yang et al., 2014b). The studies on ostracod and diatom ecology comprise ostracod-based transfer functions, stable isotopes, and trace elements from shells (Frenzel et al., 2010; Zhu et al., 2010a).

As the cores from the eastern subbasin are not exceeding core lengths of 4.5 m, the long core NC08/01 was used as a reference core in this thesis (Figure 1.10). Sediments retrieved with NC 08/01 are dark to light grey and consist mostly of silt and clay with single thin intercalated sandy layers and some dropstones (e.g., Kasper et al., 2015). The chronologic frame of NC 08/01 was established on radiometric dating (^{210}Pb , ^{137}Cs) and 24 reservoir-corrected radiocarbon ages (Kasper et al., 2015). Reservoir effects are known to complicate the development of trustworthy dating lakes on the TP (Wang et al., 2015b). However, for NC08/01, the reservoir corrected radiocarbon ages were verified by magnetostratigraphic studies (Haberzettl et al., 2015; Kasper et al., 2012) and OSL dating (Long et al., 2013; Haberzettl et al., 2019). Overall, the chronology of NC08/01 indicates a continuous sedimentation throughout the last 24 kyrs.

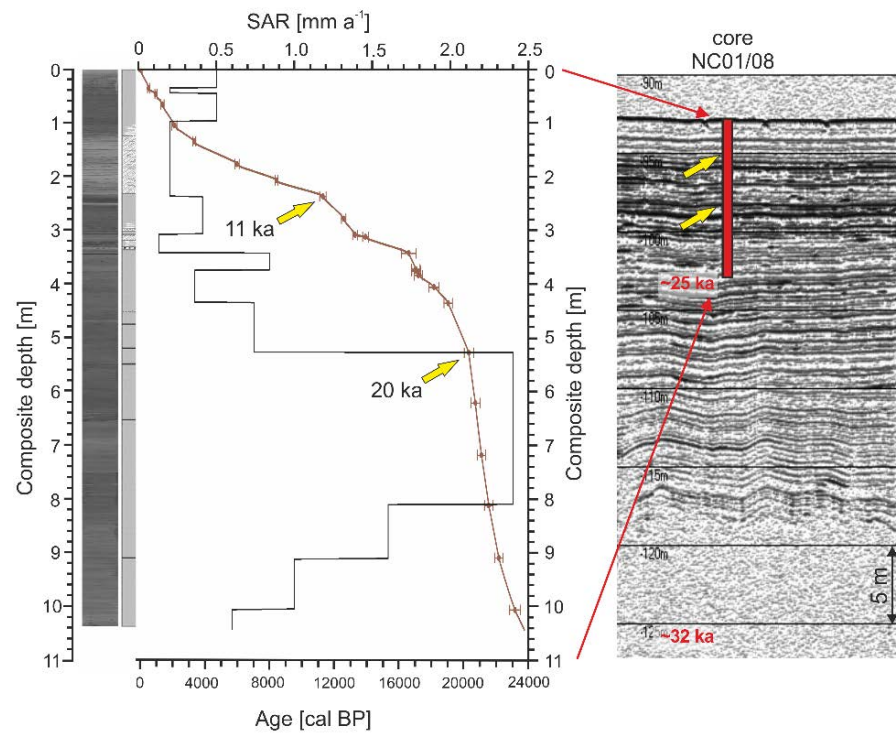


Figure 1.10: Right: Lithology, chronology and sediment accumulation rates (SAR) from NC08/01 modified after T. Haberzettl and Kasper et al. (2015); Left: Section of SES Profile Jena06-13 with the projected core length.

Chapter 2: Data and Methods

The hydro-acoustic datasets utilized in this thesis were acquired during four joint Sino-German research expeditions (Table 2.1).

Table 2.1: Overview of all hydro-acoustic surveys, their sources, and configurations, interpreted in this thesis. SES: sediment echo sounder, MCS= Multichannel Seismic.

Year	Acquisition method	Device	Source frequency range (main frequency)	Recording channels (channel spacing)	Max. vertical resolution	Horizontal resolution / bin size	No. of profiles / length
2005 2006	SES	Innomar SES-96 & SES-2000 light	4-12 kHz	1	Setting dependent (12.1 - 73 cm)	~7% of water depth	~530 km
2014	MCS	GI-airgun (2x0.1L)	50-500 Hz (250 Hz)	32 channels (2 m)	~1.6 m	3-5 m	13 profiles ~110 km
		Falmouth Bubble Pulser	10-1700 Hz (320 Hz)		~1.3	1 m	
2016	SES	Innomar SES-2000 light	Mainly 10 kHz	1	~ 7.3 cm	~7% of water depth	91 profiles ~860 km
	MCS	GI-airgun (2x0.1L)	50-500 Hz (250 Hz)	32 channels (2 m)	~1.6 m	1 m	

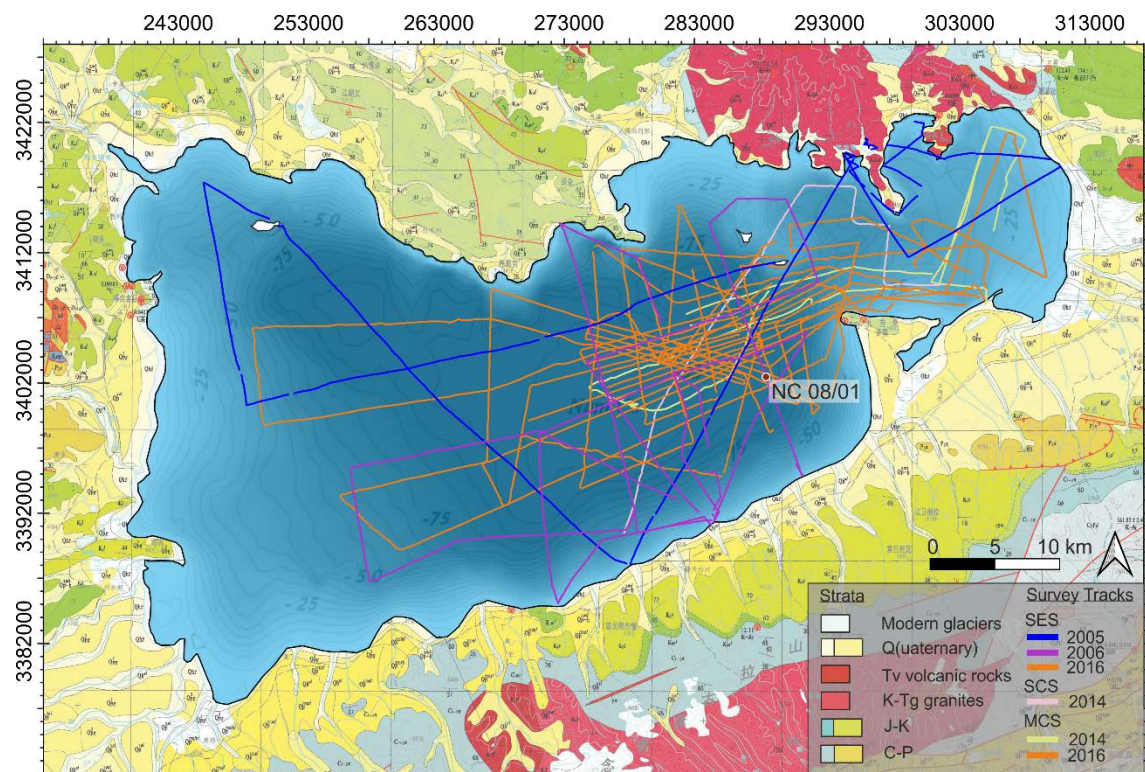


Figure 2.1: Survey tracks of Sino-German research cruises from 2005 to 2016, embedded on the geological map of the Nam Co area (Wu et al., 2011, modified); Location of Core NC08/01 is marked with a dot. Bathymetric isolines taken from (Wang et al., 2009), respective color scale is extending from 0 to -98 m water depth; Map-projection in UTM 46N.

In September 2005 & 2006, two expeditions using a parametric sub-bottom profiler were conducted by the University of Jena, Germany, and the Institute of Tibetan Plateau Research of the Chinese Academy of Sciences (ITP-CAS). The seismic profiles surveyed in the years 2005 and 2006 sum up to a total length of approx. 530 km (blue & purple profiles, Figure 2.1).

In June/July 2014, the Universities of Jena and Bremen and the ITP-CAS conducted a multichannel seismic pre-site survey expedition under funding support of the DFG priority program TiP coordination. 13 multichannel (MCS) and eight single-channel seismic (SCS) profiles of approx. 160 km length were recorded (pink & yellow profiles, Figure 2.1).

In June /July 2016, a comprehensive survey was jointly carried out by the same cooperation partners as part of a DFG funding proposal to support the ICDP initiative 'NamCore'. During the expedition, MCS and parametric sub-bottom profiler data were acquired simultaneously onboard a small vessel. More than 860 km of profiles were recorded (orange profiles, Figure 2.1).

2.1 Parametric sub-bottom profiler

The parametric (non-linear) Innomar SES-96 light and SES-2000 light (Innomar Technologie GmbH, Rostock, Germany) are dual-frequency subbottom-profiler devices. A parametric sediment echosounder (SES) simultaneously transmits two primary signals of slightly different high frequencies (e.g., 100 and 110 kHz). Their interaction generates a secondary low frequency by interference (in this case, 10 kHz). This secondary frequency can be chosen between 4 and 15 kHz.

For the survey in 2005 and 2006, the SES-transducer was mounted on a rubber boat. In 2016, the SES-Transducer was mouthed port side of the small vessel and recorded simultaneously to the MSC acquisition. The recording parameters were adjusted during the surveys. A sample rate of 50 kHz (10 μ s) and varying gain (around 50 dB) were applied during recording. In 2005 and 2006, the mid-frequencies vary between 4-12 kHz, and the recorded pulse length between 2 and 5. The vertical resolution of the SES depends on the sound velocity in water and the effective pulse duration. The sound velocity in lake water was calculated, according to Sheriff (1991), for different depths, temperatures, and salinities (Mügler et al., 2008), resulting in an average velocity of 1460 m/s. Hence, the vertical resolution depends on the specific setting but may vary between 12.1 cm and 73 cm for the 2005/2006 survey. The 2016 data were commonly recorded with a secondary frequency of 10 kHz and one pulse, ensuing in a vertical resolution of 7.3 cm. The horizontal resolution of the SES depends on the driving speed and is approx. 7% of the water depth (Innomar, n.d.). The acquired data were stored in the .ses format and handled with the Innomar ISE Post-Processing Software and later converted into standard SEG-Y format. The 2016 SES data were stored in the RAW data format and converted to SEG-Y. The 2016 data were filtered, and the envelope was calculated within the Kingdom Software by IHS. No motion sensor correction was

applied to the datasets. The SES datasets were integrated into the Kingdom Software (see Chapter 2.4).

2.2 Multichannel Seismic

For the multichannel surveys, equipment of the working group MTU (Marine Technology/Environmental Research, Bremen University) was used. As seismic source, a Soderberg generator/injector (GI) airgun was utilized. The GI-gun chambers were operated with a chamber volume of 0.1 L each, resulting in an emitted frequency range of 50-500 Hz (main frequency 250 Hz). Pressurized air was provided by two diving compressors (Bauer Mariner 320) combined with an air buffer bottle to ensure a constant air pressure of ~100 bar. However, the low atmospheric pressure at an altitude of 4725 masl led to compressor failures/inefficiencies, resulting in irregular drops in gun air pressure down to 50 bar. Thus, the shot rate was adjusted depending on the available air pressure and the vessel's speed.

A conventional analog streamer (Teledyne Marine) with a total length of 64 m, comprising 32 channels at 2 m spacing, was towed for signal recording. Onboard, data were recorded with the custom-designed Marine Multi-Channel Seismic Acquisition System (MaMuCS; Dr. Hanno Keil, MTU, University of Bremen). The sample rate in 2016 was set to 125 μ s and the recording length to 2000 ms. The raw data were stored in the standard seismic format SEG-Y.

Navigation data were acquired with a portable GPS onboard the vessel and were processed and corrected for GPS data scatter and outliers.

In 2014, MCS profiles were recorded in parallel with two seismic sources. Besides the GI-air gun, a Bubble Pulser (Falmouth) of the University Jena with an emitted frequency range of 10-1700 Hz (main frequency ~300 Hz) was operated. Additional 50 km of single-channel recordings of a low signal-to-noise ratio were acquired in 2014, which are not incorporated in this thesis. The MCS dataset recorded in 2014 was processed by Fabian Gernhardt (now Meisenbacher) in the progress of his master thesis. The MCS dataset recorded in 2016 was processed in the course of this thesis. For a detailed description of data processing, see Chapter 2.3.

2.3 Multichannel seismic data processing

Multichannel seismic data processing aims to improve the seismic image quality and the reliable interpretation of the geological subsurface. These goals are achieved by enhancing the signal to noise (S/N) ratio and migrating seismic events to their correct subsurface position.

The advantage of MCS compared to single channel seismic (SCS) is given by recording reflected seismic waves with several receivers (channels) and the consequent manifold coverage of the subsurface. By using the technique of common midpoint (CMP) binning and stacking, all signals

with the common reflection point on the subsurface are gathered and stacked. In this process, incoherent noise is significantly reduced, and hence the S/N ratio is enhanced (Yilmaz, 2001).

The sequence of all processing steps applied to the NamCo-GeoB16 dataset is schematically shown in Figure 2.2. Standard processing steps were applied, as documented in Yilmaz (2001). The steps were executed with Schlumberger's VISTA 2014 Desktop Seismic Data Processing Software (Version 2014.002.5433). In general, all profiles of GeoB16 followed the same routine. However, all profiles required individual boundary conditions. These were adjusted according to the acquisition parameters during variable weather conditions, air pressures, or shot-rates of the GI gun.

2.3.1 Pre-Processing

The location of each source and receiver pair and their midpoint on the subsurface were calculated for each shot using the custom-made program WinGeoapp (© Hanno Keil, Marine Technology – Environmental Research, Department of Geosciences

at the University of Bremen). WinGeoapp calculates these geographic coordinates by combining GPS navigation data, shot times, and relative distance between GPS and source/receiver.

Midpoints were then grouped along the profile track in defined 2D area patches (bin) on the subsurface to create common midpoint (CMP) gathers. All traces assigned to a CMP gather are assumed to image the same point on the subsurface and will be summed-up during CMP-stacking to enhance the S/N ratio. The CMP bin size is set based on a compromise between sufficient noise attenuation (larger bins) and the high horizontal resolution (smaller bins) and depends on the channel spacing, the ship's speed, and the GI-gun shot-rate. For this dataset, a bin size of 1 x 5 m in along and across-track direction, respectively, was chosen in the attempt to preserve the highest possible horizontal resolution in the shallower subsurface. This bin size left the possibility to be adjusted during interpretation by creating 'multi-stacks' and stacking a chosen amount of CMP bins (see Chapter 2.3.4 for details).

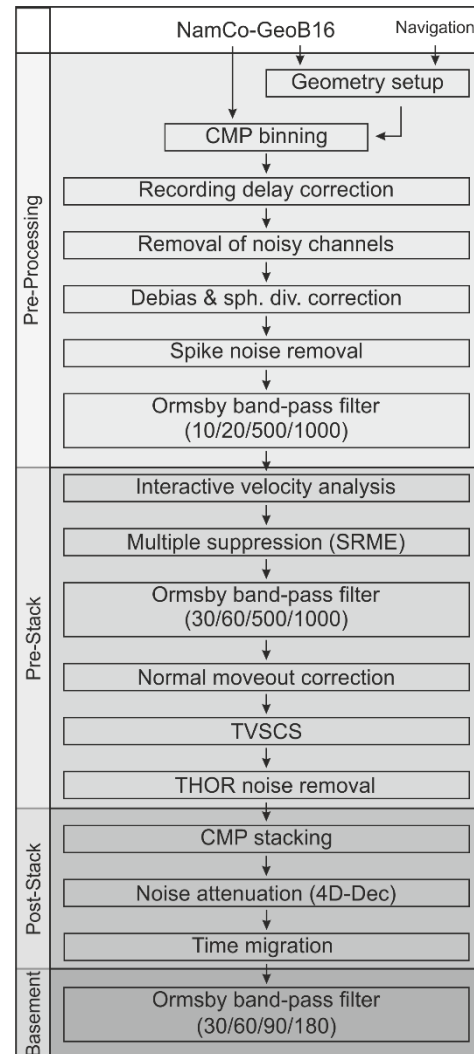


Figure 2.2: Schematic multichannel seismic data processing sequence applied on the NamCo-GeoB16 dataset.

After CMP binning, a 'debias' was applied in order to center the amplitudes of each trace. In the same processing step, noisy channels were deleted, and the recording delay between trigger time and shooting time was corrected. As the channel quality and the gun delay varied during data acquisition, the channel selection and bulk shift correction was adjusted for each profile. With the spherical divergence correction, the loss of energy due to the spherical spreading of the source signal was readjusted using a constant water velocity of 1460 m/s.

In the next step, an Ormsby frequency bandpass filter (filter flanks: 10-20 and 500-1000 Hz) and a '2D-despiking' were applied to suppress coherent noise from ship and wave action and remove random, high amplitude noise bursts, respectively (Figure 2.3A).

2.3.2 Pre-Stack Processing

A realistic subsurface velocity model is needed for seismic processing in order to enhance the multiple suppression, correct the subsequent normal moveout, and conduct a reliable time migration at the end of the processing sequence. Thus, an interactive velocity analysis was performed for all profiles with variable lake floor morphology, visible acoustic basement reflectors, or large fault throws. For profiles with uniform strata, a laterally constant velocity model was created and applied.

Due to the shallow water in the study area (< 100 m) and the partly high reflectivity of the lake floor, the MCS data contain several multiple reflections, which significantly hinder data interpretation. A surface-related multiple elimination (SRME) method was applied to reduce multiple energy. SRME is a 4-step, resource, and time-consuming procedure. It includes the interpolation of the data set to equal offsets, the prediction of a multiple model, and the subtraction of the predicted model from the pre-processed data (Verschuur, 2006). Theoretically, only primaries and interbed-multiples remain after SRME (Verschuur, 2006). SRME application proved to be particularly useful for multiple suppression in the western sub-basin of Nam Co (Figure 2.3B).

A narrow Ormsby bandpass filter (30-60 and 500-1000 Hz) was applied to attenuate low-frequency coherent noise further after multiple-suppression.

In MCS data, the traces assigned to the same CMP gather inhabit travel-time differences due to the individual source-receiver distances of each trace (offset). The normal moveout (NMO) describes the travel-time difference between a seismic event at zero offset and any other offset. In a CMP gather, the NMO eventuates in a hyperbola with increasing offset depending on the seismic velocities and has to be corrected before CMP-stacking.

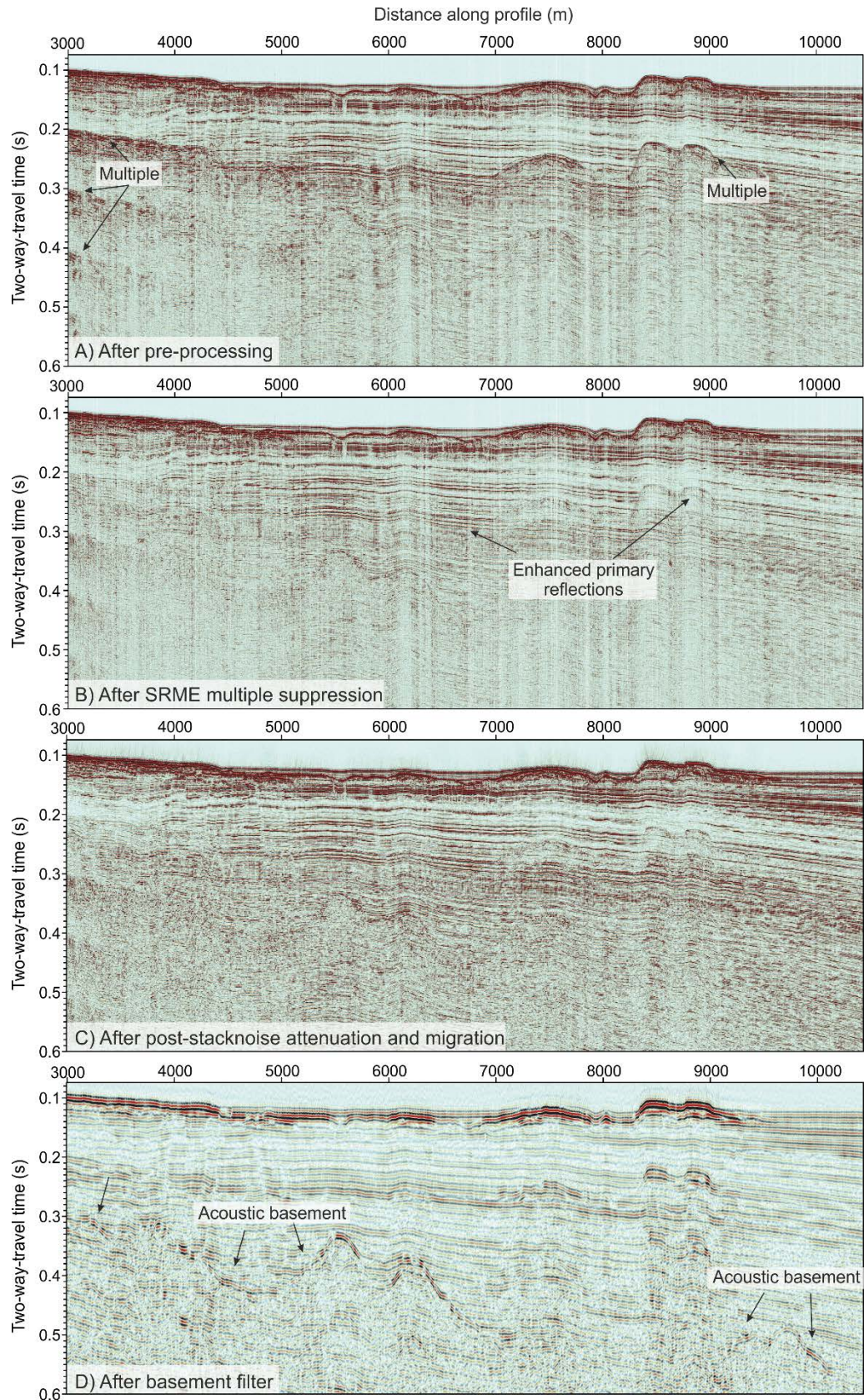


Figure 2.3: Seismic Processing steps visualized on the example of Profile GeoB16-400. A) Constant velocity CMP stack (1600 m/s) after pre-processing, containing multiples; B) CMP Stack after multiple energy suppression with SRME; C) Time migration and noise attenuation (4D-Dec, THOR), and TVSCS; D) Bandpass filter application to enhance the acoustic basement reflector.

In general, the acquisition of the GeoB16 dataset was made in fair weather conditions. Hence, relative vertical movements between source and receiver due to waves could be neglected for most profiles. Residual statics correction was only necessary in three profiles.

Time variant surface consistent scaling (TVSCS) was chosen to preserve uniform energy distribution in the scaling of traces. An alternative sequence without the application of TVSCS was additionally performed for individual profiles to secure information for further amplitude interpretation (e.g., Chapter 4).

The non-linear VISTA tool 'THOR' is especially useful in eliminating random noise and preserving the coherent signal along the entire traces. THOR uses a threshold-based median replacement of a defined amount of neighboring traces in the frequency domain to detect noise based on its incoherence (Butler, 2012). THOR was applied to all profiles just prior to CMP-Stacking.

2.3.3 Post-stack Processing

CMP-stacking was achieved by averaging all traces within one CMP gather. This processing step enhances the S/N ratio by preserving coherent signal and suppressing incoherent noise.

In some cases, trace interpolation was necessary before CMP-stacking to fill single empty bins. Equidistant trace-spacing ensured smooth operation of post-stack noise attenuation and migration. Surface coordinates of the interpolated traces were calculated using a Python code.

After CMP-stacking, the tool '4D Dec', which eliminates incoherent noise overlying all frequencies, was applied. 4D-Dec identifies and removes energy, which cannot be cross-correlated to energy peaks of continuous reflections in neighboring traces. The algorithm utilizes user-defined windows in time and space direction and a maximal expected dip angle in order to remove white noise without neglecting dipping geological structures. Especially in the deeper section, 4D-Dec significantly improved the noise removal and thus image quality.

As a final processing step, the Finite-Difference (FD) Migration was applied to move dipping events into their supposedly true subsurface positions and collapse diffractions (Yilmaz, 2001). Using the velocity models created during the interactive velocity analysis, the FD migration increased the spatial resolution and yielded a seismic image of the subsurface (Figure 2.3C). However, the streamer length limited the imaging of steeply dipping events at depth.

2.3.4 Basement processing

Depending on the necessary signal enhancement and available fold, several 1x5 meter bins can be stacked together ('multi-stacking'). This stacking can also be applied after migration to enhance special geological features, particularly at depth. In combination with an Ormsby bandpass filter

with a low high cut frequency (30-60 and 90-180 Hz), the multi-stacking significantly improved the identification of a bedrock reflection (see Figure 2.3D).

2.4 Data integration and interpretation

Multichannel seismic data, SES data, and core data were integrated into the IHS Kingdom software package. Further, geographic information system (GIS) applications, like QGIS and ArcGIS, have been utilized to facilitate the correlation of geological features with published information and conduct various data analyses.

2.4.1 Seismic Stratigraphy

An essential step within the seismic interpretation is the application of sequence stratigraphy and facies analysis. Each reflector coincides with a short period of similar depositional conditions in a geological sense. That implies they correspond to conformable changes in depositional regime, like energy level, sedimentation rates, deposition environment, input source, or pore contents (Veeken, 2006).

In all seismic profiles, seismic facies are distinguished based on reflection parameters, such as configuration, continuity, relative amplitude, and frequency following the seismic-stratigraphic interpretation techniques described by Mitchum Jr et al. (1977) and Brown Jr & Fisher (1980). Examples of principle and modified internal configurations as introduced by (Mitchum Jr et al., 1977) are included in Chapter 3 for SES and Chapter 4 for MCS data.

2.4.2 Horizon maps, calculations, and grids

The Kingdom Software enables the identification and mapping of seismic reflectors and faults. The calculation of seismic attributes like similarity, average energy and coherence supported this identification process. After the picking process, the time-based horizons are converted into grids of 10 by 10 meters by applying the 'flex gridding' algorithm, which creates a smooth surface constrained by the smallest possible distance to the data points. By applying a time-depth-conversion using an average velocity of 1600 m/s and simple math operations, depth and thickness grids were created. Thickness maps reveal not only information on the distribution of facies due to the identification of paleo-depocentres; they also indicate the timing of faults. Various factors have to be considered for interpreting thicknesses, such as former accommodation space, influence of erosion, deposition process, and lithology (Einsele, 2000; Miall, 2010).

2.4.3 Fault database

The recognition of faults is a product of the initial horizon tracing process restricted to single profiles. Faults, which are continuing across multiple profiles, have to be assigned to fault planes to

visualize their 3D behavior. To incorporate all faults into this process, a database including various faults characteristics, e.g., dip, dip direction, fault displacement, throw, heave, the according rates, or the overall extension along profiles (see Chapter 5) was set up. The according characteristics were calculated via python scripts, based on the extracted fault and horizon information from the Kingdom Software. This approach allowed fast data computation for the comprehensive data set and allowed quick data reproduction in case of changed interpretation while reducing human error.

2.4.4 SES and Core intergration

As the SES surveys were acquired over a period of 10 years and before or after the summer monsoon season, the data hold dissimilar lake-level references. To ensure comparability throughout the dataset, the same base level for all profiles was adjusted to the relative depth of the Core NC08/01 (93 mbll).

In 2008, the 10.4 m long piston core NC08/01 was retrieved in the center of the western subbasin (30.73°N, 90.78°E) (Doberschütz et al., 2014; Kasper et al., 2015). Published analyses include, e.g., AMS-¹⁴C dating, grain size distribution, XRF scanning, geochemical and micropaleontological analysis (e.g., Doberschütz et al., 2014; Kasper et al., 2012, 2015).

The core was integrated in the Kingdom Software based on the fundamental assumptions of faster sound velocities in sediment than in lake water and correctly measured core depth. According to the identified acoustic units in the SES data (see Chapter 3, Figure 3.3), a velocity model was created (Table 2.2; average velocity = ~1540 m/s). Water content and density measurements from NC08/01 were considered (Kasper pers. comm.). Sound velocity in the lake water was calculated to be 1460 m/s (see Chapter 2.1) and perfectly fit the sound velocity at the core location. In general, reflections in the SES Profile Jena06-13 correlate with silt content variations (Chapter 3, Figure 3.3). Detected increased sand contents at a core depth of, e.g., 2.8-3 m may be deposited in thin layers not detected by the SES.

Table 2.2: Sound velocities used to integrate Core NC08/01 with the hydro-acoustic data.

Subsea (m)	Two-way-travel time (s)	Interval velocity (m/s)
-93.0	0	1459
0	0.1275	
2.5	0.13091	1466
5.5	0.1349	1504
6.3	0.13593	1553
10.4	0.141	1619

Chapter 3:

Sediment distribution processes and lake-level variations since the LGM in the Tibetan lake Nam Co – reconstructed from high-resolution hydro-acoustic data

Nora Schulze^a, Thomas Kasper^b, Gerhard Daut^b, Volkhard Spieß^a, Junbo Wang^{cd}, Liping Zhu^{cd}

^a Faculty of Geosciences, University of Bremen, Klagenfurter Strasse 2-4, 28359 Bremen, Germany

^b Friedrich-Schiller-University Jena, Institute of Geography, Physical Geography, Löbdergraben 32, 07743 Jena, Germany

^c Key Laboratory of Tibetan Environment Changes and Land Surface Processes (TEL) /Nam Co Observation and Research Station (NAMORS), Institute of Tibetan Plateau Research, Chinese Academy of Sciences, Beijing 100101, China

^d CAS Center for Excellence in Tibetan Plateau Earth Sciences, Beijing 100101, China

Keyword list: sedimentation, transportation processes, interflow, suspension cloud, sediment echo sounder

Highlights:

- Interflows and hyperpycnal flows drive sediment distribution in Nam Co
- Stable summer stratification and lake level steer sedimentation
- 100 m lake-level variation in the last 20.5 kyrs
- Supra-regional paleoclimate and regional meltwater impact influence lake level

3.1 Abstract

Under the aspect of global warming, glacier thawing, and precipitation changes, the reconstruction of former lake level responses to climate change has gained focus. Here, we present a lake level reconstruction from Nam Co for the last 20.5 kyrs based on geophysical data. We investigated sediment echo sound data from 2006 to 2016, acquired on the third-largest lake on the Tibetan Plateau. By performing an acoustics stratigraphic analysis, we gained new insights into the modern sedimentation processes. Interflows and hyperpycnal flows affected by a stable summer stratification steer the sediment distribution in the lake. Eventually, modern sediment deposition is restricted to a water depth greater than 66 m below lake level (mbll). Based on the current situation (lake level at 4724.5 meters above sea level (masl)), we tested the reconstruction of absolute lake-level variations from 20.5 ka to today. The first-order estimate of a stable stratification for the onset of fine sedimentation during the Holocene and high lake-level periods fits lacustrine sediment core

and onshore observations of paleo-shorelines. For low lake level situations, the sedimentation is predominantly steered by hyperpycnal flows. During the LLGM and the Late Glacial, the onlapping sedimentation is connected to morphological paleo beach ridges. Hence, we identified absolute lake-level stands of ~80 to 58 mbll from 20.5 ka to 16.9 ka and relative variations for the sediments onlaps between 16.5 and 13.4 ka. Around 12.2 ka, the water level rose to a maximum of +16.1 m above lake level (4740.6 masl) and dropped again to a minimum at 11.4 ka. During the Holocene, short lake-level minima occurred during a general high water level, indicating severe oscillation. The sediment accumulation rate increased drastically during the Holocene, which emphasizes the enhanced input derived from the Nyainqêntanglha Mountain Range.

3.2 Introduction

3.2.1 Motivation

The Tibetan Plateau (TP) is well known as the 'Third Pole' or the 'Water Tower of Asia', which underlines its importance as a water source for the Asian population (Immerzeel et al., 2020). In order to study how climate variability affects the terrestrial water resources, sediments of endorheic lake basins on the TP offer unique opportunities. The sensitive lacustrine archives present valuable insights into past lake levels and hence the interplay of precipitation, evaporation, and glacier melting in the past (Günther et al., 2016).

High- and low amplitude variations of paleo lake-levels have been detected on various time scales, and the drawn inferences about paleoclimate vary over the TP (e.g., Alivernini et al., 2018; Fan et al., 2012; Wang et al., 2016; Yu et al., 2019). One reason for this variability is related to atmospheric circulation. Depending on the geographic location, the interplay of Indian summer monsoon (ISM), East Asian monsoon, Westerlies, and polar air masses can differ. Moisture availability and evaporation are, therefore, not uniform over the TP (Herzschuh, 2006). Further, local glacier melting may overprint the regional influence of the atmospheric circulation (Jia et al., 2001). Ongoing paleoclimate research is compulsory to disentangle local and over-regional effects on the paleoclimate. However, some paleoclimate periods are of significance on the entire TP, like the Heinrich-Event 1 from ca. 16 to ca. 14 ka, and help validate climate reconstruction based on different proxies.

In recent years, lake level research on Nam Co focused on beach remnants and lake terraces (e.g., Daut et al., 2010; Lehmkuhl et al., 2002; Schütt et al., 2008; Zhou et al., 2020; Zhu et al., 2002), biogeochemical studies on sediment cores (e.g., Doberschütz et al., 2014; Kasper et al., 2013, 2015; Mügler et al., 2010; Zhu et al., 2015) or recent changes observed via remote sensing (e.g., Kropáček et al., 2012; Zhu et al., 2010). Onshore terraces are excellent evidence for former lake level stands.

However, time constraints are limited, as dating is challenging (Yu et al., 2019). Moreover, the preservation of all beach terraces onshore is not always given, e.g., by erosion during repeated transgressive-regressive lake level fluctuations (Kong et al., 2011).

So far, only Daut et al. (2010) studied submerged beach remains in Nam Co, demonstrating lower lake-level variations. Based on hydro-acoustic data, the authors defined four acoustic units and detected five paleo-shoreline indicators at 10/15 m, 30 m, 45 m, 70 m, and 95 m below lake level (mbll). Only the shallowest beach remains have been matched to the Little Ice Age, whereas all deeper lake levels were conjectured to have formed prior to the Holocene (Daut et al., 2010).

Lake sediments have been studied on short cores (<4.5 m) in the shallow eastern subbasin and one 10 m long piston core (NC08/01) in the center of the main basin dating back 24 kyrs (Figure 3.1). The sedimentation rates from NC 08/01 confirm Nam Co being a high-resolution paleoclimate archive. Implications on paleoclimate and relative lake level variations have been drawn from, e.g., granulometric parameters, minerogenic input indicators, leaf-wax biomarkers (*n*-alkanes) and compound-specific stable isotopes, as well as pollen assemblages (Günther et al., 2015; Kasper et al., 2015; Zhu et al., 2015). Analysis of ostracod assemblages, giving absolute lake-level variations, is limited to 4 kyrs BP (Kasper et al., 2013). While Wang et al., (2015a) have analyzed surface sediments across Nam Co, no focused study on lake recent and paleo-sedimentation processes has been conducted, which would be urgently needed to draw conclusions about paleoenvironmental and paleoclimatic conditions.

Here, we utilize seismo-acoustic data ground-truthed by sediment core information from sedimentary records to investigate temporal variations in the sedimentary regime of the past 24 ka. This study aims to conceptually understand the sediment distribution processes in Nam Co and their possible relation to water column stratification. In this way, we target absolute lake-level fluctuations since the Local Last Glacial Maximum (LLGM) and discuss the positive and negative lake-level variations regarding observed oscillations in other Tibetan lakes. Further, we deliver detailed estimates on sediment fluxes, sediment sources, and depocenters for low lake level stands during the Holocene.

3.2.2 Study site / Geologic and climate setting

Nam Co (30° 30' –30° 35'N, 90°16' –91° 05'E) is an endorheic basin situated on the central TP north of the Nyainqêntanglha Mountain Range at an altitude of 4724.5 masl (meters above sea level; in June 2016; (Hydroweb, n.d.) (Figure 3.1). More than 60 small streams feed the lake, with most input sourced from the southern and eastern mountain chains. The total catchment area of the Nam Co basin is ~10,680 km² (Zhou et al., 2013), and the surface area of Nam Co is ~2,021 km² (in June 2016; Hydroweb, n.d.).

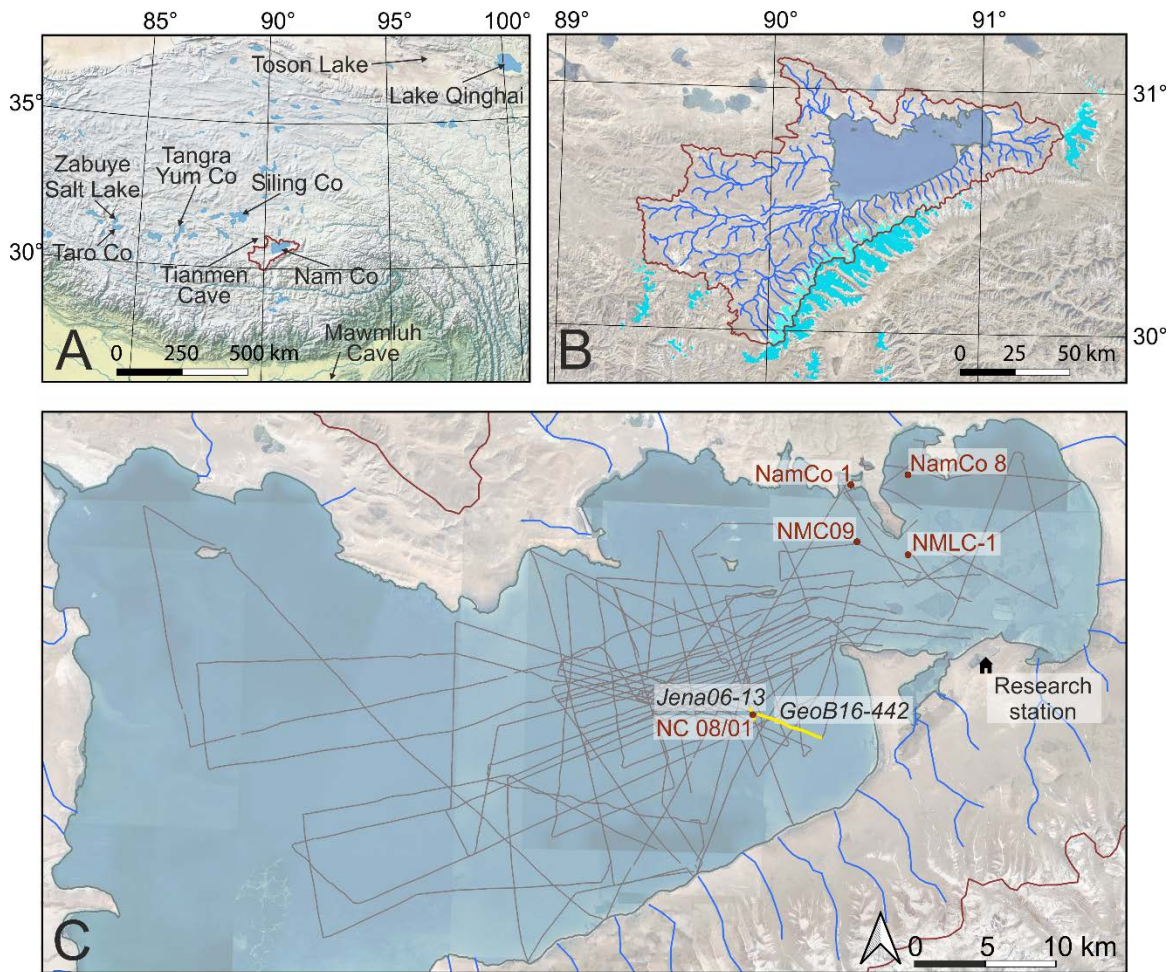


Figure 3.1: A) Location of Nam Co and its drainage area (red outline) on the Tibetan Plateau. B) Drainage area of the Nam Co basin with its inflow water network (dark blue; Wang et al. (2009a), modified) and draining glaciers (cyan). Glaciers draining outside the basin are marked in dark cyan. Glacier dataset retrieved from GLIMS & NSIDC (2005). C) Acquired SES profiles in 2005, 2006, and 2016 by the Universities of Jena and Bremen in collaboration with the ITP. Profiles Jena06-13 (Figure 3.3) and GeoB16-442 (Figure 3.4) are highlighted in yellow. All maps in UTM projection.

Morphologically, Nam Co can be divided into the western or main basin with a maximum water depth of 98 m, and the eastern sub-basin with a maximum water depth of about 60 m. The entire lake volume was calculated by Zhu et al. (2010b) to be about 86.4 km³ (in 2004). Deposits near the lakeshore are composed of unconsolidated Pleistocene to Holocene sediments of glacial, glaciofluvial, and fluvial origin. Lehmkuhl et al. (2002) have found glacial remains in the lake's vicinity in the southern part of the catchment, but moraines are reported to have not reached the lake (Schütt et al., 2008). Surface sediments in the shallow lakeshore areas are fine to very coarse, whereas, in the central basin areas > 80 mbll, the main fractions are silt and clay (Wang et al., 2015a).

The Nam Co region is dominated by arid to semi-arid continental climate (Wang et al., 2019) and the mean annual temperature at the Nam Co Research Station is 0°C. The annual precipitation is approximately 450 mm/yr (Zhu et al., 2010b), of which >90% is received during the summer monsoon season from May to September (Huang et al., 2017). Nam Co is a dimictic lake with stable

thermal stratification from June to November (Huang et al., 2017). Measured specific conductivity and pH are $1850 \mu\text{S cm}^{-1}$ and 9.2, respectively (Wang et al., 2010). For approximately 90 days during the winter season, Nam Co is covered by lake ice (Wang et al., 2019). Glaciers cover 2 % of the lake's catchment and recently contribute about 20-40 % to the total lake input water volume (Adnan et al., 2019; Biskop et al., 2016). On long time scales, the influence of meltwater run-off changes on the lake level is still debated (e.g., Zhou et al., 2013). In the last decades, the lake level is rising on average by 0.3 m/yr, about a third of the seasonal variability (Adnan et al., 2019; Kropáček et al., 2012). This behavior on different time scales emphasizes the sensitivity of Nam Co's lake level to changes in the water balance (Haberzettl et al., 2019).

3.2.3 General lake sedimentary processes

Rivers and streams are, besides aeolian input, the primary conveyors of terrestrial sediment into the Nam Co basin (Dietze et al., 2014). In general, sediment is further distributed via gravitation-driven processes (Parsons et al., 2007). At a river mouth, flow evolution depends besides viscosity and flow dynamics on the density difference between the inflow (rf) and the standing water-body (rw) (Mulder, 2011) (Figure 3.2). Originally, Bates (1953) defined three flow types: overflow (hypopycnal flow, Figure 3.2A) if $rf < rw$, homopycnal flow if $rf = rw$, and underflow (hyperpycnal flow, Figure 3.2B) if $rf > rw$. Hyperpycnal flows dilute on their way into the basin and gradually lose the ability to transport load. At the lofting point (LP, Figure 3.2B), the hyperpycnal flow reverses its negative buoyancy as a

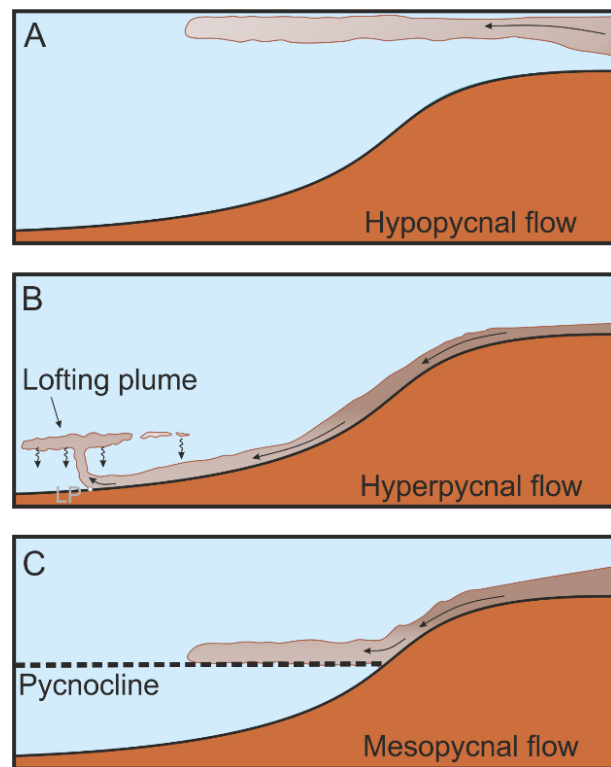


Figure 3.2: Comparison between hypopycnal (A, inflow density < lake-water density), hyperpycnal (B, inflow density > lake-water density) and mesopycnal flows (C, inflow density = lake-water density). After Mulder (2011) and Zavala et al. (2011).

consequence of the progressive loss of suspended load by deposition out of the flow (Zavala et al., 2011). In alpine lakes, it is often observed that sediment-rich water enters a well-stratified lake as an intraflow (mesopycnal flow, Figure 3.2C) (Mulder & Alexander, 2001; Scheu et al., 2018). The sediment-rich river water has a higher density than the preheated surface water of the lake but lower density than the lake water due to the high amount of cold freshwater (Cortés et al., 2014; Scheu et

al., 2015). Thus, the suspension cloud propagates above a pycnocline (Mulder, 2011). Particle settling out of suspension is related to particle diameter and shape, turbulence, and viscosity within the water column (e.g., Ferguson & Church, 2004).

3.3 Methods

3.3.1 Sediment Echo Sounder data

In summer 2016, a Sino-German research-team from the Universities of Bremen and Jena and the Institute of Tibetan Plateau Research - Chinese Academy of Science (ITP-CAS) jointly carried out a seismo-acoustic survey on Nam Co. We acquired an extended high-resolution sediment echo sounder (SES) data set of ~860 km length during the expedition. About 530 km of SES data had been previously acquired by the University of Jena and the ITP-CAS in 2005 and 2006 (Figure 3.1). Similar parametric sediment echosounder devices (Innomar 96 and 2000-light; Innomar Technologie, Rostock, Germany) were used for all surveys. We calculated seismic velocities in lake water, according to Sheriff (1991), for different depths, temperatures, and salinities (Mügler et al., 2008), resulting in an average velocity of 1460 ms^{-1} . For the 2016 data set, we achieved a maximum subbottom penetration of 18 m. The vertical resolution of the SES depends on the sound velocity in water and the effective pulse duration. During the 2016 cruise, we commonly used the setting of 10 kHz and one pulse, ensuing in a vertical resolution of 7.25 cm. The vertical resolution of the 2005/2006 SES data is minimum 12 cm (Daut et al., 2010). The horizontal resolution for the device used is <7% of the water depth (Innomar, 2015). The 2016 SES data processing included filtering and despiking, but no motion correction due to the lack of a motion sensor. To ensure the correct integration of the three surveys, we took the water depth at core site NC 08/01 (93 mbl; Figure 3.1) as reference.

3.3.2 SES data interpretation

We based the identification of reflectors on their acoustic properties. For data interpretation and mapping, we used 'The Kingdom Software' Version 2016 and 2019 by IHS. Further, we computed seismic attributes *envelope* and *average energy* for optimal reflector tracing. Tools like *flattening* of older horizons, based on the idea of a flat lake floor at the time of high lake level deposition, were applied to ensure a consistent process and best performance. We calculated standard error deviations of the onlapping-depths for the uppermost reflectors (RIX-XII) based on the deviation from the average depth of a reflector for all profiles and the picking precision of $\pm 0.0001 \text{ s}$ (TWT). A basinwide clear identification of reflectors older than RVIII was not possible due to the variable profile spacing.

Within the Kingdom Software, we performed gridding of thickness maps with a *flex gridding* algorithm. Based on the extent of the sediment units, their thicknesses, and ages, we calculated estimates for total sediment accumulation rates. We use a simple approximation by adding up the squared grid cells columns of 50 × 50 m by their thickness value.

3.3.3 Age Model and Integration of SES and Core data

Hitherto, sediments comprising the past 24,000 years have been retrieved in the 10.4 m long piston core NC08/01 retrieved in the center of the main basin (Figure 3.1). The age model was based on 24 AMS ¹⁴C ages and a reservoir effect correction of 1,420 years (Doberschütz et al., 2014; Kasper et al., 2015). The top 30 cm were corrected with ¹³⁷ Cs and ²¹⁰ Pb radiometric data (Kasper et al., 2012).

Integrating the SES data with the available core data enabled us to generate a stratigraphic frame with reliable age markers. We utilized the calculated sound velocity of 1460 m/s for the water column and a gradually increasing velocity model for the lake sediments for the depth-time conversion of the core logs (see Chapter 2.4.4).

3.4 Results

The hydro-acoustic dataset comprises five acoustic facies (AF1-5, Table 1), which build up four acoustic units (AU1-4). Moreover, we identified 13 reflectors (R0- RXII). These horizons mark either top or bottom of the acoustic units (R0, RVIII, RXII) or subdivide AU3 and AU4 internally (Figure 3.3).

3.4.1 Description of Acoustic Facies

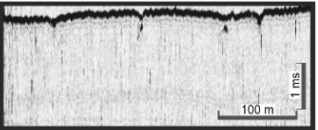
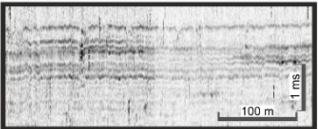
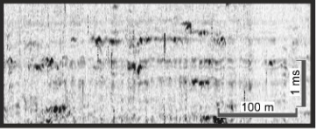
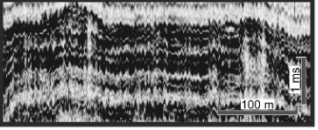
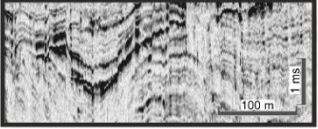
We identified five acoustic facies (AF) based on continuity, internal reflection configuration, amplitude, and frequency (Mitchum Jr et al., 1977) (Table 3.1). AF1 is characterized by continuous, parallel, very low amplitude reflections with low frequency. AF2 is represented by continuous, parallel, and low to medium amplitude reflections with medium to high frequency. AF3 has a similar character as AF2. However, reflectors are less continuous, the configuration is hummocky with high amplitude spots or patches, and the frequency is medium. Features of AF4 are continuous, parallel, high amplitude reflections with medium frequency. AF5 is characterized by discontinuous, partly disrupted, or contorted reflectors. AF5 has low amplitude reflections of varying frequencies.

3.4.2 Description of Acoustic Units

Based on the shape of sequences and acoustic facies, we defined four acoustic units (AU) (Figure 3.3):

AU1 is generally built up by well-layered reflectors, which occur basinwide with local variations. In the western and northern central basin, AF1, 2, and 4 are alternating. The unit top is conform and shows no sign of erosion. In the west, a few (normal) faults penetrate the unit. In contrast, the south-east central basin AU1 is built up by AF5. Depressions occur in varying sizes in a range of several hundred meters width and ~3 to 5 m depth with exceptions of up to 14 m depth. In the south-central basin, the top of AU1 shows erosional truncations of folded sediment packages.

Table 3.1: Acoustic facies recognized in SES data of Nam Co and their geological interpretation.

Acoustic Facies (AF)	Characteristics	Geologic Interpretation
AF1 	Transparent to good continuity Horizontal, parallel, even Very low amplitude Low frequency	Calm sedimentation milieu with continuous sediment input Fine, lacustrine high-stand deposits
AF2 	Good continuity Parallel, even Low to medium amplitude Medium to high frequency	Calm sedimentation milieu Alternating grain sizes Transition from high to low or low to high lake level
AF3 	Irregular continuity Hummocky, sometimes interrupted with high amplitude spots or patches Low to medium amplitude Medium frequency	Calm sedimentation milieu Alternating grain sizes, drop stones, event input Transition from high to low or low to high lake level
AF4 	Good continuity Horizontal, parallel High amplitude Medium frequency	High-energy sedimentation milieu with coarse grain sizes Lacustrine low-stand deposits
AF5 	Irregular continuity Contorted, disrupted Low to medium amplitude Varying frequency	Faulted and/or glacially deformed post-deposition, former SF1 to SF 4

AU2 is built up by AF4 and AF3 and shows patches of irregular, high amplitude reflectors. In the west, reflectors are conformably overlying AU1. The detected faults in AU1 also penetrate AU2. However, only a few endure above the top of the unit. In the south-eastern part of the basin, AU2 infills the depressions of the underlying AU1. Therefore, thickness is very variable with values up to 14 m (e.g., at the core position in Figure 3.1). The incisions are filled stepwise with either AF2 or AF3. The basic topography is not leveled out entirely after AU2 deposition. The top of AU2 is a prominent high-amplitude reflector (R0) and represents an unconformity. In the south-east, R0 has an irregular behavior, while in the west, it has a shallow angle, and its unconformity is less distinct.

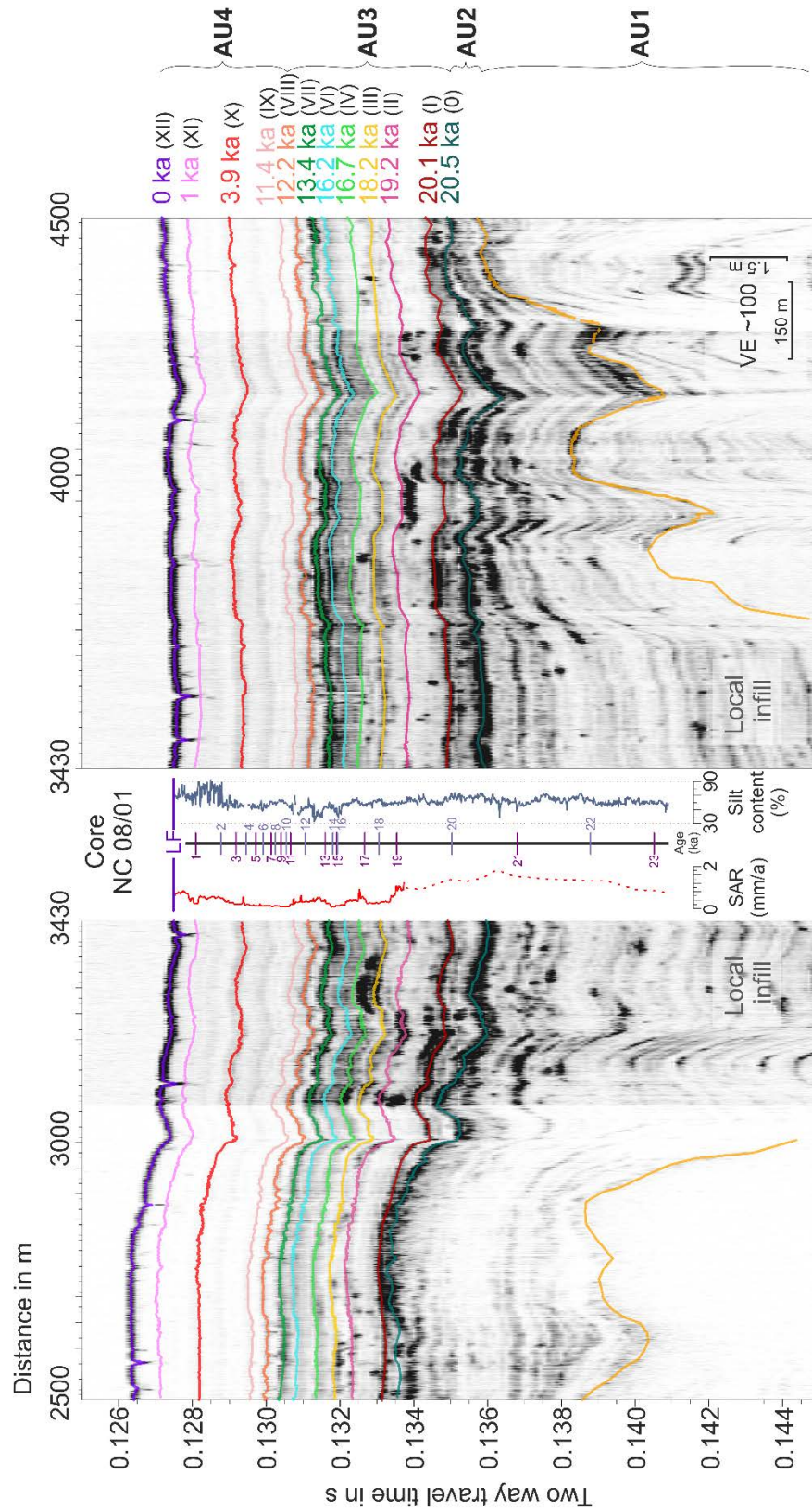


Figure 3.3: Integration of Core NC 08/01 and SES profile Jena06-13. The SES profile is split at the core location to highlight the core logs of Sediment Accumulation Rate (SAR, red) and silt content percentages (dark blue). The solid and dotted SAR curve indicates a sample distance of 1 cm and 30 cm, respectively. The tracea reflectors correlate well with recorded silt content variations. Profile recorded with 12 kHz and 1 pulse.

AU3 is onlapping AU2. The unit is built up by horizontally alternating AF1 to 4. Locally, minor facies variations occur in this unit as AF3 transforms smoothly into AF2. AU3 inhabits a basin intern constant thickness of ~3 m, thinning towards the lake flanks. A local exception with a thickness of 6 m occurs in the south-east. The top of AU3 is a high-amplitude conform reflector (RVIII).

AU4 is conformably overlaying AU3. The unit is remarkably uniform throughout the entire basin. Internally, the unit is exclusively composed of AF1. The unit thickness is varying between 2 and 3 m in the main basin. In the north-east and north-west small depocenters with thicknesses of up to 4.5 m exist. Internal sediment packages thin out towards the lake flanks (Figure 3.4). The top of AU4 is the modern lake floor (LF =XII).

3.4.3 Additional reflectors and amplitude anomalies

AU3 comprises seven internal reflectors (RI-RVII), while AU4 includes three internal reflectors (RIX-RXI) (Figure 3.3). These reflectors onlap underlying deposits and show decreasing amplitude variations basinward along the reflector (Figure 3.4B). Over a distance of one kilometer, the amplitude can decrease, and reflectors become indistinguishable.

3.4.4 Integration of Core data and hydro-acoustic data

Figure 3.4 shows the SES profile Jena06-13, with 12 of the 13 reflectors used in this study. The determined acoustic reflectors RII and RVII correlate perfectly with the formation tops LGM and H1, respectively, as defined by Kasper et al. (2015). All other reflectors in the hydro-acoustic data relate very well with silt content changes in the core (core logs, Figure 3.3). We used these congruencies to pinpoint the ages of the reflectors directly to the age assignment by Kasper et al. (2015). Therefore, the 12 interpreted reflectors are dated relatively to ages between 20.5 ka and today (see 3.4.5). As we could not trace the reflector RV in this SES section, we calculated the respective age of 16.5 ka based on linear interpolation. Hence, AU3 comprises the period from 20.5 ka to 12.2 ka and AU4 from 12.2 ka to today.

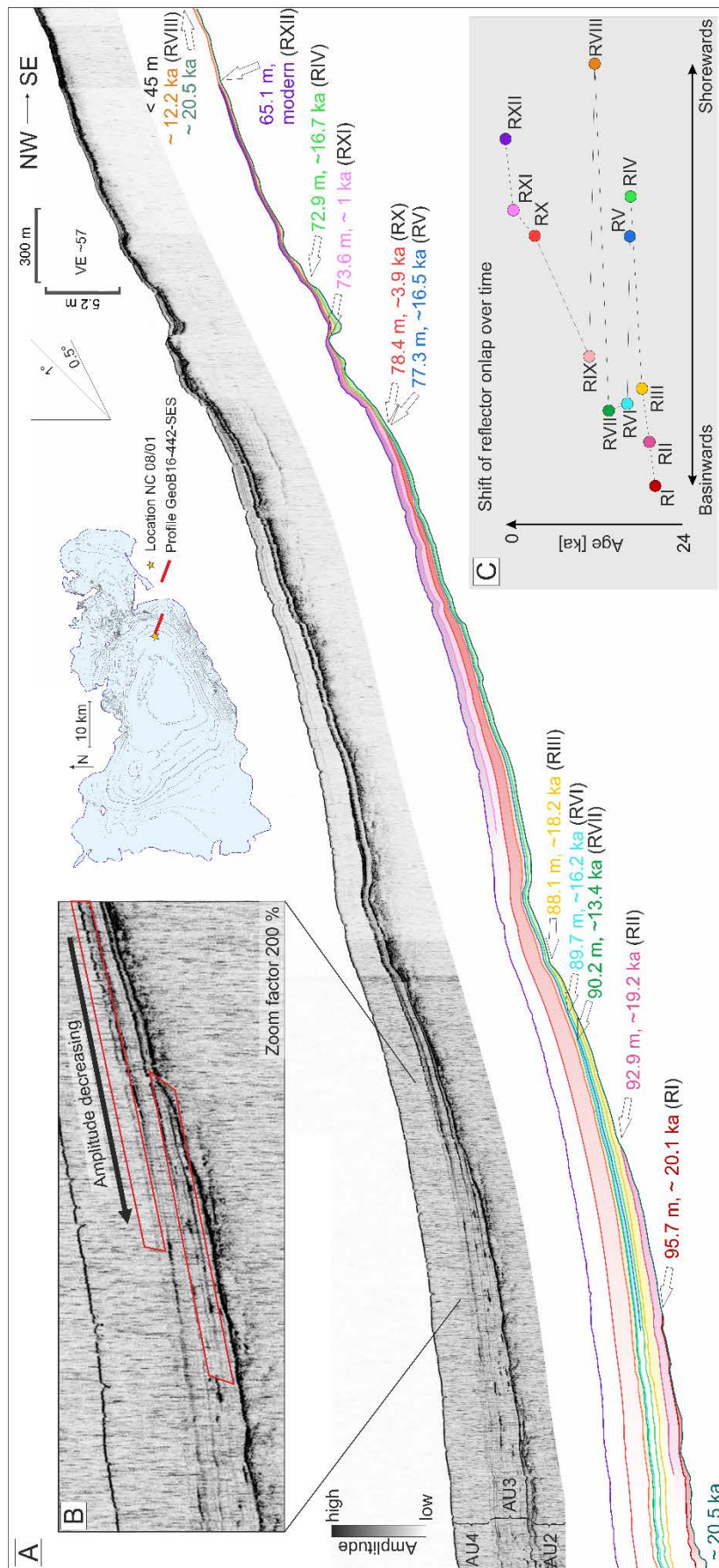


Figure 3.4: A) Onlapping reflectors at the example of SES Profile GeoB16-442-SES, displayed as the acoustic data envelope. The corresponding line drawing beneath visualizing the different reflectors and their age (same color scheme as in Figure 3.3). B) Blowup of onlapping reflectors quickly decreasing in amplitude towards the basin. C) Plot of reflector-onlap shifting basin- and shorewards through time. Please note the vertical exaggeration and its implication on slope angles for A and B.

3.4.5 Sediment distribution characteristics

As the AU1 and 2 are either deformed or infilling existing topography, we focus here on AU3 and AU4 to describe the sedimentation behavior observed in the SES data. Figure 3.4 depicts an exemplary SES profile reaching the south-eastern flank of the central basin and shows the onlapping characteristics of the reflectors (RI to RXII).

The lowermost reflector in Figure 3.4 is the top of AU2 (R0) with an age of 20.5 kyrs. Sediments of AU4 onlap on R0. In detail, these are RI of 20.1 ka at a depth of 95.7 mbll. RII of 19.2 ka at a depth of 92.9 mbll, RIII of 18.2 ka at a depth of 88.1 mbll, and RIV of 16.7 ka at a depth of 72.9 mbll. These onlaps correlate with morphological steps of the underlying topography. RV to RVII onlap the respective younger reflector. RV of 16.5 ka onlaps RIV at a depth of 77.3 mbll. The 16.2 ka old RVI onlaps RV at a depth of 89.7 mbll, and RVII of 13.4 ka onlaps RVI at a depth of 87.6 ± 2.66 mbll. RVIII of 12.2 ka covers all sediments, and its termination could be identified (on one profile) at a depth of 46.1 mbll. Onlapping the 12.2 ka reflector, RIX of approximately 11.4 ka was recorded in five profiles with an average depth of 84.5 ± 1.2 mbll. We could identify the reflectors younger than RIX in all 40 coastal profiles. They onlap onto the 12.2 ka reflector. The 3.9 ka old RX onlaps at a depth of 79.3 ± 2.7 mbll, the 1 ka old RXI onlaps at a depth of 74.4 ± 2.4 mbll, and the modern sediments (RXII) onlap at a water depth of 65.9 ± 1.8 mbll

3.4.6 Sediment extents and thicknesses during the Holocene

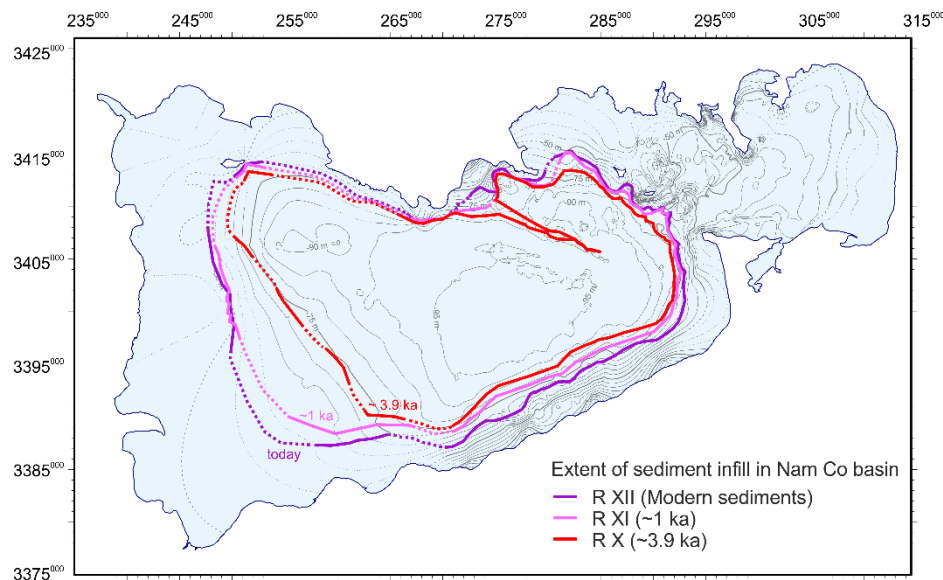


Figure 3.5: Extent of Holocene reflectors in the Nam Co basin. Dotted lines are interpolated sections. Bathymetric isopachs in grey represent the interpolated modern lake floor water depth, derived from SES 2005-2016; uncertainties are dotted.

The extents of the three topmost reflectors of AU4 (RX, RXI, RXII) and an interpolation of the modern lake floor bathymetry are mapped out basinwide due to their identification on all shore-near SES profiles (Figure 3.5).

Compared to the modern bathymetry, the outline of RX shows local deviations. Along the lake's southern flank, the RX onlap is parallel to the modern isolines of about -85 m. RX runs along the -80 m isolines in the east but diverts by more than 10 m in the northern tip. In the north, the reflector onlaps onto a scarp feature trending from NW to SE, reaching into the basin between -85 and -80 m. In the north-west and west, the RX extent strays by -10 to -5 m from the modern -80 m isoline. RX represents the top of a sub-layer with RVIII as the bottom reflector. On the thickness distribution map (Figure 3.6A) for this sub-layer from 12.2 ka (bottom) to 3.9 ka (top), we can identify maximum thicknesses, reaching 2.2 m in the north of the basin and ~1 m in the south.

The maximum extent of RXI roughly follows the 75 mbll isoline and is, besides small exceptions, parallel to the maximum size of RX. In the north-east, RXI's outline has a curvier shape than the RX outline and onlaps in shallower water depth. The most significant difference to the RX border is visible in the west and south-west. The outline diverges +15/+20 m from the 75 mbll isoline, which may be affected by scarce data in the bathymetric model, unable to mirror the real bathymetry. For the thickness of the sub-layer from 3.9 ka to 1 ka (Figure 3.4B), we measured values exceeding 1 m in the north-west, while

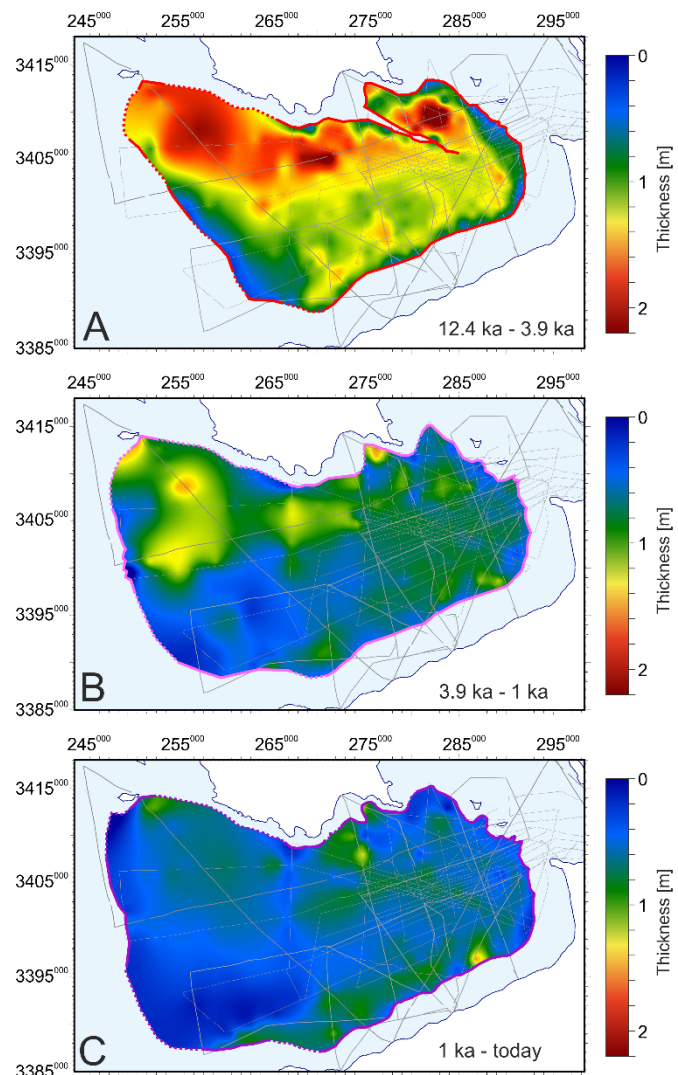


Figure 3.6: Thickness distribution for the three time-slices, highlighting the shift of enhanced sediment deposition from the north to slightly more deposition along the southern flanks of Nam Co through the past 12.4 ka. A) 12.4 to 3.9 ka B) 3.9 to 1 ka C) 1ka to today. The same color bar is applied for A, B, and C.

the rest of the basin shows minor variations between 0.6 and 0.9 m.

The extent of modern sedimentation generally follows the isoline of 66 mbll water depth. Exceptions occur in the north-east and west, where the border of the modern sedimentation extent reaches up to +15 m shallower. The thickness of this uppermost layer from 1 ka to today (Figure 3.4C) is very uniform, with an average of 0.6 m but a slightly increased thickness along the southern flank of the basin.

The calculated sediment deposition rates vary significantly from 12.2 ka to today. We calculated the lowest rate of $9.5 \times 10^4 \text{ m}^3/\text{yr}$ for the oldest part of AU4, a rate of $19 \times 10^4 \text{ m}^3/\text{yr}$ for the time-slice of 3.9 to 1 ka, and $45 \times 10^4 \text{ m}^3/\text{yr}$ for the most recent sediments (Table 3.2).

Table 3.2: Calculated sediment volumes and total accumulation rates for three time-slices of AU4.

Unit	Sediment Volume	Total accumulation rate
1 ka to today	0.45 km^3	$45 \times 10^4 \text{ m}^3/\text{yr}$
3.9 ka to 1.0 ka	0.57 km^3	$19.7 \times 10^4 \text{ m}^3/\text{yr}$
12.2 ka to 3.9 ka	0.81 km^3	$9.8 \times 10^4 \text{ m}^3/\text{yr}$

3.5 Discussion

3.5.1 Correlation of AF and AU with sediment characteristics

Reflections in the hydro-acoustic data are created by changes of impedance caused by changes in sediment physical properties, like variable amounts of sediment components, porosity, or pore fluid. Amplitude and continuity changes of hydro-acoustic reflectors are often directly correlated to lithology and may represent, e.g., changing energy level during deposition (Veeken, 2006). During high lake levels, fine-grained sediments are deposited with uniform thickness over large areas in a low energy lacustrine environment (Wu et al., 2006; Xiao et al., 2013) and eventuate in low-amplitude seismic facies. During lake-level low stands, high-amplitude seismic facies found in deeper areas of the basin indicate coarser material deposited in a high energy environment proximate to the shoreline (Wu et al., 2006; Xiao et al., 2013).

Accordingly, we interpreted our defined facies (see 3.4.1) as follows: AF1 correlates with lacustrine sediments deposited during a lake-level highstand. AF2 and AF3 correlate with lacustrine sediments deposited during the transition from a lake-level highstand to a low lake-level lowstand or vice versa. High amplitude spots or patches may be related to dropstones and ice-rafted material. AF4 correlates with lacustrine sediments deposited during a lake-level lowstand. AF 5 correlates with lacustrine sediments deformed after deposition.

The here-defined units of acoustic units coincide well with the units described by Daut et al. (2010). With the exception that we separated the second unit of Daut et al. (2010) into two distinguishable units, AU1 and AU2.

The facies distribution indicates significant lake-level variations during the deposition of AU1, AU2, and AU3. The low amplitude facies of AU4, however, was deposited in an environment with a significantly higher lake level than the prior units (see 3.5.3).

3.5.2 Sedimentation in Nam Co

3.5.2.1 Main sediment transport via intraflows

The investigated SES data lack erosional features as well as indicators for tectonic influence on sediment distribution within AU3 and 4. Thus, the onlapping behavior of the observed reflectors (RI-RXII) (Figure 3.4) must be a result of sedimentation processes, either depending on the lake level or inflow events.

We observed no modern deposits of clay and silt-sized sediments above a water depth of -66 m. This restriction of sedimentation to deeper water could be connected to the stratification of the water column in Nam Co, which under current conditions establishes from early June to early November (Wang et al., 2019). Moreover, it emerges that allochthonous and autochthonous sediment settling in water depth shallower than 66 m is hampered due to the high flow velocity of the incoming sediment or due to internal waves (Figure 3.7).

Cold meltwater and (monsoonal) precipitation with high amounts of suspended load or dissolved load enters Nam Co primarily during the summer and fall season, with mean summer flow rates $200\text{--}300\text{ m}^3\text{ s}^{-1}$ (Zhou et al., 2013). Therefore, we expect that the sediment-rich river-water has a higher density than the preheated surface water of the saline standing water-body but a lower density than the deeper lake water due to the high amount of cold freshwater (e.g., Scheu et al., 2015). When reaching the lake water, sand size and coarser particles will deposit close to the shore. The remaining suspended fine silt and clay sediment will be transported in a density-driven flow downslope until the density equilibrium is reached (Mulder & Alexander, 2001). The intraflow will then distribute its load in a suspension cloud along the pycnocline (Figure 3.7).

The assumption of intraflows acting as the primary sedimentation process within Nam Co correlates well with the overall fine-grained sediment in the basin (in NC08/01 average grain size: $\sim 15\mu\text{m}$; Kasper et al., 2015) and the observed basinward amplitude loss within seismic units (e.g., SU4, Figure 3.4). With increasing shore distance and the expansion of the flow, the flow velocity decreases, and particles settle dependent on their grain size and density (Zavala et al., 2011). This

leads to the basinward increase in sediment thickness shore (Figure 3.7) and, at the same time, allows draping of the sediment deposits over existing topography in the basin.

Anthropogenic ^{137}Cs distribution from the slopes to the center of the basin (Wang et al., 2015) correlates to the proposed conditions of sedimentation. The smaller concentrations along the slopes can be explained by grain size fractioning or the age of the sediments as the ^{137}Cs in older sediment already depleted. The same can be estimated for the distribution of ^{210}Pb in the surface sediments (Wang et al., 2015). However, the distribution of ^{137}Cs in all samples indicated that fine sediment is initially deposited basinwide to some minor extent.

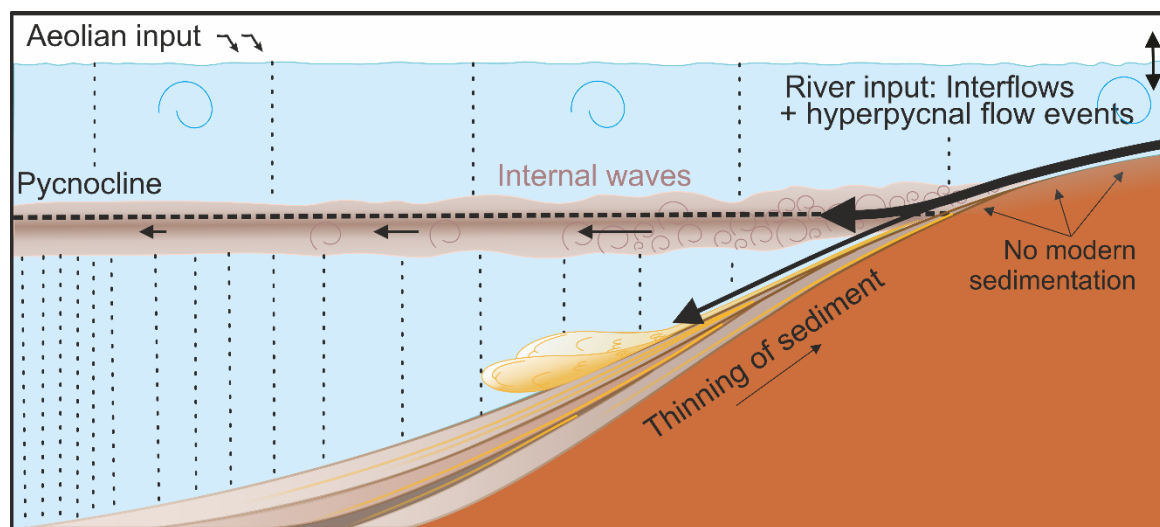


Figure 3.7: Combination of possible sedimentation processes in Nam Co. Interflows (mesopycnal flows) transport suspended, fine-grained material along the pycnocline into the basin, where particles fall out with decreasing flow velocity. No modern sedimentation takes place above the pycnocline. Sketch not to scale.

3.5.2.2 Modern pycnocline depth

Several studies support the hypotheses of an existing boundary layer in Nam Co: The surface sediment distribution examined by Wang et al. (2015a) showed a striking correlation of sediment grain size to water depth. The authors indicated a border at approximately 60 m water depth below which the variation of mean grain size markedly decreased (Wang et al., 2015a). 60 m is also the depth below which Li (2019) observed pollen assemblages. Above 60 m, no deposition or preservation of pollen occurred. Time-limited monitoring data from Wang et al. (2020) and Kai et al. (2020) show a thermocline at 50 m water depth for October 2011. However, turbidity measurement data from Kai et al. (2020) display a small variation in turbidity in the interval from 60 to 70 m water depth. As the highest turbulence occurs in this time-limited data at the lake bottom from 75 to 93 m water depth (Kai et al., 2020), this points to a weak interflow and a simultaneous hyperpycnal flow at the measurement location (Figure 3.1). This fits well with the observed restriction of sedimentation to 66 m.

3.5.2.3 Sedimentation events by hyperpycnal flows

High amplitude reflectors, which show a decreasing amplitude downslope (Figure 3.4B inlay) but are no laterally spacious features, are potentially a result of sustained hyperpycnal flows (Zavala et al., 2011) (Figure 3.7). These have been observed in many lakes (e.g., Mulder & Chapron, 2011). The correlation of the grain size log from core NC08/01 and the high amplitude reflectors indicate the occurrence of sediment layers with >10% sand content. A sustained hyperpycnal flow, which forms at river mouths as a quasi-steady extension of the stream, can transport sand into the basin (Mulder, 2011; Zavala et al., 2011). Usually, sustained hyperpycnal flows are connected to flood events or (tectonic active) basins with steep slopes (Milliman & Syvitski, 1992; Mutti et al., 1996). The slopes in Nam Co are generally flat (<2° slope) at the river mouths, and fine-grained material is prevailing in the Nam Co basin (Wang et al., 2015a). Thus, sustained hyperpycnal flows have rather been events in the past 24 ka than standard sediment input process and might have increased during dry glacial conditions with low lake level stands.

3.5.3 Lake level reconstruction based on primary sedimentation process

The sedimentation processes in Nam Co (intraflows and hyperpycnal flows (see 3.5.2.1 and 3.5.2.3; Figure 3.7) are presumably independent of the lake level. However, the onlap of sedimentation and the associated lateral grain-size grading are subject to the lake level, and hence the depth of the pycnocline.

While Nam Co behaves dimictic and the lake turns over twice a year, we assume that the contemporary pycnocline establishes at a depth of 66 mbll due to stable thermal conditions. Based on the first-order estimate of a stationary pycnocline depth of 66 mbll, we test the applicability of the onlap-depth of the identified reflectors (RI-RXII) in AU3 and AU4 towards an absolute lake level reconstruction. Further, we compare our implications for AU1-2 and our results for AU3-4 with lake-level reconstructions from other Tibetan lakes (Figure 3.1) to highlight controversies and over-regional similarities associated with paleoclimate variations.

AU1

Based on the internal acoustic structure of AU1 sediments, we expect lacustrine deposition under varying lake-level conditions. Subsequently, the sediments of AU1 were deformed and partially eroded. This could be the result of glacier impact, grounded lake ice, or permafrost conditions, as proposed by Daut et al. (2010). Ensuing flooding events connected to ice melting during the glacier retreat led to the filling of incisions (for more details, see Chapter 5).

AU2 - prior 21 ka

The sedimentation at the base of AU2 results from rapid flooding and very high lake level, as the fill is draping the former topography and not stepwise infilling and onlapping on top of AU1. Only in some steep incisions we observe a focused, divergent filling. This behavior fits very well with the highest proposed lake level and the associated lake level terrace of +30 m (Lehmkuhl et al., 2002). Around 30 ka, various lakes on the TP show indication of high stands as well, e.g., Toson Lake (Fan et al., 2012) or Selin Co (Li et al., 2009). Jia et al. (2001) identified 16 lakes with records of a lake-expanding event from 40 to 28 ka. The high lake stands are associated with a period of enhanced Indian monsoon on the TP (Shi et al., 2001).

The amplitude change in the acoustic data implies that the lake level decreases from the bottom to the top of AU2. This indicates that the climate became cooler and drier during the 'youngest glacial stage' (Lehmkuhl & Haselein, 2000). The paleoclimate shift is also in agreement with Kasper et al. (2015), who propose a low lake level for Nam Co until 20 ka. Further, we associate the detected submerged lake level terraces of -85 m and -90 m (Daut et al. 2010) to the top of AU2 and, therefore, to the lake level drop during the cooling phase of the youngest glacial stage (Figure 3.8B). The lake level decline to this very shallow lake resulted in the strong reflector R0, which we identified as an unconformity.

Indication of a dry and cold LLGM is widespread on the TP as suggested by the mean effective moisture curve (Herzschuh, 2006) and speleothem data (Dutt et al., 2015; Dykoski et al., 2005) (Figure 3.8 F&G). Some lakes on the TP desiccated or evolved into salt lakes during the LGM, while other lakes remained relatively stable (Jia et al., 2001 and references therein). Drier conditions until ca. 20.5 ka BP are the result of the enhanced influence of the Westerlies bringing cold and dry air masses to the TP (Porter & Zhisheng, 1995) and the reduced summer monsoon intensity (Sirocko et al., 1993).

AU3 (RI – RVIII) - 21ka -12.4 ka

The lake-level reconstruction from R0 to RVIII (Figure 3.8A) shows two low and two high lake-level phases within this unit, which we associate with cold/dry and warm/moist climatic periods. The first cold phase lasts until ~19 ka, which correlates with globally reported LGMs between 23-19 ka. The second cold phase starts after the Late Glacial, around 16.7 ka, and ends with Heinrich event 1 (H1) at 13.4 ka (Figure 3.6). These separate lake-level phases illustrate a higher climatic variability within the proposed continuous 'youngest glacial stage' from 24 to 15 ka by Lehmkuhl & Haselein (2000).

From 20.5 ka to 16.7 ka, the onlap depths of RI-RIV from 95.7 mbl to 72.9 mbl indicate a constant lake level rise by about 25 m. The onlap depths correlate to morphological steps in the

lake-floor topography, representing paleo-beach ridges. Thus, the onlaps indicating absolute water depths beneath the wave base. Hence, our first-order estimate of a 66 m water column above the onlap depth is not applicable during shallow lake levels. Consequently, assuming a wave base of ~15 m, the lake level from 20.5 to 16.7 ka rose from about 80 to 58 mbll. Increased terrigenous sediment input and increasing clay and decreasing silt content at Core Site NC08/01 also support a rapid lake expansion (Kasper et al., 2015). Therefore, our results constrain the timing of enhanced deglaciation at Nam Co between 19.2 and 16.7 ka. A recovery of lake level after the LGM was shown for 73 lakes, not only on the TP but in entire China by Fang (1991). Most of the rapid lake level rises are associated with glacial meltwater input (Jia et al., 2001) but also, the increasing strength of the ISM (Zhu et al., 2015) is influencing the hydrological balance.

Our reconstruction shows a short and distinct highstand around 16.7 ka. After 16.7 ka, the lake level drops quickly until 16.2 ka (Figure 3.8A). The Inflow-Evaporation-Index (Kasper et al., 2015) shows a small peak at 17 ka and decreases quickly after (Figure 3.8D). Other lakes in the vicinity express no evidence of lake level dropping (Kotlia et al., 2017). Applying the first-order estimate, the lake-level variation would make up to 16.8 m. As we lack further indication of a local phenomenon capable of a lake level change four times the increase of the last three decades, we confound the strict application of a stable pycnocline depth for the Late Glacial and during Heinrich 1. Instead, we assume a relative lake level increase associated with an inflow event at 16.7. A recorded peak in sediment accumulation rate (Figure 3.3) and terrigenous mineralogic input (Kasper et al., 2015) at the Core Site NC08/01 support this.

From 16.2 ka to 13.4 ka, the reconstructed lake level appears to be low (Figure 3.8A). Fitting our curve, speleothem data from the Mawmluh Cave record lowest $\delta^{18}\text{O}$ values from 16.5 to 15.5 ka (Dutt et al., 2015) (Figure 3.8K). Sediment accumulation rate in the core NC08/01 remained low while the silt content decreased by 10 %, and clay content increased (Kasper et al., 2015). Hence, we assume a reduced fluvial input due to dry and cold climate conditions. This corresponds to Zhu et al. (2015), who infer a northward shift of the ISM at 16.5 ka, which brought only limited moisture to the TP.

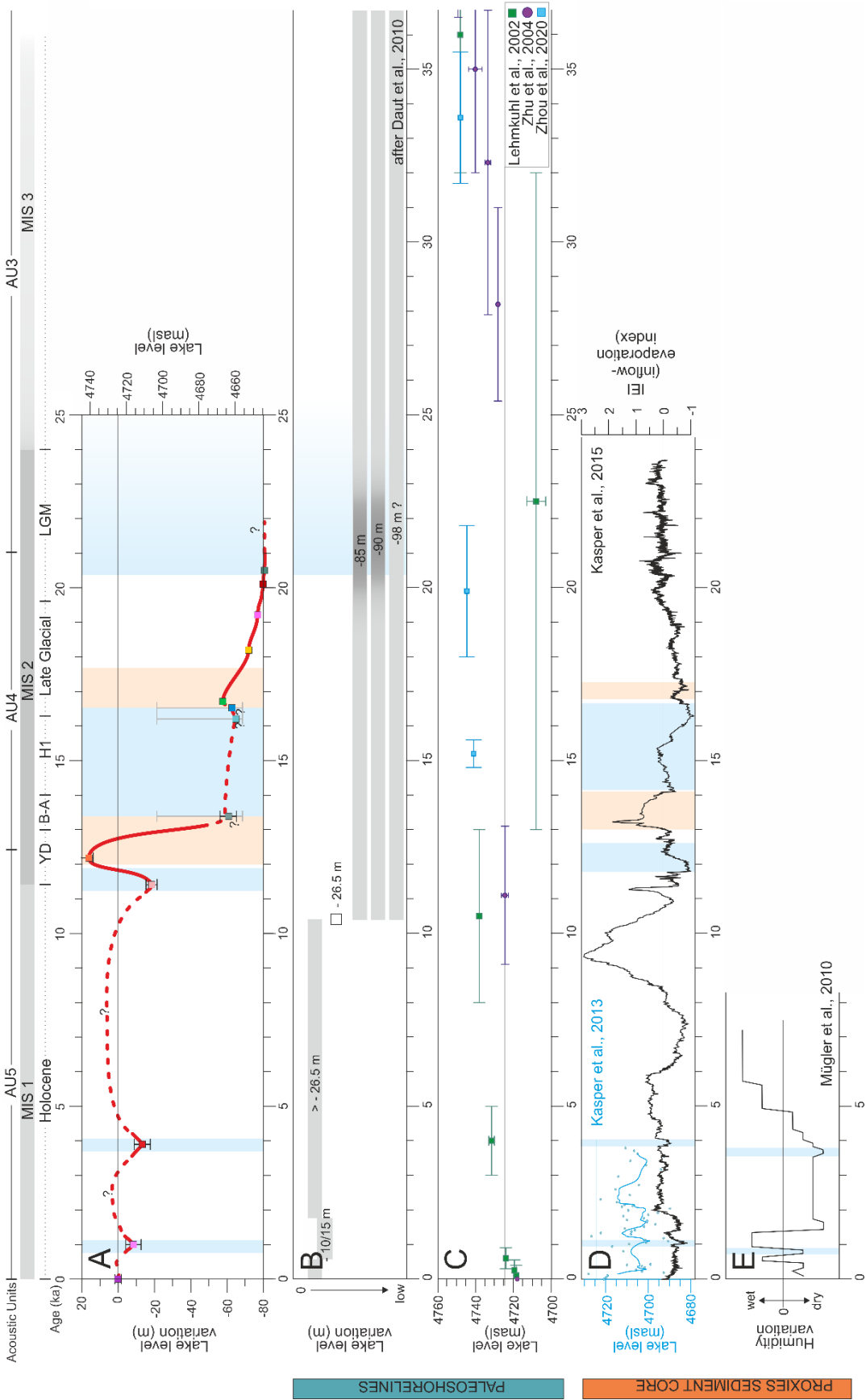


Figure 3.8, part 1: see Figure description next page.

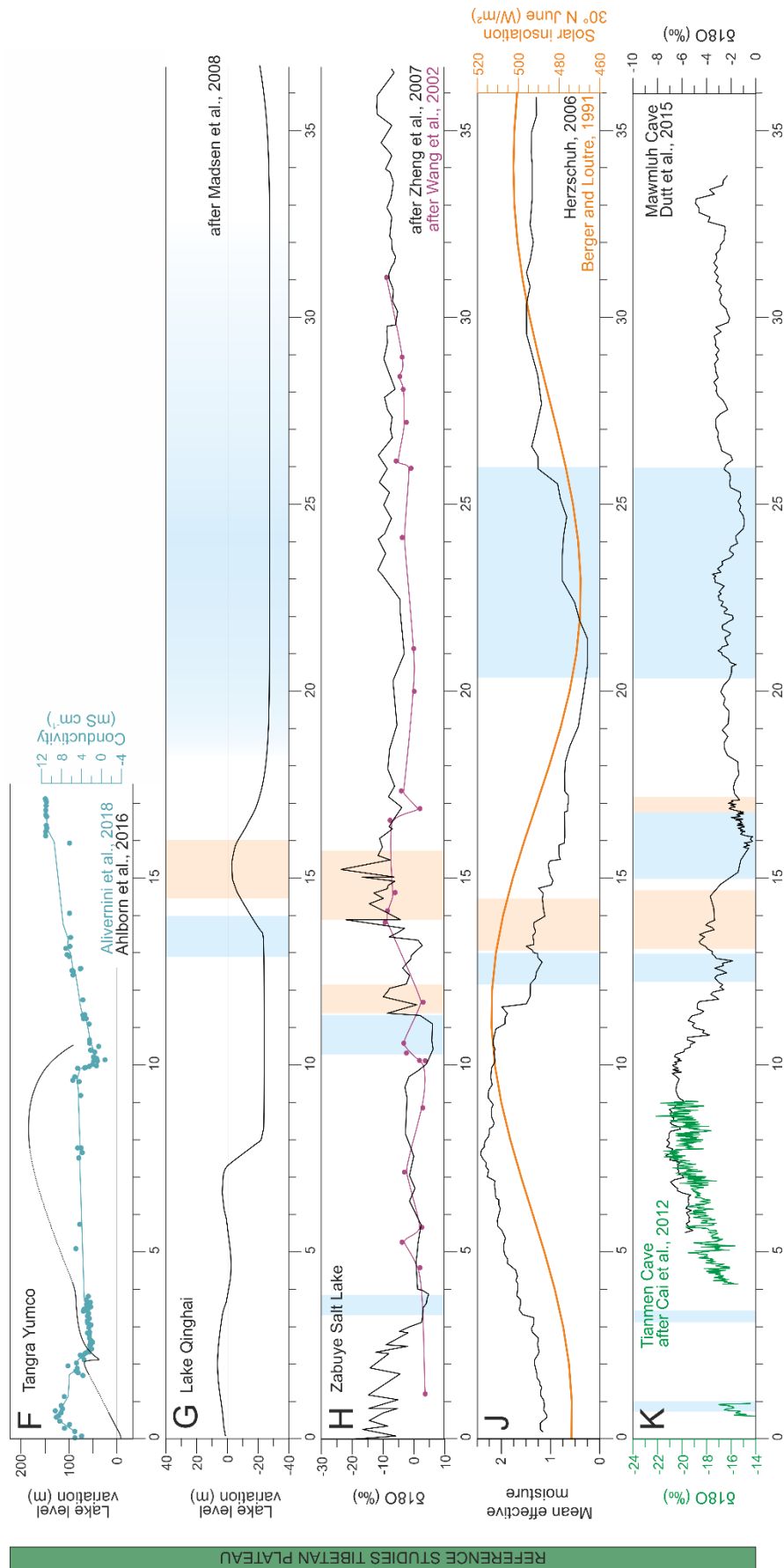


Figure 3.8, part 2: Lake-level reconstruction A) based on seismic reflector analyses relative to the recent high stand situation and (this study); B, C) based on submerged onshore terraces in Lake Nam Co; D, E) based on proxy analysis of sediment cores retrieved in Nam Co; F) based on ostracods and lacustrine deposits from Tangra Yumco; G) based on paleo-shorelines and lacustrine sediments from Lake Qinghai; H) $\delta^{18}O$ reconstruction from Zabuye Salt Lake; J) Solar insolation for 30° N and mean effective moisture curve for the Tibetan Plateau K) $\delta^{18}O$ reconstruction speleothem data from caves in NW India and central Tibet. For the location of lakes and caves, please refer to Figure 3.1.

Ice coverage of the lake is very likely in this period as dropstones occur in the core (Kasper et al., 2015). Neither our acoustic data nor the core sediments imply lake level high stands of +32.5 m (4754 masl; 19.9 ± 1.9 ka) or +16.5 m (4741 masl; 15.2 ± 0.4 ka), as dated by Zhou et al. (2020) (Figure 3.8C). Instead, Nam Co's low lake level and associated cold climate around 16-14 ka BP are supported by several lacustrine records on the TP, e.g., Pumoyum Co (Wang et al., 2016), Tangra Yumco (Günther et al., 2016), or Lake Qinghai (Figure 3.8G) (Ji et al., 2005b). These lakes show a subsequent increase in lake level after 14 ka.

We reconstructed the most significant reflector onlap shift between RVII and RVIII (Figure 3.8A). Consequently, we infer a rapid rise in lake level between 13.4 and 12.2 ka BP. This period correlates with the Bolling-Allerod warming. The sediment onlap of RVIII at 46.1 mbl matches the terrestrial lake terrace at 4737 masl observed by Lehmkuhl et al. (2002) (Figure 3.8C). This supports our assumption of a stable pycnocline, steering sedimentation processes during highstands similar to the modern situation.

AU4 (RIX – RXII) – 12.4 – 0 ka

Our reconstruction infers a similar rapid drop of lake level between 12.2 and 11.4 ka than the rise between 13.4 and 12.2 ka. From RVIII to RIX, the lake level drops by about 35 m. Hence, our lake level curve shows a short and distinct high stand at about 12.2 ka and a low stand at 11.4 ka. The lake-level maxima correlate very well to Sumxi Co and Longmu Co, where Gasse et al. (1991) and Liu et al. (2016) found evidence for a distinct high lake level from 12.8 to 11.3 ka as a reaction of a warm, humid pulse at 12.5 kyrs followed by a short cold and dry condition until 10 ka. The lake level of Siling Co had a low stand from 12 to 10 ka (Gu et al., 1994). Wang et al. (2002) report a severe Younger Dryas (YD) event at 11.5 kyr BP in Zabuye Salt Lake, fitting to our curve. Other authors (e.g., Kasper et al., 2015; Herzsuh, 2006; Dutt et al., 2015; or Dykoski et al., 2005) propose a colder and dryer climate from 13 ka on (Figure 3.8).

AU4 has the lowest relative amplitude and represents high lake level deposition (see 4.5). After the lake level minimum at 11.4 ka, we, therefore, assume a rapid lake level rise (dotted line, Figure 3.8A) and a subsequent comparably high lake level with only minor fluctuations, indicating a relatively long-term (Holocene) stable lacustrine environment. After 10 kyr BP, most lake-level proxy curves (Figure 3.8) trend to their maxima, indicating available moisture and rising lake levels on the TP. This episode is often referred to as the 'Holocene Climate Optimum' (Kotlia et al., 2017). The Lakes Sumxi Co, Tso Kar in the NW, Donggi Cona, Lake Qinghai in the NE, and Siling Co, Tangra Yumco in the center TP had their highest lake levels in the middle Holocene as confirmed by many multiproxy studies (Ahlborn et al., 2016; Alivernini et al., 2018; Avouac et al., 1996; Dietze et al., 2013; Ji et al., 2005a; Shi et al., 2017b; Wünnemann et al., 2010).

The identified reflectors RX and RXI are embedded in AU4 and occur basinwide. Thus, we assume a stable high lake level with fast, short lake-level drops rather than extreme inflow events between the lowstands. The lake level dropped to 79.3 ± 2.7 mbll at 3.9 ka and 74.4 ± 2.4 mbll at 1 ka. Also, the reflectors at 3.9 ka and 1 ka align perfectly with units in core Nam Co 8 (Figure 3.8E) (Mügler et al., 2010), which the authors interpreted as indicators of arid conditions representative for the entire Tibetan Plateau (Mischke & Zhang, 2010; Mügler et al., 2010). According to (Mischke & Zhang, 2010), the cold event around 4.2 ka is stated to be the most widespread climatic cooling over the TP during the Holocene. In Core Nam Co, short, low lake-level events down to 10-15 mbll were observed around 1.5 ka and during the Little Ice Age (Daut et al., 2010).

Analyzing the sediment extent and the thickness distribution of these subunits (Figure 3.5), we infer that the sediment input 3.9 kyrs ago arrived from the tributaries in the west and the eastern sub-basin into the basin. Deposition focused in the northern part of the main basin and a small depocenter east of the scarp feature, striking NW-SE. From 12.2 to 3.9 ka, the total accumulation rate is small, indicating a small discharge from the catchment.

After 3.9 ka, sediment deposition was predominantly sourced from the southern flanks. The total accumulation rate doubled in comparison to the last time slice from 12.2 to 3.9 kyrs. This could be attributed to more erosion in the Nyainqêntanglha Mountain Range due to enhanced glacial melting or more precipitation. Since 1 ka, the main basin has not experienced significant sediment input from the eastern subbasin. Along the southern slope, more material reached the flanks in the west than in the east. Likely, this sediment originated from the drainage of the glaciated areas in the Nyainqêntanglha Mountain Range. The significant increase in the total accumulation rate indicates enhancing meltwater supply through the Holocene.

Taking only the snapshot of the low lake-level events, one could interpret rising lake-levels for the Holocene. These would contradict other local results from Mügler et al. (2010) or Schütt et al. (2010), who report decreasing lake levels for the past 200 years. Instead, our results are evidence of short term lake level variability on millennial scales. This highlights that, e.g., the observed lake terraces do not necessarily imply a continuous decline in water level (Lehmkuhl et al., 2002; Zhou et al., 2020), but that a high-frequency oscillation is more likely (Schütt et al., 2008).

3.6 Conclusion

The investigation of ground-truthed hydro-acoustic data has given us new insights into the sediment distribution processes in Nam Co. The modern sedimentation in the lake basin comprises clayey and silty sediments, creating a very low acoustic amplitude. A detailed facies analysis and reflector tracing on nearly 1400 km of SES profiles revealed a limitation of modern sedimentation

to water depth below 66 m. We inferred that interflows and turbiditic underflows control the modern sediment distribution and transport dissolved material derived by the rivers into the lake basin. The height of a contemporary boundary layer, most likely a pycnocline, steers the prevailing interflows and limits fine sediment deposition to below 66 mbll.

By correlating the SES data to the core logs of NC01/08, we extended our analysis back in time. We identified 13 individual seismic reflectors, assigned with ages reaching back to 20.5 ka. Further, we tested the first-order estimate of a stable boundary layer steering the onset of fine sedimentation over this period.

During the LLGM, the sediment onlaps correlate with paleo beach ridges and indicate an absolute water depth of about 15 m below past lake level. Thus, the lake level was lowest from 20.5 ka until 19.2 ka with about 80 mbll. Deglaciation at Nam Co occurred synchronously with other lakes on the TP and reached 58 mbll at 16.7 ka. For dry paleoclimatic episodes and lower lake levels than today, the parameters for establishing a water column stratification require additional investigation. Thus, the sediment onlaps from 16.5 to 13.4 ka relate to relative lake-level variations between ~60 and ~20 mbll. However, the onlap depths of seismic reflectors at 12.2 ka and during the Holocene correlate with observed paleo-shorelines onshore and fit a stable boundary layer at 66 m water depth. In the Early Holocene, during a general high water level, lake-level drops occurred at 11.4 ka to 18.6 ± 2.99 mbll., at 3.9 ka to 13.4 ± 4.4 mbll, and at 1 ka to 8.5 ± 4.2 mbll. Eventually, our first-order estimate of a stable pycnocline depth for the last 20.5 kyrs is restricted to the high lake-level periods.

Generally, lake-level variations at Nam Co are associated with atmospheric circulation changes. However, we perceive fast variations in lake level between 13.4 ka and 11.4 ka, which are more likely resulting from the interaction of local meltwater and the climate-induced P/E variability. Sediment deposition shifted its focus from the northern part of the basin before 3.9 ka to a modern, very uniform sediment distribution. The significant increase in total accumulation rate during the past 12.2 kyrs emphasizes sediment input growth derived from the Nyainqêntanglha Mountain Range due to enhanced glacier melting.

3.7 Acknowledgements

This study was funded by the German Research Foundation (DFG) (grants SP296/36-1, SP296/36-2, DA 563/3-1), and is part of the ICDP project 'Seismic Pre-Site Survey for ICDP Drilling Locations at Lake Nam Co'. Further funding for data acquisition was provided by the Strategic Priority Research Program of Chinese Academy of Sciences (XDA20070101) and the Chinese Ministry of Science and Technology project (2012FY111400). We are grateful to Schlumberger for

providing the VISTA 2D/3D Seismic Data Processing software package and to IHS for providing the Kingdom Software for seismic interpretation.

Chapter 4:

Climate-induced lake-level variations of the Tibetan lake Nam Co since the Middle Pleistocene – inferred from seismic stratigraphic analysis

Nora Schulze^a, Volkhard Spieß^a, Gerhard Daut^b, Junbo Wang^{cd}, Liping Zhu^{cd}

^a Faculty of Geosciences, University of Bremen, Klagenfurter Strasse 2-4, 28359 Bremen, Germany

^b Friedrich-Schiller-University Jena, Institute of Geography, Physical Geography, Löbdergraben 32, 07743 Jena, Germany

^c Key Laboratory of Tibetan Environment Changes and Land Surface Processes (TEL) /Nam Co Observation and Research Station (NAMORS), Institute of Tibetan Plateau Research, Chinese Academy of Sciences, Beijing 100101, China

^d CAS Center for Excellence in Tibetan Plateau Earth Sciences, Beijing 100101, China

Keyword list: Tibetan Plateau, Age model, Marine Isotope Stages, multichannel reflection seismic, lacustrine sediment, hydro-acoustic

Highlights:

- Seismic stratigraphy based on >860 km high-resolution multichannel profiles
- Cyclic alternation of lacustrine high and low lake-level sediments
- Record over eight glacial-interglacial cycles back to 712 ka
- Moisture availability regulated by the atmospheric circulation steers lake level

4.1 Abstract

The endorheic lake Nam Co is the third largest lake in the central Tibetan Plateau and is located at the modern intersection of Asian Summer Monsoon, Westerlies, and Asian Winter Monsoon air masses. Thus, the lacustrine sediments of Nam Co offer an essential archive in order to assess the extent of climate pattern dynamics in response to past climate change. Here, we introduce a detailed and prime seismic stratigraphy study based on identifying and mapping seismic units down to more than half of the sedimentary infill, utilizing more than 860 km of high resolution multichannel seismic data. In this study, we deduce the depositional environments during dry and wet periods, which aid in understanding the temporal and spatial climatic conditions in the Tibetan Plateau. Our investigations revealed cyclic lacustrine high and low lake level sequences, which correlate with the global glacial cycles. The derived age model indicates the unique record of eight glacial-interglacial cycles back to 712 ka. Significant high or low lake-level stands result from the local

input-evaporation-ratio, which is strongly dependent on the moisture availability regulated by the atmospheric circulation. By comparing the lake-level record of Nam Co with global and supra-regional records, we investigate the importance of precipitation and temperature variability within periods of wet, interglacial, and dry, glacial conditions. We conclude that the hydrology of the Nam Co basin is primarily steered by the precipitation of the Asian Summer monsoon. The local contribution of enhanced meltwater or potentially thawing permafrost is notable during the high amplitude lake-level variation of MIS 5. The lacustrine sediments of Nam Co offer, all in all, an extensive climate archive and a promising prospect for the future ICDP NamCore drilling project.

4.2 Introduction

4.2.1 Paleoclimate reconstructions on the Tibetan Plateau

The Tibetan Plateau (TP) is the highest and largest Plateau on Earth. It is commonly referred to as the 'Third Pole' or the 'Water Tower of Asia' as it comprises an extensive amount of mountain glaciers and constitutes the primary freshwater source for more than one-fifth of the world's population (Immerzeel et al., 2010). The potential vulnerability of current and future water resources is of significant concern to society. This strengthens the importance of investigating the climate evolution on the TP in order to assess the extent of climate pattern dynamics in response to future climate change (Hou et al., 2017; Sun et al., 2015).

The climate of the TP is influenced by a complex interplay of multiple atmospheric circulations including the Asian Summer Monsoon system (ASM), comprehending the East Asian Summer Monsoon (EASM) and the Indian Summer Monsoon (ISM), the subtropical jet stream (i.e., the Westerlies), as well as polar air masses (i.e., winter monsoon) (An et al., 1991; Chen et al., 2008; Zhu et al., 2015). This configuration is steering the geographical and seasonal moisture supply (An et al., 2012; Hou et al., 2017). Remarkably, the ASM precipitation during the summer months provides the main supply to the TP. Hence, the reconstruction of the monsoonal variability and the extent of the monsoonal influence on the TP in the past are of significant interest to enhance climate predictions.

In vicinity to the TP, monsoonal sequences based on wind-proxies in the Arabian Sea (Clemens & Prell, 2003) and the Chinese Loess Plateau (An et al., 1991; Sun et al., 2006, 2015) or based on precipitation-proxies in speleothems (Cai et al., 2012; Cheng et al., 2016a, 2016b) and ice cores (Thompson et al., 2018) have been investigated.

Regardless of the progress in revealing ASM variability on orbital and millennial scales, the paleo-spatial and -temporal extent of the AMS is still under debate (Tang et al., 2017; Wang et al., 2014, 2017).

Lake sediment records from the TP are particularly sensitive to climate variations and provide excellent key climate archives (Street & Grove, 1979). Many deglacial to Holocene lacustrine paleoenvironmental records exist on the TP, proving a close relation of moisture evolution on the TP and lake-level fluctuations (Saini et al., 2017) and a tight coupling between summer insolation and Holocene moisture records (Mayewski et al., 2004). However, it is still unclear whether the precipitation or temperature changes have been dominant features of the observed environmental changes (Saini et al., 2017). Moreover, only a few records from the TP cover several glacial-interglacial cycles. Sediment cores from Salt Lake Zabuye cover the last 128 kyrs (Zheng et al., 2007). In the Tianmen cave, speleothems grew periodically during interglacial stages, allowing precipitation reconstruction of MIS 5 a, c, and e. Scattered terrestrial paleo-shoreline datings have been reported from various lakes. The most ancient lake-level high stands on the TP were dated by Kong et al. (2011) at Lake Tangra Yum Co to 271 ka (+365 m) and Siling Co to 216 ka (+66 m). Other high stands are attributed to MIS 5 or MIS 3 interglacial stages, and a discussion on plateau-wide connected lakes (Zhu et al., 2004) or synchronous respectively asynchronous high stands of single lakes on the TP is ongoing (Jonell et al., 2020; Long et al., 2015; Shi et al., 2017a; Zhang et al., 2020). The modern extent of the monsoonal influence on the TP (Wang et al., 2014) (Figure 4.1) depends on the strength of the monsoonal winds and the position of the Intertropical Convergence Zone (ITCZ) (Cheng et al., 2012; Wang et al., 2014). It is generally accepted that in times of intensified ASM, the influence of the cold and dry Westerlies is weakened, and more humidity from the Indian Ocean trespasses the Himalayas (An et al., 2011), reaching the Tibetan Plateau. The temperature rise during strong summer monsoon leads to an increase in precipitation but at least in the Holocene, not necessarily to an advance of the glacier snowline while increasing meltwater runoff (Schäfer et al., 2002). In general, increased rainfall and melting glaciers are the driving factor for lake waxing on the plateau by shifting the inflow–evaporation ratio to more positive values (Fang, 1991). While some authors state a synchronous climate response of lakes over the TP (e.g., Shi et al., 2001; Yang et al., 2004), other authors see spatial and temporal variations in responses to temperature or precipitation (Kong et al., 2011).

To date, continuous, late Quaternary records from the TP are lacking. Hence, the observed > 680 m of lacustrine sediments in the Nam Co basin promise an extensive climate archive. The endorheic lake Nam Co is the third largest lake in the central Tibetan Plateau and is located at the modern intersection of East Asian, Indian monsoon and cold Westerlies and polar air masses (Figure 4.1). The extent of the air systems are expected to have shifted over Nam Co in the past (Günther et al., 2015; Zhu et al., 2015).

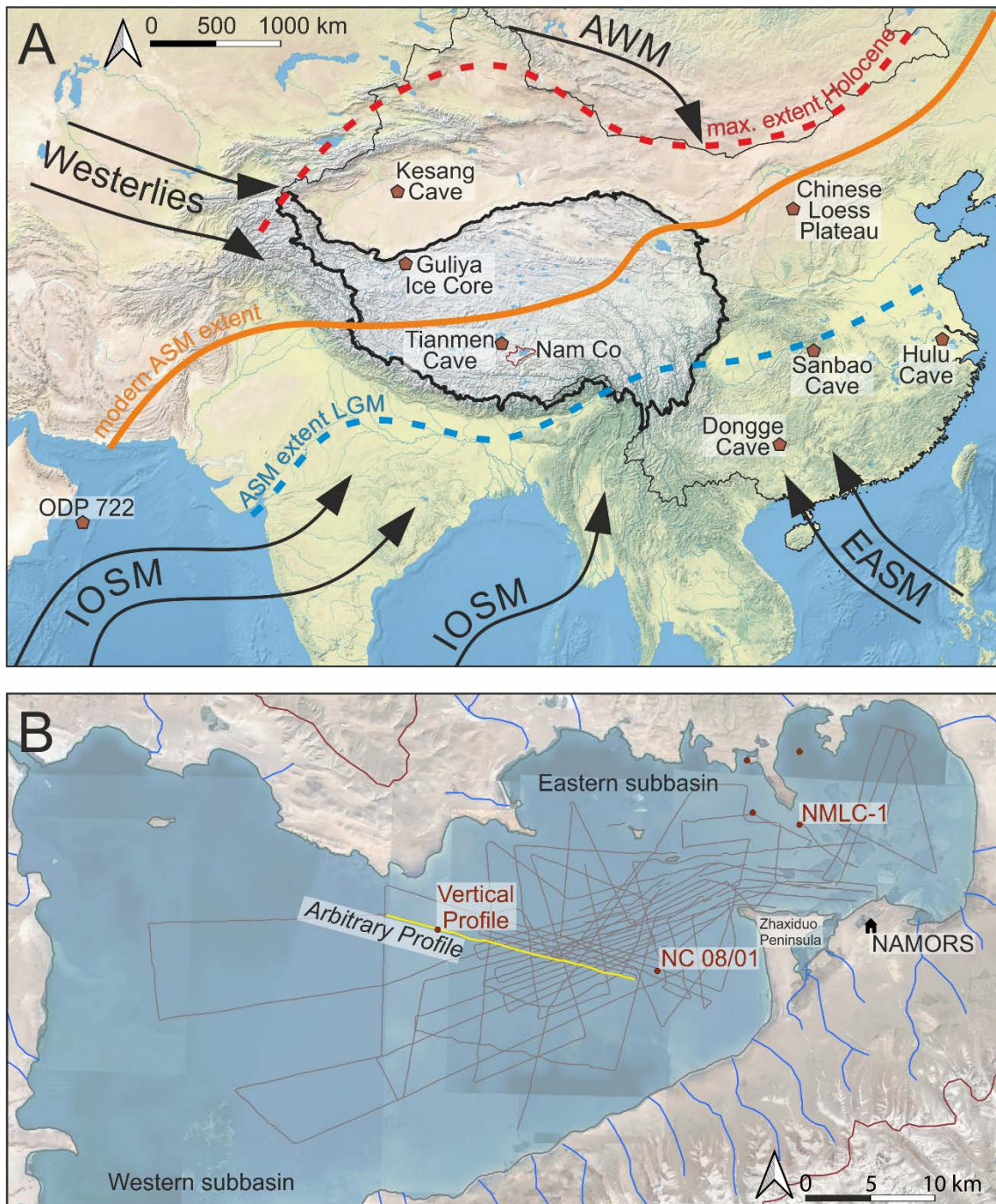


Figure 4.1: A) Location of monsoon records (see text for details); Cave locations indicated speleothem $\delta^{18}\text{O}$ records, the Summer Monsoon Index (Clemens and Prell, 2003) is retrieved from ODP 722 in the Arabian Sea. Influencing atmospheric circulation systems of the Tibetan Plateau are indicated with black arrows, IOSM= Indian Ocean Summer Monsoon, EASM=East Asian Summer Monsoon, AWM= Asian Winter Monsoon. The solid orange line depicts the recent extent of the Asian Summer Monsoon (ASM), the dotted red line the maximal ASM extent during the early to middle Holocene, and the blue dotted line the ASM extent during the Last Glacial Maximum (LGM). B) Multichannel seismic profiles acquired on Lake Nam Co (grey lines) and location of sediment cores of prior studies (Kasper et al., 2015; Doberschütz et al., 2014; Li et al., 2008). The vertical profile (Figure 4.5) and the Arbitrary Profile of GeoB16-393 and GeoB16-446 (yellow line) are highlighted.

This study focuses on high resolution multichannel seismic reflection data to highlight the long and high-resolution climate archive Nam Co offers. We present the seismic stratigraphy and the reconstruction of the relative lake level since the Middle Pleistocene. Moreover, we deduce the depositional environments during the glacial and interglacial periods, which aid in understanding the temporal and spatial climatic conditions on the Tibetan Plateau.

4.2.2 Geologic and climatic setting of the Nam Co region

Nam Co (30°30'–30°35'N, 90°16'–91°50'E) is an endorheic lake on the central Tibetan Plateau north of the Nyainqêntanglha Mountain Range at an altitude of 4718 m above sea level (masl) (Figure 4.1). The modern lake covers an area of ~2,026 km² (in 2010) (Zhang et al., 2014) and reaches a maximum water depth of 98 m. The lake volume was calculated by Huang et al. (2017) to be about 86.4 km³ for 2004. More than 60 streams feed the lake from all sides, with most input from the southern and eastern mountain chains. The total catchment area is ~10,680 km² (Zhou et al., 2013). The surrounding terrain consists of Permian to Cretaceous sedimentary and ultramafic intrusive rocks and Tertiary granites (Keil et al., 2010, and references therein). Deposits near the lakeshore are composed of unconsolidated Pleistocene to Holocene sediments of glacial, glaciofluvial, and fluvial origin (Schütt et al., 2008). Also, lacustrine and aeolian sediments occur within the catchment (Doberschütz et al., 2014; Lehmkuhl et al., 2002). Glacial geomorphological studies by Schütt et al. (2008) found inundated moraines of MIS 2 or 4 in the southwest of Nam Co. In the southeast, glacial remains have not reached the lake (Lehmkuhl et al., 2002). The Nam Co region is dominated by an arid to semi-arid continental climate and a mean annual temperature of about 0°C (Wang et al., 2019). Annual evaporation from the lake surface is challenging to assess, and values vary from 635 mm to 832±59 mm (Lazhu et al., 2016; Ma et al., 2016). The yearly precipitation is approximately 450 mm (Wang et al., 2019), with 90% of the rain falling during the summer monsoon season from May to September (Huang et al., 2017). During monsoon season, mainly southern wind directions are recorded, while westerly winds prevail from January to May (Keil et al., 2010). The annual mean wind speed is 4 m/s (Wang et al., 2019). The strongest winds occur during wintertime with 45 storm days of > 32 m/s wind speed (Keil et al., 2010).

4.2.3 Research results on Nam Co's lake-level variation

The inflow (precipitation and meltwater) to evaporation (I/E) ratio is steering the response of Nam Co's lake level (Kasper et al., 2015). Modern water balance observations show that runoff from unglaciated areas accounts for 55–65% of the total water input, whereas direct precipitation accounts for 23–28% and meltwater inflow for 7–22% (Zhou et al., 2013). Modeling results from Biskop et al. (2015) for the period from 2001 to 2010 indicate that the relative contribution of glacier

runoff plays a relatively minor role. In contrast, according to Zhou et al. (2013), meltwater runoff changes have the most substantial impact on the lake level variations on long time scales.

Sediments covering the past 24,000 years have been recovered in the 10.4 m long piston core NC08/01 retrieved in the center of the western subbasin of Nam Co (Figure 4.1). Sedimentation rates (SR) between 0.13 mm/yr for the Holocene and ~2.4 mm/yr for the early glacial have been measured (Kasper et al., 2015; Doberschütz et al., 2014). Changes in sedimentation patterns correlate to lake level variations in the past 20.5 kyrs (see Chapter 3). Core information on the history of the lake older than 24 ka is lacking.

Ages and heights of Late Pleistocene shoreline deposits have been documented around Nam Co partially contradictory. With respect to the present lake level (4824.5 masl), Zhu et al. (2004) propose a lake level high stand of 136 m (4860 masl) 115.9±12.1 ka (MIS 5e) ago. This was refuted by Kong et al. (2011), who state that lacustrine deposits occur clearly below 4750 masl. At 4750 m, the Nam Co discharges to small lakes in the NW and then to Siling Co (Kong et al., 2011). The authors dated lacustrine pebbles from 4740 masl to 53-36 ka (MIS 3). Lehmkuhl et al. (2002) propose a high stand of about 24 m (4748 masl) between 32 and 40 ka. The latest research by Zhou et al. (2020) dates a bedrock terrace at 4751 masl to 81.5±9 ka (MIS 5a) and a terrace at 4747 masl to a period from 29 to 57 ka (MIS 3).

4.3 Methods

4.3.1 Acquisition and processing of MCS data

In total, 89 high-resolution seismic profiles with a combined length of over 860 km were obtained in June/July 2016 using a Sercel air gun (in Mirco mode setting with 0.1 l volume, 250 Hz main frequency) and a 32 channel streamer with 2-meter channel spacing. This data accompanies ~160 km of single and multichannel data from a prior survey in 2014. The multichannel seismic surveys have been jointly carried out by the Universities of Bremen and Jena and the Institute of Tibetan Plateau Research - Chinese Academy of Sciences. All seismic profiles were digitally recorded in SEG-Y format and processed in Vista™ software by Schlumberger. Processing included: trace editing, geometry, binning, bandpass filtering, CMP-sorting, interactive velocity analysis, multiple suppression using SRME, normal move-out correction, time-variant surface consistent scaling, stacking, and time-migration. Bin distance is 1 m, which defines the maximal horizontal resolution. Defined by the main frequency of the source, the data's vertical resolution is ~2 m.

4.3.2 Interpretation procedures of MCS data

We performed the seismic interpretation, including horizon and fault management and gridding, within the IHS Kingdom Suite 2016/2019 software packages. Thickness values calculated with IHS Kingdom Suite are apparent thickness values based on the subtraction of two gridded reflector maps in two way travel time (TWT). However, the discrepancy of apparent to true thickness due to inclined horizons by faulting is considered negligible. Gridding was performed for 10x10 m cells using a flex gridding algorithm. We defined fault polygons for each unit before creating horizon and thickness maps in order to prevent miscalculated thicknesses at faults.

The MCS dataset is converted from TWT to depth by a constant velocity of 1460 ms⁻¹ for the water column and an average velocity of 1600 ms⁻¹ for sediments.

We created a super-gather amplitude curve (Figure 4.5A) by stacking the envelope (absolute) amplitude data of ten neighboring common midpoints (CMPs) at a representative location (90° 36' 21" E, 30° 45' 54" N; Figure 4.1). The amplitude curve was smoothed by a running average of 4 ms for reasons of presentation.

4.4 Results

4.4.1 Perceptions from Multichannel seismic data

Multichannel seismic surveys conducted in 2014 and 2016 prove the existence of more than 680 meters of sedimentary deposits as the mostly undisturbed layers with continuous sedimentation allowed a signal penetration of >1 s TWT (Figure 4.2A). All MCS profiles show a cyclic alternation of high and low reflection amplitudes throughout the record (Figure 4.2A). The sediments are disrupted by faulting, especially in the western basin (Figure 4.2B). The faults are not penetrating the most recent deposits.

In the 2016 MCS data, we detected acoustic basement reflectors (Figure 4.2B). By using adapted low-frequency processing (see methods), we were able to amplify reflections at greater depth that are partially overprinted by multiple energy (Figure 4.2B).

Moreover, we confirmed two subbasins in the Nam Co basin morphology proposed by Daut et al. (2010). A tectonic sill trending NW-SE, from a small peninsula in the NW to the Zhaxiduo Peninsula, separates the lake basin into the eastern and the western subbasins (Figure 4.1) (Chapter 5). In this study, we focus on the western subbasin.

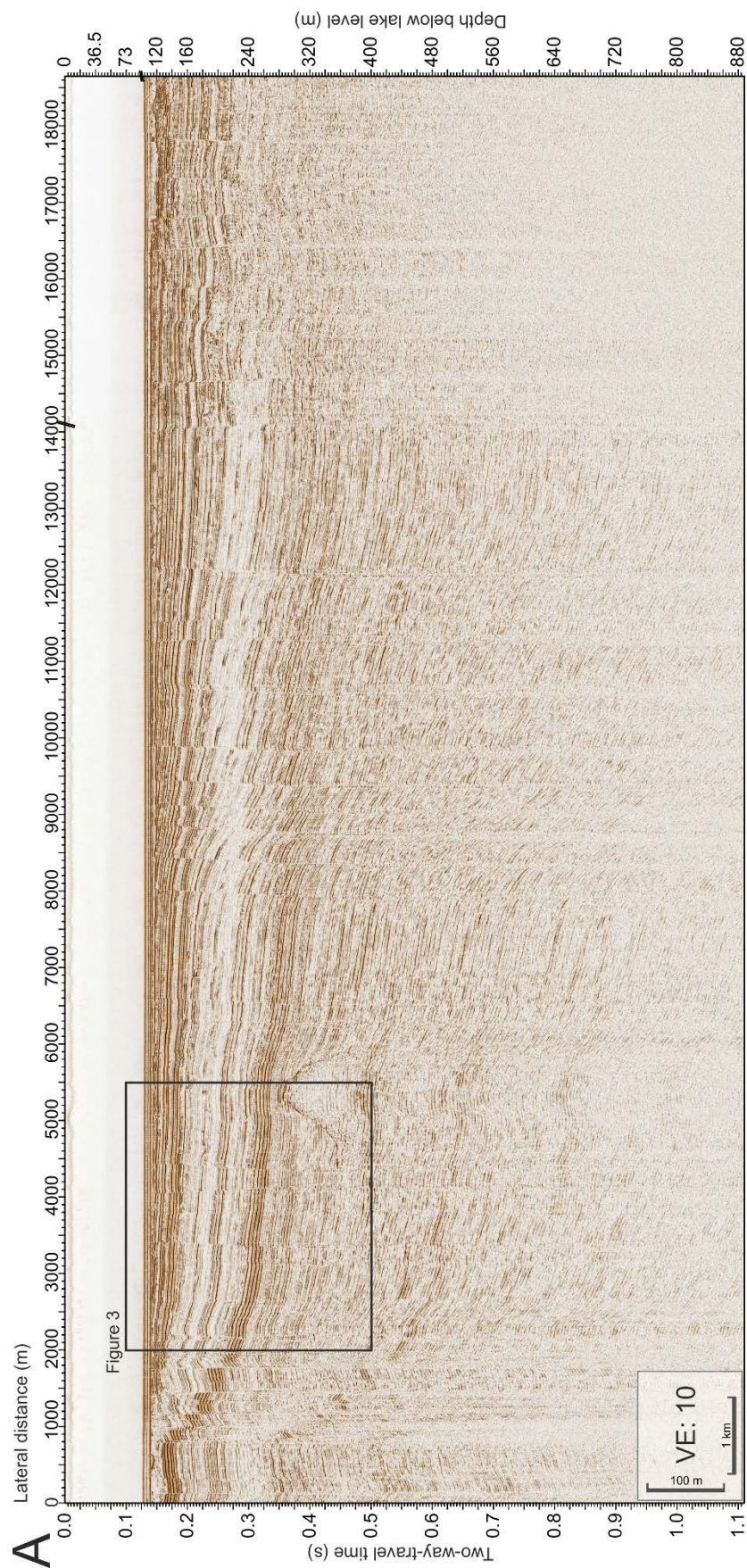


Figure 4.2 A: Arbitrary Line of Seismic Profiles GeoB16-393 and GeoB16-446. Time depth conversion in water column with 1460m/s and in sediment with 1600m/s.

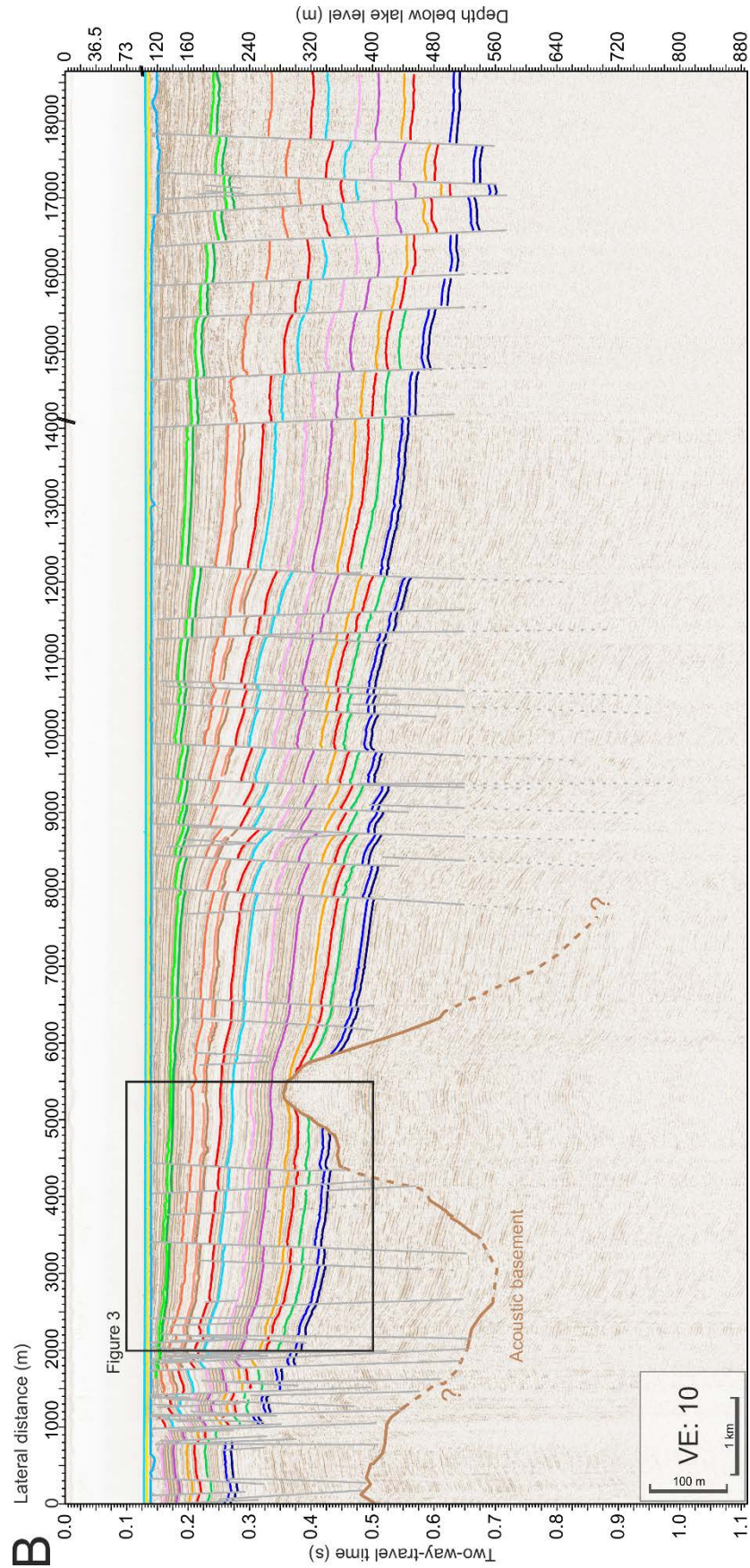


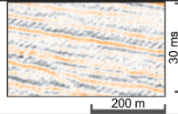
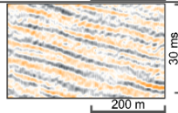
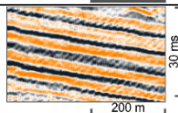
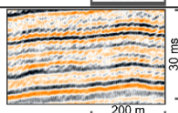
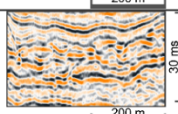
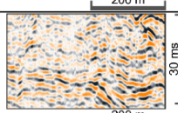
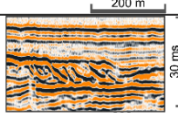
Figure 4.2B: Accoring Line drawing of the arbitrary seismic profile. Time depth conversion in water column with 1460m/s and in sediment with 1600m/s.

4.4.2 Seismic stratigraphy

Four main seismic facies (Table 4.1) occur in the MCS dataset. Following the seismic-stratigraphic interpretation techniques described by Mitchum Jr et al. (1977), we assigned these seismic facies using reflection amplitude, frequency, continuity, and configuration (Table 4.1). As a result of this seismic facies classification, we define 17 seismic units (SU1-17) (Figure 4.3). The seismic reflectors (SR0 to 17) are designated boundaries of the interpreted seismic units (Figure 4.3).

4.4.2.1 Seismic Facies

Table 4.1: Seismic facies recognized in the 2D seismic data set. Data examples taken from Profile GeoB16-393. Scale and vertical exaggeration of 10 applies for all examples.

Seismic facies (SF)	Reflection amplitude	Reflection frequency	Reflection continuity	Reflection configuration	Example of MCS dataset
SF1a	low	low	parallel continuous	even parallel	
SF1b	medium to low	medium high	parallel continuous	even to wavy parallel	
SF2a	high	high	parallel continuous	even parallel	
SF2b	medium to high	medium low	parallel continuous	even to wavy parallel	
SF3a	medium to high	varying	discontinuous	hummocky	
SF3b	medium to low	varying	discontinuous	chaotic	
SF4	medium to high	medium high	semi continuous	prograding oblique	

SF1a is characterized by low amplitude reflections. Reflection frequency is low, and the reflections are continuous and even parallel.

SF1b is characterized by medium-low amplitude reflections. Reflection frequency is medium to high, and the reflections are well-stratified, continuous, and even parallel to wavy parallel.

SF2a is characterized by high amplitude reflections. Reflection frequency is high, and the reflections are well-stratified, continuous, and even parallel.

SF2b is characterized by medium-high amplitude reflections. Reflection frequency is medium to low, and the reflections are well-stratified, continuous, and even parallel to wavy parallel.

SF3 is characterized by discontinuous reflections and a varying reflection frequency. SF3a has medium to high amplitudes, and the internal reflection configuration is hummocky. SF3b has medium to low amplitudes, and the internal reflection configuration is hummocky to chaotic.

SF4 is characterized by medium to high amplitude reflections. Reflection frequency is medium to high. The reflections are semi-continuous, and the internal reflection configuration is stratified and parallel. The external form is oblique- or complex- obliquely-shaped.

4.4.2.2 Seismic Units and Reflectors

The seismic units were identified and defined within the western basin. An NW-SE-striking tectonic zone prevents the validation of continuous seismic units between the western and the eastern basin. Except for the bedrock reflector (SR0) and the youngest reflectors (SR15 to SR17), all reflectors are disrupted by faults (e.g., Figure 4.2).

SR0 represents the top of the acoustic basement (Figure 4.3B). By adapted low-frequency processing, we could identify a bedrock reflector close to the northern shore of the western basin of the lake. Signal penetration below the bedrock reflector is diminished. The unit beneath SR0 has no internal structure, and the acoustic facies appears transparent in the low-frequency seismic images. However, the energy of multiples overprints the facies. The basement has a significant topography. In the NW of the basin, SR0 dips with an angle of $\sim 13^\circ$ steeply towards the center (Figure 4.2B), indicating the bedrock at greater depth. In the south of the basin, we could not identify any bedrock reflectors.

SU1 includes all sediments above the acoustic basement (SR0) to the first continuous reflector (SR1). Multiple reflections superimpose real reflections, which constrains the seismic facies classification. The top of SU1 (SR1), however, onlaps topographic bedrock highs (Figure 4.3). As the bedrock inhabits significant topography, this unit varies significantly in thickness, with sections up to 380 m thick.

SU2 lies conformal on SU1. The unit is built up by SF1b. On the survey profiles covering the NW part of the lake, the unit top (SR2) and internal facies are recognized straightforward, while in the center, multiple energy masks the internal structure of SU2 at depth. SU 2 is about 10 ± 2 m thick.

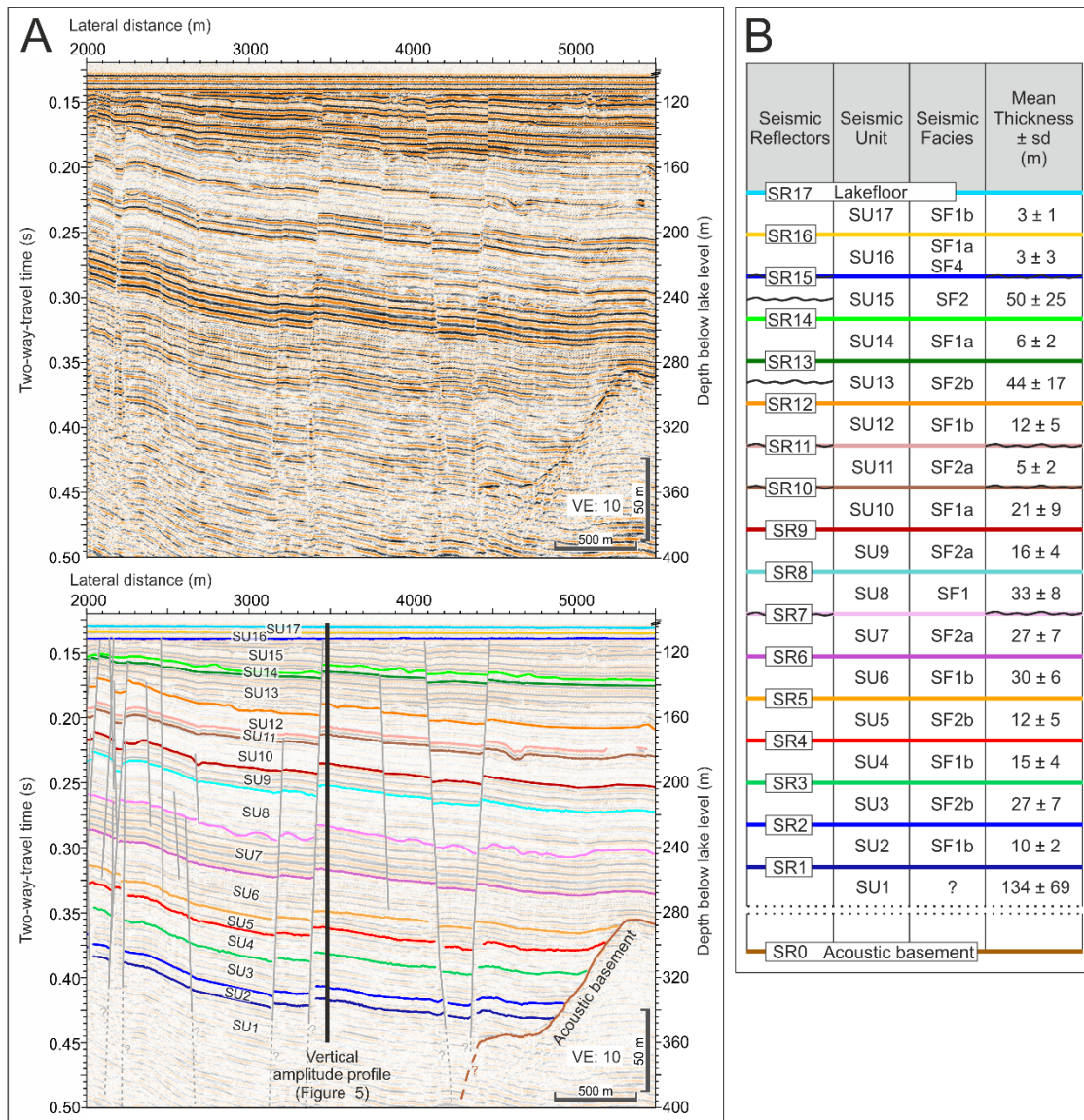


Figure 4.3: Seismic-based unit definition. A) Example of MCS Data of Profile NamCo16-393 (zoom as shown in Figure 4.2) and corresponding line drawing, showing all identified seismic reflectors (colored horizons) and seismic units (SU); B) Table of all seismic reflectors (SR), seismic units (SU), attributes seismic facies (SF), and the mean thickness and standard deviation for each SU.

SU3 lies conformal on SU2. The unit is built up by SF2b. SU3 shows a thickness gradient with 20 m thickness in the north and around 30 m thickness in the western center of the basin. On average, SU3 is 27 ± 7 m thick.

SU4 lies conformal on SU3. The unit is built up by SF1b. SU4 is very uniform and about 15 ± 4 m thick.

SU5 lies conformal on SU4. The unit is built up by SF2b. SU5 is very uniform and about 12 ± 5 m thick.

SU6 lies conformal on SU5. The unit is built up by SF1b. From N to S, SU6 shows a slight thickness gradient from 25 to 35 m. On average, SU6 is about 30 ± 6 m thick.

SU7 lies conformal on SU6. The unit is built up by SF2a. The top of SU7 (SR7) shows local unconformities, indicating a truncation of underlying reflectors. The most prominent truncation in the NW and northern center of the basin show a maximum of 4 m of erosion within limited extents. On average, SU7 is 27 ± 7 m thick.

SU8 lies mostly conformal on SU7. Exceptions are the unconformities of SR7, especially in the NW and northern center of the basin. The unit is built up by SF1b. A noticeable transition into SF1a occurs for the upper third of the unit. SU8 is about 33 ± 8 m thick.

SU9 lies conformal on SU8. The unit is built up by SF2a. SU9 is uniform and about 16 ± 4 m thick.

SU10 lies conformal on SU9. The unit is built up by SF1a. The top of SU10 (SR10) shows local minor unconformities, resulting in a stronger reflector but not necessarily an erosional truncation. Towards the East, SR10 is conformal to SR9 and not continuously traceable. SU10 shows an increasing thickness trend from 10 to 30 m towards the center of the basin. On average, SU10 is 21 ± 9 m thick.

SU11 lies unconformably on SU10. The unit is built up by SF2b. The top of SU11 (SR12) behaves similarly to SR11, also showing local minor unconformities. On average, SU11 is 5 ± 2 m thick.

SU12 lies conformal on SU11 towards the E, while for the rest of the basin, SU12 rests on the minor unconformity of SR11. The unit is built up by SF1b. SU12 is about 12 ± 5 m thick.

SU13 lies conformal on SU12. The unit is built up by SF2a. Internally an uncontinuous and unconformable reflector occurs. This unconformity shows local erosional truncations in the western center of the basin of a maximum of 18 m. The unconformity created a strong reflector in some areas. Sediments directly beneath the unconformity appear hummocky in their reflection geometry. SU13 inhabits a significant thickness gradient towards the E, with thickness increasing by 40m. On average, SU13 is 44 ± 17 m thick.

SU14 lies conformal on SU13. The unit is built up by SF1a. SU14 is very uniform, with a thickness of 6 ± 2 m.

SU15 lies conformal on SU14. The unit is built up by a mixture of SF2a, SF2b, SF1b, and two internal uncontinuous and unconformable reflectors. The first unconformity indicates local erosional truncations of maximal 8 m in the eastern center of the basin. In the west, the reflector lies conformably above SR14. The sediments below the unconformity have a greater reflection amplitude, while the overlying sediments can be attributed to SF1b. The second unconformity is restricted to the eastern center of the basin. The sediments below the unconformity are even parallel and can be attributed to alternations of SF1b and SF2b. Above the unconformity, the facies shifts to high amplitude facies SF2a and the hummocky geometry of SF3a. Local erosional truncations are

limited vertically to a few meters. The top of SU15 (SR15) is truncating SU15 and expresses an irregular, high amplitude reflector. SU15 inhabits a significant thickness gradient towards the East, with thicknesses increasing by 80 m. On average, SU15 is 50 ± 25 m thick.

SU16 rests unconformably on SU15. In the west, the bottom reflector (SR15) is parallel to the lake floor, while in the eastern center of the basin, SR15 truncates SU15 by up to 20 m. Sediments of SF4 and SF1 infill the incisions. SF1 is also found in the rest of the basin. The top of SU16 (SR16) is parallel to the lake floor. On average, SU16 is 3 ± 3 m thick.

SU17 lies conformal on SU16. The unit is built up by SF1a. SU17 is a very uniform unit with a thickness of 3 ± 1 m.

4.4.2.3 Seismic reflectivity and sedimentation rates

The integration of Core NC08/01 with the MCS data showed that the reflectivity changes in the acoustic data coincide with variations in grain size and sedimentation rate at the core location (Chapter 3). Low seismic reflectivity of SU17 in the MCS data correlates with a low sedimentation rate of 0.2 mm/yr, descriptive for the Holocene (approximately MIS 1). High seismic reflectivity in the MCS also correlates with higher sedimentation rates at the core location. However, Core NC08/01 (see Figure 4.1) is situated in an infilled erosional structure of SR15. Sedimentation rates for sediments older than the LGM may be biased by focused deposition. Therefore, the sedimentation rates at the core location corresponding to SU16 are not representative of the entire basin.

4.5 Interpretation and Discussion

4.5.1 Depositional environments of seismic facies

All seismic profiles investigated in this study highlight cyclic changes in reflectivity. Variations in reflection amplitude and continuity of hydro-acoustic data usually correlate directly to variations in lithology and energy level during deposition (Veeken, 2006). The primary sediment source of Nam Co remains constant through time, and the widespread, continuous character of the reflections indicates deposition in a continuously lacustrine environment. Thus, reflection variations must be linked to changes in grain size and sedimentation rate. The deposited grain sizes, in turn, result from changes in the transportation processes as the shoreline shifted from high to low lake level stands and vice versa and from the sediment availability (Ju et al., 2012) (see Chapter 3).

Low amplitude seismic facies indicate sediment deposition in a low-energy lacustrine environment (Figure 4.4A) (Wu et al., 2006; Xiao et al., 2013). Therefore, SF1 links to fine-grained sediments, which typically deposit with uniform thickness over large areas during high lake levels.

High amplitude seismic facies, however, deposit in a high-energy lacustrine environment (Wu et al., 2006; Xiao et al., 2013). Therefore, SF2 indicates coarser material, which deposits subsequent to a short transport in the lake and hence, proximate to the shoreline during a lake level low stand (Figure 4.4B).

Based on the connection of low amplitude seismic facies to low energy depositional environment, we interpret all SUs of SF1 as high lake level sediment, deposited under quiet conditions with sediment sources far away from the basin center. Vice versa, we interpret all SUs of SF2 as low lake-level sediments, deposited under high energy conditions with sediment sources close to the basin center.

While some studies found a positive correlation of grain size and precipitation (e.g., Peng et al., 2005; Zhang et al., 2003) or grain size and temperature (Ju et al., 2012), we agree with Wan et al. (2004) that these correlations occur on short time scales (years to decades) and grain size-lake-level-correlations are representative on millennial time scales.

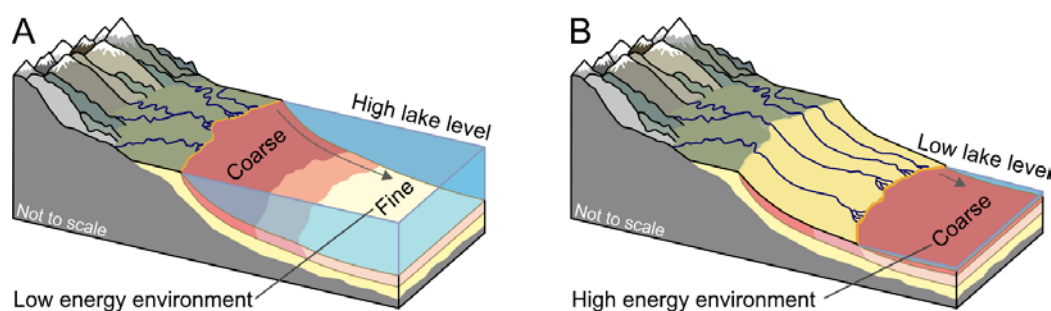


Figure 4.4: Sketch of depositional environments of seismic facies. A) high lake-level scenario with grain size sorting towards the basin along a long transport path (arrow). B) Low lake-level scenario with deposition of coarse sediment in the center of the basin along a short transport path (arrow).

The acoustic characteristics of SF 3 are typical for fluvial or mass-transport deposits, which may form by mechanisms such as slide/slumps or debris flows (Mitchum Jr et al., 1977).

SF4 inhabits the geometry of prograding sediments or point bars. We attribute SF4 to fluvial channel migration or delta-deposits (Mitchum Jr et al., 1977) in a shallow lacustrine setting.

4.5.2 Chronology of relative lake-level variations

4.5.2.1 Relative lake level

The demonstrated connection of seismic reflectivity and lake level stands provides the unique tool to reconstruct relative lake level changes at Nam Co. We reconstructed a relative lake-level curve based on the envelope reflection amplitude at a location on Profile GeoB16-393 (90° 36' 21.72" E 30° 45' 54.33" N) (see Figure 4.1 for location, Figure 4.3 for vertical profile on

MCS). At this location, the facies are very distinctive for all units below SR15 due to limited multiple energy overprint and are, hence, representative for the entire lake. The generated envelope amplitude curve (Figure 4.5, A) shows small scale amplitude variations throughout the section and within units, while significant amplitude variations appear at the interpreted seismic unit boundaries (SFs, colored diamonds, Figure 4.5).

4.5.2.2 Age correlation

To ascertain a chronology of Nam Co's sediments, we correlate the relative lake level curve with the global $\delta^{18}\text{O}$ record of benthic foraminifera (LR04) (Lisiecki & Raymo, 2005). The $\delta^{18}\text{O}$ record itself represents changes in global ice volume, temperature, and salinity (Lisiecki & Raymo, 2005). Strong coupling between winter and summer monsoon and ice volume changes has been demonstrated by the high correlation between loess grain size and speleothem $\delta^{18}\text{O}$ changes with the LR04 record (e. g. Sun et al., 2015; Porter and An, 1995; Cheng et al., 2009). Thus, the ages of the glacial terminations and interglacial-glacial transitions, inferred from the benthic $\delta^{18}\text{O}$, provide adequate time controls (Sun et al., 2015). This further allows a comparison of the local Nam Co record to the established global record of climatic conditions, including temperature and sea level (see 4.5.3.2).

For the correlation, we proceed in two steps.

As the transitions from low to a high lake level environment are particularly pronounced (e.g., SR2, 6, or 10), we correlate these quick changes to the rapid transitions from glacial to interglacial periods of the global $\delta^{18}\text{O}$ record (Figure 4.5A, black connecting lines).

The first step of the correlation based on nine tie points (Figure 4.5A, black connecting lines) highlights a timeframe back to MIS 17/18. Using the ages of the glacial-interglacial transition of the $\delta^{18}\text{O}$ record and the thicknesses of the seismic units, we calculated linear sedimentation rates (LSR) for each full glacial-interglacial cycle (Figure 4.5B).

This results in LSRs around 0.52 mm/yr for the cycles: MIS17&16, MIS 13&12, MIS 11&10, MIS 7&6, and MIS 2 to 5. Two cycles, MIS 15&14 and MIS 9&8, show lower rates of 0.3 mm/yr. As, globally, MIS 14 and MIS 8 are both less distinct glacial periods, an LSR of ~0.52 mm/yr is a representative value for a 'standard' glacial cycle at Nam Co. The uniform LSRs indicate that the conditions for the entire cycles (except for MIS 14 and 8) and the ratio of interglacial to glacial period are constant through the last ~712 kyrs.

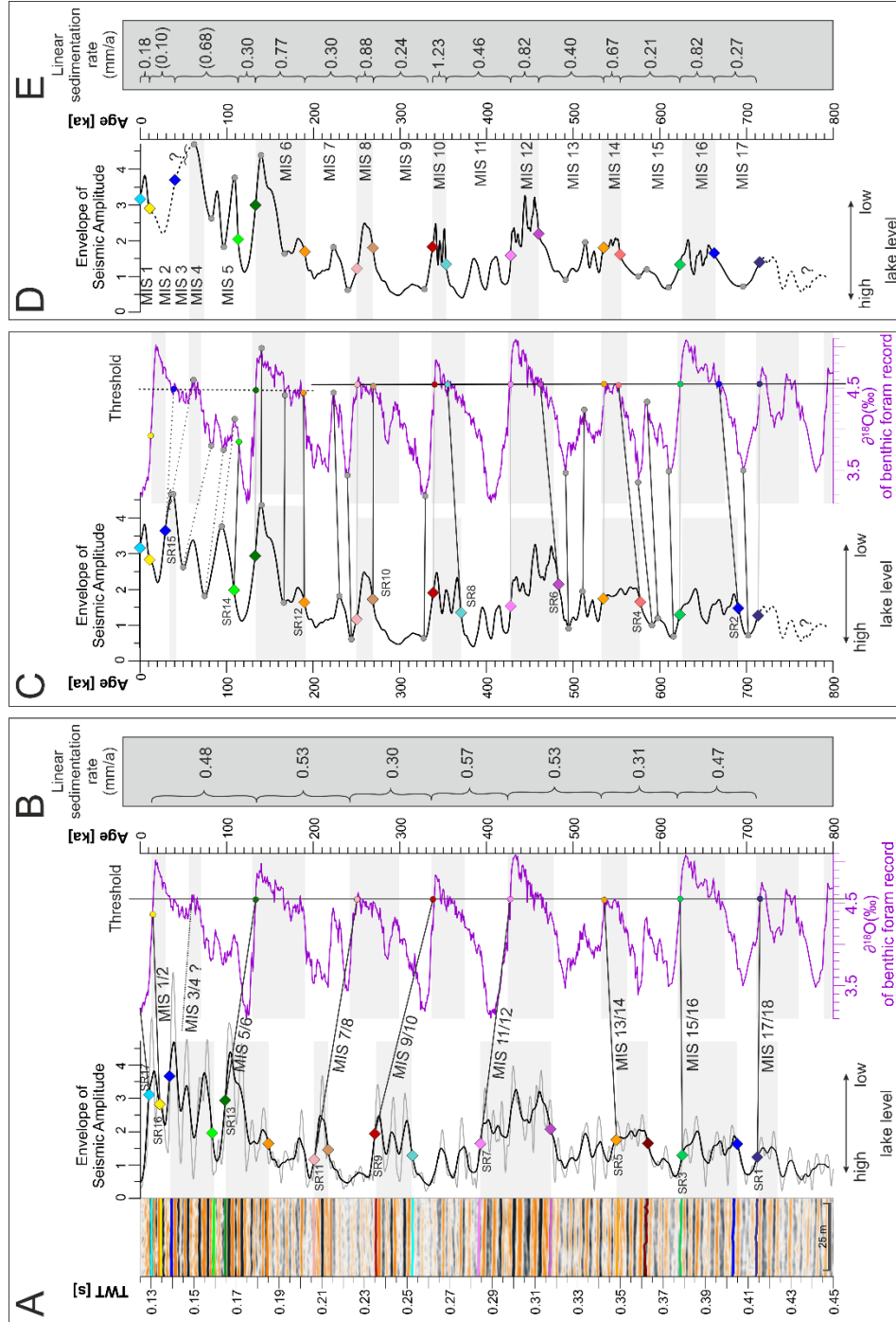


Figure 4.5: Correlation of the envelope amplitude curve representing lake-level variations, with the global $\delta^{18}O$ record of benthic foraminifera (purple) (Lisiecki & Raymo, 2005). For simplicity, the 4ms-running-average (black) of the envelope amplitude curve (grey) is shown; A) First Step: Correlation of the glacial-interglacial transitions (odd-numbered SR1-13 and SR16, colored diamonds); B) Linear sedimentation rates (LSR) of full glacial cycles; C) Second Step: Correlation of the interglacial-glacial transitions based on a threshold value of 4.55‰ (even-numbered SR2-14, colored diamonds) and the correlation of additional markers (grey dots); D) Final age-corrected envelope amplitude curve; E) Linear sedimentation rates (LSR) of the glacial and interglacial periods.

The LR04 record holds a 'saw-tooth'-shape, displaying the sharp side at the transition from glacial to interglacial stage. The fast variation occurs from 4.55 ‰ to 4.05 ‰ $\delta^{18}\text{O}$ for each glacial-interglacial transition. As the glacial stages 14 and 8 are expressed weakly in the seismic data, we chose a threshold at the upper range of 4.55 ‰ for the second step of the age correlation (Figure 4.5A). The intersections with the $\delta^{18}\text{O}$ curve are assigned to the transitions from interglacial to glacial period (Figure 4.5C). The age correlation is further supported by additional data points at distinct curve minima or maxima (grey dots, Figure 4.5C), resulting in 31 tie points overall. The correlation of SR15 bears a challenge. The horizon is not penetrated by Core NC08/01 and must therefore be older than 24 ka. This discloses a hiatus (wavy line, Figure 4.6), with sediments of MIS 3 & 4 possibly missing in the lake record at the location of the vertical section.

The result of the second age correlation (Figure 4.5D) emphasizes that the cyclic changes of lake level are correlating well to the global record of $\delta^{18}\text{O}$. Consequently, we identify 17 marine isotope stages corresponding to our interpreted seismic units. The oldest interpreted reflector, SR1, is about 712 kyr old. This results in an average LSR of 0.5 mm/yr for the interpreted section. Considering that SU1 is, on average, 134 ± 69 m (max. 350 m) thick, the entire lacustrine record down to the bedrock, however, might span more than 1 Ma.

4.5.3 Sedimentary responses to climate forcing

4.5.3.1 Linear sedimentations rates

The calculated linear sedimentation rates between 0.1 and 1.23 mm/yr are comparable to the low LSRs <1 mm/yr of other high altitude lakes on the TP (Wang et al., 2015b). It is prominent in our data that the LSRs of glacial periods are, in general, 2 to 3 times larger than the LSR of interglacial periods (Figure 4.5E). The results from the sediment cores taken in Nam Co confirm this observation for the youngest glacial cycle (e.g., core NMCL-1; Li et al., 2008). The sediment core NC08/01 defines low sedimentation rates for the 2.5 m thick Holocene silt-sized sediments with an LSR of 0.2 mm/yr (Doberschütz et al., 2014), while sediment of the late glacial have an LSR of about 0.7 mm/yr (Kasper et al., 2015). Hence, glacier meltwater contributes to a high proportion of suspended allochthonous sediments to the lake (Doberschütz et al., 2014). Also, the observation of higher LSR during dry glacial periods than during interglacial periods at Nam Co fits to records from sediment cores outside the TP, e.g., from Lake Xingkai in NE China (Long et al., 2015) and assorts a supra-regional reduction of lake extents during glacial stages.

4.5.3.2 Global atmospheric circulation and local responses

Overall, we recognize eight glacial-interglacial cycles in the lacustrine deposits (Figure 4.5A). The lake-level curve perfectly resembles the glacial-interglacial transitions as represented in the

benthic LR04 curve. The choice of a threshold of 4.55‰ for the interglacial-glacial transitions agrees with An et al. (2011), who accentuate that the ASM strength is the weakest at a $\delta^{18}\text{O}$ of 4.5‰. Hence, the long-term strength of the ASM controls the duration of periods, which resemble glacial and interglacial conditions on the TP, supporting the comparatively short glacial conditions at Nam Co. In the following, we refer to glacial conditions as dry periods and interglacial conditions as wet periods at Nam Co. As we recognize a shift towards a lower threshold at MIS 6, the influence of the ASM in the Nam Co area must have decreased. However, An et al. (2011) infer the weakening of the ASM long-term amplitude from 370 to 300 ka.

Figure 4.6 compares the lake-level curve (Figure 4.6A), derived from seismic amplitudes, with proxy records connected to different atmospheric circulation systems and global climate indicators. The $\delta^{18}\text{O}$ curves (Figure 4.6B-E) matches the sea-surface temperature (SST; Figure 4.6J) changes during the interglacial, and the sea-level changes during the glacial stages (Shakun et al., 2015). Some deviations in the Nam Co lake-level curve (Figure 4.6A) within dry or wet periods are associated with significant SST or sea-level variations not reflected in the $\delta^{18}\text{O}$ record. Other deviations (Figure 4.6) are related to local responses of the Inflow-Evaporation-Ratio, indicating that either the extent of the prevailing atmospheric circulations shifted or that local responses to climate variations occurred.

From MIS 17 to MIS 13, the amplitude changes of the lake-level curve in dry or wet periods occur on a small scale. This behavior compares well to records from the Chinese Loess Plateau (CLP) (Sun et al., 2006). The normalized mean quartz grain size (Figure 4.6G) is positively correlated with the wind strength of the winter monsoon (An et al., 1991). During MIS 13, larger values of normalized magnetic susceptibility (Figure 4.6F) indicate precipitation and an enhanced ASM reaching the CLP (Zhou et al., 1990). Also, speleothem records from the Kesang Cave support this (Cheng et al., 2016b). Even though the cave is located in western China and dominated by the Westerlies, the speleothems reflect summer precipitation changes of the ASM (Cheng et al., 2016b). However, the lake level curve of Nam Co is less affected, and the LSR for MIS 13 is high compared to other periods of interglacial climate conditions. Hence, moist air masses did not reach the inner TP extensively at MIS 13, and dry winds predominated the Nam Co area until MIS 12.

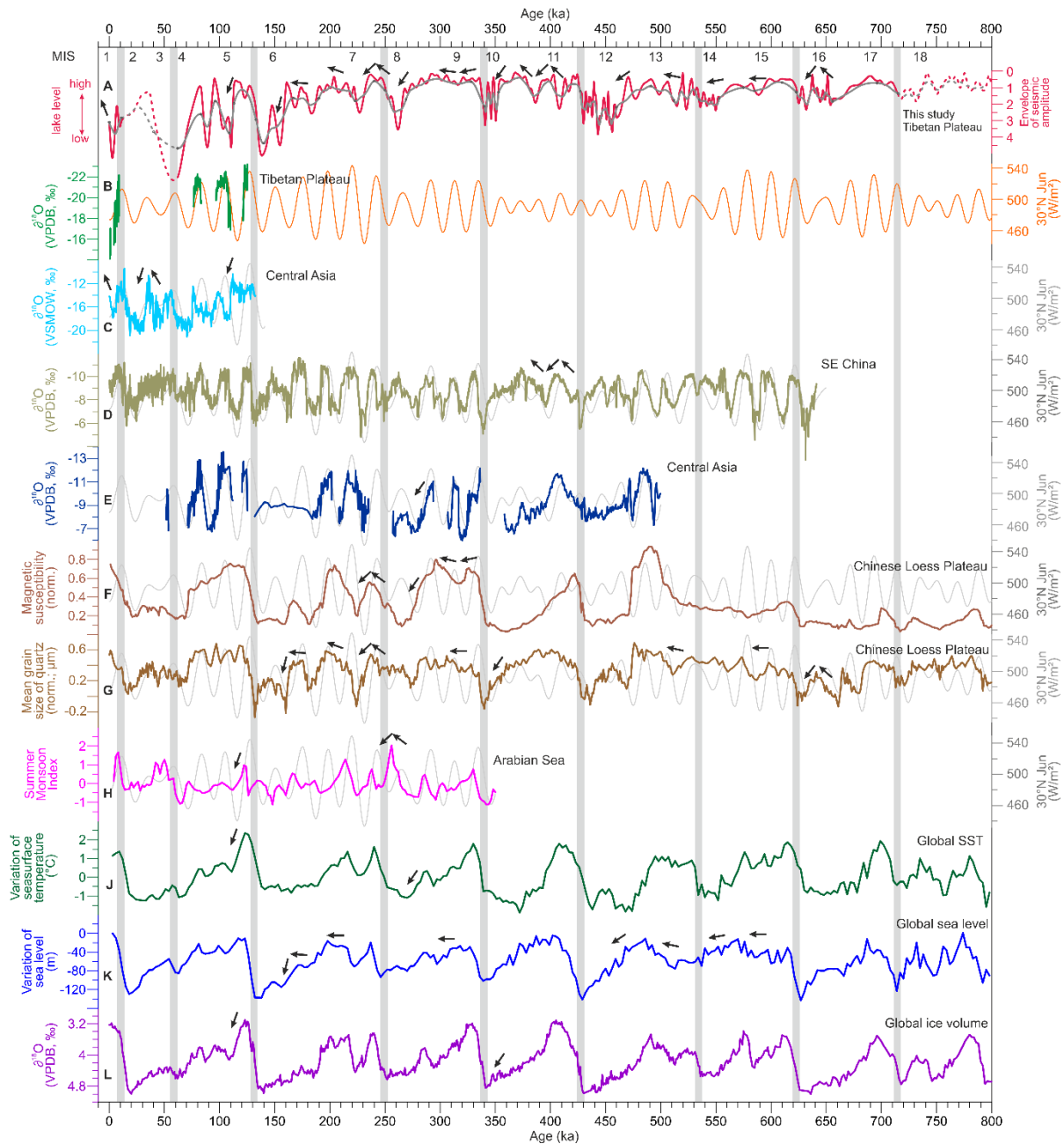


Figure 4.6: Comparison of the age-correlated lake-level curve with proxy records of atmospheric circulation and climate. A) Lake level cure of Nam Co based on the envelope of seismic amplitude (this study); B) $\delta^{18}\text{O}$ record of the Tianmen cave speleothem in vicinity to Nam Co (Cheng et al., 2016b) and summer insolation at 30°N (Berger & Loutre, 1991); C) Ice core record from the Guliya ice cap ; D) Composite Speleothem record for four cave in SE China (Cheng et al., 2016a); E) Speleothem record from the Kesang Cave in Western China (Cheng et al., 2016b); F) Normalized magnetic susceptibility record from the Chinese Loess Plateau (Sun et al., 2006); G) Normalized mean grain size of quartz particles from the Chinese Loess Plateau (Sun et al., 2006); H) Summer Monsoon Index derived from multiple proxies of a sediment core from the Arabian Sea (Clemens & Prell, 2003); I) Normalized record of global sea surface temperature (Shakun et al., 2015); J) Normalized record of global sea level (Shakun et al., 2015); K) Global $\delta^{18}\text{O}$ record of benthic foraminifera (LR04) (Lisiecki & Raymo, 2005). The summer insolation curve at 30°N is plotted for comparison with plots C-H. Gray vertical bars highlight the glacial terminations. Black arrows hint at the correlation of the lake level curve and other records.

With the onset of MIS 11, various Asian records indicate an enhanced ASM (Figure 4.6D, E, F) (Cheng et al., 2016a, 2016b; Sun et al., 2006). The lake level curve shows two internal cycles within the wet period, which do not resemble the CLP or global records. The winter monsoon on the CLP is weak (Figure 4.6G), and moisture reaching the CLP focused on the first half of MIS11 (Figure 4.6F). It appears that the precision-driven variability of $\delta^{18}\text{O}$ recorded in the SE China speleothems (Figure 4.6D) is synchronous with the curve from Nam Co, highlighting the interplay of the ASM and the Westerlies during MIS 11. The noticeable facies transition in the upper third of the unit marks the dominance of the ASM, reaching the inner TP at the end of MIS 11.

During dry periods from MIS 16 to MIS 10, the lake level curve shows quick, small-scale variability, possibly associated with strong Westerlies or winter monsoon winds. The sediments deposited in Nam Co during dry periods create a high seismic amplitude. One reason for this might be their heterogeneous composition of grain sizes. Coarser sediments deposit in the high energy environments basin-wide during a low lake level. During ice-covered periods of the lake, aeolian sediments derived by strong winds are trapped on the lake ice and reach the lake floor during melting phases. Significantly high LSRs, e.g., of the short MIS 10, indicate that more sediments reached the lake basin. This may be connected to intensified meltwater phases and thawing permafrost.

The high lake-level periods during interglacial conditions at MIS 9 and 7 correlate perfectly with increased precipitation (Figure 4.6F) and reduced winter monsoon influence (Figure 4.6G) registered in the CLP. Hence, the ASM expanded further to the west. The ASM influence during MIS 9 is continuously strong at Nam Co, as indicated by the smooth, high lake level and the low LSR. Around 270 ka, the curve is declining towards a short and unpronounced dry phase corresponding to the MIS 8 glacial stage. The reported high stand at Tangra Yumco of + 300 m at this time (Kong et al., 2011) appears not to be synchronous with Nam Co and the global records. The thin sediment layer of SU 11 and the uncontinuous top reflector imply a short, low lake-level stand with patchy sediment deposition and a fast lake level rise at MIS 7. The high lake level at Siling Co around 216 ka (Kong et al., 2011) emphasizes a supra-regional response to atmospheric circulation in the area. Towards the MIS 6 glacial stage, the Nam Co curve correlates well with steps in the global sea level drop (Figure 4.6K) and the enhancing winter monsoon winds (Figure 4.6G).

Even though the CLP record signals a constant moisture availability and a very weak winter monsoon, the lake-level curve of Nam Co emphasizes a high amplitude variability synchronous to the MIS 5 sub-stages. The highest peak appeared during MIS 5e, but also the interglacial sub-stages MIS 5c and MIS 5a are distinctive. The significant lake-level drop after MIS 5e correlates well with the global temperature decrease (Figure 4.6J). As the $\delta^{18}\text{O}$ record of the nearby Tianmen Cave

(Figure 4.6B) indicates high moisture availability for all interglacial sub-stages of MIS 5, we interpret the lake-level curve to respond locally to temperature variation. This is supported by the difference of the Guliya ice core record (Figure 4.6C) from the Kunlun Mountains in central Asia compared to the global temperature record (Figure 4.6I). The Guliya ice core may also resemble precipitation variations delivered from the Westerlies and local moisture recycling (Figure 4.6C) (An et al., 2017; Thompson et al., 2018), but this would not be compliant with the record from the CLP. Hence, during MIS 5e, 5c, and 5a, sizable amounts of meltwater might have contributed to the rapid lake-level shifts at Nam Co. The lake-level curve further supports the detected paleo-terrace dated to MIS 5a (Zhou et al., 2020). Also, $\delta^{18}\text{O}$ records of Zabuye Salt Lake in the Southwestern TP show fast amplitude variations during the interglacial substages of MIS 5, attributed to local characteristics of climatic change (Zheng et al., 2007).

The seismic record may contain a hiatus at the location of the vertical section, as we could not unambiguously assign ages for MIS 4 to 2. While we could observe only local effects of sediment redistribution or small erosional truncation during prior dry periods, the reflector SR15 truncates sediments by up to 20 m. The spatial extent of the incisions, limited to the eastern center of the basin, might indicate, e.g., grounded lake ice or a glacial advance reaching Nam Co. A remaining shallow proglacial lake could cause the lack of an evident hiatus in the north-west of the basin. However, the sourcing direction of the glacier remains unclear. Most likely, glaciers from the Nyainqêntanglha in the south fed an ice advance. Lehmkuhl & Haselein (2000) postulated two glacial advances alternating with a high lake-level period at Nam Co in the past 100 kyrs. Adding some age control, Lehmkuhl et al. (2002) refined this to 1) an 'older glacier advance' between 70 and 50/40 ka, which reached down to modern lake level, 2) a lake level highstand of +30 m (4751 masl) between 40 to 32 ka, which eroded and incised the previous moraine and 3) a 'youngest glacial stage' from 32 ka until around 18-13 ka, which terminated upstream. While the associated cliff of the maximum lake level of +30 m has been dated controversially to post-LGM by Schütt et al. (2008), results from Zhou et al. (2020) support Lehmkuhl et al. (2002), pinpointing the lake terrace of the high stand to an age of 33.6 ± 1.9 ka. Dating of pebble samples by Kong et al. (2011) found +20 m above the modern lake level also indicates an age of ~ 36 ka. Therefore, deposition and deformation of SU 15 must have taken place earlier.

The prograding infill of the glacial erosional structures is associated with a significant sediment input. Hence, a significant flooding event (Cukur et al., 2013) and a fast lake level rise enhanced by glacial meltwater and thawing permafrost preceded the high stand at 33.6 ± 1.9 ka.

The lake-level amplitude of the following high stand is smaller than amplitude variations registered at MIS 5 (Figure 4.6A). This fits results from Zhou et al. (2020), who suggest higher lake

levels during MIS 5 than during MIS 3 at Nam Co. At Zabuye Salt Lake, however, the total $\delta^{18}\text{O}$ amplitude variations of MIS 5 are not exceeding those of MIS 4 and remain smaller than those of MIS 3 (Zheng et al., 2007). Together with recent studies (Kong et al., 2011; Long et al., 2015; Shi et al., 2017a), this indicates that lake level responses may occur asynchronously over the TP, as has been reported for Holocene lake-level behavior (Jia et al., 2001), and that the existence of large connected lakes during MIS 3 or MIS 5e is not supported.

4.6 Conclusion

The high-resolution multichannel seismic profiles acquired in Nam Co express cyclic changes of low and high seismic reflection amplitude. We compile the direct dependency to lake-level, as the seismic amplitude variations relate to sedimentation rates and grain-size sorting during transportation. The low energy environment during high lake-level stands allows for fine-grained materials to settle, while during low lake levels, the high energy environment transports coarser material to the center of the lake basin.

By correlating glacial and interglacial cycles corresponding to the Marine Isotope Stages to the observed lake-level cycles, we developed a seismic stratigraphy. The interpreted section of the seismic data encloses eight glacial cycles back to 712 ka. With lacustrine sediments infilling the Nam Co basin by more than 670 m, the deepest sediments may be more than one million years old.

Calculated linear sedimentation rates show almost constant values for full glacial-interglacial cycles, with low rates during wet (interglacial) and high rates during dry (glacial) periods, indicating similar environmental influences in the Nam Co area through time.

Based on the seismic stratigraphy, we compared the relative lake level curve with records of global and supra-regional climate proxies. Our investigations yield that the long-term as well as short-term lake-level behavior of Nam Co correlates well to the shift of the ASM. This implies that precipitation is the main driving factor of lake-level variation at Nam Co. Divergence from the global pattern occurs during MIS 5, when quick, high amplitude lake-level variations between the interglacial substages may have been caused by enhanced meltwater supply and thawing permafrost. The enhanced meltwater runoff is a direct response to local temperature variability. Observed erosional truncations during glacial stages are generally restricted to local sediment redistributions. However, between 70 and 40 ka, a spatially restricted erosion in the south-eastern lake basin could be associated with a glacier advance from the Nyainqêntanglha Mountain Range south of Nam Co.

In general, Nam Co's lake level responses between 712 ka and 70 ka show a direct connection to the strength of the Asian summer monsoon, and hence the here presented data emphasize the comprehensive climate archive that Nam Co offers.

4.7 Acknowledgements

This study was funded by the German Research Foundation (DFG) (grants SP296/36-1, SP296/36-2, DA 563/3-1), and is part of the ICDP project 'Seismic Pre-Site Survey for ICDP Drilling Locations at Lake Nam Co'. Further funding for data acquisition was provided by the Strategic Priority Research Program of Chinese Academy of Sciences (XDA20070101) and the Chinese Ministry of Science and Technology project (2012FY111400). We are grateful to Schlumberger for providing the VISTA 2D/3D Seismic Data Processing software package and to IHS for providing the Kingdom Software for seismic interpretation. Further, we want to thank Bor Gonzalez Usach for his help coding python scripts.

Chapter 5:

The transtensional tectonic system at Nam Co, Tibet

- Results from high-resolution 2D seismic data

Nora Schulze^a, Jerome van der Woerd^b, Volkhard Spieß^a, Junbo Wang^{cd}, Liping Zhu^{cd}

^a Faculty of Geosciences, University of Bremen, Klagenfurter Strasse 2-4, 28359 Bremen, Germany

^b Institut de Physique du Globe de Strasbourg, UMR 7516 CNRS, Université de Strasbourg, Strasbourg, France

^c Key Laboratory of Tibetan Environment Changes and Land Surface Processes (TEL) / Nam Co Observation and Research Station (NAMORS), Institute of Tibetan Plateau Research, Chinese Academy of Sciences, Beijing 100101, China

^d CAS Center for Excellence in Tibetan Plateau Earth Sciences, Beijing 100101, China

Keyword list: Tibetan Plateau, lake, Nam Tso, extension, strike-slip, slip rate

Highlights:

- Manifold faults offer a unique study of extensional throw rates, direction, and timing
- Primary NW-SE strike-slip faults created wrench zone, separating two sub-basins
- Secondary normal faults initiated ~350 ka (MIS 10) and disclosed distributed extension across the basin
- WNW-ESE extension with total cumulative throw up to 315 m
- Intermittent throw rates range from ~0.3 to 0.9 mm/yr in the last 350 kyrs

5.1 Abstract

By analyzing ~1000 km of high-resolution 2D seismic data from Nam Co (Co = Tibetan for lake), we identified an unexpected large amount of more than 550 fault structures observed within the basin. We present evidence for extensional tectonics from connected NW-SE strike-slip and N-S normal faults. Primary faults along a NW-SE directed wrench zone are parallel to the dextral Beng Co Fault to the NE of Nam Co. Moreover, we observed secondary N-S extending normal faults and grabens, soft domino faulting, as well as indicators for negative flower structures. Simple end-member models of either extension or strike-slip do not represent the complexity of the setting. Therefore, we propose a transtensional tectonic setting with a dominant extensional component within Nam Co. Our measurements highlight in great details that the tectonic activity initiated ~350 kyrs ago (Middle Pleistocene) and was continuously active except for the period of MIS 5e and since the Holocene. Our analysis reveals that cumulative throw rates in the study area are in the

range from 0.3 mm/yr in WSW-ENE direction to 0.9 mm/yr in WNW-ESE direction for the last 350 kyrs. Lateral extension rates range between 0.5 and 0.7 mm/yr. Although rates and amounts of extension found in Nam Co seem secondary when compared to the nearby Gulu Graben (<12%), our rates indicate that Nam Co faults contribute nearly half of the total extension when compared to the southern Yadong-Gulu rift system, or ~7% when compared to the whole south Tibet extension. Our finding, the first one to document extension since the Middle Pleistocene in southern Tibet, will contribute to a better understanding of the extensional regime in the Tibetan Plateau.

5.2 Introduction

5.2.1 E-W extension on the Tibetan Plateau

The onset of E-W extension and the connected tectonic behavior of the Tibetan Plateau (TP) are still widely and controversially debated. Major N-S trending rifts south of the Bangong Suture and numerous small grabens north of the Bangong Suture characterize the TP's modern shape (Armijo et al., 1986). The most prominent rift, the Yadong-Gulu-Rift, extends for more than 500 km across the Yarlung-Zangbo suture (Figure 5.1). Based on GPS measurements, normal faulting accommodates 15%–20% of the total E-W extensional strain in the present day (Elliott et al., 2010).

The initiation times for the onset of W-E extension vary broadly from Middle Miocene to Early Pliocene ages (Figure 5.1). Besides, Mahéo et al. (2007) constructed the hypothesis of not one but two phases of extension: one phase of SW-NE directed rifting around 14–10 Ma and a second more accelerated phase after 5 Ma. Support for the latter hypothesis is given by the Shuang Hu graben (13.5 Ma and 4 Ma) (Blisniuk et al., 2001; Mahéo et al., 2007), the Xuro Co –Tangra Yumco graben system (13 & 6 Ma) (Dewane et al., 2006), or the Ama Drime Range (Kali et al., 2010; Leloup et al., 2010). Armijo et al. (1986) state that normal faulting, directed $N96^{\circ}E \pm 7$, has been the dominant tectonic regime north of the Himalayas in the last 2 ± 0.5 million years.

Figure 5.1 summarizes initiation ages and fault throw or slip rates on grabens and rifts, and the Beng Co strike-slip fault in the vicinity to Nam Co (Co = Lake). The compilation reveals that the initiation of N-S-extension occurred during the middle to late Miocene.

Several models to explain the crustal thinning and the interaction of the E-W extension and the Himalayan arc evolution have been introduced. Based on the observation of synchronous onset of regional extension, some authors (e.g., Dewey et al., 1988; Elliott et al., 2010; England & Houseman, 1989; Molnar et al., 1993) endorse the theory of gravitational collapse: when maximum sustainable crustal thickness was reached, the crust started to spread under gravitational stresses (Elliott et al., 2010; Styron et al., 2015). In comparison, other authors (e.g., Copley & McKenzie, 2007; DeCelles et al., 2002; Kapp et al., 2005b) deduce from the faster rates of rifting in southern compared to

northern Tibet that rifting is triggered by progressive underthrusting of the Indian Plate beneath the southern plateau (Styron et al., 2015).

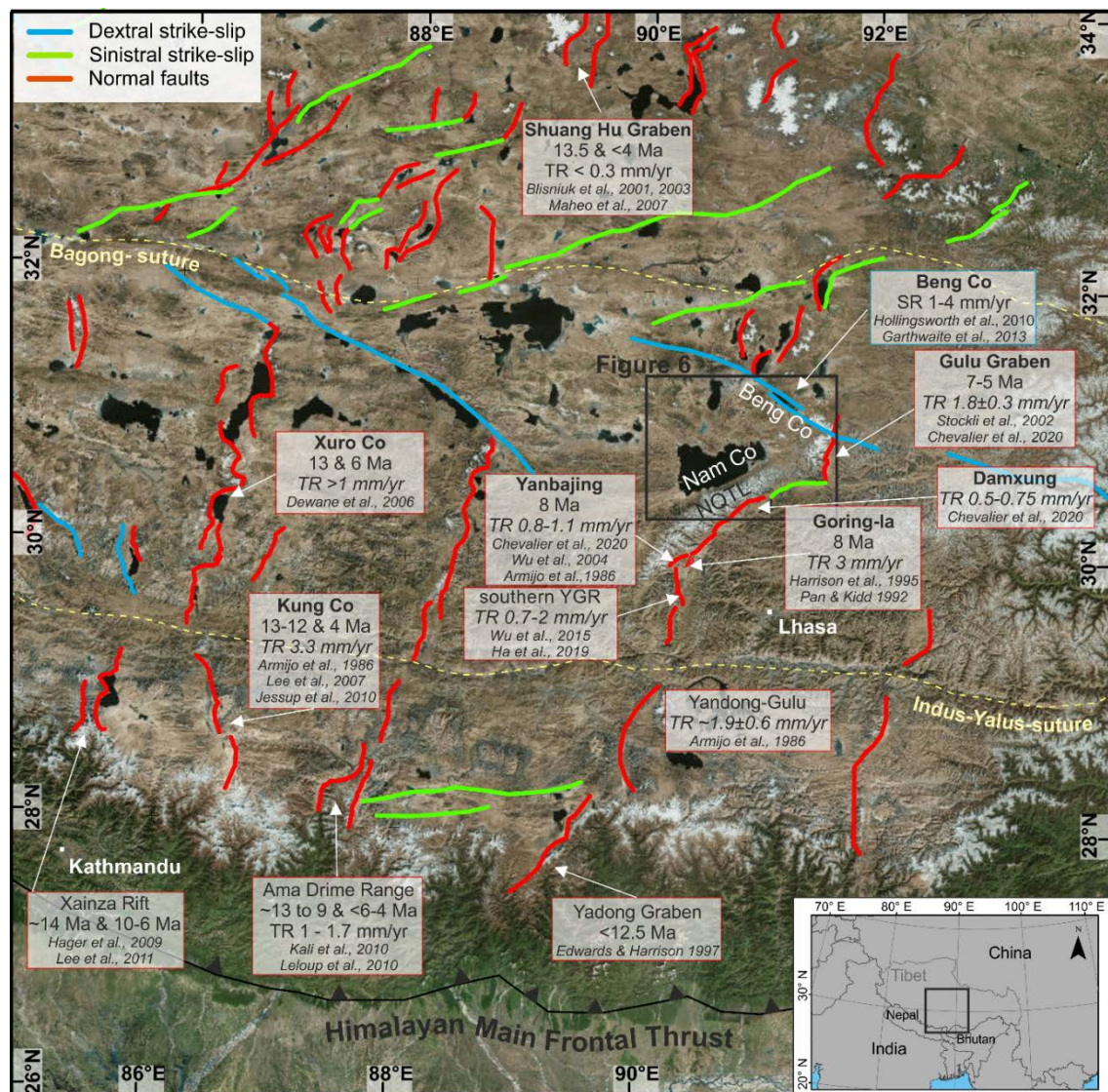


Figure 5.1: Overview map of the eastern central Tibetan Plateau with comprehension of currently active faults. Initiation ages, fault throw rates (TR), or slip rates (SR) are given where applicable. NQTL = Nyainqêntanglha Mountain Range. Sources: HimaTibetMap 1.0 fault database of Taylor & Yin (2009) and Styron et al. (2010). World Imagery ESRI 10.4, Projection in UTM 46N.

The most discussed models on South Tibetan deformation are the 'oroclinal bending' (e.g., Li & Yin, 2008; Ratschbacher et al., 1994), the 'radial spreading' (e.g., Copley & McKenzie, 2007; England et al., 1988), the 'lateral extrusion' (e.g., Lacassin et al., 2004; Tapponnier et al., 1982), and the 'oblique convergence' (e.g., McCaffrey, 1992; Seeber & Armbruster, 1984). Please refer to Styron et al. (2011) and McCallister et al. (2014) for thorough summaries.

In the Nam Co area, the 'lateral extrusion' and the 'oblique convergence' models endorse extension towards the East, supported by geodetic data (Styron et al., 2011), while the other two models suggest expansion to the south or the west.

Strong support for the lateral extrusion model is given by Armijo et al. (1989). In Armijo et al.'s (1989) kinematic model, only a small number of crucial strike-slip faults in Central Tibet accommodate the eastward extrusion of material (Hollingsworth et al., 2010). To fit the model of Tapponnier et al. (1982) and Armijo et al. (1989), relatively high slip rates are required (Styron et al., 2011). This demand stands in contrast to observations along the Beng Co dextral strike-slip fault, north of the Gulu graben (Figure 5.1). Instead of the proposed >10 mm/yr-20 mm/yr (Armijo et al., 1989), strike-slip rates of 1-4±1 mm/yr (Garthwaite et al., 2013), 3-4 mm/yr (Hollingsworth et al., 2010; pers. comm.), and 7.7 mm/yr (Ryder et al., 2014) were measured.

To fit the lateral extrusion model proposed by Armijo et al. (1989), Nam Co would have to contain an additional NW-SW strike-slip fault and small W-E extension rates. Otherwise, a continuous deformation model like the oblique convergence model, where slow slip rates distribute eastward motion across many active structures throughout the region (England & Houseman, 1989), might be prevailing.

5.2.2 Regional tectonic setting around Nam Co

According to Armijo et al. (1986, 1989), the dextral strike-slip faults near the Bangong Nujiang suture are linked kinematically to the N-S rifts. Nam Co is located at a key position to understand this interaction of recent E-W extensional faulting and the older but still active strike-slip faulting (e.g., the dextral NW-SE Beng Co Fault and the SW-NE extensional grabens and the Yadong-Gulu rift) (Figure 5.1).

Nam Co is an endorheic lake, which covered 2026 km² in 2010 (Zhang et al., 2017). It is situated in a basin north of the Nyainqêntanglha (NQTL) Mountains, a high SW-NE elongated mountain range with peaks > 7000 m above sea level. To the East of Nam Co, the East Nyainqêntanglha Mountains are located N-S, and to their East, the Gulu graben evolved. Chapter 4 highlighted the long record of lacustrine sediments spanning more than 715 kyrs. So far, it has not been studied how and when the Nam Co basin developed. Hypotheses exist that the Nam Co basin developed as an extensional, half-graben structure or a pull-apart feature. However, the basin may have also evolved during the Oligocene to Lower Miocene as a foreland basin of the NQTL as insinuated by Pullen et al. (2008). The fault system within Nam Co is exemplary for the TP along the Jiali Fault zone (between the suture zones of Bangong-Nujiang in the north and the Indus-Yalu-Suture in the south) (Figure 5.1). We expect that the tectonic setting displayed at Nam Co is consistent with the regional tectonics and that the predominant W-E direction has steered the faulting in the Nam Co

basin. Still, the interaction of the Nam Co basin, the NQTL, and the graben structures of the Yarlung- Gulu rift has not been evaluated in much detail. The NQTL acts as a natural border along which the extension is re-oriented (Armijo et al., 1986). Instead of N-S rifts, the Yagong-Gulu Rift extension is propagating SW-NE along the weak zone of a former low-angle thrust or strike-slip fault leading to sinistral faulting along its Damxung section, the only place in south Tibet where left-lateral faulting occurs presently south of Bangong (Armijo et al., 1989). Extension rates along the Yadong-Gulu rift decrease from north (3-6 mm/yr) to south (~1.3 mm/yr) (Chevalier et al., 2020).

The presented data from Nam Co will significantly contribute to the, so far, little available data and help establish a local and regional model while contributing to the existing thought on over-regional models for the TP. Moreover, we take up the hypotheses that the local tectonics are continuously active. The faults are active for extended time periods instead of rapid stress relief events, as major seismological events solely occur along the major faults around Nam Co (e.g., 2008 south of Yanbajin; 1951 & 1952 close to Gulu) (U.S. Geological Survey, n.d.).

5.3 Material and methods

5.3.1 2D Reflection seismic surveys data

Two acoustic surveys have been conducted on Lake Nam Co. In 2014, multi-channel seismic (MCS) profiles of ~110 km length were acquired. In 2016, we acquired MCS profiles of 860 km length. The surveys were carried out in cooperation with the Friedrich-Schiller-University Jena, the Institute of Tibetan Plateau Research, and the University of Bremen.

5.3.2 Acquisition

The acoustic survey in 2014 utilized either a Sercel two-chamber Mini GI airgun (in micro setting: 2x 0.1 L chamber volume) with a frequency range between 50- 500 Hz or a Falmouth bubble pulser with a frequency range between 10-1700 Hz. Recording was conducted with a Teledyne streamer of 32 channels and 64 m active length (2 m channel spacing with one hydrophone per channel) for 13 profiles. The MCS survey in 2016 utilized the same Sercel two-chamber Mini GI airgun in combination with the Teledyne streamer as 2014 for all 91 profiles.

5.3.3 Processing and interpretation

The following processing steps were applied to the 2016 MCS data using the processing software VISTA by Schlumberger: Pre-Processing (gun delay, trace editing, spherical divergence), frequency bandpass filtering, despiking, velocity-model design, surface-related multiple elimination (SRME) based on velocity model, time-variant surface consistent scaling, pre-stack noise attenuation,

velocity-model based NMO corrections and common midpoint (CMP) stacking, post-stack noise attenuation, and post-stack time migration. The processing sequence of the 2014 data partially included residual statics elimination and multiple attenuation using predictive deconvolution.

The processing technique allowed substantial enhancement of the signal-to-noise ratio and enlarged the overall imaging depth by suppressing multiples and ambient noise. The seismic data's vertical resolution is <2 m, as it generally depends on the central signal frequency of the source (~250 Hz, Mini GI airgun). The CMP bin size (1 m) defines the horizontal resolution.

We integrated the processed profiles into the interpretation software *The Kingdom Software* 2016.1 & 2019 by IHS ('*Kingdom*') for visual interpretation under the usage of seismic attributes such as similarity, envelope, frequency, and average energy as well as specific filters. Identified and interpreted seismic reflectors (SR) and faults are the basis for this study (see Chapter 4). Overall, we picked and analyzed 17 SR on all seismic images.

5.3.4 Characterization and classification of faults

We anticipate to interconnect faults within Nam Co and the surrounding tectonic system by classifying the faults, calculating throw and heave data, and determining displacements, extension, and vertical displacement rates. To allow a statistical approach, we used a semi-automated way to process the information using python. We calculated the fault throw data from exported horizon information created in *Kingdom* (e.g., SR9, Figure 5.4). We computed faults length, angle, and apparent strike from the exported fault picks, also generated in *Kingdom*.

5.3.5 Application of H - T-Plots

The faults revealed by the MCS data inhabit a high lateral and spatial resolution, allowing the characterization of faults with the method introduced by Hongxing & Anderson (2007): by plotting the horizons against the throw of a fault, in so-called H-T-Plots, information about initiation time, inactive phases and time of highest slip rates are visualized. The maximum throw of a fault indicates the time of initiation as the associated sediment unit was offset from all tectonic events since initiation.

5.4 Results

The high-resolution MCS data indicate a lacustrine infill of up to 680 m in the Nam Co basin. A detailed seismic facies analysis (Chapter 4) allowed the identification of 17 seismic reflectors (SR) throughout the MCS dataset (e.g. Figure 5.2A) down to about 550 m depth below lake level. The chronology of the reflectors is based on the correlation of alternating seismic facies to global Marine Isotope stages (Chapter 4). The sedimentation during wet, interglacial conditions is characterized

by low sedimentation rates and low amplitude seismic facies, while dry periods during glacial condition result in high sedimentation rates and high seismic amplitude facies. The timeframe spans about 715 kyrs, starting with the deepest continuous reflector traced in the MCS dataset (SR1; e.g., Figure 5.2A).

The MSC dataset revealed an extensive occurrence of faults in the lake sediments. We observed e.g., more than 550 faults displacing SR 9 (end of MIS10) within an area of 430 km²; an amount previously unknown. Figure 5.2A exemplarily shows the seismic unit succession in a characteristic fault setting in scale 1:1. Most faults show a normal fault behavior on the 2D seismic profiles; only a few faults in the south inhabit a reverse fault characteristic (Figure 5.3).

5.4.1 Fault initiation and behavior

The H-T Plots reveal that the seismic units are offset by non-constant throws (Figure 5.2B). However, during MIS 5e and for the Holocene, all H-T plots indicate a constant throw for the bottom and top reflectors of the according units (Figure 5.2B, SR13-14 and SR 15-17). With very little exception, the faults show an initiation time within MIS 10 (Figure 5.2C). The faults express an initial post-depositional faulting phase, followed by a syn-depositional behavior after initiation until Upper Pleistocene times (Figure 5.2). The highest throw rates (fastest fault growth) of 1.5 occurred during MIS 2-5d. Strikingly, the majority of the faults do not penetrate the uppermost sediment unit (above SR15) of about 15 meters below lake floor (Figure 5.2A).

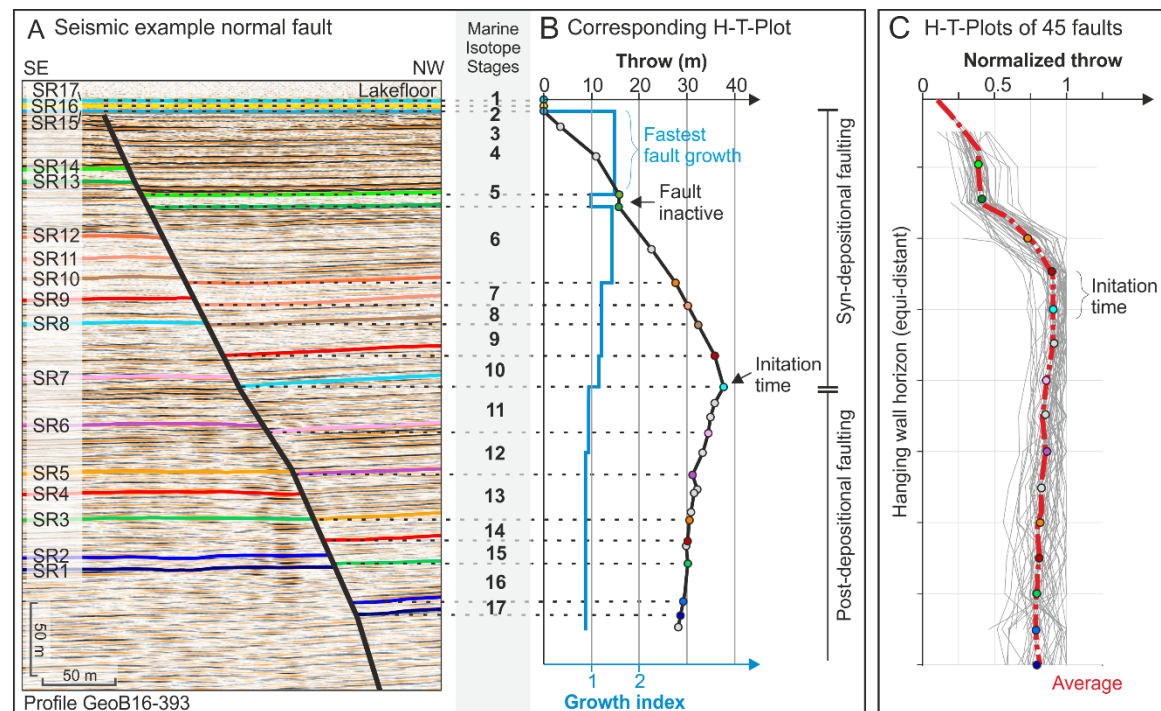


Figure 5.2: A) Seismic example of a typical normal fault in scale 1:1, here on Profile GeoB16-393 (extent shown in Figure 5.6). Seventeen seismic reflectors (SR) are highlighted. Stratigraphic marine isotope stages (MIS) are assigned to the

seismic units (as shown in Chapter 4). B) Fault characterization after Hongxing & Anderson (2007). The Horizon-Throw-Plot (H-T-Plot) shows post-depositional behavior before the initiation time (SR8, top MIS 11) and syn-depositional behavior after initiation time until SR 15. The uppermost units (SR15-17) are not penetrated. C) Compilation of H-T-Plots of a representative amount of 45 faults in the western sub-basin of Nam Co with throw values for more than ten horizons. The individual plots of each fault are normalized to the maximum throw of each fault (gray lines). The mean of all plots is highlighted in red. The average initiation time is within MIS 10.

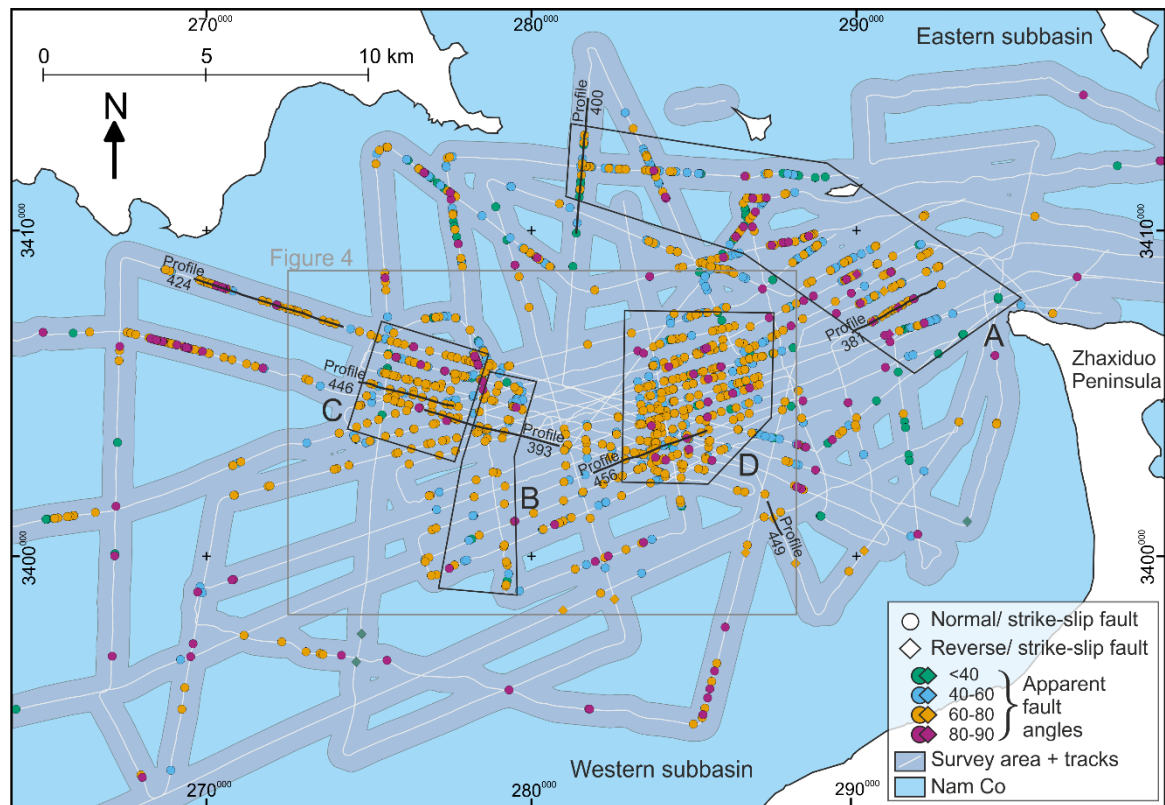


Figure 5.3: Amount and types of faults in the western sub-basin of Nam Co. Circles indicate normal fault and diamonds reverse fault behavior. Apparent fault angles along-track are color-coded. Areas A, B, C, D are marked with black polygons. Projection in UTM 46N.

5.4.2 Fault classification and identification of fault surfaces

The depth of faulting is very variable and the acoustic bedrock reflector hampers the tracing of fault into the bedrock. Apparent dips of faults (perpendicular to profile direction) vary between 30° and 90° throughout the western sub-basin (Figure 5.3). Additional to the apparent fault dip, throw and heave, we considered apparent dip direction and fault depth to identify continuing fault planes in the Nam Co basin and assign them to three classes (Figure 5.4). Most fault planes in the western sub-basin strike N-S. In the westernmost part, the strike is more NNE-SSW directed, while in the eastern part, it has an NNW -SSE tendency (Figure 5.4).

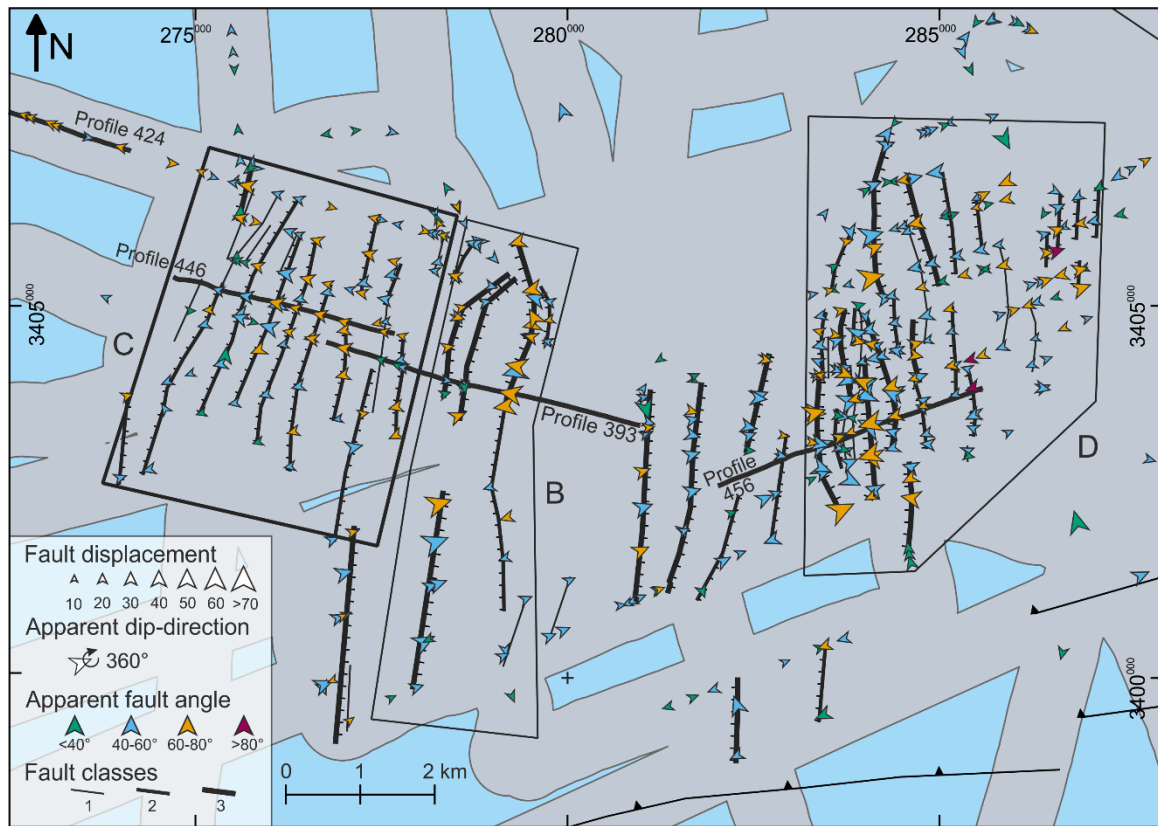


Figure 5.4: Exemplary close-up map (extent shown in Figure 5.3) of fault data from horizon SR 9, comprising apparent dip direction (direction of arrowhead), amount of throw (size of arrow symbol), and displacement (color of arrow symbol) for each fault. An interpretation of fault planes is shown with black connecting lines, and their classification is highlighted by line thickness. Projection is UTM 46N.

5.4.3 Areas

According to the behavior of the faults, we differentiated four areas in the lake (A, B, C, D) (Figure 5.3).

Area A

Area A lies at the boundary of the shallower eastern sub-basin to the deeper western sub-basin. In the southeastern part within Area A, faults are significantly steep, with apparent angles between 70° and 90° (Figure 5.5, up). The fault distance is small, resulting in a very high fault abundance (about 20 fault planes along 500 m). Reverse faults and roll-over anticlines occur. Several faults in Area A penetrate the lake floor. Throws often exceed the imaged depth of reflectors, which masks any correlation between hanging and footwall. Therefore, horizons identified in the western sub-basin are not traceable across Area A into the eastern sub-basin.

In the northwestern section of Area A, the faults show similar dips as in the southeastern section, however, the sedimentary units are not as deformed and rotated as in the SE (Figure 5.5, down). Here, the lake floor reflectivity is very dominant, and the according strong multiple prohibits the continuous tracing of horizons into the eastern sub-basin.

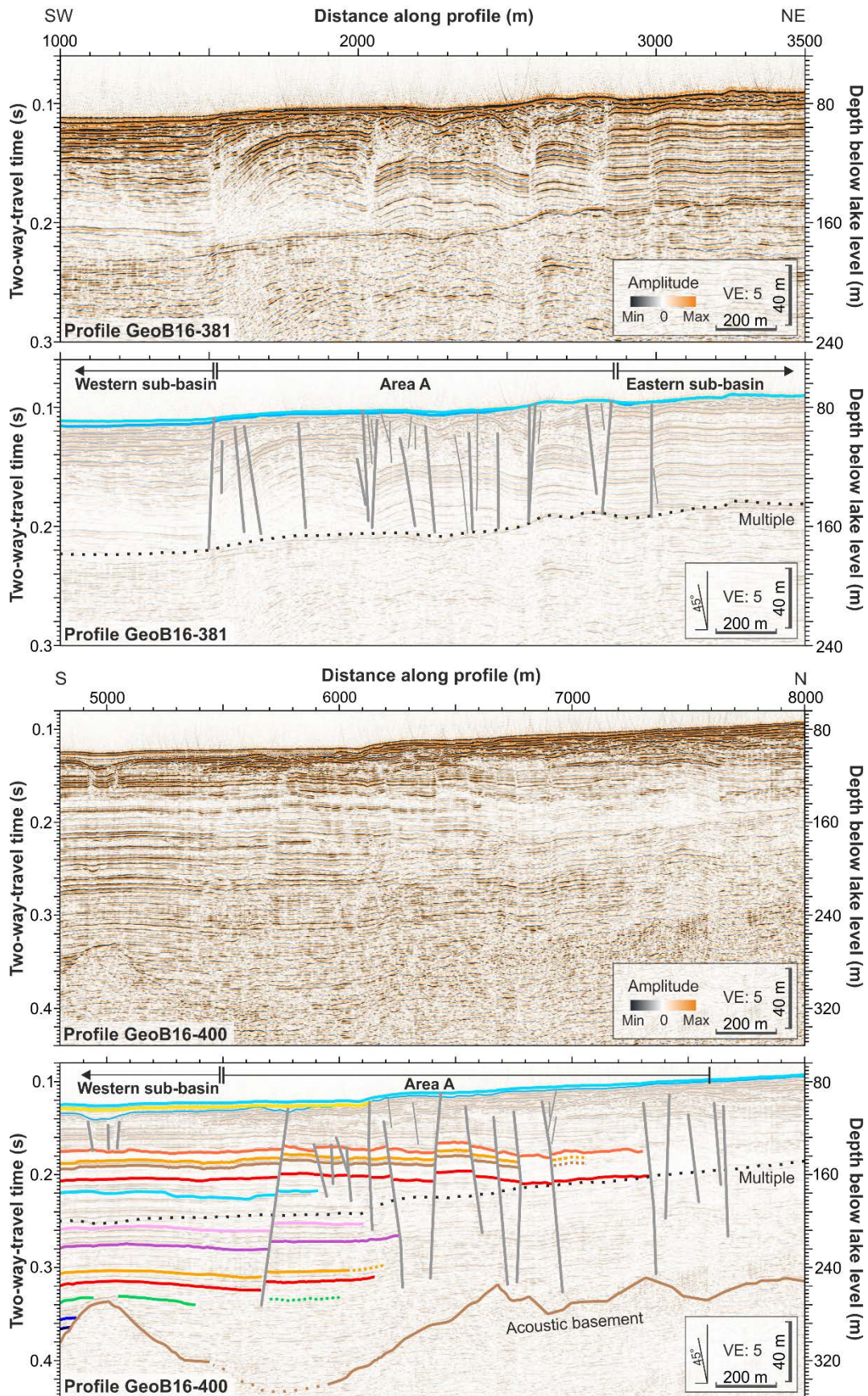


Figure 5.5: Section of seismic profile GeoB16-381 as example for the southeastern part of Area A and section of seismic profile GeoB16-400 as example for the northwestern part of Area A. Profiles vertically exaggerated by 5. Simple depth conversion with 1600 m/s. Profile locations are marked in Figure 5.3. Same horizon color scheme used as in Figure 5.2A.

Area B

Area B is defined by mainly two extensive, semi-parallel normal faults, striking N-S (Figure 5.4); the western fault is dipping east, while the eastern fault is dipping west. In the northern half of Area B, two less-rated faults are substituting the one major fault plane present in the southern part (Figure 5.4; 5.6). The apparent fault angles of all faults are, on average, 60° . The faults actively bind a depression over a distance of 560 to 870 m in the W-E direction. Some of the largest throws of the entire data set, up to 40 m, occur at the southern end of the western fault and the northern part of the eastern fault (Figure 5.4). Accordingly, throws are decreasing in the opposite direction along the two faults. We calculated the sediment accumulation rates (SAR) for hanging- and footwall of the eastern fault (Box, Figure 5.6) since fault initiation exemplarily: SAR of 0.43 mm/yr for the footwall and SAR of 0.54 mm/yr for the hanging wall.

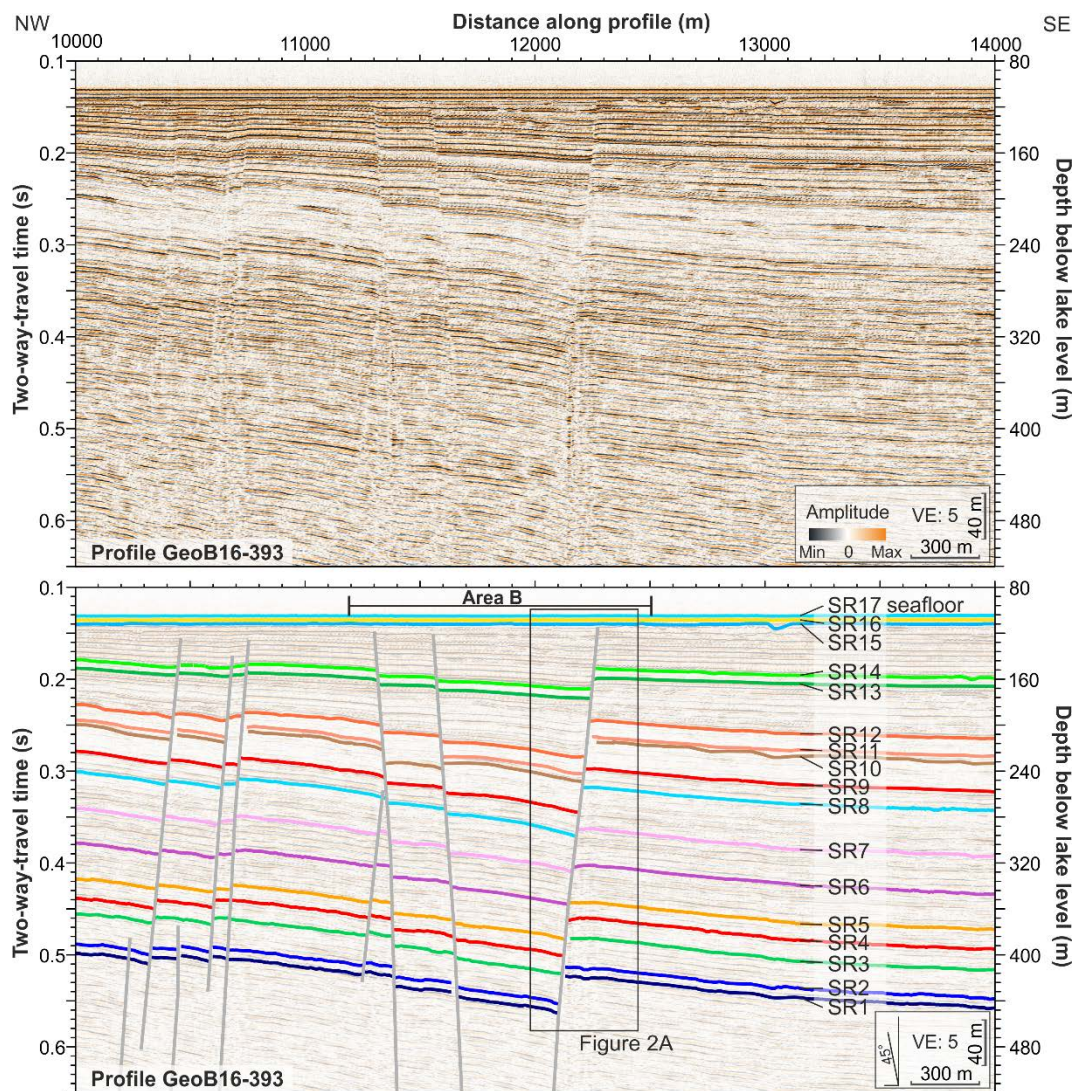


Figure 5.6: Section of seismic profile NamCo-GeoB16-393 as example for Area B. Profile vertically exaggerated by 5. Simple depth conversion with 1600 m/s. Profile location is marked in Figure 5.3. Horizon color scheme the same as in Figure 5.2A.

Area C

Area C excels for all faults dipping in the same NW direction (Figure 5.7). The fault angles vary only slightly around 65° , along the same profile and between parallel profiles. The fault spacing is between 300 m and 450 m. No overall subsidence is happening with respect to the sediment units, while the faults themselves show throws of up to 20 m and create local accommodation space.

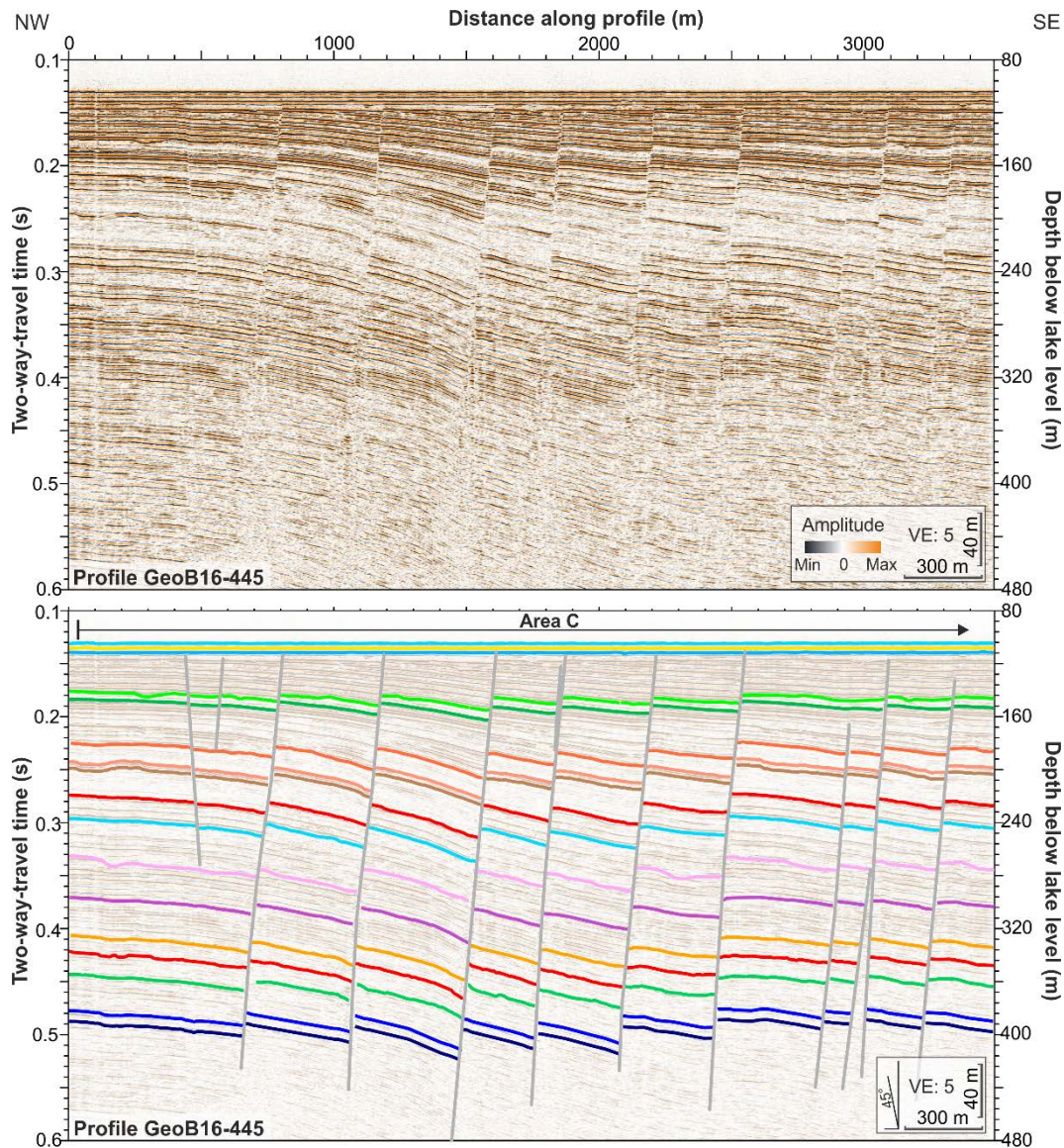


Figure 5.7: Section of seismic profile NamCo-GeoB16-446 as example for Area C. Profile vertically exaggerated by 5. Simple depth conversion with 1600 m/s. Profile location is marked in Figure 5.3. Horizon color scheme same as in Figure 5.2A.

Area D

Area D comprises a fault zone with many short overlapping faults (in map view). In the west of the area, faults are dipping eastwards, and in the East, faults are dipping westwards, building a structure with steeper and shorter faults towards the center (Figure 5.8).

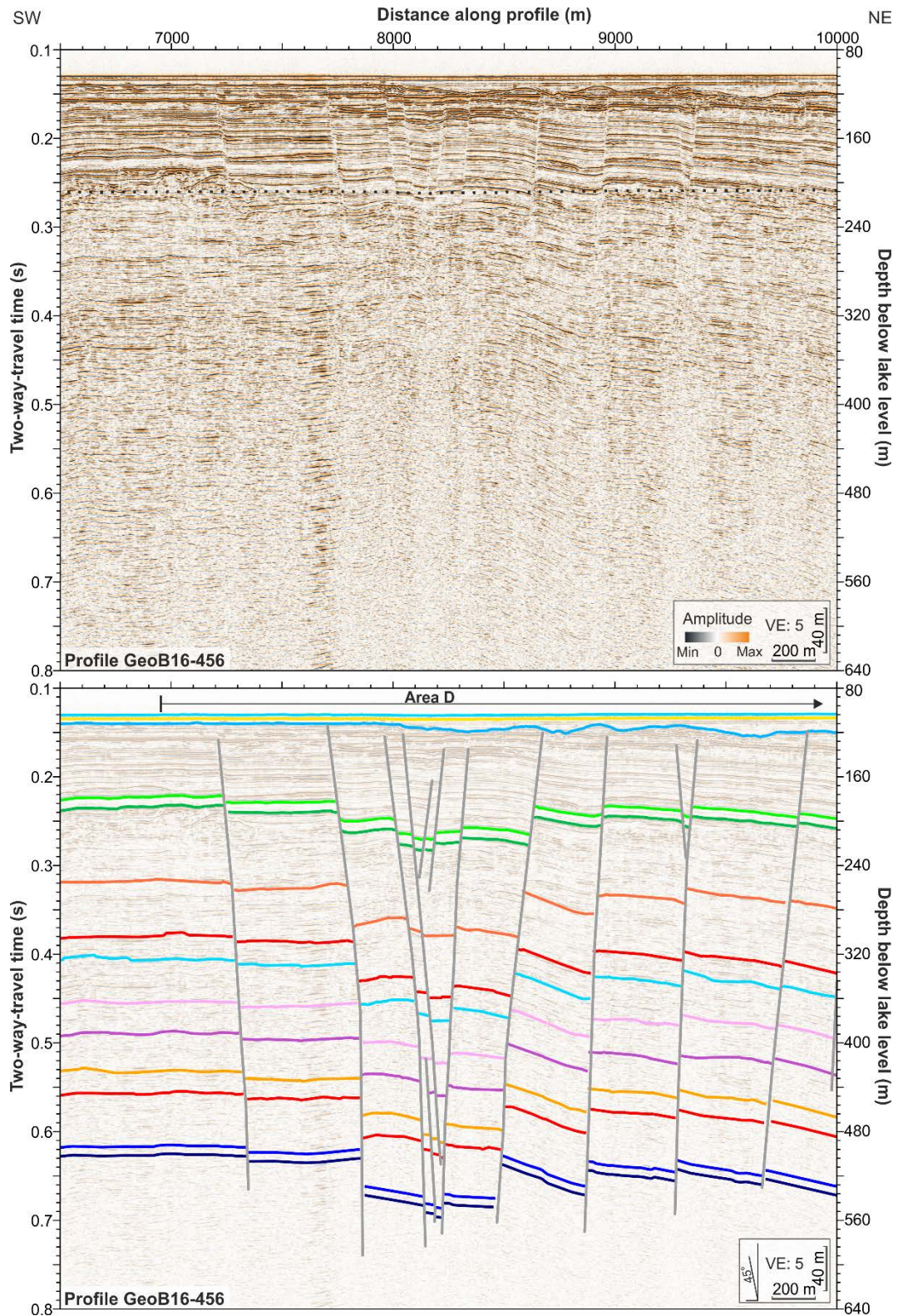


Figure 5.8: Section of seismic profile NamCo-GeoB16-456 as example for Area D. Profile vertically exaggerated by 5. Simple depth conversion with 1600 m/s. Profile location is marked in Figure 5.3. Horizon color scheme the same as in Figure 5.2A.

The fault spacing decreases from about 200 m between the outer faults to about 50 m in the center. Several faults show large throws of more than 40 m. Faults of opposing dip direction are intersecting, creating v-shapes. However, the penetration of the seismic data does not image whether these fault pairs converge to single fault surfaces in greater depth (y-shapes). Overall, the faults are organized in a graben like structure.

Faults on the northwestern flank and reverse faults in the south

North-west of Area D (Figure 5.3), the fault spacing decreases until upslope. Close to the lakeshore (Profiles GeoB16-393 and GeoB16-424; Figure 5.9), faults arise in high density. High-angle normal faults of opposing dip direction and of different vertical length occur. The fault throws vary widely, and over a distance of one kilometer, cumulative throws of 80 m develop.

The identified reverse throws in the south and southwest of Nam Co inherit very steep apparent dipping angles of up to 85° while showing only minimal throws (max. 5 m) (e.g., Profile GeoB-449; Figure 5.9).

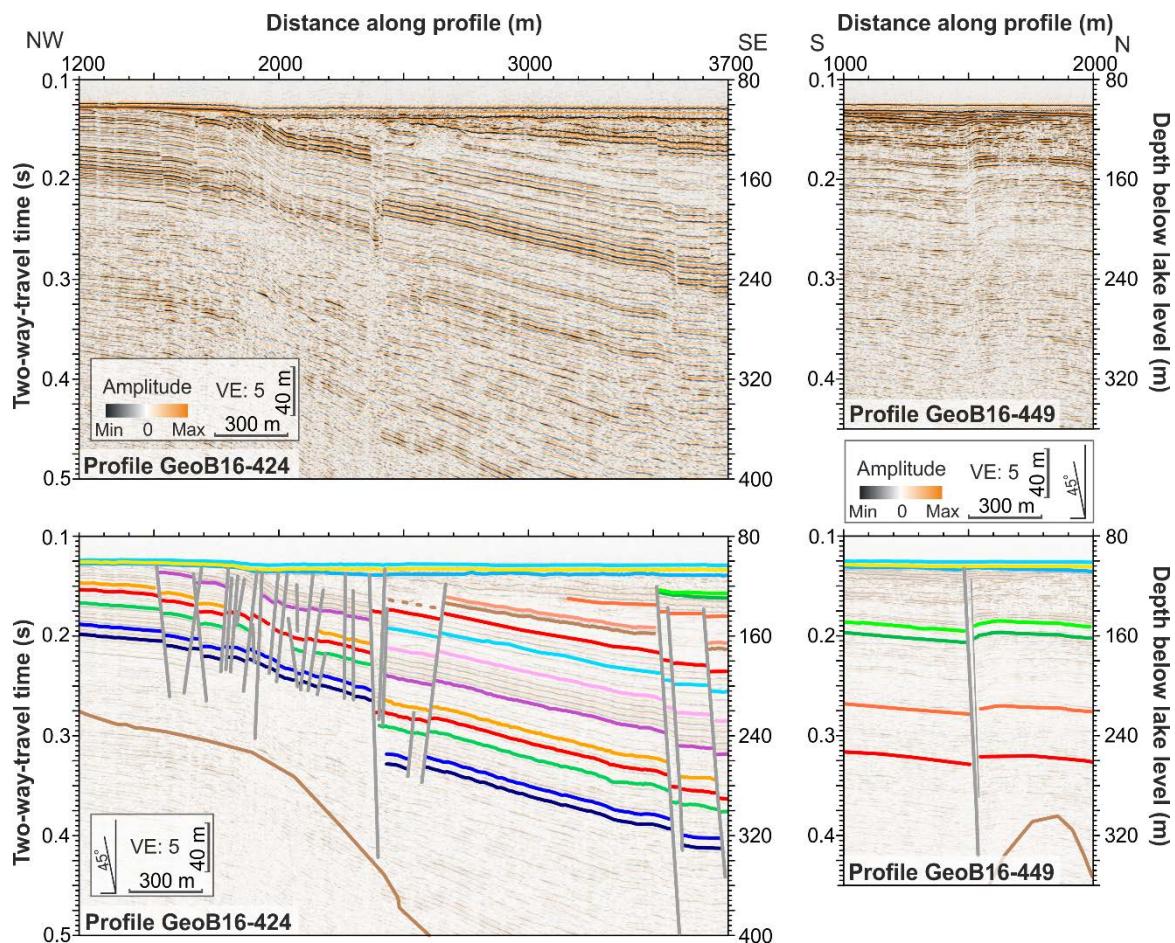


Figure 5.9: Sections of seismic profiles NamCo-GeoB16-424 and GeoB16-449. Profiles vertically exaggerated by 5. Simple depth conversion with 1600 m/s. Profile locations are marked in Figure 5.3. Horizon color scheme the same as in Figure 5.2A.

5.5 Discussion

5.5.1 Character of observed faults

We distinguish two categories of faults in the recorded fault system in the Nam Co lacustrine sediments. The NW-SE directed faults of Area A are primary, based on their large throws and acoustic basement penetration. All faults in the western sub-basin, including the Areas B, C, and D, are defined as secondary faults

Under the assumption of normal fault behavior, an initiation time in the Middle Pleistocene, around 350 ka, was distinguished for the N-S-directed secondary growth faults. As we could not detect an initiation time pattern within the western sub-basin, a synchronous spatial evolution of the lake basin is likely. Our survey presents a yet unpaired data set in Tibet, as due to resolution and age control, few studies exist on tectonically active phases in the Pleistocene.

The H-T-Plots do not show a constant throw value before initiation but a decreasing throw with depth (Figure 5.2). This might indicate either compaction of older sediment units or a keystone fault (Hongxing & Anderson, 2007). This type of fault penetrates downward into older pre-kinematic layers while growing upward into younger syn-kinematic layers with time (Hongxing & Anderson, 2007). Since initiation, the fault characteristics express a mostly continuous tectonic activity until about 40 ka. The syn-sedimentary behavior might have prevented considerable stress build-up in the past. The H-T-Plots imply that the fastest growth rate occurred during deposition from MIS 5d to MIS 3 (Figure 5.2). This could be an artifact due to an unconformity and a possible associated hiatus of MIS 3-4 sediments (Chapter 4).

Only faults in Area A penetrate the lake floor. The apparent tectonic inactivity during the Holocene as well as during MIS 5e coincides with phases of very high lake level during wet, interglacial conditions at Nam Co. Even though this concurrence needs further inspection, a potential correlation of imposed water load and pore pressure on seismological events is striking. Hence, the reduced imposed water load during lower lake level periods than in MIS 1 and 5e might induce fault activity. This might be a similar relationship as has been observed close to the Dead Sea Transform Fault, where groundwater extraction triggered seismicity (Wetzler et al., 2019). The normal fault throw characteristics also agree with the fact that few earthquakes are reported from the Nam Co area (Figure 5.10) and that significant earthquakes (>6 Magnitude) have only occurred along the Yadong-Gulu Graben (U.S. Geological Survey, n.d.).

5.5.2 Unresolved basin evolution of Nam Co

The bounding faults that presumably generated the Nam Co Basin are not within the data set and are more likely located at the lake's rims, i.e., along the southern flank or outside of the modern

lake. Therefore, the hypotheses that the Nam Co basin developed as an extensional, graben structure rather than a pull-apart feature still has to be proven. Indications for a SW-NE trending normal fault along the northern rim of the NQTL have been suggested (Tapponnier & Molnar, 1977) as incorporated in the HimTibetMap-1.0 (Styron et al., 2010)(dotted orange line, Figure 5.10), although later fieldwork has not confirmed active faulting there (Armijo et al., 1986). Until further proof, the possibility of thermal subsidence rather than tectonic has to be considered as an additional explanation for the lack of major faults.

5.5.3 Extensional and strike-slip characteristics of defined areas

Differently directed stress vectors in the Nam Co basin created diverse areas with unique fault patterns. Some fault characteristics of the four main areas within the western sub-basin (A, B, C, D) can be attributed to two different tectonic regimes. When applicable, both interpretations are included in the detailed perceptions following:

Area A

The area separating the eastern and the western sub-basin closely resembles a wrench zone. The steep dipping angles of faults, the inclined bedding of units, as well as the uplifted Zhaxiduo Peninsula and islands along that zone indicate NW-SE directed strike-slip faults bounding a typical wrench tectonic setting. The southeastern part of the zone has undergone more compressional stress along strike, whereas in the northwestern part, the geometry of the faults led to less compression and, therefore, less deformation (Figure 5.10A). As some wrench zone faults penetrate the lake floor, this zone emerges to be still active. In the past, the wrench zone has likely led to a different evolution of the eastern and the western part of the lake. The later, more profound subsidence (extension) of the western part resulted in a relative depth difference. As a result, hard grounds developed in the flatter eastern sub-basin during lake level low stands. Hard grounds may also be the cause for low penetration of the seismic signal in the entire eastern sub-basin.

Area B

The interpretation for the geologic structure in Area B is a simple (extensional) graben, given the amount of subsidence and the fault angles of 60-70°. Here, the largest throws (40 m) inside the western basin are measured. The direction of fault surfaces in Nam Co is in accordance with the directed stress field for the formation of the regional rift systems (Armijo et al., 1986).

Area C

At first glance, Area C resembles a textbook example of domino faulting (see Scenario 1, Figure 5.10B). Yet, most domino fault systems rest on an underlying decollement fault or detachment (Fossen, 2016). A low-angle-fault has not been detected in the seismic data, but an alternative explanation, as stated by Fossen (2016), is possible: A mechanically weak layer of clay or salt could

be acting as a mobile medium at the base of the rotating fault blocks. Using the fault angles of 65° and 10° for the angle of rotation, while neglecting internal strain, we calculated an extension of 6.6% by using the formula by Brun & Choukroune (1983): $\varepsilon = \frac{\sin(\alpha+\theta)}{\sin \theta} - 1$, where ε = extension, α = dip angle of bedding, and θ = dip angle of the fault plane. As the lake sediments are unconsolidated and are showing slight folding within the blocks, a 'soft' domino model, as described by Fossen (2016), is very likely. This allows for slight variations in fault size, fault displacement, and folding of layers as observed in Area C. Likewise, the inclined blocks in Area C could be caused by block rotation in a strike-slip environment (see Scenario 2, Figure 5.10C). Dextral strike-slip faults, striking NW-SE, bordering Area D create a clockwise rotation of blocks. However, this hypothesis stays speculative as the along strike movement cannot be quantified.

Area D

The dense and steep faulting, lateral overlapping of short faults, and the cross-section geometry (Figure 5.7) indicate a negative flower structure (Fossen, 2016). This feature is typical for a strike-slip regime. Moreover, the varying amounts of throw along the fault plane indicate movement up and down along the fault plane. The flower structure's overall strike direction would be NW-SE and should be dextral to fit the regional context (see Scenario 2, Figure 5.10C). The surface expression of the faults point to modern activity. However, the penetration of the seismic data hampers a statement about the fault plane behavior at greater depth. For a negative flower structure, the fault planes converge in-depth into one single fault plane and create typical 'y' shapes. Fault planes that do not converge but create 'v'-shaped structures could also be interpreted as alternating E-W half-graben structures (see Scenario 1, Figure 5.10B).

NW slope

The abundant faults detected on the northwestern slope of Nam Co (Profiles GeoB-393 and GeoB-424; Figure 5.9) west of Area D resemble the evolution of ramp-flat-ramp-faults with extensive hanging wall deformation (Fossen, 2016) or horst-and-graben structures (Figure 9B) that extend to the East into the domino fault system (Area C).

Reverse faults in the south and framework of primary faults

The few observed reverse faults in the SW study area (Figure 5.3) inhabit negligible throws but steep fault angles and are hence most likely strike-slip induced. We identify two parallel faults in NW- SE direction, which fit to the two strike-slip faults proposed to reach Nam Co in the NW by Schneider et al. (2003) and Molnar & Tapponnier (1978) (dotted orange in Figure 5.10A).

A possible connection of the strike-slip faults in the basin and the proposed faults onshore points to an older initiation age of the faults. Therefore, we consider the southern NW- SE directed strike-slip faults as primary (purple, Figure 5.10).

Schneider et al. (2003) also identified a thrust fault (Duba Fault) and a parallel strike-slip fault (brown in Figure 5.10A) reaching Nam Co in the SE. Also, from observations at the Gulu Graben, Pullen et al. (2008) suggest a thrust fault zone entering Nam Co in the SE. However, we identified only a few minor faults in the area, which inhabit nearly no throws. Therefore, no clear distinguishing between reverse or strike-slip faults is possible. The faults might also be reactivated features that are created due to the interplay of the strike-slip wrench zone and the sub-parallel strike-slip faults in the center of the basin. As the two strike-slip fault zones slightly converge towards the south-east (Figure 5.10), the increased stress created the observed reverse faulting.

Neither Taylor et al. (2003), Taylor & Yin (2009) nor Styron et al. (2010, 2011) have included NW-SE directed faults parallel to the Beng Co fault in their compilation maps (e.g., HimaTibetMap 1.1). Our interpretation of satellite images (GoogleEarth, n.d.) (white lines, Figure 5.10A) concludes in a likely continuation of the NW-SE wrench fault zone on land further to the northwest, coinciding with the compilation of Tapponnier and Molnar (1977), Wu et al. (2011) or Armijo, et al. (1986; 1989) an to the SE (indicated purple line, Figure 5.10A).

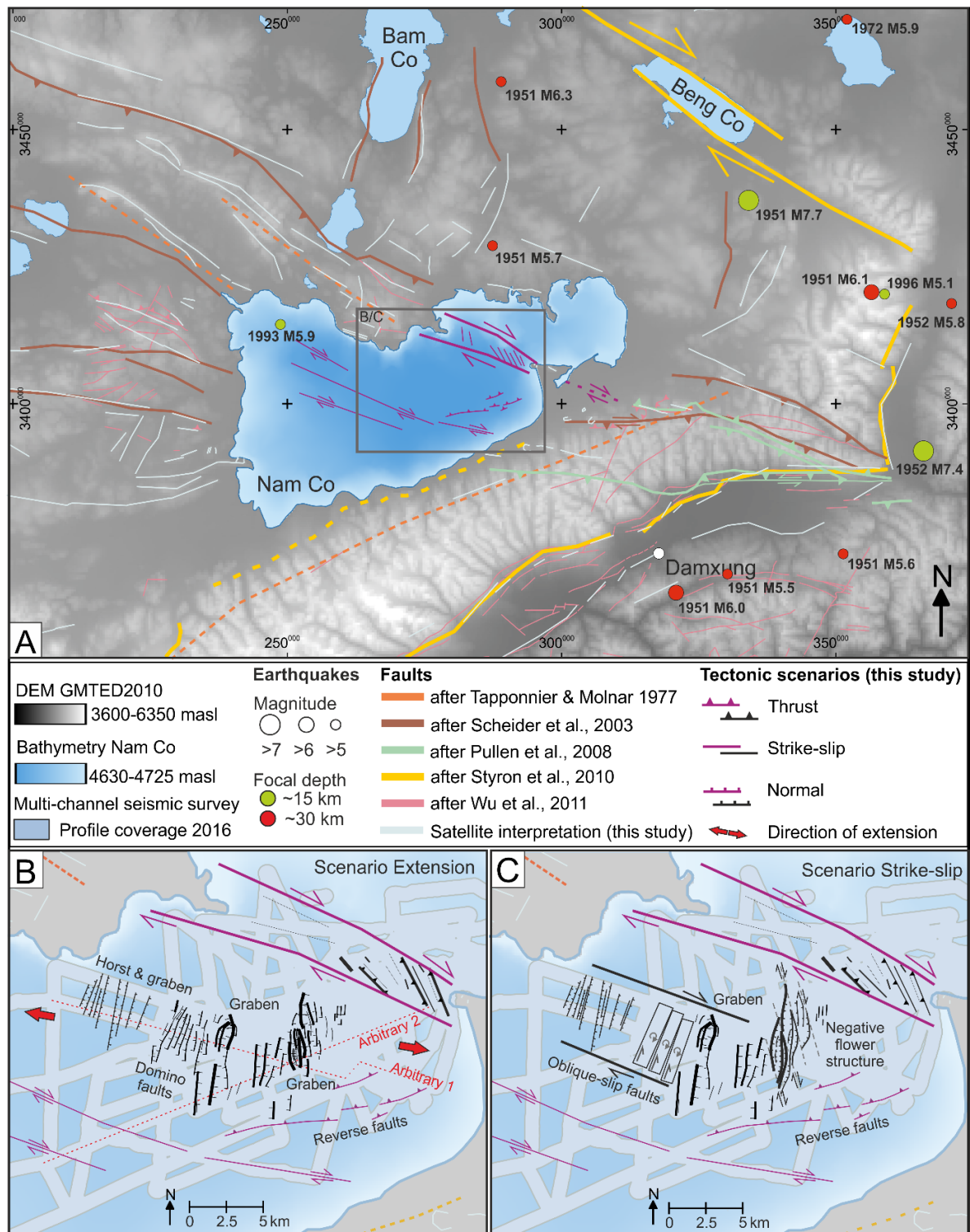


Figure 5.10: A) Regional tectonic system compiled from Molnar & Tapponnier (1978), Schneider et al. (2003), Pullen et al. (2008), Styron et al. (2010), and Wu et al. (2011) as well as own satellite observations. Inferred faults are indicated with dotted lines. The interpretation of primary faults in the Nam Co basin is shown in purple. B) & C) illustrate the interpretation of local tectonic system of secondary faults in black. Fault classification is given with line thicknesses. Extent of B and C as indicated in A. All maps are projected in UTM 46N.

To keep up with Armijo et al.'s assumption (1986) of equal rates on the main faults, the major strike-slip faults should inhabit >10 to 20 mm/yr of slip. Slip rates along the Beng Co strike-slip fault to the north-east of Nam Co, measured by Hollingsworth et al. (2010) and Garthwaite et al. (2013) have been in the range of 1-4 mm/yr. Ryder et al. (2014) assessed a slip rate of 7.7 mm/yr. The movement estimation of the wrench zone within Nam Co needs to be studied further. However, the strike-slip fault could be compensating the strain difference between expectation and measurement at the dextral Beng Co fault.

5.5.4 Interpretation of extensional and strike-slip-dominated scenarios

The characteristics of the faults within the western basin are not allowing a clear distinction between strike-slip and normal dip-slip faults. Therefore, we introduce two endmember-models (Scenario 1 -Extension and Scenario 2 -Strike-slip) to demonstrate the interplay of the different areas and the connection to the regional fault system.

Scenario 1 and Scenario 2 depict possible tectonic settings of Nam Co with the network of dip-slip and strike-slip faults, respectively. Both scenarios have in common that the wrench zone to the north and one or more NW-SE striking strike-slip faults to the south (primary faults, Figure 5.10A) bind the secondary tectonic system of the western sub-basin. These primary faults most likely continue on land, and probably more extensively towards the northwest.

Scenario 1 - Extension Setting

Framed by the primary faults (purple, Figure 5.10B), extensional features are aligned in the western sub-basin. Striking NNE-SSW, a Horst and Graben fault pattern, is followed by domino faults and a major graben. With a slight change in strike, direction follows an NNW-SSE striking complex half-graben system, built up by various overstepping faults of different lengths and throws.

The identification of the main strike directions being NNE-SSW in the western and NNW-SSE in the eastern part of the sub-basin (Figure 5.10B) allowed us to calculate extension rates across two directions through the lake, approximately perpendicular to the strike. As the bedding angles are on average 2° but always < 5°, we assume a nearly horizontal setting and calculate the extension as shown by Bogen & Schweickert (1985). In WNW-ESE direction along Arbitrary (line) 1 (Figure 5.10B), the lateral extension rate is 0.7 mm/yr, which accounts for ~1.1% in the last 350 kyrs. The cumulative throw rate (TR), accordingly, is 0.9 mm/yr. In WSW-ENE direction along Arbitrary 2 (B), the lateral extension rate is 0.5 mm/yr, which accounts for ~0.7% in the last 350 kyrs, and the TR is 0.3 mm/yr.

Cumulative throw rates of 0.9 mm/yr in WNW-ESE direction across the basin are comparable with values from other regional extensional grabens. Recent measurements from Chevalier et al. (2020) and Wu et al. (2004, 2015) from the southern Yadong-Gulu graben, the Yanbajing Graben,

and Damxung (Figure 5.1) are in the same range. Compared to the Gulu Graben in the north, where the extension rates are found to be larger (Chevalier et al., 2020; Ryder et al., 2014), the throw rates from Nam Co are about one third to half the magnitude. In central Tibet, W-E extension is less prominent, and the throw rates are one order of magnitude smaller: In the Shuang Hu graben, cumulative TR is less than 0.3 mm/yr within the last ~230 kyrs (Blisniuk & Sharp, 2003).

Armijo et al. (1986) have observed an extension of about 1% per million years across south Tibet. Across the Yadong-Gulu rift, Armijo et al. (1986) imply an average extension rate of 1.4 ± 0.8 mm/yr. Chevalier et al. (2020) measured decreasing late Quaternary extension rates from north to south: 3-6 mm/yr north of the Gulu bend and 1.3 ± 0.3 mm/yr for the southern Yadong-Gulu rift.

Therefore, lateral extension within Nam Co is proceeding on rates about half the magnitude of the Yadong Gulu rift. This emphasizes the prominent role of the extensive N-S striking rift system on the TP.

In Nam Co, maximum throws occur in Area A and Area B, with a max 40 m. Absolute fault throw along individual master faults, as described by Armijo et al. (1986), is significantly greater than the individual faults within Nam Co. All of Armijo's observed rift systems have throws exceeding 2 km (Armijo et al., 1986). However, faulting along the entire NW- SE profile 393 (section shown in Figure 5.6), for example, created a total subsidence of 136 m. Normal dip-slip faults can entirely explain the subsidence of the basin; however, the features in Areas C & D imply a strike-slip component in the local tectonic system.

Scenario 2 - Strike-slip dominated setting:

Framed by the primary faults (purple, Figure 5.10C), oblique-slip faults border the central graben to the west, and negative flower structures are located to the east. The interpretation of Area D as a negative flower structure infers that its strike-slip faults are dying out towards the SW.

The most prominent adaptation compared to Scenario 1 is the change in fault classification. In order to allow rotated blocks in Area C, two parallel strike-slip faults are introduced to border the Areas A and C. These faults have not been identified as strike-slip in the seismic data, but a lack of throw could have masked them from detection. These additional faults inhabit the largest fault class and downgrade the faults of the wrench zone, most likely. In this setting, the reverse faults in the south-east could be reactivated by strike-slip if the strike-slip faults are not transferring movement to the normal faults. The stress vector is increasing the dextral force on the fault in the south. Alternatively, the southernmost strike-slip fault would remain in the highest fault class. The strike-slip scenario contains an extensional component in nearly W-E direction. Its strength is possibly decreased compared to Scenario 1.

Feasibility

The seismic data support both scenarios. Almost certainly, none of the end-member model represents the actual tectonic system adequately. Most likely, a combination of the two models resembles reality best. More plausible, in our opinion, is a transtensional model with major extension features. Reasons for that are the simpler geometry and mechanism architecture. The detected faults in Scenario 1 can be explained with less bounding faults than Scenario 2, which needs additional faults for which no hard proof yet exists.

Our assumptions about fault behavior in depth are tentative. According to Cogan et al. (1998), the geometry of the Yadong-Gulu rift and other rift systems imply that lateral flow within the middle crust steered the extension of the Tibetan Plateau crust at depth. From there, low-angle shear zones could have developed to accommodate extension. However, deformation in the upper, brittle crust reveals little how extension was accommodated in the lower crust and mantle lithosphere (Fossen, 2016). Most recent earthquake events in Yanbajing (Damxung event, 2008) occurred with focal depths of 4-11 km (Elliott et al., 2010) while the 1993 earthquake in the NW of Nam Co was reported with a focal depth of 33 km (U.S. Geological Survey, n.d.) (Figure 5.10).

5.6 Conclusion

The Nam Co sediments reveal a local diverse tectonic system influenced by the regional tectonic movements. Nam Co inhabits an NW-SE strike-slip zone, parallel to the dextral Beng Co fault. The so-called wrench zone separated the eastern from the western sub-basin and initiated the development of the western sub-basin into a sedimentary depocenter. This NW-SE strike-slip zone is in agreement with the 'lateral extrusion' model suggested by Armijo et al. (1989) and could comprehend the difference between expected and recently measured slip rates along the Beng Co fault.

Besides the primary strike-slip fault zone, the western sub-basin contains extensive secondary faulting. A clear distinguishing between an extensional and a purely strike-slip setting at Nam Co is not possible. Characteristic features of both scenarios can be identified, and a mixture of extension and strike-slip is most likely. We therefore hypothesize a transtensional setting with a predominant extensional component.

The faults inhabit a cumulative throw rate of 0.9 mm/yr in NWN-SES direction, comparable to other regional faults. For the center of the lake, an extension of 1% was calculated in NWN-SES direction. However, an extension rate of 0.7 mm/yr for Nam Co is about half the extension rate from faults in the Yadong-Gulu rift, emphasizing the subordinate role of the secondary faults in Nam Co.

For the observed time span from ~360 to ~40 kyrs, the measured throw and extension rates are an indicator of constant strain comprehension in this part of the TP. However, during periods of high lake levels and interglacial climate conditions, the tectonic activity of the faults seems to be inactive. This might indicate a correlation of e.g., pore pressure and seismological activity and requires further investigation.

5.7 Acknowledgements

This study was funded by the German Research Foundation (DFG) (grants SP296/36-1, SP296/36-2, DA 563/3-1), and is part of the ICDP project 'Seismic Pre-Site Survey for ICDP Drilling Locations at Lake Nam Co'. Further funding for data acquisition was provided by the Strategic Priority Research Program of Chinese Academy of Sciences (XDA20070101) and the Chinese Ministry of Science and Technology project (2012FY111400). We are grateful to Schlumberger for providing the VISTA 2D/3D Seismic Data Processing software package and to IHS for providing the KINGDOM Software for seismic interpretation. Further, we want to thank Carlos Alejandro Ramos Cordova for his help in coding Python.

Chapter 6: Conclusion and Outlook

Within this thesis, the combined dataset of parametric sediment echosounder profiles, coring data, and new hydro-acoustic data was utilized to investigate the sedimentary and tectonic evolution of the lake Nam Co on the Tibetan Plateau. The here presented research contributes to the overall understanding of Nam Co's sedimentary system and tectonic setting. Consequently, this work poses an essential prerequisite for evaluating Nam Co as a potential climate archive, which could significantly advance the progress in modeling future climate changes.

The most recent set of sediment echo sounder and multichannel reflection seismic (MCS) data, acquired as a pre-site survey for the ICDP campaign 'NamCore' in 2016, built the broad database for Chapters 3, 4, and 5 of this work. The current thesis underlined the excellent suitability of high-frequency multichannel reflection seismic to study shallow-water lake setting even in challenging high altitudes and an isolated environment like Nam Co (4724 masl), conquering technological challenges, low air pressure, and logistic efforts.

The main findings of this thesis are presented in three standalone studies presented in Chapters 3 to 5. The chapters focused on the recent sediment distribution and deposition processes and lake-level variations back to the LLGM (Chapter 3), the long-term lake-level variations over eight glacial-interglacial-cycles back to 712 ka and the climatic steering factors (Chapter 4), and the tectonic setting within Nam Co (Chapter 5).

Regarding the research objectives outlined in Chapter 1.1.4, the key conclusions of this thesis are summarized in the subsequent paragraphs.

(1) Improved comprehension of lacustrine sediment distribution and deposition processes (Chapter 3)

The investigation of high-resolution SES data from 2005, 2006 & 2016 provided new insights into the sediment distribution processes in Nam Co. A detailed facies analysis and reflector tracing was conducted on nearly 1400 km of profiles. The comprehensive SES data revealed a limitation of modern sedimentation to water depth deeper than 66 m. Moreover, modern sediments younger than 1 ka are generally characterized by a very low amplitude seismic facies typical for a high lake-level environment.

A sedimentological model (Figure 3.7) representative for the observed sediment distribution was developed. The model proposes that clay and silt-sized sediment reached far into the basin via interflows. The height of a contemporary boundary layer, most likely a pycnocline, steered the interflow and limited fine sediment deposition to below 66 mbl. The suggested model fits the

reported spatial variability of surface sediment samples (Wang et al., 2012; 2015a), e.g., the anthropogenic ^{138}Cs or Pb or n-alkane.

By correlating the SES data to the core logs of NC01/08, 13 individual reflectors could be assigned ages reaching back to 20.5 ka. All reflectors show a specific onlap depth between 46.1 to 95.7 mbll. The according units are characterized by increasing thicknesses to the basin. Also, internal reflectors with basinward-decreasing amplitude were detected. The first order approximate of a stable boundary layer is representative for high lake-level scenarios during the Holocene and a short period around 12.2 ka. During climatic periods with a low lake level, the stratification of the water column might not be at a stable water depth of 66 mbll. The identified onlaps of the reflectors until 16.7 ka are connected to morphological steps in the lake subsurface, implying that the lake level was about 15 m higher than the onlap depths. For reflectors from 16.5 to 13.4 ka, most likely underflows distributed dissolved material derived by rivers into the lake basin. Hence, the sediment onlaps during the periods with Late Glacial climatic conditions represent relative lake-level variations.

(2) Development of a seismo-stratigraphic concept of the lacustrine sediments (Chapter 4)

The so far limited stratigraphic control of the Nam Co sediments by the 10.4 m record, spanning 24 kyrs, has emphasized the need for a comprehensive seismo-stratigraphic framework.

The MCS data allowed a deep penetration to nearly 1 s TWT while preserving superb imaging quality. For the first time, acoustic basement reflectors could be identified. A customized seismic processing routine enabled the mapping of the reflector on several profiles. However, on the center of the lake, the reflection was below the seismic resolution limit, indicating that the sediment infill exceed 680 m in thickness.

Seismic units down to half of the lacustrine basin infill were identified and mapped by conducting a detailed seismic facies analysis. The entire acoustic dataset displays a cyclic alternation in seismic reflection amplitude. A direct dependency of reflection amplitude to lake-level was revealed, as the seismic amplitude variations relate to sedimentation rates and grain-size sorting during transportation. The low energy environment during high lake-level stands allows fine-grained materials to settle, corresponding to low seismic amplitudes. In contrast, during low lake levels, the high energy environment transports coarser material to the center of the lake basin represented by high seismic amplitude units. In turn, these cyclic lacustrine high and low lake level sequences correlate with the global glacial cycles. Thus, the derived age model indicated the unique record of eight glacial-interglacial cycles back to 712 ka. The presented stratigraphic analysis extents to the deepest identified continuous reflector, however, the underlying sediment might span an

additional 350 m of lacustrine infill. Thus, the deepest sediments in Nam Co could more than one million years old.

(3) Understanding the variability of lake level on long time scales and its climatic control (Chapter 4)

A relative lake-level curve was developed based on the conducted seismic facies analysis and the established seismo-stratigraphic framework (see paragraph (3)). Depositional environments during dry and wet periods were deduced, which allow an understanding of the temporal and spatial climatic conditions in the Tibetan Plateau. Significantly high or low lake-level stands result from the local input-evaporation-ratio, which is strongly dependent on the moisture availability regulated by the atmospheric circulation. Calculated linear sedimentation rates show almost constant values of 0.52 mm/yr for full glacial-interglacial cycles, with low rates (~ 0.2 mm/yr) during wet, interglacial conditions and high rates (~ 0.87 mm/yr) during dry, glacial conditions, indicating similar environmental influences in the Nam Co area through time. By comparing the relative lake-level curve to supra-regional records from speleothems, ice cores, and loess records and global records of temperature, $\delta^{18}\text{O}$, and lake-level variation, it was concluded that the hydrology of the Nam Co basin is primarily steered by the precipitation of the Asian Summer monsoon. The local contribution of enhanced meltwater or potentially thawing permafrost is, however, notable during MIS 5.

(4) Providing insights on the link between regional and supra-regional tectonics (Chapter 5)

The analysis of more than 970 km of high-resolution multichannel seismic data revealed manifold strike-slip and normal faults in the Nam Co basin and presented the first documentation of tectonic extension in southern Tibet since the Middle Pleistocene.

Through the detailed identification, analysis, and characterization of the observed faults, primary and secondary faults were distinguished, and two end-member models to interpret the secondary faults were introduced.

The primary strike-slip zone, crossing Nam Co from NW to SE, separated the eastern from the western sub-basin and initiated the development of the western sub-basin into a sedimentary depocenter. This 'wrench zone' is a parallel feature to the dextral Beng Co strike-slip fault in the NE and might likewise compensate for W-E extension, fitting the supra-regional strain regime. Most likely, this fault zone extends onshore and is currently active, as indicated by lake-floor-penetrating faults.

The secondary faults identified in the western subbasin of Nam Co cannot be unambiguously interpreted as either extensional or purely strike-slip as characteristic features of both end-member

scenarios are apparent. Thus, a transtensional setting with a predominant extensional component was hypothesized.

Faulting in WSW-ENE and WNW-ESE direction through the western subbasin inhabit rates of calculated, cumulative throws in the range of 0.3 mm/yr to 0.9 mm/yr, respectively. These rates are comparable to other regional faults, e.g., in the southern Yadong-Gulu rift. In total, we observed a cumulative throw of 315 m along the WNW-ESE direction. Lateral extension rates range between 0.5 and 0.7 mm/yr. Although rates and amounts of extension found in Nam Co seem secondary when compared to the nearby Gulu Graben (<12%), the rates from Nam Co indicate that its faults contributed nearly half of the total extension when compared to the southern Yadong-Gulu rift system, or ~7% when compared to the whole south Tibet extension.

Moreover, the analysis indicated continuous fault activity since the initiation of faulting around 350 ka. Short exceptions are periods of very high lake levels during wet, interglacial conditions prevailing in MIS 5e and since the Holocene. This requires further detailed investigation but might indicate a correlation between groundwater pressure and seismicity.

All in all, Nam Co represents a yet unparalleled lacustrine archive comprising potentially more than one million years of sedimentary history. A successful ICDP drilling campaign will significantly enhance our understanding of the past climate system and contribute to assessing future climate change and its implications on society, ecology, and the economy.

This thesis raised new questions that may be approached by future research:

In the scope of the SES data analysis, several indicators of former beach ridges were identified. However, a spatial correlation between single SES profiles was not unambiguously possible. Most of these features habit an apparent topography and no to minor sediment cover as resolved by the SES. A multibeam survey close to the shorelines would enable the examination of recently drowned beach ridges and terraces. A multibeam survey would further enlighten the spatial distribution pattern of surface sediments close to major river inlets. The occurrence of delta lobes or meander pathways could be investigated and enhance the understanding of recent sedimentary processes in Nam Co.

The stratigraphic framework presented in Chapter 4 revealed the good overall accordance of the relative lake-level curve and the glacial cycles over a time span of 17 MIS. However, the age correlation of MIS 3 and 4 proved to be challenging at the location of the reference site. The seismo-

stratigraphy of these sediments could be further improved by applying the used method on multiple reference sites in the basin and creating a composite lake-level curve.

The analysis of the faults in Na co has revealed an almost continuous activity of the extensional faults. During high lake-level periods of MIS 5 e and the Holocene, however, faulting appears to have stopped. While the assumption was made that the water level and the associated pore pressure may hinder fault movement, this requires further investigation. The focus on a more detailed analysis of thicknesses and throws within seismic units of high lake levels (e.g., MIS 11) might promote a correlation of high lake level and fault inactivity.

The question of how the Nam Co basin initially formed remains open for speculation. Fieldwork might reveal bounding dip-slip faults onshore parallel to the northern flank of the Nyainqêntanglha Mountain Range. Also, the Zhaxiduo Peninsula and the area north and south of the wrench zone might be a promising research target to endorse the dextral strike-slip activity and to estimate displacement rates on the strike-slip faults and their contribution to the overall E-W extension in southern Tibet.

With the granted Drilling Initiative NamCore by ICDP, all interested parties' funding efforts are ongoing. The successful retrieval of sediment cores in Nam Co would allow for interdisciplinary and integrated research on long and continuous proxy time-series of past climate, ecosystems, tectonics, and biosphere (Haberzettl et al., 2019). The here presented geophysical investigation revealed Nam Co's structural and stratigraphic framework. The thorough correlation between core data and seismic reflection profiles and a comparison between seismic facies analysis and lithology would further elaborate the spatial and temporal reconstruction of Nam Co's evolution.

Acknowledgments

"You Can't Climb Up A Mountain With Downhill Thoughts." Having reached the peak and looking back, I want to thank everyone who helped me get to where I am now. I definitely could not have succeeded without a bunch of people who accompanied me along the way:

My thanks go to Prof. Dr. Volkhard Spieß for offering me this interesting and challenging project, for his supervision work and advice, and for the possibilities to join research cruises, attend workshops and get teaching experience while being part of his workgroup 'Marine Technology' at the University of Bremen.

I thank Prof. Dr. Sebastian Krastel for appraising this thesis as the second evaluator and having a flexible schedule.

Special thanks goes to my thesis committee: To Jerome van der Woerd, Gerhard Daut, and Tilmann Schwenk for their time, expertise, and readiness to help.

Fieldwork in Tibet would not have been possible without the help of our Chinese colleagues. I would like to mention Junbo Wang, Jianting Ju, and Liping Zhu out of a big group of helping fellow researchers and students.

This study was funded by the Deutsche Forschungsgemeinschaft (DFG, German Research Foundation) within the IODP Priority program (Grant SP296/36-1, Grant SP296/36-2). I would also like to express my gratitude to GLOMAR for providing funding support, thereby enabling my attendance at AOGS 2017 in Singapore and a workshop in Potsdam.

From the bottom of my heart, I would like to thank my colleagues: Aisgo, Angela, Anna, Fenna, Hanno, Helga, Julia, Lena, Niko, Noemi, Opeyemi, Stefan, Tilmann, and Zsuzsi. Thanks for your help in data processing, for the discussions, for coffee/fresh-air breaks, for listening, for reading, for just making the office the place to be.

And last of all, I owe my friends Fenna, Rebecca, and Carlos, and my parents and Bor an outstanding heartfelt debt of gratitude. For all the support, for warm words in times of despair, for sharing thoughts, in-depth-discussions and wise counseling, por Homeoffice todo incluido, paseos no importa el tiempo y montones de hojas. For always being there for me.

Danke für alles. Muchas gracias.

List of Figures

Figure 1.1: Geographical location of the Tibetan Plateau	21
Figure 1.2: NamCore Logo of the ICDP Nam Co Drilling Project	23
Figure 1.3: Tectonic reconstructions of the India-Eurasia-Collision	26
Figure 1.4: Sketches of proposed tectonic models.....	27
Figure 1.5: Tectonic map of the Tibetan Plateau.....	28
Figure 1.6: Distribution of earthquakes in and around the TP.....	28
Figure 1.7: Catchment area of Nam Co on the geologic map of the area.....	29
Figure 1.8: Sketch depicting the summer monsoon circulation.....	30
Figure 1.9: Basic pattern of summer circulation during the Last Glacial and the Holocene.....	30
Figure 1.10: Lithology, chronology and SAR from NC08/01.....	33
Figure 2.1: Survey tracks of Sino-German research cruises	35
Figure 2.2: Schematic multichannel seismic data processing sequence	38
Figure 2.3: Seismic Processing steps visualized on the example of Profile GeoB16-400.....	40
Figure 3.1: Location of Nam Co and its drainage area on the Tibetan Plateau. B) Drainage area of the Nam Co basin with its inflow water network C) Acquired SES profiles.....	48
Figure 3.2: Comparison between hypopycnal, hyperpycnal and mesopycnal flows	49
Figure 3.3: Integration of Core NC 08/01 and SES profile Jena06-13	53
Figure 3.4: A) Onlapping reflectors at the example of SES Profile GeoB16-442-SES, B) Blowup of onlapping reflectors quickly decreasing in amplitude towards the basin. C) Plot of reflector-onlap shifting basin- and shorewards through time.	55
Figure 3.5: Extent of Holocene reflectors in the Nam Co	56
Figure 3.6: Thickness distribution for the time-slices A) 12.4 to 3.9 ka B) 3.9 to 1 ka C) 1ka to today	57
Figure 3.7: Combination of possible sedimentation processes in Nam Co	60
Figure 3.8: Lake-level reconstruction	65
Figure 4.1: A) Location of monsoon records and B) Multichannel seismic profiles.	74
Figure 4.2 A: Arbitrary Line of Seismic Profiles GeoB16-393 and GeoB16-446.....	78
Figure 4.3: Seismic-based unit definition.	82
Figure 4.4: Sketch of depositional environments of seismic facies	85
Figure 4.5: Correlation of the envelope amplitude curve representing lake-level variations, with the global $\delta^{18}\text{O}$ record of benthic foraminifera	87
Figure 4.6: Comparison of the age-correlated lake-level curve with proxy records of atmospheric circulation and climate.....	90

Figure 5.1: Overview map of the eastern central Tibetan Plateau with comprehension of currently active faults	97
Figure 5.2: A) Seismic example of a typical normal fault in scale 1:1 B) Fault characterization C) Compilation of H-T-Plots of a representative amount of 45 faults	101
Figure 5.3: Amount and types of faults in the western sub-basin of Nam Co.....	102
Figure 5.4: Exemplary close-up map of fault data from horizon SR 9.....	103
Figure 5.5: Section of seismic profile GeoB16-381 as example for the southeastern part of Area A and section of seismic profile GeoB16-400 as example for the northwestern part of Area A.....	104
Figure 5.6: Section of seismic profile NamCo-GeoB16-393 as example for Area B	105
Figure 5.7: Section of seismic profile NamCo-GeoB16-446 as example for Area C.....	106
Figure 5.8: Section of seismic profile NamCo-GeoB16-456 as example for Area D	107
Figure 5.9: Sections of seismic profiles NamCo-GeoB16-424 and GeoB16-449.....	108
Figure 5.10: A) Regional tectonic system B) & C) illustrate the interpretation of local tectonic system of secondary faults	113

List of Tables

Table 1.1: List of sediment cores from Nam Co	32
Table 2.1: Overview of all hydro-acoustic surveys on Nam Co	35
Table 2.2: Sound velocities used to integrate Core NC08/01 with the hydro-acoustic data.	43
Table 3.1: Acoustic facies recognized in SES data of Nam Co	52
Table 3.2: Calculated sediment volumes and total accumulation rates	58
Table 4.1: Seismic facies recognized in the 2D seismic data set.....	80

References

- Adnan, M., Kang, S., Zhang, G., Saifullah, M., Anjum, M. N. & Ali, A. F. (2019). Simulation and Analysis of the Water Balance of the Nam Co Lake Using SWAT Model. *Water*, 11(7), 1383. <https://doi.org/10.3390/w11071383>
- Ahlborn, M., Haberzettl, T., Wang, J., Henkel, K., Kasper, T., Daut, G., Zhu, L. & Mäusbacher, R. (2016). Synchronous pattern of moisture availability on the southern Tibetan Plateau since 17.5 cal. ka BP-the Tangra Yumco lake sediment record. *Boreas*. <https://doi.org/10.1111/bor.12204>
- Alivernini, M., Akita, L., Ahlborn, M., Börner, N., Haberzettl, T., Kasper, T., Plessen, B., Peng, P., Schwalb, A., Wang, J. & others. (2018). Ostracod-based reconstruction of Late Quaternary lake level changes within the Tangra Yumco lake system (southern Tibetan Plateau). *Journal of Quaternary Science*, 33(6), 713–720. <https://doi.org/10.1002/jqs.3047>
- An, Z., Clemens, S. C., Shen, J., Qiang, X., Jin, Z., Sun, Y., Prell, W. L., Luo, J., Wang, S., Xu, H., Cai, Y., Zhou, W., Liu, X., Weiguo, L., Shi, Z., Yan, L., Xiao, X., Chang, H., Wu, F., ... Lu, F. (2011). Glacial-interglacial Indian summer monsoon dynamics. *Science*, 333(6043), 719–723. <https://doi.org/10.1126/science.1203752>
- An, Z., Colman, S. M., Zhou, W., Li, X., Brown, E. T., Jull, A. T., Cai, Y., Huang, Y., Lu, X., Chang, H. & others. (2012). Interplay between the Westerlies and Asian monsoon recorded in Lake Qinghai sediments since 32 ka. *Scientific Reports*, 2, 619. <https://doi.org/10.1038/srep00619>
- An, Z., Kukla, G. J., Porter, S. C. & Xiao, J. (1991). Magnetic susceptibility evidence of monsoon variation on the Loess Plateau of central China during the last 130,000 years. *Quaternary Research*, 36(1), 29–36. [https://doi.org/10.1016/0033-5894\(91\)90015-W](https://doi.org/10.1016/0033-5894(91)90015-W)
- An, Z., Kutzbach, J. E., Prell, W. L. & Porter, S. C. (2001). Evolution of Asian monsoons and phased uplift of the Himalaya-Tibetan plateau since Late Miocene times. *Nature*, 411(6833), 62–66. <https://doi.org/10.1038/35075035>
- Anslan, S., Rad, M. A., Buckel, J., Galindo, P. E., Kai, J., Kang, W., Keys, L., Maurischat, P., Nieberding, F., Reinosch, E. & others. (2020). Reviews and syntheses: How do abiotic and biotic processes respond to climatic variations in the Nam Co catchment (Tibetan Plateau)? *Biogeosciences*, 17(5), 1261–1279. <https://doi.org/https://doi.org/10.5194/bg-17-1261-2020>
- Armijo, R., Tapponnier, P. & Han, T. (1989). Late Cenozoic right-lateral strike-slip faulting in southern Tibet. *Journal of Geophysical Research: Solid Earth*, 94(B3), 2787–2838. <https://doi.org/https://doi.org/10.1029/JB094iB03p02787>
- Armijo, R., Tapponnier, P., Mercier, J. & Han, T.-L. (1986). Quaternary extension in southern Tibet: Field observations and tectonic implications. *Journal of Geophysical Research: Solid Earth*, 91(B14), 13803–13872. <https://doi.org/10.1029/JB091iB14p13803>
- Avouac, J.-P., Dobremez, J.-F. & Bourjot, L. (1996). Palaeoclimatic interpretation of a topographic profile across middle Holocene regressive shorelines of Longmu Co (western Tibet). *Palaeogeography, Palaeoclimatology, Palaeoecology*, 120(1-2), 93–104. [https://doi.org/10.1016/0031-0182\(96\)88700-1](https://doi.org/10.1016/0031-0182(96)88700-1)
- Bates, C. C. (1953). Rational theory of delta formation. *Aapg Bulletin*, 37(9), 2119–2162. <https://doi.org/10.1306/5CEADD76-16BB-11D7-8645000102C1865D>
- Berger, A. & Loutre, M.-F. (1991). Insolation values for the climate of the last 10 million years. *Quaternary Science Reviews*, 10(4), 297–317.
- Biskop, S., Maussion, F., Krause, P. & Fink, M. (2015). What are the key drivers of regional differences in the water balance on the Tibetan Plateau? *Hydrology & Earth System Sciences Discussions*, 12(4). <https://doi.org/10.5194/hessd-12-4271-2015>
- Biskop, S., Maussion, F., Krause, P. & Fink, M. (2016). Differences in the water-balance components of four lakes in the southern-central Tibetan Plateau. *Hydrology & Earth System Sciences*, 20(1). <https://doi.org/10.5194/hess-20-209-2016>
- Blisniuk, P. M., Hacker, B. R., Glodny, J., Ratschbacher, L., Bi, S., Wu, Z., McWilliams, M. O. & Calvert, A. (2001). Normal faulting in central Tibet since at least 13.5 Myr ago. *Nature*, 412(6847), 628–632. <https://doi.org/10.1038/35088045>

- Blisniuk, P. M. & Sharp, W. D. (2003). Rates of late Quaternary normal faulting in central Tibet from U-series dating of pedogenic carbonate in displaced fluvial gravel deposits. *Earth and Planetary Science Letters*, 215(1), 169–186. [https://doi.org/10.1016/S0012-821X\(03\)00374-1](https://doi.org/10.1016/S0012-821X(03)00374-1)
- Bogen, N. L. & Schweickert, R. A. (1985). *Magnitude of crustal extension across the northern Basin and Range province: constraints from paleomagnetism*. [https://doi.org/10.1016/0012-821X\(85\)90054-8](https://doi.org/10.1016/0012-821X(85)90054-8)
- Bolch, T., Yao, T., Kang, S., Buchroithner, M., Scherer, D., Maussion, F., Huintjes, E. & Schneider, C. (2010). A glacier inventory for the western Nyainqentanglha Range and the Nam Co Basin, Tibet, and glacier changes 1976–2009. *The Cryosphere*, 4, 419–433. <https://doi.org/10.5194/tc-4-419-2010>
- Boos, W. R. & Kuang, Z. (2010). Dominant control of the South Asian monsoon by orographic insulation versus plateau heating. *Nature*, 463(7278), 218–222. <https://doi.org/10.1038/nature08707>
- Brown Jr, L. & Fisher, W. (1980). *Seismic-Stratigraphic Interpretation of Depositional Systems and its Role in Petroleum Exploration (Part 1)*.
- Brun, J.-P. & Choukroune, P. (1983). Normal faulting, block tilting, and decollement in a stretched crust. *Tectonics*, 2(4), 345–356. <https://doi.org/10.1029/TC002i004p00345>
- Buckel, J., Reinosch, E., Hördt, A., Zhang, F., Riedel, B., Gerke, M., Schwalb, A. & Mäusbacher, R. (2020). Insights in a remote cryosphere: A multi method approach to assess permafrost occurrence at the Qugaqie basin, western Nyainqentanglha Range, Tibetan Plateau. *The Cryosphere Discussions*, 1–33. <https://doi.org/10.5194/tc-2020-114>
- Butler, P. (2012). Strong Noise—Removal and Replacement on Seismic Data. *CSEG Rec*, 37, 34–37.
- Cai, Y., Zhang, H., Cheng, H., An, Z., Edwards, R. L., Wang, X., Tan, L., Liang, F., Wang, J. & Kelly, M. (2012). The Holocene Indian monsoon variability over the southern Tibetan Plateau and its teleconnections. *Earth and Planetary Science Letters*, 335, 135–144. <https://doi.org/10.1016/j.epsl.2012.04.035>
- Chen, F., Yu, Z., Yang, M., Ito, E., Wang, S., Madsen, D. B., Huang, X., Zhao, Y., Sato, T., Birks, H. J. B. & others. (2008). Holocene moisture evolution in arid central Asia and its out-of-phase relationship with Asian monsoon history. *Quaternary Science Reviews*, 27(3), 351–364. <https://doi.org/10.1016/j.quascirev.2007.10.017>
- Chen, G.-S., Liu, Z. & Kutzbach, J. (2014). Reexamining the barrier effect of the Tibetan Plateau on the South Asian summer monsoon. *Climate of the Past*, 10(3), 1269. <https://doi.org/10.5194/cp-10-1269-2014>
- Cheng, H., Edwards, R. L., Sinha, A., Spötl, C., Yi, L., Chen, S., Kelly, M., Kathayat, G., Wang, X., Li, X. & others. (2016a). The Asian monsoon over the past 640,000 years and ice age terminations. *Nature*, 534(7609), 640–646. <https://doi.org/10.1038/nature18591>
- Cheng, H., Sinha, A., Wang, X., Cruz, F. W. & Edwards, R. L. (2012). The Global Paleomonsoon as seen through speleothem records from Asia and the Americas. *Climate Dynamics*, 39(5), 1045–1062. <https://doi.org/10.1007/s00382-012-1363-7>
- Cheng, H., Spötl, C., Breitenbach, S. F., Sinha, A., Wassenburg, J. A., Jochum, K. P., Scholz, D., Li, X., Yi, L., Peng, Y. & others. (2016b). Climate variations of Central Asia on orbital to millennial timescales. *Scientific Reports*, 6, 36975. <https://doi.org/10.1038/srep36975>
- Chevalier, M.-L., Tapponnier, P., van der Woerd, J., Leloup, P., Wang, S., Pan, J., Bai, M., Kali, E., Liu, X. & Li, H. (2020). Late Quaternary Extension Rates Across the Northern Half of the Yadong-Gulu Rift: Implication for East-West Extension in Southern Tibet. *Journal of Geophysical Research: Solid Earth*, 125(7), e2019JB019106. <https://doi.org/10.1029/2019JB019106>
- Clemens, S. C. & Prell, W. L. (2003). A 350,000 year summer-monsoon multi-proxy stack from the Owen Ridge, Northern Arabian Sea. *Marine Geology*, 201(1–3), 35–51. [https://doi.org/10.1016/S0025-3227\(03\)00207-X](https://doi.org/10.1016/S0025-3227(03)00207-X)
- Cogan, M. J., Nelson, K., Kidd, W. & Wu, C. (1998). Shallow structure of the Yadong-Gulu rift, southern Tibet, from refraction analysis of Project INDEPTH common midpoint data. *Tectonics*, 17(1), 46–61. <https://doi.org/10.1029/97TC03025>
- Cong, Z., Kang, S., Gao, S., Zhang, Y., Li, Q. & Kawamura, K. (2013). Historical trends of atmospheric black carbon on Tibetan Plateau as reconstructed from a 150-year lake sediment record. *Environmental Science & Technology*, 47(6), 2579–2586. <https://doi.org/10.1021/es3048202>

- Copley, A. & McKenzie, D. (2007). Models of crustal flow in the India-Asia collision zone. *Geophysical Journal International*, 169(2), 683–698. <https://doi.org/10.1111/j.1365-246X.2007.03343.x>
- Cortés, A., Fleenor, W., Wells, M., de Vicente, I. & Rueda, F. (2014). Pathways of river water to the surface layers of stratified reservoirs. *Limnology and Oceanography*, 59(1), 233–250. <https://doi.org/doi:10.4319/lo.2014.59.1.0233>
- Cruz, R., Harasawa, H., Lal, M., Wu, S., Anokhin, Y., Punsalmaa, B., Honda, Y., Jafari, M., Li, C. & Ninh, N. H. (2007). *Climate Change 2007: Impacts, Adaptation and Vulnerability. Contribution of Working Group II to the Fourth Assessment Report of the Intergovernmental Panel on Climate Change*. Cambridge University Press, Cambridge, UK and New York, NY.
- Cukur, D., Krastel, S., Demirel-Schlüter, F., Demirbag, E., Imren, C., Niessen, F., Toker, M., Group, P.-W. & others. (2013). Sedimentary evolution of Lake Van (Eastern Turkey) reconstructed from high-resolution seismic investigations. *International Journal of Earth Sciences*, 102(2), 571–585. <https://doi.org/10.1007/s00531-012-0816-x>
- Cuo, L. & Zhang, Y. (2017). Spatial patterns of wet season precipitation vertical gradients on the Tibetan Plateau and the surroundings. *Scientific Reports*, 7(1), 1–10. <https://doi.org/10.1038/s41598-017-05345-6>
- Daut, G., Mäusbacher, R., Baade, J., Gleixner, G., Kroemer, E., Mügler, I., Wallner, J., Wang, J. & Zhu, L. (2010). Late Quaternary hydrological changes inferred from lake level fluctuations of Nam Co (Tibetan Plateau, China). *Quaternary International*, 218(1-2), 86–93. <https://doi.org/10.1016/j.quaint.2010.01.001>
- De Batist, M. & Chapron, E. (2008). Lake systems: sedimentary archives of climate change and tectonics. *Palaeogeography, Palaeoclimatology, Palaeoecology*, 2(259), 93–95. <https://doi.org/10.1016/j.palaeo.2007.10.016>
- DeCelles, P. G., Robinson, D. M. & Zandt, G. (2002). Implications of shortening in the Himalayan fold-thrust belt for uplift of the Tibetan Plateau. *Tectonics*, 21(6), 1062. <https://doi.org/10.1029/2001TC001322>
- Dewane, T., Stockli, D., Hager, C., Taylor, M., Ding, L., Lee, J. & Wallis, S. (2006). Timing of Cenozoic EW Extension in the Tangra Yum Co-Kung Co Rift, south-central Tibet. *AGU Fall Meeting Abstracts*.
- Dewey, J. F., Shackleton, R. M., Chengfa, C. & Yiyin, S. (1988). The tectonic evolution of the Tibetan Plateau. *Philosophical Transactions of the Royal Society of London. Series A, Mathematical and Physical Sciences*, 327(1594), 379–413. <https://doi.org/10.1098/rsta.1988.0135>
- Dietze, E., Maussion, F., Ahlborn, M., Diekmann, B., Hartmann, K., Henkel, K., Kasper, T., Lockot, G., Opitz, S. & others. (2014). Sediment transport processes across the Tibetan Plateau inferred from robust grain size end-members in lake sediments. *Climate of the Past*, 10, 91–106. <https://doi.org/10.5194/cp-10-91-2014>
- Dietze, E., Wünnemann, B., Hartmann, K., Diekmann, B., Jin, H., Stauch, G., Yang, S. & Lehmkuhl, F. (2013). Early to mid-Holocene lake high-stand sediments at Lake Donggi Cona, northeastern Tibetan Plateau, China. *Quaternary Research*, 79(3), 325–336. <https://doi.org/10.1016/j.yqres.2012.12.008>
- Ding, L., Xu, Q., Yue, Y., Wang, H., Cai, F. & Li, S. (2014). The Andean-type Gangdese Mountains: Paleoelevation record from the Paleocene-Eocene Linzhou Basin. *Earth and Planetary Science Letters*, 392, 250–264. <https://doi.org/10.1016/j.epsl.2014.01.045>
- Doberschütz, S., Frenzel, P., Habertzettl, T., Kasper, T., Wang, J., Zhu, L., Daut, G., Schwalb, A. & Mäusbacher, R. (2014). Monsoonal forcing of Holocene paleoenvironmental change on the central Tibetan Plateau inferred using a sediment record from Lake Nam Co (Xizang, China). *Journal of Paleolimnology*, 51(2), 253–266. <https://doi.org/10.1007/s10933-013-9702-1>
- Dutt, S., Gupta, A. K., Clemens, S. C., Cheng, H., Singh, R. K., Kathayat, G. & Edwards, R. L. (2015). Abrupt changes in Indian summer monsoon strength during 33,800 to 5500 years BP. *Geophysical Research Letters*, 42(13), 5526–5532. <https://doi.org/10.1002/2015GL064015>
- Dykoski, C. A., Edwards, R. L., Cheng, H., Yuan, D., Cai, Y., Zhang, M., Lin, Y., Qing, J., An, Z. & Revenaugh, J. (2005). A high-resolution, absolute-dated Holocene and deglacial Asian monsoon record from Dongge Cave, China. *Earth and Planetary Science Letters*, 233, 71–86. <https://doi.org/10.1016/j.epsl.2005.01.036>
- Einsele, G. (2000). *Sedimentary basins: evolution, facies, and sediment budget*. Springer.
- Elliott, J., Walters, R., England, P., Jackson, J., Li, Z. & Parsons, B. (2010). Extension on the Tibetan plateau: recent normal faulting measured by InSAR and body wave seismology. *Geophysical Journal International*, 183(2), 503–535. <https://doi.org/10.1111/j.1365-246X.2010.04754.x>

- England, P. & Houseman, G. (1989). Extension during continental convergence, with application to the Tibetan Plateau. *Journal of Geophysical Research: Solid Earth*, 94(B12), 17561–17579. <https://doi.org/10.1029/JB094iB12p17561>
- England, P., Houseman, G., Osmaston, M. & Ghosh, S. (1988). The mechanics of the Tibetan Plateau. *Philosophical Transactions of the Royal Society of London. Series A, Mathematical and Physical Sciences*, 301–320. <https://doi.org/10.1098/rsta.1988.0089>
- England, P. & McKenzie, D. (1982). A thin viscous sheet model for continental deformation. *Geophysical Journal International*, 70(2), 295–321. <https://doi.org/10.1111/j.1365-246X.1982.tb04969.x>
- Fan, Q., Ma, H., Cao, G., Chen, Z. & Cao, S. (2012). Geomorphic and chronometric evidence for high lake level history in Gahai Lake and Toson Lake of north-eastern Qaidam Basin, north-eastern Qinghai-Tibetan Plateau. *Journal of Quaternary Science*, 27(8), 819–827. <https://doi.org/10.1002/jqs.2572>
- Fang, J.-Q. (1991). Lake evolution during the past 30,000 years in China, and its implications for environmental change. *Quaternary Research*, 36(1), 37–60. [https://doi.org/10.1016/0033-5894\(91\)90016-X](https://doi.org/10.1016/0033-5894(91)90016-X)
- Farinotti, D., Huss, M., Fürst, J. J., Landmann, J., Machguth, H., Maussion, F. & Pandit, A. (2019). A consensus estimate for the ice thickness distribution of all glaciers on Earth. *Nature Geoscience*, 12(3), 168–173. <https://doi.org/10.1038/s41561-019-0300-3>
- Ferguson, R. & Church, M. (2004). A simple universal equation for grain settling velocity. *Journal of Sedimentary Research*, 74(6), 933–937. <https://doi.org/10.1306/051204740933>
- Fossen, H. (2016). *Structural geology*. Cambridge University Press. ISBN: 978-1-107-05764-7.
- Frenzel, P., Wroczynka, C., Xie, M., Zhu, L. & Schwalb, A. (2010). Palaeo-water depth estimation for a 600-year record from Nam Co (Tibet) using an ostracod-based transfer function. *Quaternary International*, 218(1), 157–165. <https://doi.org/10.1016/j.quaint.2009.06.010>
- Garthwaite, M. C., Wang, H. & Wright, T. J. (2013). Broad-scale interseismic deformation and fault slip rates in the central Tibetan Plateau observed using InSAR. *Journal of Geophysical Research: Solid Earth*, 118(9), 5071–5083. <https://doi.org/10.1002/jgrb.50348>
- Gasse, F., Arnold, M., Fontes, J. C., Fort, M., Gibert, E., Huc, A., Bingyan, L., Yuanfang, L., Qing, L., Melieres, F. & others. (1991). A 13,000-year climate record from western Tibet. *Nature*, 353(6346), 742–745. <https://doi.org/10.1038/353742a0>
- GEBCO-Compilation-Group. (2020). *GEBCO_2020 Grid*. <https://doi.org/10.5285/a29c5465-b138-234d-e053-6c86abc040b9>
- GLIMS, & NSIDC. (2005). *Global Land Ice Measurements from Space glacier database. Compiled and made available by the international GLIMS community and the National Snow and Ice Data Center, Boulder CO, U.S.A. (updated 2020)*. <https://doi.org/10.7265/N5V98602>
- GoogleEarth. (n.d.). Retrieved December 4, 2017, from <http://www.earth.google.com>
- Gu, Z., Liu, J., Yuan, B., Liu, T. & Zhang, G. (1994). Lacustrine authigenic deposition expressive of environment and the sediment record from Siling Co, Xizang (Tibet), China. *Quaternary Sciences*, 2, 02.
- Guillot, S. & Replumaz, A. (2013). Importance of continental subductions for the growth of the Tibetan plateau. *Bulletin de La Société Géologique de France*, 184(3), 199–223. <https://doi.org/10.2113/gssgfbull.184.3.199>
- Günther, F., Thiele, A., Biskop, S., Mäusbacher, R., Haberzettl, T., Yao, T. & Gleixner, G. (2016). Late quaternary hydrological changes at Tangra Yumco, Tibetan Plateau: a compound-specific isotope-based quantification of lake level changes. *Journal of Paleolimnology*, 55(4), 369–382. <https://doi.org/10.1007/s10933-016-9887-1>
- Günther, F., Witt, R., Schouten, S., Mäusbacher, R., Daut, G., Zhu, L., Xu, B., Yao, T. & Gleixner, G. (2015). Quaternary ecological responses and impacts of the Indian Ocean Summer Monsoon at Nam Co, Southern Tibetan Plateau. *Quaternary Science Reviews*, 112, 66–77. <https://doi.org/10.1016/j.quascirev.2015.01.023>
- Gupta, A. (2008). *Large rivers: geomorphology and management*. John Wiley & Sons.
- Haberzettl, T., Daut, G., Schulze, N., Spiess, V., Wang, J., Zhu, L. & others. (2019). ICDP workshop on scientific drilling of Nam Co on the Tibetan Plateau: 1 million years of paleoenvironmental history, geomicrobiology, tectonics and paleomagnetism derived from sediments of a high-altitude lake. *Scientific Drilling*, 25, 63–70. <https://doi.org/10.5194/sd-25-63-2019>

- Haberzettl, T., Henkel, K., Kasper, T., Ahlborn, M., Su, Y., Wang, J., Appel, E., St-Onge, G., Stoner, J., Daut, G. & others. (2015). Independently dated paleomagnetic secular variation records from the Tibetan Plateau. *Earth and Planetary Science Letters*, 416, 98–108. <https://doi.org/10.1016/j.epsl.2015.02.007>
- Herrmann, M., Lu, X., Berking, J., Schütt, B., Yao, T. & Mosbrugger, V. (2010). Reconstructing Holocene vegetation and climate history of Nam Co area (Tibet), using pollen and other palynomorphs. *Quaternary International*, 218(1-2), 45–57. <https://doi.org/10.1016/j.quaint.2009.05.007>
- Herzschuh, U. (2006). Palaeo-moisture evolution in monsoonal Central Asia during the last 50,000 years. *Quaternary Science Reviews*, 25(1), 163–178. <https://doi.org/10.1016/j.quascirev.2005.02.006>
- Hijioka, Y., E. Lin, J.J. Pereira, R.T. Corlett, X. Cui, G. E. I., R.D. Lasco, E. Lindgren, & Surjan, A. (2014). *Asia* ([Barros, V.R., C.B. Field, D.J. Dokken, M.D. Mastrandrea, K.J. Mach, T.E. Bilir, M. Chatterjee, K.L. Ebi, Y.O. Estrada, R.C. Genova, B. Girma, E.S. Kissel, A.N. Levy, S. MacCracken, P.R. Mastrandrea, and L.L. White (eds.)], Ed.; pp. 1327–1370). Cambridge University Press, Cambridge, United Kingdom and New York, NY, USA.,
- Hock, R., Rasul, G., Adler, C., Caceres, B., Gruber, S., Hirabayashi, Y., Jackson, M., Käb, A., Kang, S., Kutuzov, S. & others. (2019). *High Mountain Areas: In: IPCC Special Report on the Ocean and Cryosphere in a Changing Climate*.
- Hollingsworth, J., Wernicke, B. & Ding, L. (2010). Fault slip-rate estimate for the right-lateral Beng Co strike-slip fault, based on Quaternary dating of displaced paleo-lake shorelines. *AGU Fall Meeting Abstracts*.
- Hongxing, G. & Anderson, J. K. (2007). Fault throw profile and kinematics of Normal fault: conceptual models and geologic examples. *Geol. J. China Univ*, 13(75), e88.
- Hou, J., D'Andrea, W. J., Wang, M., He, Y. & Liang, J. (2017). Influence of the Indian monsoon and the subtropical jet on climate change on the Tibetan Plateau since the late Pleistocene. *Quaternary Science Reviews*, 163, 84–94. <https://doi.org/10.1016/j.quascirev.2017.03.013>
- Huang, L., Wang, J., Zhu, L., Ju, J. & Daut, G. (2017). The Warming of Large Lakes on the Tibetan Plateau: Evidence From a Lake Model Simulation of Nam Co, China, During 1979–2012. *Journal of Geophysical Research: Atmospheres*. <https://doi.org/10.1002/2017JD027379>
- Hydroweb. (n.d.). Retrieved 11, 2020, from http://hydroweb.theia-land.fr/hydroweb/view/L_namco?lang=en
- Immerzeel, W. W., Lutz, A., Andrade, M., Bahl, A., Biemans, H., Bolch, T., Hyde, S., Brumby, S., Davies, B., Elmore, A. & others. (2020). Importance and vulnerability of the world's water towers. *Nature*, 577(7790), 364–369. <https://doi.org/10.1038/s41586-019-1822-y>
- Immerzeel, W. W., Van Beek, L. P. & Bierkens, M. F. (2010). Climate change will affect the Asian water towers. *Science*, 328(5984), 1382–1385. <https://doi.org/10.1126/science.1187443>
- Innomar. (n.d.). *Innomar SES-2000 light Sub-Bottom Profiler* (accessed 06.08.2018). <https://www.innomar.com/ses2000light.php>
- Innomar. (2015). *SES-2000 medium-100 Sub-Bottom Profiler*.
- Ji, J., Shen, J., Balsam, W., Chen, J., Liu, L. & Liu, X. (2005a). Asian monsoon oscillations in the northeastern Qinghai-Tibet Plateau since the late glacial as interpreted from visible reflectance of Qinghai Lake sediments. *Earth and Planetary Science Letters*, 233(1), 61–70. <https://doi.org/10.1016/j.epsl.2005.02.025>
- Ji, S., Xingqi, L., Sumin, W. & Matsumoto, R. (2005b). Palaeoclimatic changes in the Qinghai Lake area during the last 18,000 years. *Quaternary International*, 136(1), 131–140. <https://doi.org/10.1016/j.quaint.2004.11.014>
- Jia, Y., Shi, Y., Wang, S., Jiang, X., Li, S., Wang, A. & Li, X. (2001). Lake-expanding events in the Tibetan Plateau since 40 kaBP. *Science in China Series D: Earth Sciences*, 44(1), 301–315. <https://doi.org/10.1007/BF02912000>
- Jonell, T. N., Aitchison, J. C., Li, G., Shulmeister, J., Zhou, R. & Zhang, H. (2020). Revisiting growth and decline of late Quaternary mega-lakes across the south-central Tibetan Plateau. *Quaternary Science Reviews*, 248, 106475. <https://doi.org/10.1016/j.quascirev.2020.106475>
- Ju, J., Zhu, L., Feng, J., Wang, J., Wang, Y., Xie, M., Peng, P., Zhen, X. & Lü, X. (2012). Hydrodynamic process of Tibetan Plateau lake revealed by grain size: Case study of Pumayum Co. *Chinese Science Bulletin*, 57(19), 2433–2441. <https://doi.org/10.1007/s11434-012-5083-5>

- Kai, J., Wang, J., Ju, J., Huang, L., Ma, Q., Daut, G. & Zhu, L. (2020). Spatio-temporal variations of hydrochemistry and modern sedimentation processes in the Nam Co basin, Tibetan Plateau: Implications for carbonate precipitation. *Journal of Great Lakes Research*. <https://doi.org/10.1016/j.jglr.2020.04.006>
- Kali, E., Leloup, P., Arnaud, N., Mahéo, G., Liu, D., Boutonnet, E., Van der Woerd, J., Liu, X., Liu-Zeng, J. & Li, H. (2010). Exhumation history of the deepest central Himalayan rocks, Ama Drime range: Key pressure-temperature-deformation-time constraints on orogenic models. *Tectonics*, 29(2). <https://doi.org/10.1029/2009TC002551>
- Kapp, J. L., Harrison, T. M., Kapp, P., Grove, M., Lovera, O. M. & Lin, D. (2005a). Nyainqentanglha Shan: a window into the tectonic, thermal, and geochemical evolution of the Lhasa block, southern Tibet. *Journal of Geophysical Research: Solid Earth*, 110(B8). <https://doi.org/10.1029/2004JB003330>
- Kapp, P., DeCelles, P. G., Gehrels, G. E., Heizler, M. & Ding, L. (2007). Geological records of the Lhasa-Qiangtang and Indo-Asian collisions in the Nima area of central Tibet. *Geological Society of America Bulletin*, 119(7-8), 917–933. <https://doi.org/10.1130/B26033.1>
- Kapp, P., Yin, A., Harrison, T. M. & Ding, L. (2005b). Cretaceous-Tertiary shortening, basin development, and volcanism in central Tibet. *Geological Society of America Bulletin*, 117(7-8), 865–878. <https://doi.org/10.1130/B25595.1>
- Kasper, T., Frenzel, P., Haberzettl, T., Schwarz, A., Daut, G., Meschner, S., Wang, J., Zhu, L. & Mäusbacher, R. (2013). Interplay between redox conditions and hydrological changes in sediments from Lake Nam Co (Tibetan Plateau) during the past 4000cal BP inferred from geochemical and micropaleontological analyses. *Palaeogeography, Palaeoclimatology, Palaeoecology*, 392, 261–271. <https://doi.org/10.1016/j.palaeo.2013.09.027>
- Kasper, T., Haberzettl, T., Doberschütz, S., Daut, G., Wang, J., Zhu, L., Nowaczyk, N. & Mäusbacher, R. (2012). Indian Ocean Summer Monsoon (IOSM)-dynamics within the past 4 ka recorded in the sediments of Lake Nam Co, central Tibetan Plateau (China). *Quaternary Science Reviews*, 39, 73–85. <https://doi.org/10.1016/j.quascirev.2012.02.011>
- Kasper, T., Haberzettl, T., Wang, J., Daut, G., Doberschütz, S., Zhu, L. & Mäusbacher, R. (2015). Hydrological variations on the Central Tibetan Plateau since the Last Glacial Maximum and their teleconnection to inter-regional and hemispheric climate variations. *Journal of Quaternary Science*, 30(1), 70–78. <https://doi.org/10.1002/jqs.2759>
- Keil, A., Berking, J., Mügler, I., Schütt, B., Schwalb, A. & Steeb, P. (2010). Hydrological and geomorphological basin and catchment characteristics of Lake Nam Co, South-Central Tibet. *Quaternary International*, 218(1), 118–130. <https://doi.org/10.1016/j.quaint.2009.02.022>
- Kidd, W. S. F., Dewey, J. F. & participants, G. (1988). *Geological Map of the Academia Sinica-Royal Society Geotraverse: Route Across the Xizang-Qinghai (Tibetan) Plateau, South Sheet - Lhasa to Tanggula Pass 1: 500,000*. Royal Society.
- Kidd, W. S. & Molnar, P. (1988). Quaternary and active faulting observed on the 1985 Academia Sinica-Royal Society Geotraverse of Tibet. *Philosophical Transactions of the Royal Society of London. Series A, Mathematical and Physical Sciences*, 327(1594), 337–363. <https://doi.org/10.1098/rsta.1988.0133>
- Kong, P., Na, C., Brown, R., Fabel, D., Freeman, S., Xiao, W. & Wang, Y. (2011). Cosmogenic ¹⁰Be and ²⁶Al dating of paleolake shorelines in Tibet. *Journal of Asian Earth Sciences*, 41(3), 263–273. <https://doi.org/10.1016/j.jseaes.2011.02.016>
- Kotlia, B. S., Yadav, R. R. & Juyal, N. (2017). “Third pole: The last 20,000 years”: Parts 1-3. *Quaternary International* 454, 85–89. <https://doi.org/10.1016/j.quaint.2017.08.058>
- Kropáček, J., Braun, A., Kang, S., Feng, C., Ye, Q. & Hochschild, V. (2012). Analysis of lake level changes in Nam Co in central Tibet utilizing synergistic satellite altimetry and optical imagery. *International Journal of Applied Earth Observation and Geoinformation*, 17, 3–11. <https://doi.org/10.1016/j.jag.2011.10.001>
- Lacassin, R., Valli, F., Arnaud, N., Leloup, P. H., Paquette, J. L., Haibing, L., Tapponnier, P., Chevalier, M.-L., Guillot, S., Maheo, G. & others. (2004). Large-scale geometry, offset and kinematic evolution of the Karakorum fault, Tibet. *Earth and Planetary Science Letters*, 219(3-4), 255–269. [https://doi.org/10.1016/S0012-821X\(04\)00006-8](https://doi.org/10.1016/S0012-821X(04)00006-8)
- Langille, J., Jessup, M., Cottle, J. & Ahmad, T. (2014). Kinematic and thermal studies of the Leo Pargil Dome: Implications for synconvergent extension in the NW Indian Himalaya. *Tectonics*, 33(9), 1766–1786. <https://doi.org/10.1002/2014TC003593>

- Lazhu, Yang, K., Wang, J., Lei, Y., Chen, Y., Zhu, L., Ding, B. & Qin, J. (2016). Quantifying evaporation and its decadal change for Lake Nam Co, central Tibetan Plateau. *Journal of Geophysical Research: Atmospheres*, 121(13), 7578–7591. <https://doi.org/10.1002/2015JD024523>
- Lehmkuhl, F. & Haselein, F. (2000). Quaternary paleoenvironmental change on the Tibetan Plateau and adjacent areas (Western China and Western Mongolia). *Quaternary International*, 65, 121–145. [https://doi.org/10.1016/S1040-6182\(99\)00040-3](https://doi.org/10.1016/S1040-6182(99)00040-3)
- Lehmkuhl, F., Klinge, M. & Lang, A. (2002). Late Quaternary glacier advances, lake level fluctuations and aeolian sedimentation in Southern Tibet. *Zeitschrift Für Geomorphologie. Supplementband*, 126, 183–218.
- Leloup, P., Mahéo, G., Arnaud, N., Kali, E., Boutonnet, E., Liu, D., Xiaohan, L. & Haibing, L. (2010). The South Tibet detachment shear zone in the Dinggye area: Time constraints on extrusion models of the Himalayas. *Earth and Planetary Science Letters*, 292(1), 1–16. <https://doi.org/10.1016/j.epsl.2009.12.035>
- Li, C., Yan, F., Kang, S., Chen, P., Han, X., Hu, Z., Zhang, G., Hong, Y., Gao, S., Qu, B. & others. (2017). Re-evaluating black carbon in the Himalayas and the Tibetan Plateau: concentrations and deposition. *Atmos. Chem. Phys*, 17, 11899–11912. <https://doi.org/10.5194/acp-17-11899-2017>
- Li, D., Li, Y., Ma, B., Dong, G., Wang, L. & Zhao, J. (2009). Lake-level fluctuations since the Last Glaciation in Selin Co (lake), Central Tibet, investigated using optically stimulated luminescence dating of beach ridges. *Environmental Research Letters*, 4(4), 045204. <https://doi.org/10.1088/1748-9326/4/4/045204>
- Li, D. & Yin, A. (2008). Orogen-parallel, active left-slip faults in the Eastern Himalaya: Implications for the growth mechanism of the Himalayan Arc. *Earth and Planetary Science Letters*, 274(1-2), 258–267. <https://doi.org/10.1016/j.epsl.2008.07.043>
- Li, M., Kang, S., Zhu, L., You, Q., Zhang, Q. & Wang, J. (2008). Mineralogy and geochemistry of the Holocene lacustrine sediments in Nam Co, Tibet. *Quaternary International*, 187(1), 105–116. <https://doi.org/10.1016/j.quaint.2007.12.008>
- Li, M., Wang, J., Zhu, L., Wang, L. & Yi, C. (2012). Distribution and formation of monohydrocalcite from surface sediments in Nam Co Lake, Tibet. *Quaternary International*, 263, 85–92. <https://doi.org/10.1016/j.quaint.2007.12.008>
- Li, Q. (2019). Distribution and vegetation representation of pollen assemblages from surface sediments of Nam Co, a large alpine lake in the central Tibetan Plateau. *Vegetation History and Archaeobotany*, 28(4), 365–377. <https://doi.org/10.1007/s00334-018-0699-2>
- Li, Q., Lu, H., Zhu, L., Wu, N., Wang, J. & Lu, X. (2011). Pollen-inferred climate changes and vertical shifts of alpine vegetation belts on the northern slope of the Nyainqentanglha Mountains (central Tibetan Plateau) since 8.4 kyr BP. *The Holocene*, 0959683611400218.
- Lin, X., Zhu, L., Wang, Y., Wang, J., Xie, M., Ju, J., Mäusbacher, R. & Schwalb, A. (2008). Environmental changes reflected by n-alkanes of lake core in Nam Co on the Tibetan Plateau since 8.4 kaB. P. *Chinese Science Bulletin*, 53(19), 3051–3057. <https://doi.org/10.1007/s11434-008-0313-6>
- Lisiecki, L. E. & Raymo, M. E. (2005). A Pliocene-Pleistocene stack of 57 globally distributed benthic delta 18O records. *Paleoceanography*, 20(1). <https://doi.org/10.1029/2004PA001071>
- Liu, X.-J., Madsen, D. B., Liu, R., Sun, Y. & Wang, Y. (2016). Holocene lake level variations of Longmu Co, western Qinghai-Tibetan Plateau. *Environmental Earth Sciences*, 75(4), 301. <https://doi.org/10.1007/s12665-015-5188-7>
- Long, H., Shen, J., Haberzettl, T., Fuchs, M., Frechen, M. & Wang, J. (2013). High-resolution OSL chronology of a sediment core from Lake Nam Co on the southern Tibetan Plateau: Comparison with radiocarbon dating. *EGU General Assembly Conference Abstracts*, 15, 959.
- Long, H., Shen, J., Wang, Y., Gao, L. & Frechen, M. (2015). High-resolution OSL dating of a late Quaternary sequence from Xingkai Lake (NE Asia): Chronological challenge of the “MIS 3a Mega-paleolake” hypothesis in China. *Earth and Planetary Science Letters*, 428, 281–292. <https://doi.org/10.1016/j.epsl.2015.07.003>
- Lu, X., Herrmann, M., Mosbrugger, V., Yao, T. & Zhu, L. (2010). Airborne pollen in the Nam Co Basin and its implication for palaeoenvironmental reconstruction. *Review of Palaeobotany and Palynology*, 163(1), 104–112. <https://doi.org/10.1016/j.revpalbo.2010.10.004>

- Ma, N., Szilagyi, J., Niu, G.-Y., Zhang, Y., Zhang, T., Wang, B. & Wu, Y. (2016). Evaporation variability of Nam Co Lake in the Tibetan Plateau and its role in recent rapid lake expansion. *Journal of Hydrology*, 537, 27–35. <https://doi.org/10.1016/j.jhydrol.2016.03.030>
- Mahéo, G., Leloup, P.-H., Valli, F., Lacassin, R., Arnaud, N., Paquette, J.-L., Fernandez, A., Haibing, L., Farley, K. & Tapponnier, P. (2007). Post 4 Ma initiation of normal faulting in southern Tibet. Constraints from the Kung Co half graben. *Earth and Planetary Science Letters*, 256(1), 233–243. <https://doi.org/10.1016/j.epsl.2007.01.029>
- Mayewski, P. A., Rohling, E. E., Stager, J. C., Karlén, W., Maasch, K. A., Meeker, L. D., Meyerson, E. A., Gasse, F., van Kreveld, S., Holmgren, K. & others. (2004). Holocene climate variability. *Quaternary Research*, 62(3), 243–255. <https://doi.org/10.1016/j.yqres.2004.07.001>
- McCaffrey, R. (1992). Oblique plate convergence, slip vectors, and forearc deformation. *Journal of Geophysical Research: Solid Earth (1978-2012)*, 97(B6), 8905–8915. <https://doi.org/10.1029/92JB00483>
- McCallister, A. T., Taylor, M. H., Murphy, M. A., Styron, R. H. & Stockli, D. F. (2014). Thermochronologic constraints on the late Cenozoic exhumation history of the Gurla Mandhata metamorphic core complex, southwestern Tibet. *Tectonics*, 33(2), 27–52. <https://doi.org/10.1002/2013TC003302>
- Miall, A. D. (2010). *The geology of stratigraphic sequences*. Springer Science & Business Media.
- Milliman, J. D. & Syvitski, J. P. (1992). Geomorphic/tectonic control of sediment discharge to the ocean: the importance of small mountainous rivers. *The Journal of Geology*, 100(5), 525–544. <https://doi.org/10.1086/629606>
- Mischke, S. & Zhang, C. (2010). Holocene cold events on the Tibetan Plateau. *Global and Planetary Change*, 72(3), 155–163. <https://doi.org/10.1016/j.gloplacha.2010.02.001>
- Mitchum Jr, R. M., Vail, P. R. & Sangree, J. B. (1977). Seismic stratigraphy and global changes of sea level: Part 6. Stratigraphic interpretation of seismic reflection patterns in depositional sequences: Section 2. Application of seismic reflection configuration to stratigraphic interpretation. In *Seismic Stratigraphy-Applications to Hydrocarbon Exploration* (pp. 117–133). AAPG Special Volumes.
- Molnar, P., England, P. & Martinod, J. (1993). Mantle dynamics, uplift of the Tibetan Plateau, and the Indian monsoon. *Reviews of Geophysics*, 31(4), 357–396. <https://doi.org/10.1029/93RG02030>
- Molnar, P. & Tapponnier, P. (1975). Cenozoic tectonics of Asia: effects of a continental collision. *Science*, 189(4201), 419–426. <https://doi.org/10.1126/science.189.4201.419>
- Molnar, P. & Tapponnier, P. (1978). Active tectonics of Tibet. *Journal of Geophysical Research: Solid Earth*, 83(B11). <https://doi.org/10.1029/JB083iB11p05361>
- Mügler, I., Gleixner, G., Günther, F., Mäusbacher, R., Daut, G., Schütt, B., Berking, J., Schwalb, A., Schwark, L., Xu, B., Yao, T., Zhu, L. & C, Y. (2010). A multi-proxy approach to reconstruct hydrological changes and Holocene climate development of Nam Co, Central Tibet. *Journal of Paleolimnology*, 43(4), 625–648. <https://doi.org/10.1007/s10933-009-9357-0>
- Mügler, I., Sachse, D., Werner, M., Xu, B., Wu, G., Yao, T. & Gleixner, G. (2008). Effect of lake evaporation on deltaD values of lacustrine n-alkanes: a comparison of Nam Co (Tibetan Plateau) and Holzmaar (Germany). *Organic Geochemistry*, 39(6), 711–729. <https://doi.org/10.1016/j.orggeochem.2008.02.008>
- Mulder, T. (2011). Gravity processes and deposits on continental slope, rise and abyssal plains. In *Developments in Sedimentology* (Vol. 63, pp. 25–148). Elsevier. [https://doi.org/10.1016/S0070-4571\(11\)63002-1](https://doi.org/10.1016/S0070-4571(11)63002-1)
- Mulder, T. & Alexander, J. (2001). The physical character of subaqueous sedimentary density flows and their deposits. *Sedimentology*, 48(2), 269–299. <https://doi.org/10.1046/j.1365-3091.2001.00360.x>
- Mulder, T. & Chapron, E. (2011). *Flood deposits in continental and marine environments: character and significance*. <https://doi.org/10.1306/13271348St613436>
- Mutti, E., Davoli, G., Tinterri, R. & Zavala, C. (1996). The importance of ancient fluvio-deltaic systems dominated by catastrophic flooding in tectonically active basins. *Memorie Di Scienze Geologiche*, 48, 233–291.
- Nábelek, J., Hetényi, G., Vergne, J., Sapkota, S., Kafle, B., Jiang, M., Su, H., Chen, J., Huang, B.-S. & others. (2009). Underplating in the Himalaya-Tibet collision zone revealed by the Hi-CLIMB experiment. *Science*, 325(5946), 1371–1374. <https://doi.org/10.1126/science.1167719>
- Özacar, A. A. (n.d.). *Personal webpage*. Retrieved June 2017, from <https://www.geo.arizona.edu/~ozacar/models~1.htm>

- Parsons, J. D., Friedrichs, C. T., Traykovski, P. A., Mohrig, D., Imran, J., Syvitski, J. P., Parker, G., Puig, P., Buttle, J. L., Garc'ia, M. H. & others. (2007). The mechanics of marine sediment gravity flows. *Continental Margin Sedimentation: From Sediment Transport to Sequence Stratigraphy*, 37, 275–334.
- Peng, Y., Xiao, J., Nakamura, T., Liu, B. & Inouchi, Y. (2005). Holocene East Asian monsoonal precipitation pattern revealed by grain-size distribution of core sediments of Daihai Lake in Inner Mongolia of north-central China. *Earth and Planetary Science Letters*, 233(3–4), 467–479. <https://doi.org/10.1016/j.epsl.2005.02.022>
- Porter, S. C. & Zhisheng, A. (1995). Correlation between climate events in the North Atlantic and China during the last glaciation. *Nature*, 375(6529), 305–308. <https://doi.org/10.1038/375305a0>
- Prell, W. L. & Kutzbach, J. E. (1992). Sensitivity of the Indian monsoon to forcing parameters and implications for its evolution. *Nature*, 360(6405), 647–652. <https://doi.org/10.1038/360647a0>
- Pullen, A., Kapp, P., Gehrels, G. E., DeCelles, P. G., Brown, E. H., Fabijanic, J. M. & Ding, L. (2008). Gangdese retroarc thrust belt and foreland basin deposits in the Damxung area, southern Tibet. *Journal of Asian Earth Sciences*, 33(5), 323–336. <https://doi.org/10.1016/j.jseaes.2008.01.005>
- Qiu, J. (2008). China: the third pole. *Nature*, 454(7203), 393–396. <https://doi.org/10.1038/454393a>
- Ratschbacher, L., Frisch, W., Liu, G. & Chen, C. (1994). Distributed deformation in southern and western Tibet during and after the India-Asia collision. *Journal of Geophysical Research: Solid Earth*, 99(B10), 19917–19945. <https://doi.org/10.1029/94JB00932>
- Rodda, J. C. (2007). Invited Opinion Piece Refreshing world water affairs. *Water Policy*, 9(6), 645–648. <https://doi.org/10.2166/wp.2007.123>
- Royden, L. H., Burchfiel, B. C. & van der Hilst, R. D. (2008). The geological evolution of the Tibetan Plateau. *Science*, 321(5892), 1054–1058. <https://doi.org/10.1126/science.115537>
- Ryder, I., Wang, H., Bie, L. & Rietbrock, A. (2014). Geodetic imaging of late postseismic lower crustal flow in Tibet. *Earth and Planetary Science Letters*, 404, 136–143. <https://doi.org/10.1016/j.epsl.2014.07.026>
- Saini, J., Günther, F., Aichner, B., Mischke, S., Herzschuh, U., Zhang, C., Mäusbacher, R. & Gleixner, G. (2017). Climate variability in the past~ 19,000 yr in NE Tibetan Plateau inferred from biomarker and stable isotope records of Lake Donggi Cona. *Quaternary Science Reviews*, 157, 129–140. <https://doi.org/10.1016/j.quascirev.2016.12.023>
- Schäfer, J. M., Tschudi, S., Zhao, Z., Wu, X., Ivy-Ochs, S., Wieler, R., Baur, H., Kubik, P. W. & Schlüchter, C. (2002). The limited influence of glaciations in Tibet on global climate over the past 170 000 yr. *Earth and Planetary Science Letters*, 194(3), 287–297. [https://doi.org/10.1016/S0012-821X\(01\)00573-8](https://doi.org/10.1016/S0012-821X(01)00573-8)
- Scheu, K. R., Fong, D., Monismith, S. G. & Fringer, O. B. (2015). Sediment transport dynamics near a river inflow in a large alpine lake. *Limnology and Oceanography*, 60(4), 1195–1211. <https://doi.org/10.1002/lno.10089>
- Scheu, K. R., Fong, D., Monismith, S. G. & Fringer, O. B. (2018). Modeling Sedimentation Dynamics of Sediment-Laden River Intrusions in a Rotationally-Influenced, Stratified Lake. *Water Resources Research*, 54(6), 4084–4107. <https://doi.org/10.1029/2017WR021533>
- Schneider, W., Mattern, F., Wang, P. & Li, C. (2003). Tectonic and sedimentary basin evolution of the eastern Bangong-Nujiang zone (Tibet): a Reading cycle. *International Journal of Earth Sciences*, 92(2), 228–254. <https://doi.org/10.1007/s00531-003-0311-5>
- Schütt, B., Berking, J., Frechen, M., Frenzel, P., Schwalb, A. & Wrozyna, C. (2010). Late Quaternary transition from lacustrine to a fluvio-lacustrine environment in the north-western Nam Co, Tibetan Plateau, China. *Quaternary International*, 218(1), 104–117. <https://doi.org/10.1016/j.quaint.2009.05.009>
- Schütt, B., Berking, J., Frechen, M. & Yi, C. (2008). Late Pleistocene lake level fluctuations of the Nam Co, Tibetan Plateau, China. *Zeitschrift Für Geomorphologie, Supplementary Issues*, 52(2), 57–75. <https://doi.org/10.1127/0372-8854/2008/005252-0057>
- Searle, M. (2020). *India: Asia Collision and Tibet*. <https://doi.org/10.1016/B978-0-12-409548-9.12493-5>
- Seeber, L. & Armbruster, J. (1984). Some elements of continental subduction along the Himalayan front. *Tectonophysics*, 105(1–4), 263–278. [https://doi.org/10.1016/0040-1951\(84\)90207-5](https://doi.org/10.1016/0040-1951(84)90207-5)

- Shakun, J. D., Lea, D. W., Lisiecki, L. E. & Raymo, M. E. (2015). An 800-kyr record of global surface ocean $\delta^{18}\text{O}$ and implications for ice volume-temperature coupling. *Earth and Planetary Science Letters*, 426, 58–68. <https://doi.org/10.1016/j.epsl.2015.05.042>
- Sheriff, R. E. (1991). Encyclopedic dictionary of exploration geophysics: Soc. *Expl. Geophys.*
- Shi, X., Furlong, K. P., Kirby, E., Meng, K., Marrero, S., Gosse, J., Wang, E. & Phillips, F. (2017a). Evaluating the size and extent of paleolakes in central Tibet during the late Pleistocene. *Geophysical Research Letters*, 44(11), 5476–5485. <https://doi.org/10.1002/2017GL072686>
- Shi, X., Kirby, E., Furlong, K. P., Meng, K., Robinson, R., Lu, H. & Wang, E. (2017b). Rapid and punctuated Late Holocene recession of Siling Co, central Tibet. *Quaternary Science Reviews*, 172, 15–31. <https://doi.org/10.1016/j.quascirev.2017.07.017>
- Shi, Y., Yu, G., Liu, X., Li, B. & Yao, T. (2001). Reconstruction of the 30–40 ka BP enhanced Indian monsoon climate based on geological records from the Tibetan Plateau. *Palaeogeography, Palaeoclimatology, Palaeoecology*, 169(1–2), 69–83. [https://doi.org/10.1016/S0031-0182\(01\)00216-4](https://doi.org/10.1016/S0031-0182(01)00216-4)
- Sirocko, F., Sarnthein, M., Erlenkeuser, H., Lange, H., Arnold, M. & Duplessy, J. C. (1993). *Century-scale events in monsoonal climate over the past 24,000 years*. <https://doi.org/10.1038/364322a0>
- Street, F. A. & Grove, A. (1979). Global maps of lake-level fluctuations since 30,000 yr BP. *Quaternary Research*, 12(1), 83–118. [https://doi.org/10.1016/0033-5894\(79\)90092-9](https://doi.org/10.1016/0033-5894(79)90092-9)
- Styron, R. H., Taylor, M. H. & Murphy, M. A. (2011). Oblique convergence, arc-parallel extension, and the role of strike-slip faulting in the High Himalaya. *Geosphere*, 7(2), 582–596. <https://doi.org/10.1130/GES00606.1>
- Styron, R., Taylor, M. & Okoronkwo, K. (2010). Database of active structures from the Indo-Asian collision. *Eos, Transactions American Geophysical Union*, 91(20), 181–182. <https://doi.org/10.1029/2010EO200001>
- Styron, R., Taylor, M. & Sundell, K. (2015). Accelerated extension of Tibet linked to the northward underthrusting of Indian crust. *Nature Geoscience*, 8(2), 131–134. <https://doi.org/10.1038/NGEO2336>
- Su, Y., Gao, X., Liu, Q., Hu, P., Duan, Z., Jiang, Z., Wang, J., Zhu, L., Doberschütz, S., Mäusbacher, R. & others. (2013). Mechanism of variations in environmental magnetic proxies of lake sediments from Nam Co, Tibet during the Holocene. *Chinese Science Bulletin*, 58(13), 1568–1578. <https://doi.org/10.1007/s11434-012-5324-7>
- Sun, J., Zhou, T., Liu, M., Chen, Y., Shang, H., Zhu, L., Shedayi, A. A., Yu, H., Cheng, G., Liu, G. & others. (2018). Linkages of the dynamics of glaciers and lakes with the climate elements over the Tibetan Plateau. *Earth-Science Reviews*. <https://doi.org/10.1016/j.earscirev.2018.06.012>
- Sun, Y., Clemens, S. C., An, Z. & Yu, Z. (2006). Astronomical timescale and palaeoclimatic implication of stacked 3.6-Myr monsoon records from the Chinese Loess Plateau. *Quaternary Science Reviews*, 25(1–2), 33–48. <https://doi.org/10.1016/j.quascirev.2005.07.005>
- Sun, Y., Kutzbach, J., An, Z., Clemens, S., Liu, Z., Liu, W., Liu, X., Shi, Z., Zheng, W., Liang, L. & others. (2015). Astronomical and glacial forcing of East Asian summer monsoon variability. *Quaternary Science Reviews*, 115, 132–142. <https://doi.org/10.1016/j.quascirev.2015.03.009>
- Tang, C., Yang, H., Pancost, R. D., Griffiths, M. L., Xiao, G., Dang, X. & Xie, S. (2017). Tropical and high latitude forcing of enhanced megadroughts in Northern China during the last four terminations. *Earth and Planetary Science Letters*, 479, 98–107. <https://doi.org/10.1016/j.epsl.2017.09.012>
- Tapponnier, P. & Molnar, P. (1977). Active faulting and tectonics in China. *Journal of Geophysical Research*, 82(20), 2905–2930. <https://doi.org/10.1029/JB082i020p02905>
- Tapponnier, P., Peltzer, G. & Armijo, R. (1986). On the mechanics of the collision between India and Asia. *Geological Society, London, Special Publications*, 19(1), 113–157. <https://doi.org/10.1144/GSL.SP.1986.019.01.07>
- Tapponnier, P., Peltzer, G., Le Dain, A., Armijo, R. & Cobbold, P. (1982). Propagating extrusion tectonics in Asia: New insights from simple experiments with plasticine. *Geology*, 10(12), 611–616. [https://doi.org/10.1130/0091-7613\(1982\)10<611:PETIAN>2.0.CO;2](https://doi.org/10.1130/0091-7613(1982)10<611:PETIAN>2.0.CO;2)
- Tapponnier, P., Zhiqin, X., Roger, F., Meyer, B., Arnaud, N., Wittlinger, G. & Jingsui, Y. (2001). Oblique stepwise rise and growth of the Tibet Plateau. *Science*, 294(5547), 1671–1677. <https://doi.org/10.1126/science.105978>

- Taylor, M. & Yin, A. (2009). Active structures of the Himalayan-Tibetan orogen and their relationships to earthquake distribution, contemporary strain field, and Cenozoic volcanism. *Geosphere*, 5(3), 199–214. <https://doi.org/10.1130/GES00217.1>
- Taylor, M., Yin, A., Ryerson, F. J., Kapp, P. & Ding, L. (2003). Conjugate strike-slip faulting along the Bangong-Nujiang suture zone accommodates coeval east-west extension and north-south shortening in the interior of the Tibetan Plateau. *Tectonics*, 22(4). <https://doi.org/10.1029/2002TC001361>
- Thompson, L. G., Yao, T., Davis, M. E., Mosley-Thompson, E., Wu, G., Porter, S. E., Xu, B., Lin, P.-N., Wang, N., Beaudon, E. & others. (2018). Ice core records of climate variability on the Third Pole with emphasis on the Guliya ice cap, western Kunlun Mountains. *Quaternary Science Reviews*, 188, 1–14. <https://doi.org/10.1016/j.quascirev.2018.03.003>
- U.S. Geological Survey. (n.d.). Retrieved 10, 2020, from earthquake.usgs.gov
- Van Hinsbergen, D. J., Lippert, P. C., Li, S., Huang, W., Advokaat, E. L. & Spakman, W. (2019). Reconstructing Greater India: Paleogeographic, kinematic, and geodynamic perspectives. *Tectonophysics*, 760, 69–94. <https://doi.org/10.1016/j.tecto.2018.04.006>
- Veeken, P. P. (2006). *Seismic stratigraphy, basin analysis and reservoir characterisation* (Vol. 37). Elsevier.
- Verschuur, D. J. (2006). *Seismic multiple removal techniques - past, present, and future*.
- Wan, G., Zhang, D. D., Zhang, F., Huang, R. & others. (2004). Environmental records of lacustrine sediments in different time scales: Sediment grain size as an example. *Science in China Series D: Earth Sciences*, 47(10), 954–960. <https://doi.org/10.1360/03yd0160>
- Wang, B., Clemens, S. C. & Liu, P. (2003). Contrasting the Indian and East Asian monsoons: implications on geologic timescales. *Marine Geology*, 201(1–3), 5–21. [https://doi.org/10.1016/S0025-3227\(03\)00196-8](https://doi.org/10.1016/S0025-3227(03)00196-8)
- Wang, J., Huang, L., Ju, J., Daut, G., Ma, Q., Zhu, L., Haberzettl, T., Baade, J., Mäusbacher, R., Hamilton, A. & others. (2020). Seasonal stratification of a deep, high-altitude, dimictic lake: Nam Co, Tibetan Plateau. *Journal of Hydrology*, 124668. <https://doi.org/https://doi.org/10.1016/j.jhydrol.2020.124668>
- Wang, J., Huang, L., Ju, J., Daut, G., Wang, Y., Ma, Q., Zhu, L., Haberzettl, T., Baade, J. & Mäusbacher, R. (2019). Spatial and temporal variations in water temperature in a high-altitude deep dimictic mountain lake (Nam Co), central Tibetan Plateau. *Journal of Great Lakes Research*, 45(2), 212–223. <https://doi.org/10.1016/j.jglr.2018.12.005>
- Wang, J., Zhu, L., Daut, G., Ju, J., Lin, X., Wang, Y. & Zhen, X. (2009a). Bathymetric survey and modern limnological parameters of Nam Co, central Tibet. *Journal of Lake Sciences*, 21, 128–134.
- Wang, J., Zhu, L., Daut, G., Ju, J., Lin, X., Wang, Y. & Zhen, X. (2009b). Investigation of bathymetry and water quality of Lake Nam Co, the largest lake on the central Tibetan Plateau, China. *Limnology*, 10(2), 149–158. <https://doi.org/10.1007/s10201-009-0266-8>
- Wang, J., Zhu, L., Wang, Y., Ju, J., Daut, G. & Li, M. (2015a). Spatial variability and the controlling mechanisms of surface sediments from Nam Co, central Tibetan Plateau, China. *Sedimentary Geology*, 319, 69–77. <https://doi.org/10.1016/j.sedgeo.2015.01.011>
- Wang, J., Zhu, L., Wang, Y., Ju, J., Xie, M. & Daut, G. (2010). Comparisons between the chemical compositions of lake water, inflowing river water, and lake sediment in Nam Co, central Tibetan Plateau, China and their controlling mechanisms. *Journal of Great Lakes Research*, 36(4), 587–595. <https://doi.org/10.1016/j.jglr.2010.06.013>
- Wang, J., Zhu, L., Wang, Y., Peng, P., Ma, Q., Haberzettl, T., Kasper, T., Matsunaka, T. & Nakamura, T. (2015b). Variability of the 14 C reservoir effects in Lake Tangra Yumco, Central Tibet (China), determined from recent sedimentation rates and dating of plant fossils. *Quaternary International*. <https://doi.org/10.1016/j.quaint.2015.10.084>
- Wang, P., Wang, B., Cheng, H., Fasullo, J., Guo, Z., Kiefer, T. & Liu, Z. (2014). The global monsoon across timescales: coherent variability of regional monsoons. *Climate of the Past*, 10(6), 2007. <https://doi.org/10.5194/cp-10-2007-2014>
- Wang, P. X., Wang, B., Cheng, H., Fasullo, J., Guo, Z., Kiefer, T. & Liu, Z. (2017). The global monsoon across time scales: Mechanisms and outstanding issues. *Earth-Science Reviews*, 174, 84–121. <https://doi.org/10.1016/j.earscirev.2017.07.006>

- Wang, R., Scarpitta, S., Zhang, S. & Zheng, M. (2002). Later Pleistocene/Holocene climate conditions of Qinghai-Xizhang Plateau (Tibet) based on carbon and oxygen stable isotopes of Zabuye Lake sediments. *Earth and Planetary Science Letters*, 203(1), 461–477. [https://doi.org/10.1016/S0012-821X\(02\)00829-4](https://doi.org/10.1016/S0012-821X(02)00829-4)
- Wang, Y., Zhu, L., Wang, J., Ju, J. & Lin, X. (2012). The spatial distribution and sedimentary processes of organic matter in surface sediments of Nam Co, Central Tibetan Plateau. *Chinese Science Bulletin*, 57(36), 4753–4764. <https://doi.org/10.1007/s11434-012-5500-9>
- Wang, Y., Zhu, L., Wang, J., Ju, J., Peng, P., Lin, X., Hu, J. & Nishimura, M. (2016). Paleohydrological processes revealed by n-alkane δD in lacustrine sediments of Lake Pumoyum Co, southern Tibetan Plateau, and their response to climate changes during the past 18.5 cal ka. *Journal of Paleolimnology*, 56(2-3), 223–238. <https://doi.org/10.1016/j.quaint.2015.10.084>
- Webb, A. A. G., Guo, H., Clift, P. D., Husson, L., Müller, T., Costantino, D., Yin, A., Xu, Z., Cao, H. & Wang, Q. (2017). The Himalaya in 3D: Slab dynamics controlled mountain building and monsoon intensification. *Lithosphere*, 9(4), 637–651. <https://doi.org/10.1130/L636.1>
- Wetzler, N., Shalev, E., Göbel, T., Amelung, F., Kurzton, I., Lyakhovsky, V. & Brodsky, E. E. (2019). Earthquake swarms triggered by groundwater extraction near the Dead Sea Fault. *Geophysical Research Letters*, 46(14), 8056–8063. <https://doi.org/10.1029/2019GL083491>
- Witt, R., Günther, F., Lauterbach, S., Kasper, T., Mäusbacher, R., Yao, T. & Gleixner, G. (2016). Biogeochemical evidence for freshwater periods during the Last Glacial Maximum recorded in lake sediments from Nam Co, south-central Tibetan Plateau. *Journal of Paleolimnology*, 55(1), 67–82. <https://doi.org/10.1007/s10933-015-9863-1>
- Wrožyna, C., Frenzel, P., Daut, G., Mäusbacher, R., Zhu, L. & Schwalb, A. (2012). Holocene lake level changes of Lake Nam Co, Tibetan Plateau, deduced from ostracode assemblage and $\delta^{18}O$ and $\delta^{13}C$ signatures of their valves. *Ostracoda as Proxies for Quaternary Climate Change. Developments in Quaternary Science*, 17, 282–295. <https://doi.org/10.1016/B978-0-444-53636-5.00016-0>
- Wu, Y., Lücke, A., Zhangdong, J., Sumin, W., Schleser, G. H., Battarbee, R. W. & Weilan, X. (2006). Holocene climate development on the central Tibetan Plateau: a sedimentary record from Cuoe Lake. *Palaeogeography, Palaeoclimatology, Palaeoecology*, 234(2-4), 328–340. <https://doi.org/10.1016/j.palaeo.2005.09.017>
- Wu, Z., Barosh, P. J., Xun, Z., Zhonghai, W., Daogong, H. & Qisheng, L. (2007). Miocene Tectonic Evolution from Dextral-Slip Thrusting to Extension in the Nyainqentanglha Region of the Tibetan Plateau. *Acta Geologica Sinica-English Edition*, 81(3), 365–384. <https://doi.org/10.1111/j.1755-6724.2007.tb00961.x>
- Wu, Z. H., Meng, X. G. & Hu, D. G. (2011). *Regional Geological Survey Report of China (Damxong)* (pp. 1–346).
- Wu, Z., Ye, P., Wang, C., Zhang, K. ang Z. H., Zheng Yonggang, Yi, J. & Li, H. (2015). The Relics, Ages and Significance of Prehistoric Large Earthquakes in the Angang Graben in South Tibet. *Earth Science - Journal of China University of Geosciences*, 24(10), 1621–1642.
- Wu, Z., Zhao, X., Wu, Z., Jiang, W., Hu, D. & Zhou, C. (2004). Quaternary Geology and Faulting in the Damxung-Yangbajain Basin. *Acta Geologica Sinica-English Edition*, 78(1), 273–282. <https://doi.org/10.1111/j.1755-6724.2004.tb00700.x>
- Wünnemann, B., Demske, D., Tarasov, P., Kotlia, B. S., Reinhardt, C., Bloemendal, J., Diekmann, B., Hartmann, K., Krois, J., Riedel, F. & others. (2010). Hydrological evolution during the last 15kyr in the Tso Kar lake basin (Ladakh, India), derived from geomorphological, sedimentological and palynological records. *Quaternary Science Reviews*, 29(9), 1138–1155. <https://doi.org/10.1016/j.quascirev.2010.02.017>
- Xiao, J., Fan, J., Zhou, L., Zhai, D., Wen, R. & Qin, X. (2013). A model for linking grain-size component to lake level status of a modern clastic lake. *Journal of Asian Earth Sciences*, 69, 149–158. <https://doi.org/10.1016/j.jseas.2012.07.003>
- Yang, K., Wu, H., Qin, J., Lin, C., Tang, W. & Chen, Y. (2014a). Recent climate changes over the Tibetan Plateau and their impacts on energy and water cycle: A review. *Global and Planetary Change*, 112, 79–91.
- Yang, Q., Jochum, K. P., Stoll, B., Weis, U., Börner, N., Schwalb, A., Frenzel, P., Scholz, D., Doberschütz, S., Haberzettl, T. & others. (2014b). Trace element variability in single ostracod valves as a proxy for hydrochemical change in Nam Co, central Tibet, during the Holocene. *Palaeogeography, Palaeoclimatology, Palaeoecology*, 399, 225–235. <https://doi.org/10.1016/j.palaeo.2014.01.014>

- Yao, T., Masson-Delmotte, V., Gao, J., Yu, W., Yang, X., Risi, C., Sturm, C., Werner, M., Zhao, H., He, Y. & others. (2013). A review of climatic controls on $\delta^{18}\text{O}$ in precipitation over the Tibetan Plateau: Observations and simulations. *Reviews of Geophysics*, 51(4), 525–548. <https://doi.org/10.1002/rog.20023>
- Yilmaz, Ö. (2001). *Seismic data analysis* (Vol. 1). Society of exploration geophysicists Tulsa, OK.
- Yu, S.-Y., Colman, S. M. & Lai, Z.-P. (2019). Late-Quaternary history of “great lakes” on the Tibetan Plateau and palaeoclimatic implications-A review. *Boreas*, 48(1), 1–19. <https://doi.org/10.1111/bor.12349>
- Zavala, C., Arcuri, M., Di Meglio, M., Diaz, H. G. & Contreras, C. (2011). A genetic facies tract for the analysis of sustained hyperpycnal flow deposits. In R. M. Slatt and C. Zavala (Ed.), *Sediment transfer from shelf to deep water—Revisiting the delivery system* (Vol. 61, pp. 31–51). AAPG Special Volumes. <https://doi.org/10.1306/13271349St613438>
- Zhang, G., Yao, T., Piao, S., Bolch, T., Xie, H., Chen, D., Gao, Y., O'Reilly, C. M., Shum, C., Yang, K. & others. (2017). Extensive and drastically different alpine lake changes on Asia's high plateaus during the past four decades. *Geophysical Research Letters*, 44(1), 252–260. <https://doi.org/10.1002/2016GL072033>
- Zhang, G., Yao, T., Xie, H., Zhang, K. & Zhu, F. (2014). Lakes' state and abundance across the Tibetan Plateau. *Chinese Science Bulletin*, 59(24), 3010–3021. <https://doi.org/10.1007/s11434-014-0258-x>
- Zhang, J., Jin, M., Chen, F., Battarbee, R. & Henderson, A. (2003). High-resolution precipitation variations in the Northeast Tibetan Plateau over the last 800 years documented by sediment cores of Qinghai Lake. *Chinese Science Bulletin*, 48(14), 1451–1456. <https://doi.org/10.1360/02wd0271>
- Zhang, P.-Z., Shen, Z., Wang, M., Gan, W., Bürgmann, R., Molnar, P., Wang, Q., Niu, Z., Sun, J., Wu, J. & others. (2004). Continuous deformation of the Tibetan Plateau from global positioning system data. *Geology*, 32(9), 809–812. <https://doi.org/10.1130/G20554.1>
- Zhang, S., Zhang, J., Zhao, H., Liu, X. & Chen, F. (2020). Spatiotemporal complexity of the “Greatest Lake Period” in the Tibetan Plateau. *Science Bulletin*, 65(16), 1317–1319.
- Zhang, Y., Li, B.-Y. & Zheng, D. (2002). A discussion on the boundary and area of the Tibetan Plateau in China. *地理研究*, 21(1), 1–8. <https://doi.org/10.11821/yj2002010001>
- Zheng, M., Yuan, H., Liu, J., Li, Y., Ma, Z. & Sun, Q. (2007). Sedimentary characteristics and paleoenvironmental records of Zabuye Salt Lake, Tibetan Plateau, since 128 ka BP. *Acta Geologica Sinica-English Edition*, 81(5), 861–879. <https://doi.org/10.1111/j.1755-6724.2007.tb01008.x>
- Zhou, J., Zhou, W., Dong, G., Hou, Y., Xian, F., Zhang, L., Tang, L., Zhao, G. & Fu, Y. (2020). Cosmogenic ^{10}Be and ^{26}Al exposure dating of Nam Co lake terraces since MIS 5, southern Tibetan Plateau. *Quaternary Science Reviews*, 231, 106175. <https://doi.org/10.1016/j.quascirev.2020.106175>
- Zhou, L., Oldfield, F., Wintle, A., Robinson, S. & Wang, J. (1990). Partly pedogenic origin of magnetic variations in Chinese loess. *Nature*, 346(6286), 737–739. <https://doi.org/10.1038/346737a0>
- Zhou, S., Kang, S., Chen, F. & Joswiak, D. (2013). Water balance observations reveal significant subsurface water seepage from Lake Nam Co, south-central Tibetan Plateau. *Journal of Hydrology*, 491, 89–99. <https://doi.org/10.1016/j.jhydrol.2013.03.030>
- Zhou, S., Kang, S., Gao, T. & Zhang, G. (2010). Response of Zhadang Glacier runoff in Nam Co Basin, Tibet, to changes in air temperature and precipitation form. *Chinese Science Bulletin*, 55(20), 2103–2110. <https://doi.org/10.1007/s11434-010-3290-5>
- Zhu, D., Meng, X., Zhao, X., Shao, Z., Xu, Z., Yang, C., Ma, Z., Wu, Z., Wu, Z. & Wang, J. (2004). Evolution of an ancient large lake in the southeast of the northern Tibetan Plateau. *Acta Geologica Sinica (English Edition)*, 78(4), 982–992. <https://doi.org/10.1111/j.1755-6724.2004.tb00220.x>
- Zhu, D., Xitao, Z., Xiangang, M., Zhonghai, W., Zhenhan, W., Xiangyang, F., Zhaogang, S., Qisheng, L. & Meiling, Y. (2002). Quaternary Lake Deposits of Nam Co, Tibet, with a Discussion of the Connection of Nam Co with Ring Co-Jiuru Co. *Acta Geologica Sinica-English Edition*, 76(3), 283–291. <https://doi.org/10.1111/j.1755-6724.2002.tb00544.x>
- Zhu, L., Lü, X., Wang, J., Peng, P., Kasper, T., Daut, G., Haberzettl, T., Frenzel, P., Li, Q., Yang, R. & others. (2015). Climate change on the Tibetan Plateau in response to shifting atmospheric circulation since the LGM. *Scientific Reports*, 5. <https://doi.org/10.1038/srep13318>

- Zhu, L., Peng, P., Xie, M., Wang, J., Frenzel, P., Wrozyna, C. & Schwalb, A. (2010a). Ostracod-based environmental reconstruction over the last 8,400 years of Nam Co Lake on the Tibetan plateau. *Hydrobiologia*, 648(1), 157–174. <https://doi.org/10.1007/s10750-010-0149-3>
- Zhu, L., Wu, Y., Wang, J., Lin, X., Ju, J., Xie, M., Li, M., Mäusbacher, R., Schwalb, A. & Daut, G. (2008). Environmental changes since 8.4 ka reflected in the lacustrine core sediments from Nam Co, central Tibetan Plateau, China. *The Holocene*, 18(5), 831–839. <https://doi.org/10.1177/0959683608091801>
- Zhu, L., Xie, M. & Wu, Y. (2010b). Quantitative analysis of lake area variations and the influence factors from 1971 to 2004 in the Nam Co basin of the Tibetan Plateau. *Chinese Science Bulletin*, 55(13), 1294–1303. <https://doi.org/10.1007/s11434-010-0015-8>

Appendix

ICDP workshop on scientific drilling of Nam Co on the Tibetan Plateau: 1 million years of paleoenvironmental history, geomicrobiology, tectonics and paleomagnetism derived from sediments of a high-altitude lake

Torsten Haberzettl, Gerhard Daut, Nora Schulze, Volkhard Spiess, Junbo Wang, Liping Zhu, and the 2018 Nam Co workshop party

Sci. Dril., 25, 63–70, 2019

<https://doi.org/10.5194/sd-25-63-2019>

This work is distributed under the Creative Commons Attribution 4.0 License.

Sci. Dril., 25, 63–70, 2019
<https://doi.org/10.5194/sd-25-63-2019>
 © Author(s) 2019. This work is distributed under
 the Creative Commons Attribution 4.0 License.



Scientific Drilling
 Open Access

ICDP workshop on scientific drilling of Nam Co on the Tibetan Plateau: 1 million years of paleoenvironmental history, geomicrobiology, tectonics and paleomagnetism derived from sediments of a high-altitude lake

Torsten Haberzettl¹, Gerhard Daut², Nora Schulze³, Volkhard Spiess³, Junbo Wang⁴, Liping Zhu⁴, and the 2018 Nam Co workshop party*

¹University of Greifswald, Institute of Geography and Geology, Physical Geography, Friedrich-Ludwig-Jahn-Str. 16, 17489 Greifswald, Germany

²Friedrich-Schiller-University Jena, Institute of Geography, Physical Geography, Löbdergraben 32, 07743 Jena, Germany

³Department of Geosciences, Marine Technology and Environmental Research, University of Bremen, Bremen, Germany

⁴Institute of Tibetan Plateau Research, Chinese Academy of Sciences, No. 16 Lincui Road, Chaoyang District, Beijing 100101, China

*A full list of authors and their affiliations appears at the end of the paper.

Correspondence: Torsten Haberzettl (torsten.haberzettl@uni-greifswald.de)

Received: 10 September 2018 – Revised: 21 November 2018 – Accepted: 22 November 2018 – Published: 12 June 2019

Abstract. The Tibetan Plateau is of peculiar societal relevance as it provides freshwater from the so-called “Water Tower of Asia” to a large portion of the Asian population. However, future climate change will affect the hydrological cycle in this area. To define parameters for future climate change scenarios it is necessary to improve the knowledge about thresholds, timing, pace and intensity of past climatic changes and associated environmental impacts. Sedimentary archives reaching far back in time and spanning several glacial–interglacial cycles such as Nam Co provide the unique possibility to extract such information. In order to explore the scientific opportunities that an ICDP drilling effort at Nam Co would provide, 40 scientists from 13 countries representing various scientific disciplines met in Beijing from 22 to 24 May 2018. Besides paleoclimatic investigations, opportunities for paleomagnetic, deep biosphere, tectonic and paleobiological studies were discussed. After having explored the technical and logistical challenges and the scientific opportunities all participants agreed on the great value and need to drill this extraordinary archive, which has a sediment thickness of more than 1 km, likely covering more than 1 Ma.

1 Introduction

With a mean elevation of > 4000 m above sea level, the Tibetan Plateau is often considered as the “Third Pole”, as it is the third largest storage of ice on earth (Qiu, 2008). Its isolated setting at high altitudes resulted from its long tectonic evolution and made it home to unique ecosystems with a large number of endemic species, particularly in aquatic systems (von Oheimb et al., 2011). The Tibetan Plateau is

also of peculiar social relevance as it is the source of several major rivers, providing freshwater from the so-called “Water Tower of Asia” to a large portion of the Asian population (Lau et al., 2010) and sediment for associated mega deltas with areas larger than $10\,000\text{ km}^2$, being home to millions of people (Cruz et al., 2007). Future climate change, as shown in the 5th IPCC assessment report (Masson-Delmotte et al., 2013), will impact the hydrological cycle in this area and consequently the ecology and economy. To define parameters

Published by Copernicus Publications on behalf of the IODP and the ICDP.

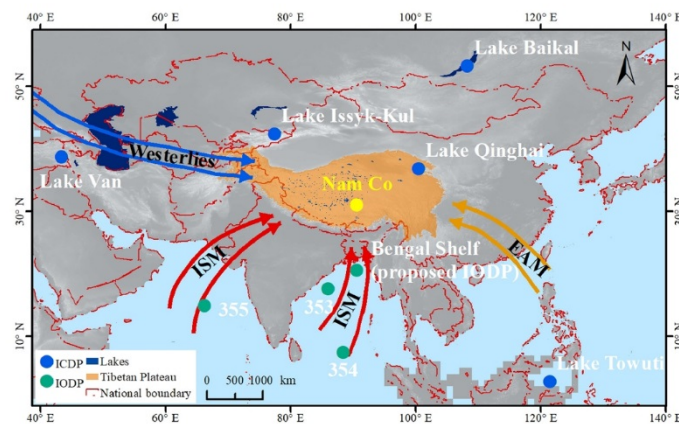


Figure 1. Strategic location of Nam Co (yellow dot) on the Tibetan Plateau (orange area) with respect to further ICDP and IODP sites (blue and green dots). Numbers represent IODP expeditions, ISM: Indian Summer Monsoon, EAM: East Asian Monsoon. Source map: Shuttle Radar Topography Mission digital elevation model (SRTM DEM) from the US Geological Survey (<https://lta.cr.usgs.gov/citation>, last access: 12 November 2018).

for future climate change scenarios and their consequences for ecosystems and society, it is necessary to improve our knowledge about the thresholds, timing, pace and intensity of past climatic changes and associated environmental impacts, not just on short (modern to Last Glacial Maximum) but also on long geologic timescales and with high resolution.

High-resolution archives, such as lacustrine sediments, are abundant on the Tibetan Plateau but the depositional histories are rather short and often discontinuous, because an arid climate led to repeated desiccation. On the northern TP, Lake Qinghai is an archive where one of the longest paleoclimatic records (32 cal ka BP) from the Tibetan Plateau was produced (An et al., 2012). On the western plateau, Bangong Co (co = lake) bears a Holocene paleoclimatic record (Fontes et al., 1996) and in the south, at Puma Yumco, paleoclimatic variations of the past 19 cal kyr BP were investigated (Nishimura et al., 2014). However, none of these investigations exceeds the Last Glacial. Thus, large and deep lacustrine systems with sizeable catchment areas, integrating regional climatic signals, represent the only suitable continuous paleoclimate archives. Previous studies have shown that Nam Co is one of those lakes (Kasper et al., 2015).

During the past 10 years, transect studies focusing on paleoclimate on the Tibetan Plateau, including Nam Co, have been carried out (Ahlborn et al., 2017; Alivernini et al., 2018; Dietze et al., 2014). In addition, physical and chemical limnological seasonal processes as well as climate parameters at Nam Co have been monitored. Further information on environmental dynamics in the Nam Co catchment is available for glacier dynamics (Bolch et al., 2010), hydrology (Krause

et al., 2010), regional geology (Wu et al., 2011), geomorphology (Keil et al., 2010) and meteorology (Ma et al., 2008). This makes the Nam Co area one of the best-surveyed areas on the Tibetan Plateau.

Because of the location of Nam Co on the central Tibetan Plateau at the intersection of westerly and monsoonal air masses (Fig. 1) and its continuous sedimentation history, it represents an ideal drilling target to disentangle long-term changes in climate. A record from Nam Co will enable the following: the relation of climate signals in Tibet to inter-regional and/or global atmospheric circulation patterns using, for example, sediment cores recovered in IODP; the study of paired ocean and continent archives in appropriate locations with adequate resolution; the investigation of upstream and downstream processes (Thurrow et al., 2009) and fill a gap in two ICDP/IODP continental scale transects (Fig. 1, N–S: Lake Baikal, Lake Qinghai, Bay of Bengal; W–E: Lake Van, Lake Issyk-Kul, Lake Towuti). These transects (especially the N–S) will contribute to the Baikal to Bengal transect, which focuses on the internal dynamics of the monsoonal system. This follows previous discussions on utilizing combined ICDP and IODP drilling projects for maximizing the scientific progress in paleoclimate research (Thurrow et al., 2009).

2 Site description

Nam Co has a flat central basin with a water depth > 95 m and a smaller and shallower basin of only about 60 m water depth in the NE (Fig. 2) (Wang et al., 2009). The lake covers

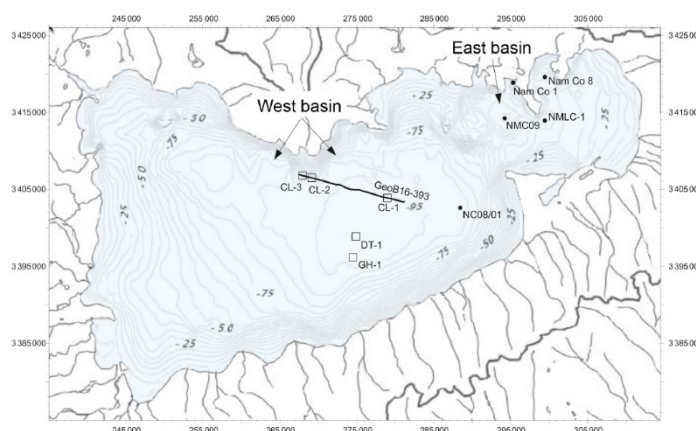


Figure 2. Bathymetry of Nam Co (Wang et al., 2009). Potential drill sites for three piston cores (CL-1, CL-2, CL-3) along profile GeoB16-393 (Fig. 4), a deep core (DT-1) and a glacial history core (GH-1) are indicated. Also indicated are previously investigated sediment cores NMLC1 (Zhu et al., 2008), Nam Co 8 (Mügler et al., 2010), NC08/01 (Kasper et al., 2015) and NMC09 (Li et al., 2017).

an area of 2015.4 km² (Zhu et al., 2010) and has a catchment area of 10 680 km² (Zhou et al., 2013). The drainage area hosts more than 60 streams, most of them draining the glaciated Nyainqêntanglha mountain range (> 7000 m a.s.l.) in the S and SW of the lake (Xie et al., 2009). Annual precipitation is around 420 mm, with more than 90 % from intensive monsoonal rainfall from June to September. Dry conditions with low precipitation prevail from October to May (Zhang et al., 2011). As Nam Co is situated in a closed basin, the water balance is primarily controlled by precipitation, evaporation, permafrost glacier meltwater, and groundwater. Annual lake-level fluctuations in the range of 2 m are clearly related to monsoonal precipitation during summer and evaporation during the rest of the year. Nowadays Nam Co is a dimictic, oligotrophic, slightly alkaline (8.04–9.85, averaging 9.21, Wang et al., 2009) and saline lake (1.851 mS cm⁻¹, Wang et al., 2009) with a waterbody that shows a stable thermal stratification during summer (June to early November) and complete oxygenation throughout the year even during ice coverage (February to mid-May). Allochthonous input by high-density underflows dominates modern sedimentation. The surface distribution patterns of many allochthonous input indicators show that sediment focusing effects occur in the deepest parts of both subbasins.

Nam Co is surrounded by Cretaceous sedimentary rocks as well as Jurassic sediments to the east, and Permian and Carboniferous rocks to the south. Magmatic rocks are found in the northeast of the lake and, together with mainly metamorphic rocks, also form the main part of the glaciated Nyainqêntanglha mountain range in the south (Fig. 3).

Although the main active faults of the Yadong–Gulu rift system lie outside the Nam Co basin (Armijo et al., 1986;

Harrison et al., 1995; Styron et al., 2010), minor faulting may occur across the basin. These faults may be either north–south-trending normal faults or northwest–southeast-trending strike-slip faults or a combination of both. Geology and tectonics (Fig. 3) as well as evidence from own seismic data (Fig. 4) indicate deformation in the Quaternary in the Nam Co basin.

3 Previous investigations

High-resolution (centennial to decadal) multiproxy studies on four sediment cores from different water depths and locations (Fig. 2, NMLC1, Zhu et al., 2008; Nam Co 8, Mügler et al., 2010; NC08/01, Kasper et al., 2015; NMC09, Li et al., 2017) within Nam Co underline the high potential of Nam Co sediments as an environmental archive. Studies integrate results from inorganic geochemistry; sedimentology; mineralogy (Doberschütz et al., 2014); organic geochemistry, including compound-specific (*n*-alkanes) stable isotopes (Günther et al., 2011); micropaleontological (ostracod and diatom ecology) analyses, including ostracod-based transfer functions (salinity, water depth) and stable isotopes, as well as trace elements from their shells (Yang et al., 2014); paleomagnetic and environmental magnetic investigations (Haberzettl et al., 2015; Kasper et al., 2012; Su et al., 2013); and modern and fossil pollen composition (Zhu et al., 2015).

The longest of the hitherto recovered sediment cores, NC08/01 (10.4 m) from the deepest part of the lake, includes many discoveries made in shorter sediment cores in earlier studies and is therefore used as a reference core. This core covers the past 24 cal kyr BP (Kasper et al., 2015), but high

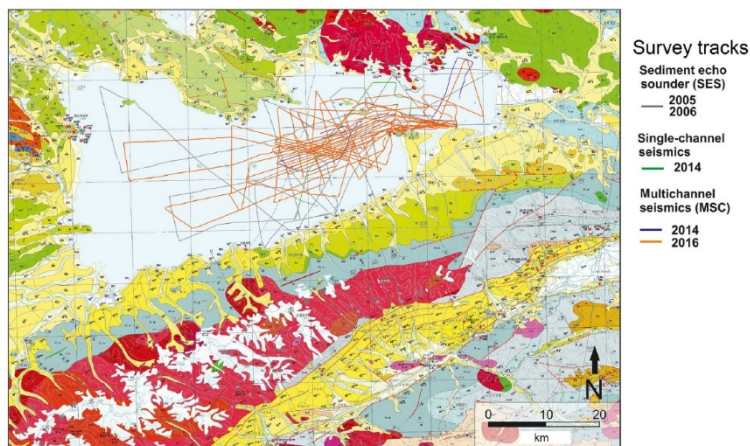


Figure 3. Geological map of the Nam Co area (green: Cretaceous; blue: Jurassic; gray: Permian and Carboniferous; red: magmatic and metamorphic; yellow: Quaternary; white: modern glaciers of the Nyainqentanglha mountain range) (Wu et al., 2011, modified) and cruise tracks of 2005/2006 echosounder (gray), 2014 single channel (green), and 2014/2016 multichannel seismic surveys (purple and orange).

stand lacustrine deposits up to 139.2 m above today's lake level of Nam Co, dated back to 115.9 ± 12.1 ka, prove the existence of the lake for a much longer period, potentially as part of an ancient megalake on the Tibetan Plateau (Zhu et al., 2004). In addition, molecular clock analyses of recent endemic gastropods (*Radix* spp.) occurring in the Nam Co area indicate that their regional diversification started > 1 Ma ago. This suggests a continuous existence of water bodies in the Nam Co area at least since the middle Pleistocene (von Ohlenstein et al., 2011).

In 2005 and 2006, about 420 km of seismic profiles (Fig. 3) was acquired with a parametric sediment echo sounder (Innomar SES 96 light), providing a signal penetration to 30–35 m sediment depth. After a preliminary deep seismic survey (signal penetration to ~ 800 m) in 2014 (~ 160 km) an extensive pre-site survey funded by the Deutsche Forschungsgemeinschaft (DFG, German Research Foundation) took place in June–July 2016 to refine the opportunities for a deep drilling ICDP project (Fig. 3). A further goal of this multichannel seismic survey (MCS) was the investigation of the tectonic framework and sedimentary environment to develop stratigraphic and evolutionary scenarios for Nam Co. For this purpose, a micro GI Gun (2×0.1 L chamber volume) combined with a multichannel streamer (Teledyne, 32 channels, 64 m active length) was utilized. In total, 91 deep penetration seismic profiles were recorded, allowing good coverage of the basin (860 km).

4 Seismic results

Seismic profiles reveal at least several hundred meters of sediment infill with varying thicknesses. In the eastern part of the lake a penetration depth of only 250 ms TWT (two-way travel time) (~ 200 m) was reached, whereas the western part allowed a penetration of > 1 s TWT (~ 800 m). Fault patterns in the sediment fill of Nam Co likely represent the predominant regional deformation in the Quaternary. Fig. 4 displays a seismic profile along the NW–SE axis of the lake (GeoB16-393), comprising well-layered sedimentary sequences down to 960 ms TWT, with densely spaced steep faults, indicating a predominant strike-slip tectonic regime. E–W-trending positive and negative flower structures (Fig. 4) indicate local subsidence and the creation of accommodation space. The interplay of tectonics and sedimentation has apparently maintained a closed basin in the late Quaternary. We suppose that during extensional phases subsidence has significantly influenced sediment accumulation within the basin. Combining the new seismic data and drilling results will provide depositional boundary conditions, e.g. timing of tectonic activity and subsidence rates.

A preliminary seismic stratigraphy was derived using overall reflection strength to distinguish high and low lake-level settings as well as transitional periods. Also, in MCS data (Fig. 4), low-amplitude seismic facies can be assigned to lake-level high stands and deposition of mostly fine-grained sediments, comparable to the modern situation. A uniform thickness of this uppermost unit is indicative of a widespread deposition of mostly suspended material. During periods of lower lake levels, higher amplitude reflectors indicate coarser

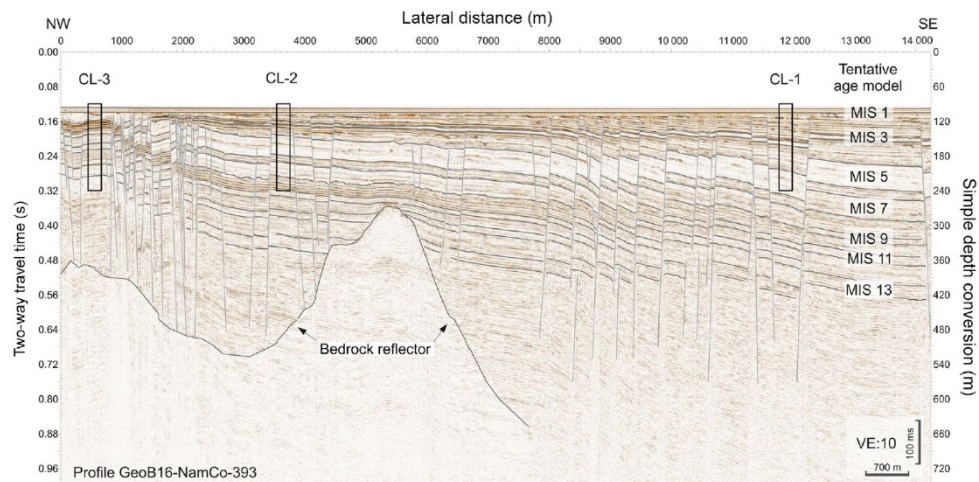


Figure 4. Multichannel seismic profile GeoB16-393 showing several hundred meters of sediment infill. Sediment thickness is increasing towards the center of the lake in the SE due to the additional subsidence of ca. 300 m. Simple depth conversion with 1500 m s^{-1} . A tentative age model is given with marine isotope stages (MISs). Potential piston coring locations (CL-1, CL-2, CL-3) at which sediment cores can well be parallelized to form a composite sediment sequence using strong reflectors in the seismic images are indicated by black boxes.

material. This and minor incisions in shallower parts of the lake as well as irregular topography hint to erosion in a shallow lake. In Fig. 4 extrapolation of the sedimentation rates and the acoustic behavior observed in the reference core confirm that at least 13 MIS stages are imaged (Fig. 4), with older sedimentary sections present.

5 Workshop

With these data in mind 40 scientists from 13 countries, representing various fields, met in Beijing from 22 to 24 May 2018 to discuss the further scientific opportunities that an ICDP drilling effort would provide. In addition, drilling strategies as well as logistical requirements of a deep drilling at Nam Co were discussed. Contributions of the participants included the following topics:

- the tectonic setting of Nam Co;
- the global relevance of a long climate record from Nam Co;
- paleoclimatological work which had been and will be carried out at Nam Co;
- seismic stratigraphy of Nam Co;
- archives for comparison;
- lake drilling project management, drilling operations, and fundamental core analyses;

- geochronology;
- bioindicators and deep biosphere;
- downhole logging;
- paleomagnetism;
- provenance analyses.

In addition, an excursion to Nam Co was planned for late 2018 to consider possible lake access points and base camps for future drilling and science teams as well as other logistic challenges.

Several discussion groups were organized to focus on the themes noted above and were charged with writing short reports to identify the major questions and develop hypotheses that will be addressed by studying Nam Co sediments through an ICDP deep drilling project. These groups included (1) sedimentology, (2) pollen, (3) bioindicators, (4) chronology and (5) tectonics. Scientific hypotheses were subsequently reviewed by all workshop participants and revisited by the breakout groups on the last day of the workshop. This reiterating process led to scientific hypotheses which can be tested by scientific drilling, such as the following for example:

- The timing and magnitude of Indian monsoon variability is controlled by eccentricity- and/or precession-driven insolation during the last million years.

- The land–ocean temperature gradient is greatest in transitions from terminations to interglacials, increasing precipitation (decreasing evaporation/inflow).
- Hemispheric climate controls species diversity, functional diversity and evolution of high-altitude ecosystems during the last 1 Ma.
- Aquatic and terrestrial biomes respond independently to environmental forcing over multiple glacial to interglacial cycles.
- High-altitude ecosystems are resilient from interglacial to interglacial which results in similar community structures and functions.
- The activity and diversity of the subsurface biosphere in high-altitude lake basins is dependent on their relationship to climate-driven carbon cycling and nutrient availability.
- The permanent lake system of Nam Co provided a refugium during glacials and, due to its unique location and size, was instrumental in the survival and recolonization of high-altitude species endemic to the Tibetan Plateau.
- The denudation rate of the Nyainqêntanglha mountain range controls sediment accumulation in the closed Nam Co basin.
- Deformation in the basin is consistent in space and time with regional tectonics.

These hypotheses will be used and revisited for the preparation of an ICDP full proposal. Participants saw dating as the most important prerequisite to be able to test the abovementioned hypotheses. It was concluded that 200 radiocarbon ages in combination with 200–400 OSL ages will provide a sound chronology for the younger part of the sequence, allowing the “calibration” of the paleomagnetic signal which should be used to date the older part. The use of U-Th dating as another dating technique was seen as questionable as more recent sediments showed a high detrital Th component. Therefore, the use of U-Th as an additional dating technique will have to be tested for older sediments. Amino acid dating might also be used for dating if suitable material can be extracted from the sediment sequence.

The last part of the workshop was dedicated to drilling strategies, on-site work and budgeting as well as outreach opportunities. Since Nam Co is characterized by ongoing tectonism, new accommodation space is constantly created in different parts of the lake. As this is a “quasi” continuous process, younger sediments are found at the top of the sequences in the southern part and older sediments at the top of the sequences in the northern part, with intermediate sequences in between (Fig. 4). Considering this architecture, one promising drilling strategy which was discussed by the participants

was to build a composite record using three to four overlapping cores in rather high resolution and of good quality, recovered from different sites (Fig. 4). Using, for example, three to four 100–150 m long piston cores (e.g. CL-1 to 3 in Fig. 4) in a N–S transect a continuous, high-core-quality composite sequence going back to MIS 13 (according to the seismic interpretation) will be obtained. These sites should be covered by triple cores. The construction of a continuous log will be improved by downhole logging data. Also possible depth shifts will be corrected using these data. This composite record will be complemented by a ~ 700–800 m long core (DT-1 in Fig. 2) going back to ~ 1 Ma which most likely can only be cored as a single hole due to time constraints. Modern process studies show that different subbasins of Nam Co show different signals. For example, oxygen isotopes reveal an offset of 2‰ between basins. Thus, the long core will be used to calibrate signal changes in proxies detected in the high-quality “short” piston cores. Finally, two ~ 100 m parallel cores forming the composite sequence GH-1 will be recovered from the very southern shore (Fig. 2) in order to investigate the role of glacial activity and its impact on the lake. The ICDP’s Deep Lake Drilling System was generally seen as a reasonable tool for drilling Nam Co as it has been successfully applied to other challenging environmental systems (e.g. the Dead Sea in Israel).

Since Nam Co is located at an altitude of 4730 m a.s.l. there was intense discussion of how much man power will be needed to guarantee a smooth drilling operation. Everybody agreed that on-site work should at least include measurements of magnetic susceptibility and density to calculate porosity, which is important for OSL dating, using a Multi-Sensor Core Logger (MSCL). A mobile nuclear magnetic resonance (NMR) device will enable water content and thus porosity to be even more precisely determined. This will be complemented by pore water extraction and a clean lab for microbiological investigations. If manpower permits microscopes could also potentially be set up on-site.

6 Conclusions

All participants agreed that Nam Co sediments hold an extraordinary potential to answer questions of global social relevance, including past, modern and future climate change, biological development, tectonic evolution, and understanding of paleomagnetic variations and water resources which are coupled to the hydrological cycle. The workshop allowed the refinement of the scientific questions and discussion of the logistical issues of a scientific drilling of Nam Co in the framework of ICDP. Moreover, it allowed the transfer of knowledge between the different participants, increasing international visibility and promoting multidisciplinary.

Data availability. No data sets were used in this article.

Team list. Guillaume St-Onge (University of Quebec, Rimouski, Canada), Fahu Chen (Institute of Tibetan Plateau Research, CAS, Beijing, China), Xingqi Liu (Beijing Normal University, Beijing, China), Xinmiao Lyu (Institute of Tibetan Plateau Research, CAS, Beijing, China), Jianting Ju (Institute of Tibetan Plateau Research, CAS, Beijing, China), Qingfeng Ma (Institute of Tibetan Plateau Research, CAS, Beijing, China), Zhonghai Wu (Chinese Academy of Geological Sciences, Beijing, China), Bernd Wünnemann (East China Normal University, Shanghai, China), Dada Yan (East China Normal University, Shanghai, China), Shuangwen Yi (Nanjing University, Nanjing, China), Hanzhi Zhang (Nanjing University, Nanjing, China), Yan Zhao (Institute of Geographic Sciences and Natural Resources Research, CAS, Beijing, China), Hongbo Zhao (China Geological Survey (Beijing Institute of Exploration Engineering), Beijing, China), Jan-Pieter Buylaert (Aarhus University, Aarhus, Denmark), Andrew Murray (Aarhus University, Aarhus, Denmark), Jerome van der Woerd (University of Strasbourg, Strasbourg, France), Peter Frenzel (Friedrich-Schiller-University, Jena, Germany), Gerd Gleixner (MPI Jena, Germany), Uli Harms (Scientific Drilling Operational Support Group ICDP, Potsdam, Germany), Klaus Reicherter (RWTH Aachen University, Aachen, Germany), Antje Schwalb (Technische Universität Braunschweig, Braunschweig, Germany), Arne Ulfers (Leibniz Institute for Applied Geophysics (LIAG), Hanover, Germany), Gábor Újvári (Research Centre for Astronomy and Earth sciences, Hungarian Academy of Sciences, Budapest, Hungary), Nivedita Mehrotra (Birbal Sahni Institute of Palaeosciences, Lucknow, India), Nicolas Waldmann (University of Haifa, Haifa, Israel), Andrea Lami (Italian National Research Council, Rome, Italy), Daniel Ariztegui (University of Geneva, Geneva, Switzerland), Natasha Barbolini (University of Amsterdam, Amsterdam, the Netherlands), Philippa Ascoug (Scottish Universities Environmental Research Centre, East Kilbride, UK), Leon Clarke (Manchester Metropolitan University, Manchester, UK), Andrew Henderson (Newcastle University, Newcastle upon Tyne, UK), Richard Staff (Scottish Universities Environmental Research Centre, East Kilbride, UK), Anders Noren (LacCore Facility, University of Minnesota, Minneapolis, USA), Trisha Spanbauer (University of Texas at Austin, Austin, USA), Joseph Stoner (Oregon State University, Corvallis, USA).

Author contributions. All authors jointly organized the workshop. TH drafted the paper and NS drafted Figs. 2 to 4. All co-authors jointly contributed to the content of the final version of the paper. Listed workshop participants enthusiastically discussed the scientific objectives of a scientific drilling at Nam Co, contributed to the compilation of the hypotheses listed above and commented on the paper.

Competing interests. The authors declare that they have no conflict of interest.

Acknowledgements. We would like to acknowledge funding from ICDP and the Institute of Tibetan Plateau Research to carry out the workshop in Beijing. We would also like to thank Thomas Kasper and Ruimin Yang for drafting Fig. 1.

Edited by: Ulrich Harms

Reviewed by: two anonymous referees

References

- Ahlborn, M., Haberzettl, T., Wang, J., Henkel, K., Kasper, T., Daut, G., Zhu, L., and Mäusbacher, R.: Synchronous pattern of moisture availability on the southern Tibetan Plateau since 17.5 cal. ka BP-the Tangra Yumco lake sediment record, *Boreas*, 46, 229–241, 2017.
- Alivernini, M., Akita, L. G., Ahlborn, M., Börner, N., Haberzettl, T., Kasper, T., Plessen, B., Peng, P., Schwalb, A., Wang, J., and Frenzel, P.: Ostracod-based reconstruction of Late Quaternary lake level changes within the Tangra Yumco lake system (southern Tibetan Plateau), *J. Quaternary Sci.*, 33, 713–720, 2018.
- An, Z., Colman, S. M., Zhou, W., Li, X., Brown, E. T., Jull, A. J. T., Cai, Y., Huang, Y., Lu, X., Chang, H., Song, Y., Sun, Y., Xu, H., Liu, W., Jin, Z., Liu, X., Cheng, P., Liu, Y., Ai, L., Li, X., Liu, X., Yan, L., Shi, Z., Wang, X., Wu, F., Qiang, X., Dong, J., Lu, F., and Xu, X.: Interplay between the Westerlies and Asian monsoon recorded in Lake Qinghai sediments since 32 ka, *Nat. Sci. Rep.*, 2, 1–6, 2012.
- Armijo, R., Tapponnier, P., Mercier, J., and Han, T. L.: Quaternary extension in southern Tibet: Field observations and tectonic implications, *J. Geophys. Res.-Sol. Ea.*, 91, 13803–13872, 1986.
- Bolch, T., Yao, T., Kang, S., Buchroithner, M. F., Scherer, D., Mausson, F., Huintjes, E., and Schneider, C.: A glacier inventory for the western Nyainqentanglha Range and the Nam Co Basin, Tibet, and glacier changes 1976–2009, *The Cryosphere*, 4, 419–433, <https://doi.org/10.5194/tc-4-419-2010>, 2010.
- Cruz, R. V., Harasawa, H., Lal, M., Wu, S., Anokhin, Y., Punsalma, B., Honda, Y., Jafari, M., Li, C., and Huu Ninh, N.: Asia – Climate Change 2007: Impacts, Adaptation and Vulnerability, Contribution of Working Group II to the Fourth Assessment Report of the Intergovernmental Panel on Climate Change, Cambridge, 469–506, 2007.
- Dietze, E., Maussion, F., Ahlborn, M., Diekmann, B., Hartmann, K., Henkel, K., Kasper, T., Lockot, G., Opitz, S., and Haberzettl, T.: Sediment transport processes across the Tibetan Plateau inferred from robust grain-size end members in lake sediments, *Clim. Past*, 10, 91–106, <https://doi.org/10.5194/cp-10-91-2014>, 2014.
- Doberschütz, S., Frenzel, P., Haberzettl, T., Kasper, T., Wang, J., Zhu, L., Daut, G., Schwalb, A., and Mäusbacher, R.: Monsoonal forcing of Holocene paleoenvironmental change on the central Tibetan Plateau inferred using a sediment record from Lake Nam Co (Xizang, China), *J. Paleolimnol.*, 51, 253–266, 2014.
- Fontes, J.-C., Gasse, F., and Gibert, E.: Holocene environmental changes in Lake Bangong basin (Western Tibet), Part I: Chronology and stable isotopes of carbonates of a Holocene lacustrine core, *Palaeogeogr. Palaeoclimatol.*, 120, 25–47, 1996.
- Günther, F., Mügler, I., Mäusbacher, R., Daut, G., Leopold, K., Gerstmann, U. C., Xu, B., Yao, T., and Gleixner, G.: Response of δD values of sedimentary n-alkanes to variations in source water isotope signals and climate proxies at lake Nam Co, Tibetan Plateau, *Quatern. Int.*, 236, 82–90, 2011.
- Haberzettl, T., Henkel, K., Kasper, T., Ahlborn, M., Su, Y., Wang, J., Appel, E., St-Onge, G., Stoner, J., Daut, G., Zhu, L., and Mäusbacher, R.: Independently dated paleomagnetic secular variation

- records from the Tibetan Plateau, *Earth Planet. Sc. Lett.*, 416, 98–108, 2015.
- Harrison, T. M., Copeland, P., Kidd, W., and Lovera, O. M.: Activation of the Nyainqentanghla shear zone: Implications for uplift of the southern Tibetan Plateau, *Tectonics*, 14, 658–676, 1995.
- Kasper, T., Haberzettl, T., Doberschütz, S., Daut, G., Wang, J., Zhu, L., Nowaczyk, N., and Mäusbacher, R.: Indian Ocean Summer Monsoon (IOSM)-dynamics within the past 4 ka recorded in the sediments of Lake Nam Co, central Tibetan Plateau (China), *Quaternary Sci. Rev.*, 39, 73–85, 2012.
- Kasper, T., Haberzettl, T., Wang, J., Daut, G., Zhu, L., and Mäusbacher, R.: Hydrological variations on the Central Tibetan Plateau since the LGM and their teleconnection to inter-regional and hemispheric climate variations, *J. Quaternary Sci.*, 30, 70–78, 2015.
- Keil, A., Berking, J., Mügler, I., Schütt, B., Schwalb, A., and Steeb, P.: Hydrological and geomorphological basin and catchment characteristics of Lake Nam Co, South-Central Tibet, *Quatern. Int.*, 218, 118–130, 2010.
- Krause, P., Biskop, S., Helmschrot, J., Flügel, W. A., Kang, S., and Gao, T.: Hydrological system analysis and modelling of the Nam Co basin in Tibet, *Adv. Geosci.*, 27, 29–36, 2010.
- Lau, W. K. M., Kim, M. K., Kim, K. M., and Lee, W. S.: Enhanced surface warming and accelerated snow melt in the Himalayas and Tibetan Plateau induced by absorbing aerosols, *Environ. Res. Lett.*, 5, 025204, <https://doi.org/10.1088/1748-9326/5/2/025204>, 2010.
- Li, C., Yan, F., Kang, S., Chen, P., Han, X., Hu, Z., Zhang, G., Hong, Y., Gao, S., Qu, B., Zhu, Z., Li, J., Chen, B., and Silanpää, M.: Re-evaluating black carbon in the Himalayas and the Tibetan Plateau: concentrations and deposition, *Atmos. Chem. Phys.*, 17, 11899–11912, <https://doi.org/10.5194/acp-17-11899-2017>, 2017.
- Ma, Y., Kang, S., Zhu, L., Xu, B., Tian, L., and Yao, T.: ROOF OF THE WORLD: Tibetan Observation and Research Platform, *B. Am. Meteorol. Soc.*, 89, 1487–1492, 2008.
- Masson-Delmotte, V., Schulz, M., Abe-Ouchi, A., Beer, J., Ganopolski, A., Rouco, J. F. G., Jansen, E., Lambeck, K., Luterbacher, J., Naish, T., Osborn, T., Otto-Bliesner, B., Quinn, T., Ramesh, R., Rojas, M., Shao, X., and Timmermann, A.: *Information from Paleoclimate Archives*, Cambridge, New York, 2013.
- Mügler, I., Gleixner, G., Günther, F., Mäusbacher, R., Daut, G., Schütt, B., Berking, J., Schwalb, A., Schwark, L., Xu, B., Yao, T., Zhu, L., and Yi, C.: A multi-proxy approach to reconstruct hydrological changes and Holocene climate development of Nam Co, Central Tibet, *J. Paleolimnol.*, 43, 625–648, 2010.
- Nishimura, M., Matsunaka, T., Morita, Y., Watanabe, T., Nakamura, T., Zhu, L., Nara, F. W., Imai, A., Izutsu, Y., and Hasuike, K.: Paleoclimatic changes on the southern Tibetan Plateau over the past 19,000 years recorded in Lake Pumoyum Co, and their implications for the southwest monsoon evolution, *Palaeogeogr. Palaeoclimatol.*, 396, 75–92, 2014.
- Qiu, J.: China: The third pole, *Nature*, 454, 393–396, 2008.
- Styron, R., Taylor, M., and Okoronkwo, K.: Database of active structures from the Indo-Asian collision, *Eos T. Am. Geophys. Un.*, 91, 181–182, 2010.
- Su, Y., Gao, X., Liu, Q., Hu, P., Duan, Z., Jiang, Z., Wang, J., Zhu, L., Doberschütz, S., Mäusbacher, R., Daut, G., and Haberzettl, T.: Mechanism of variations in environmental magnetic proxies of lake sediments from Nam Co, Tibet during the Holocene, *Chin. Sci. Bull.*, 58, 1568–1578, 2013.
- Thurrow, J., Peterson, L. C., Harms, U., Hodell, D. A., Cheshire, H., Brumsack, H.-J., Irino, T., Schulz, M., Masson-Delmotte, V., and Tada, R.: Acquiring High to Ultra-High Resolution Geological Records of Past Climate Change by Scientific Drilling, *Sci. Drill.*, 8, 46–56, <https://doi.org/10.2204/iodp.sd.8.08.2009>, 2009.
- von Oheimb, P. V., Albrecht, C., Riedel, F., Du, L. N., Yang, J. X., Aldridge, D. C., Bossneck, U., Zhang, H. C., and Wilke, T.: Freshwater Biogeography and Limnological Evolution of the Tibetan Plateau – Insights from a Plateau-Wide Distributed Gastropod Taxon (*Radix* spp.), *Plos One*, 6, e26307, <https://doi.org/10.1371/journal.pone.0026307>, 2011.
- Wang, J., Zhu, L., Daut, G., Ju, J., Lin, X., Wang, Y., and Zhen, X.: Investigation of bathymetry and water quality of Lake Nam Co, the largest lake on the central Tibetan Plateau, China, *Limnology*, 10, 149–158, 2009.
- Wu, Z. H., Meng, X. G., and Hu, D. G.: *Regional Geological Survey Report of China (Damxong)*, China University of Geosciences Press, Wuhan, China, 346 pp., 2011.
- Xie, M., Zhu, L., Peng, P., Wang, J., Wang, Y., and Schwalb, A.: Ostracod assemblages and their environmental significance from the lake core of the Nam Co on the Tibetan Plateau 8.4 ka BP, *J. Geogr. Sci.*, 19, 387–402, 2009.
- Yang, Q., Jochum, K. P., Stoll, B., Weis, U., Börner, N., Schwalb, A., Frenzel, P., Scholz, D., Doberschütz, S., Haberzettl, T., Gleixner, G., Mäusbacher, R., Zhu, L., and Andreae, M. O.: Trace element variability in single ostracod valves as a proxy for hydrochemical change in Nam Co, central Tibet, during the Holocene, *Palaeogeogr. Palaeoclimatol.*, 399, 225–235, 2014.
- Zhang, Y. J., Kang, S. C., and You, Q. L.: *Climate in Nam Co Basin, in: Modern Environmental Processes and Changes in the Nam Co Basin Tibetan Plateau*, edited by: Kang, S. C., China Meteorological Press, 15–35, 2011.
- Zhou, S., Kang, S., Chen, F., and Joswiak, D. R.: Water balance observations reveal significant subsurface water seepage from Lake Nam Co, south-central Tibetan Plateau, *J. Hydrol.*, 491, 89–99, 2013.
- Zhu, D. G., Meng, X. G., Zhao, X. T., Shao, Z. G., Xu, Z. F., Yang, C. B., Ma, Z. B., Wu, Z. G., Wu, Z. H., and Wang, J. P.: Evolution of an Ancient Large Lake in the Southeast of the Northern Tibetan Plateau, *Acta Geol. Sin.-Engl.*, 78, 982–992, 2004.
- Zhu, L., Wu, Y., Wang, J., Lin, X., Ju, J., Xie, M., Li, M., Mäusbacher, R., Schwalb, A., and Daut, G.: Environmental changes since 8.4 ka reflected in the lacustrine core sediments from Nam Co, central Tibetan Plateau, China, *The Holocene*, 18, 831–839, 2008.
- Zhu, L., Peng, P., Xie, M., Wang, J., Frenzel, P., Wroczynna, C., and Schwalb, A.: Ostracod-based environmental reconstruction over the last 8,400 years of Nam Co Lake on the Tibetan plateau, *Hydrobiologia*, 648, 157–174, 2010.
- Zhu, L., Lü, X., Wang, J., Peng, P., Kasper, T., Daut, G., Haberzettl, T., Frenzel, P., Li, Q., Yang, R., Schwalb, A., and Mäusbacher, R.: Climate change on the Tibetan Plateau in response to shifting atmospheric circulation since the LGM, *Sci. Rep.*, 5, 13318, <https://doi.org/10.1038/srep13318>, 2015.

Versicherung an Eides Statt / *Affirmation in lieu of an oath*
gem. § 5 Abs. 5 der Promotionsordnung vom 18.06.2018 /
according to § 5 (5) of the Doctoral Degree Rules and Regulations of 18 June, 2018

Ich / I, Nora Schulze
(Vorname / *First Name*, Name / *Name*)

versichere an Eides Statt durch meine Unterschrift, dass ich die vorliegende Dissertation selbständig und ohne fremde Hilfe angefertigt und alle Stellen, die ich wörtlich dem Sinne nach aus Veröffentlichungen entnommen habe, als solche kenntlich gemacht habe, mich auch keiner anderen als der angegebenen Literatur oder sonstiger Hilfsmittel bedient habe und die zu Prüfungszwecken beigelegte elektronische Version (PDF) der Dissertation mit der abgegebenen gedruckten Version identisch ist. / *With my signature I affirm in lieu of an oath that I prepared the submitted dissertation independently and without illicit assistance from third parties, that I appropriately referenced any text or content from other sources, that I used only literature and resources listed in the dissertation, and that the electronic (PDF) and printed versions of the dissertation are identical.*

Ich versichere an Eides Statt, dass ich die vorgenannten Angaben nach bestem Wissen und Gewissen gemacht habe und dass die Angaben der Wahrheit entsprechen und ich nichts verschwiegen habe. / *I affirm in lieu of an oath that the information provided herein to the best of my knowledge is true and complete.*

Die Strafbarkeit einer falschen eidesstattlichen Versicherung ist mir bekannt, namentlich die Strafandrohung gemäß § 156 StGB bis zu drei Jahren Freiheitsstrafe oder Geldstrafe bei vorsätzlicher Begehung der Tat bzw. gemäß § 161 Abs. 1 StGB bis zu einem Jahr Freiheitsstrafe oder Geldstrafe bei fahrlässiger Begehung. / *I am aware that a false affidavit is a criminal offence which is punishable by law in accordance with § 156 of the German Criminal Code (StGB) with up to three years imprisonment or a fine in case of intention, or in accordance with § 161 (1) of the German Criminal Code with up to one year imprisonment or a fine in case of negligence.*

Ort / *Place*, Datum / *Date*

Unterschrift / *Signature*